FOURIER TRANSFORM INFRARED SPECTROSCOPIC STUDIES OF POLYPEPTIDES AND MEMBRANE-ASSOCIATED PROTEINS

By

DORIAN FRANCIS KENNEDY M.Sc., B.Sc. (Hons.)

Department of Protein and Molecular Biology,
Royal Free Hospital School of Medicine,
Rowland Hill Street,
London NW3 2PF.

Submitted in fulfilment of the requirements for the degree of Doctor of Philosophy for the University of London, 1991.

ProQuest LLC.
789 East Eisenhower Parkway
P.O. Box 1346
Ann Arbor, MI 48106 – 1346

ABSTRACT

Fourier transform infrared (FTIR) spectroscopy has been used to investigate the interaction of polypeptides and proteins with model biomembranes.

The characterisation of peptides known to possess a 3_{10}-helical structure, or mixed α-/3_{10}-helical structures, was carried out. Fully stable 3_{10}-helices in organic solvent were found to absorb IR radiation in the 1666-1662 cm^{-1} range. Peptides known to contain both α- and 3_{10}-helical structures exhibit IR absorption bands characteristic of both structures. Peptides containing 3_{10}-helical structure in organic solvent altered their structure in aqueous lipid dispersion to become predominantly α-helical. Peptides containing mixed α- and 3_{10}-helices in organic solvent also altered their structure on interaction with lipids, and formed aqueous channels in the membrane. Peptides known to fold into the β-bend ribbon structure in organic solvent showed an amide I band maxima at 1648-1645 cm^{-1}. β-bend ribbon peptides were largely unaltered by the membrane environment, but formed aqueous pores in the membrane.

The mechanism of spontaneous insertion of soluble proteins into model membranes was investigated using colicin A and aerolysin. The secondary structure of colicin A remained α-helical on insertion into the membrane but it adopted a more open configuration. Aerolysin and its precursor, proaerolysin, contain predominantly β-sheet structure with a small region of hydrophobic α-helix in their soluble form. An increase in α-helical content was observed when aerolysin interacted with model membranes.

The structure of phospholipase A_2's from different sources contained a high degree of conformational homology. Conformational changes consistent with an increase α-helix and a decrease in β-sheet, and possibly β-turns, were observed on binding to lipids and a transition-state inhibitor in micellar form.

ACKNOWLEDGEMENTS

I would like to thank Prof. Dennis Chapman for his supervision of my studies.

I also wish to express thanks to the people with whom I have collaborated on various projects:-

Dr. Arend Slotboom and Prof. Gerard de Haas from the University of Utrect for the phospholipase A_2 work;

Prof. Claudio Toniolo and Dr. Mario Crisma of the University of Padova, Italy for the 3_{10}-helix studies;

Dr. Franc Pattus from EMBL, Heidelberg for the colicin A project; and

Dr. Tom Buckley from the University of Victoria, Canada for the aerolysin project.

All were most generous in providing me with samples to study and with their time, patience and advice.

Thanks a lot to Dr. Mike Jackson helping me through the projects and his invaluable advice.

Also thanks to Laks, Brenda, Trevor, Rachel, Gerald, LinYe, Jonathon and Iñaki for being a laugh.

And to Christine Hall for keeping sane and supplied with cappuccinos with extra chocolate and for producing Joe.

I am also grateful to Dr. Fred Kurzer for his advice and long suffering in explaining the joys of chemistry to me, and to Yandao and Shi for their friendliness and honesty.

And Sarah, thankyou.

I am indebted to my family and friends for seeing me through the last few years and for good times, and for providing babies for me to play with.

THIS THESIS IS FOR AMY, ROBERT AND GABRIELE AND ANY MORE THAT POP OUT.

ABBREVIATIONS USED

Aib - α-aminoisobutyric acid

ATR - attenuated total reflection

Boc - tert-butoxycarbonyl

CD - circular dichroism

$CDCl_3$ - deuterated chloroform

cmc - critical micelle concentration

$C_{10}PN$ - n-decylphosphocholine

$C_{18}PN$ - n-octadecylphosphocholine

DMPC - dimyristoyl phosphatidylcholine

DMPG - dimyristoyl phosphatidylglycerol

EGTA - ethylene glycol-bis(β-aminoethyl ether)-N,N,N',N'-tetra-acetic acid

e.m. - electromagnetic

FT - Fourier transform

FT^{-1} - inverse Fourier transform

FTIR - Fourier transform infrared

FT-NMR - Fourier transform nuclear magnetic resonance

Ge - Germanium

HHNP - 1-heptanoyl-2-heptanoylamino-2-deoxy-sn-glycero-3-phosphoglycol

IR - infrared

KBr - potassium bromide

L_α - bilayer fluid phase

L_β - bilayer crystalline phase

MES - 2-[N-morpholino]ethanesulphonic acid

NMR - nuclear magnetic resonance

OMe - methoxy

O<u>t</u>Bu - <u>tert</u>-butoxy

<u>p</u>BrBz - <u>para</u>-bromobenzoyl

<u>p</u>BrZ - <u>para</u>-bromobenzyloxycarbonyl

pbs - phosphate buffered saline

PC - phosphatidylcholine

PE - phosphatidylethanolamine

PI - phosphatidylinositol

PLA_2 - phospholipase A_2

PMSF - phenylmethylsulphonyl fluoride

$proPLA_2$ - prophospholipase A_2

PS - phosphatidylserine

SM - sphingomyelin

s/n - signal-to-noise ratio

TFE - trifluoroethanol

T_m - temperature of the main phase transition in phospholipids

Tris - tris(hydroxymethyl)aminomethane

Z - benzyloxycarbonyl

TABLE OF CONTENTS

INDEX TO FIGURES

INDEX TO TABLES

CHAPTER ONE

BIOLOGICAL MOLECULES

1.1. INTRODUCTION

A tremendous investment of resources has been directed towards studying the properties of biological systems and biomembranes in order to understand their structure and mode of function at the molecular level. This progress has enabled a greater understanding of the structure of proteins at atomic resolution in the pursuit of an understanding of the relationship between the structure and function of proteins, and of biomembranes. This has been crucial in the development of medicinal drug design as well as furthering the understanding of biomolecular systems. The work presented in this thesis describes the interaction of proteins and polypeptides with biological membranes. Therefore, the properties and structure of proteins and biomembranes are described.

Much of the information concerning these systems has been gained using biophysical techniques such as X-ray crystallography and electron diffraction, nuclear magnetic resonance (NMR) spectroscopy, circular dichroism and vibrational spectroscopy. Techniques providing information at atomic resolution, i.e. X-ray diffraction and NMR spectroscopy, have produced a wealth of information on many soluble proteins. However a severe bottleneck in information has occurred because neither technique has been successfully applied to membrane proteins, with the notable exceptions of the photosynthetic reaction centre of Rhodopseudomonas

viridis (Deisenhofer et al., 1985) and porin (Weiss et al., 1990). This has led to the application of other techniques to study membrane proteins, and the mechanisms of protein insertion into biomembranes.

This chapter is concerned with giving an introduction to the composition and characteristics of biomembranes and proteins.

1.2. BIOMEMBRANES

Biomembranes are sheet-like structures, approximately 50 - 100 Å thick composed of lipids and proteins, and also of carbohydrates attached to these molecules. The main roles of membranes are:-

i) to separate cells from their environment, thus giving cells individuality,

ii) to regulate molecular and ionic composition of the cell through membrane pumps and gates, and

iii) to control information flow between the cell and its environment through specific receptors.

The structure and function of the membrane components needs to be discussed in detail to gain a better understanding of the overall function of biomembranes.

1.3. LIPIDS

The most important characteristic of lipids is that they are amphipathic, containing a hydrophobic fatty acyl chain region and a hydrophilic headgroup region. The three major classes of lipid are glycolipids, sphingolipids and sterols.

1.3.1. Glycolipids

Glycolipids are derived from glycerol, in which one of the primary hydroxyl groups of glycerol is linked to a headgroup with the other hydroxyl groups esterified to fatty acids. The most important class of lipids in animal membranes is the phospholipid, where the headgroup

contains a substituted phosphatidic acid group.

The general structure of common phospholipids is similar to that of phosphatidylcholine (PC), shown in Fig. 1.1a, where R and R' are fatty acyl chains. The fatty acyl chains are usually between 14 and 24 carbon atoms long and may contain one or more double bonds. Other common phospholipids have a similar structure, but with a different headgroup, as illustrated in Figs. 1.1b, c and d.

1.3.2. Sphingolipids

These lipids are derived from the sphingosine molecule to which is attached a fatty acid and a headgroup. One of the commonest sphingolipid is sphinogmyelin (SM), shown in Fig. 1.2a.

Sphingomyelin and gangliosides are usually found in plasma membranes of animal cells but seldom in plants or bacteria.

1.3.3. Sterols

The best-known sterol is cholesterol in animal membranes, while ergosterol occurs in lower eukaryotes and β-sitosterol in plants. All have a similar structure to cholesterol, shown in Fig. 1.2b.

This membrane component has a relatively short acyl chain and a bulky headgroup compared to the structures of the other lipids illustrated. In the membrane, the

Fig. 1.1. The chemical structure of the common phospholipid headgroups:-

a) phosphatidylcholine (PC),
b) phosphatidylserine (PS),
c) phosphatidylethanolamine (PE),
d) phosphatidylinositol (PI).

a) PC

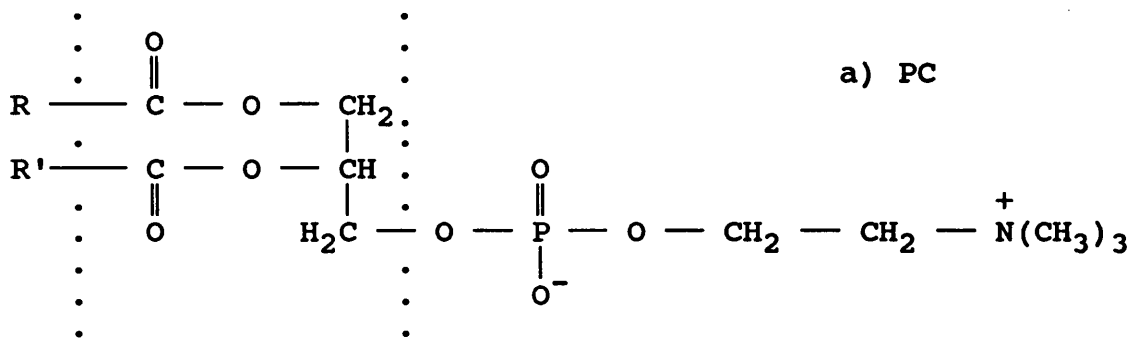

b) PS

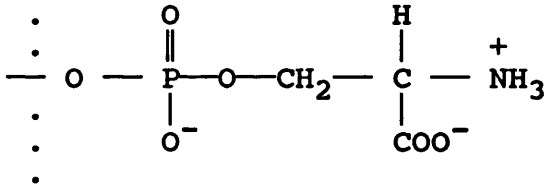

c) PE

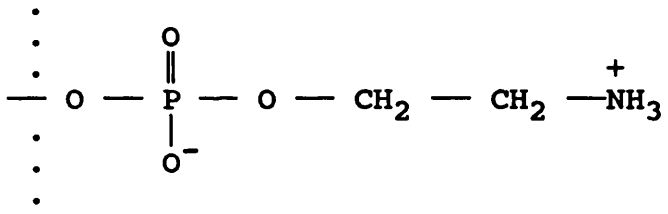

d) PI

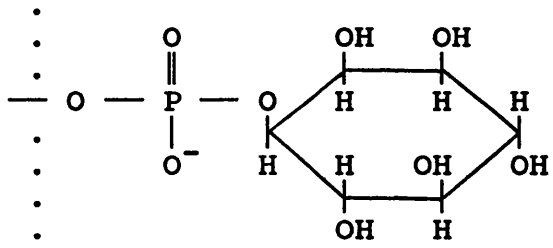

Fig. 1.2. The chemical structures of:-
a) sphingolipids,
b) cholesterol.

a)

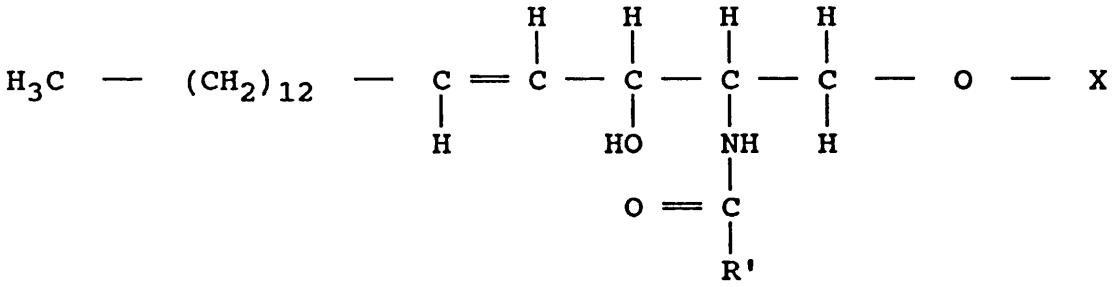

where X = 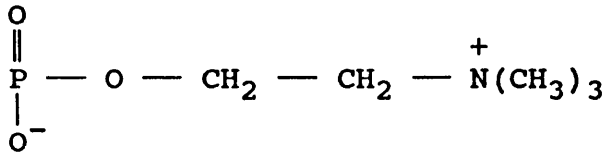 for sphingomyelin

X = glucose for glucocerebroside

X = galactose for galactocerebroside

X = oligosaccharide for ganglioside

b)

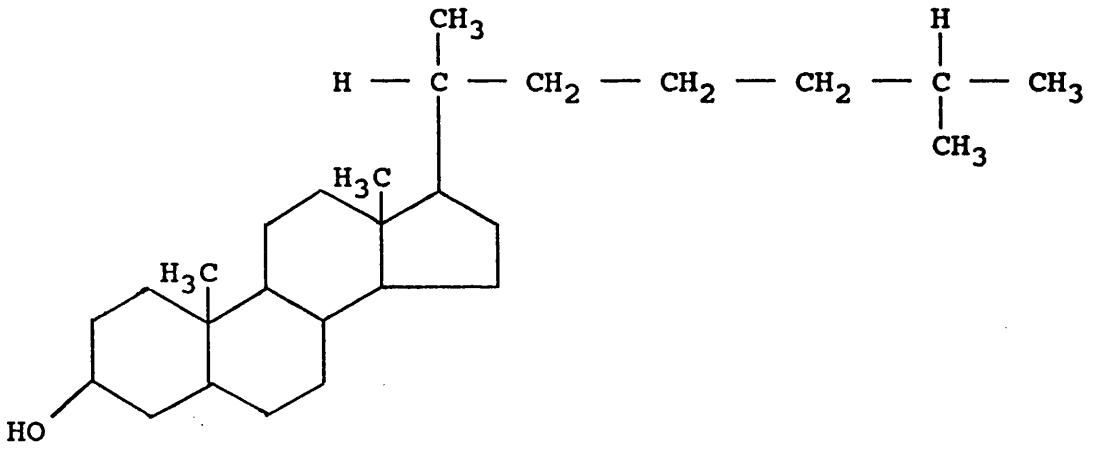

β-hydroxyl group of the cholesterol forms a hydrogen bond with the carbonyl oxygen of the ester group which links the phospholipid acyl chain with the glycerol group (Huang 1977).

1.4. BILAYER FORMATION

The amphipathic nature of phospholipids determines the structures formed by these molecules in aqueous media. Thermodynamically, the bilayer is one of the most stable configurations for lipids in aqueous media. Hydrophobic forces are the main driving forces in the formation of lipid bilayers where the acyl chains are situated in the hydrophobic core of the bilayer and the polar headgroups interact with water molecules via electrostatic interactions. Van der Waals attraction forces induce close packing of the acyl chains in the hydrophobic core of the bilayer. Bilayers are therefore held together by non-covalent interactions and, from energy minimalisation considerations, form self-sealing structures, as illustrated in Fig. 1.3.

All known biological membranes are asymmetric, that is, have a different lipid composition on either face of the bilayer. This is important for the orientation of membrane proteins. For example, the function of the Na^+/K^+-ATPase is to pump Na^+ ions out of the cell and K^+ ions into the cell. Random orientation of the protein within the membrane would result in no net transfer of Na^+ or K^+ ions across a cell membrane. It is thought

Fig. 1.3. The structure of some lipid assemblies in aqueous dispersion:-

a) vesicle,
b) bilayer, and
c) micelle.

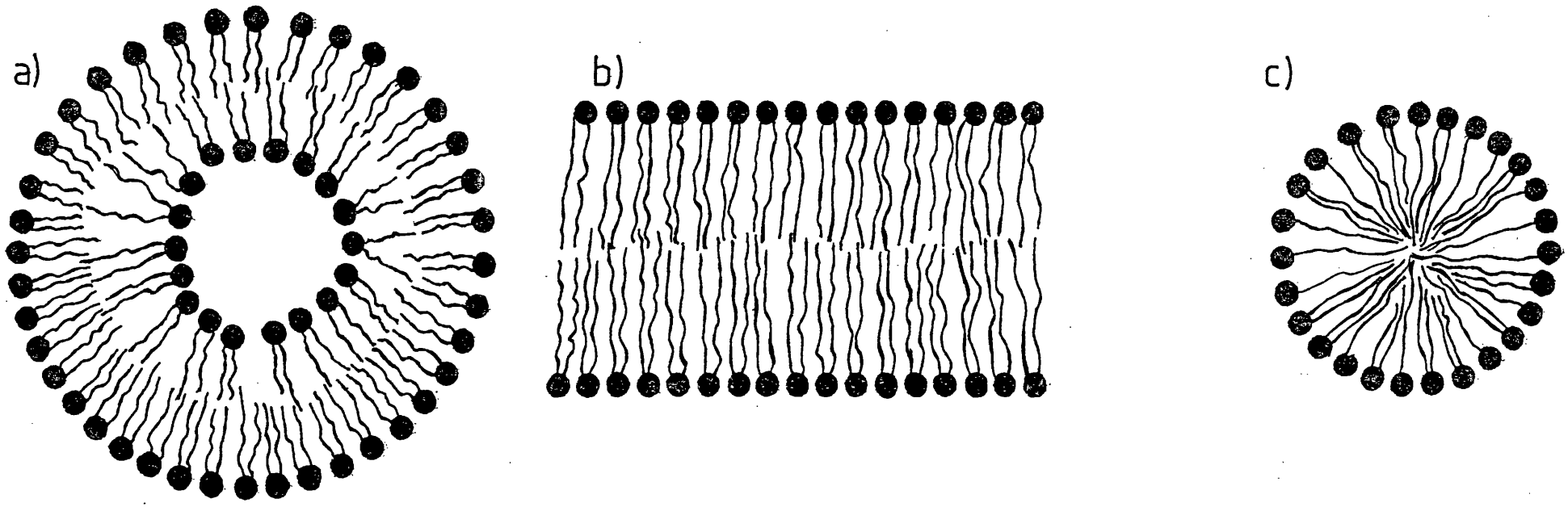
a)
b)
c)

that protein orientation is influenced by the asymmetric distribution of lipids in the membrane.

Furthermore, the asymmetry of the red blood cell membrane is important in the process of blood clot formation. The outer membrane layer contains PC and sphingomyelin (SM) which are haemocompatible and do not induce a thrombogenic response when blood proteins come into contact. However the inner membrane composition of PE and PS induces blood clotting on exposure to blood proteins. Therefore during cell damage, the exposure of the inner membrane induces a thrombogenic response. Membrane asymmetry is maintained by the difficulty of lipids diffusing from one side of the membrane to the other (see Section 1.5).

At low temperatures, the acyl chains interact favourably with each other and the bilayer crystallises to form a regular repeating pattern (L_{β} phase) with the CH_2 groups of the relatively straight acyl chains in a trans configuration. Upon heating, the bilayer loses its crystalline structure and becomes fluid (the L_{α} phase). The CH_2 groups in the L_{α} phase are a mixture of trans and gauche configurations. The gauche isomers form kinks in the acyl chain that are highly mobile along the whole length of chain, with an increasing probability of occurring near the methyl terminus. The temperature at which the transition from crystalline to fluid state occurs is known as the phase transition temperature, T_m, and, for single-lipid membranes, may occur within a 1° -

2°C temperature range due to co-operative melting.

The phase transition temperature is influenced by:-

a) the length of the acyl chain. Due to Van der Waals attraction, each CH_2 group adds approximately 0.5 kcal/mol of enthalpy to the transition,

b) the degree of unsaturation of the acyl chain, with T_m lowering as the number of double bonds increases. Double bonds introduce a kink into the acyl chain, thus preventing the close packing of the chains,

c) the position of the double bonds, with T_m being lowest when the double bond is in the middle of the acyl chain,

d) the character of the acyl chains, with T_m being reduced when the longer, more saturated, chain is nearer the polar headgroup, and

e) the structure and electrostatic nature of the headgroup. This follows that, for a given chain length, the general pattern for T_m of PE > PS > PC $\geqslant$ PG.

Due to its short acyl chain and bulky headgroup, cholesterol is unable to form bilayers or organised assemblies in aqueous solution. However introducing cholesterol into a lipid bilayer system has a major effect on the phase transition. The bulky sterol molecule disrupts the close packing of the acyl chains, allowing greater motion of the chains in the L_β phase and an increased proportion of gauche conformers (Oldfield &

Chapman, 1972). In the L_α phase, the cholesterol core restricts the acyl chains from moving freely, thus reducing the proportion of gauche conformers typical of bilayers in the L_α phase, and thereby giving the fluid bilayer a more rigid order. The resultant effect of cholesterol is to reduce T_m and the enthalpy of the phase transition, as well as reducing in the co-operativity of melting. As the cholesterol-to-lipid ratio increases, the phase transition is gradually abolished. For PC lipids, this occurs when there is a minimum of two cholesterol molecules per seven lipids.

1.5. LIPID MOBILITY

Bilayers are dynamic structures that allow the movement of membrane components. Lipids are able to rotate about their long axis with a spin correlation time in the order of 10 ns. They are capable of lateral diffusion through their monolayer by 'jumping' into vacancies in the liquid crystal. These 'jumps' occur with a frequency of 10^7 - 10^8 s^{-1} in the L_α phase, giving a lateral diffusion coefficient of 10^{-11} - 10^{-15} m^2s^{-1}. Lateral diffusion of lipids is several orders of magnitude lower than this in the L_β phase. Transbilayer movement also occurs, but this is a much slower phenomena apparently because it requires the lipid polar headgroup to pass through the hydrophobic core of the bilayer. This occurs on a time scale of approximately once every two weeks.

It is thought that the particular distribution of fatty acyl chains present in a membrane provides the appropriate membrane fluidity at a particular environment temperature to match diffusion rates or rates of metabolic processes required for a tissue. Bacteria regulate fluidity by changing the lipid composition of the membrane whereas with animal membranes, it is easier to alter fluidity by changing the proportion of cholesterol present.

1.6. PROTEINS

The role of proteins in biological function is widespread and diverse. The largest class of proteins are the enzymes, of which about two thousand different types are known. Other types of proteins include storage and transport proteins, toxins, hormones, structural and contractile proteins, and protective proteins in blood.

Proteins can be separated into two general categories:-

i) soluble (or globular) proteins, (e.g. haemoglobin, myoglobin, concanavalin A), and

ii) membrane proteins, illustrated in Fig. 1.4, of which there are 4 subgroups

a) peripheral - these are bound mainly by ionic forces to the lipid polar headgroup or to other proteins in the membrane and can be removed by raising the ionic strength of the buffer,

Fig. 1.4. Examples of membrane proteins.

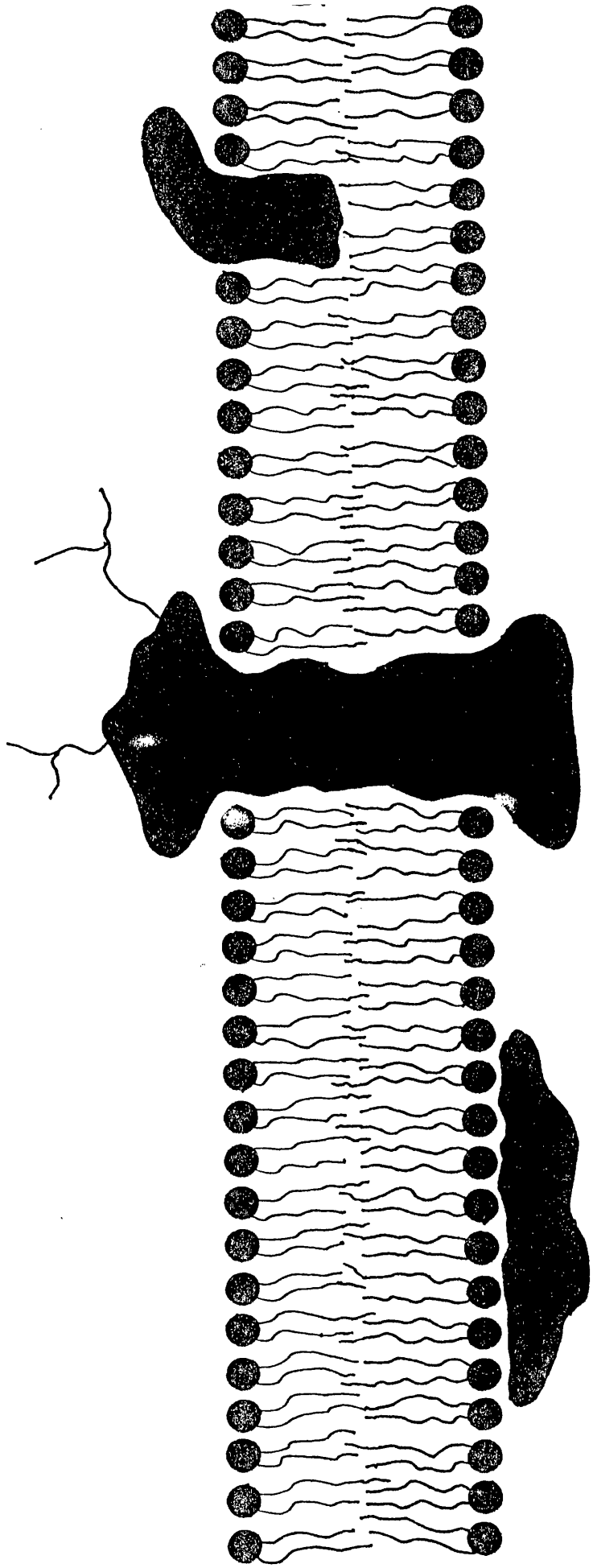

b) integral membrane proteins that may span the lipid bilayer once (e.g. glycophorin) or more than once (e.g. many of the transmembrane ion channels, such as Ca^{2+} ATPase, Na^{+}/K^{+}-ATPase and bacteriorhodopsin). These proteins can only be removed from the membrane by use of detergents, 8M urea or 6 M guanidinium chloride solutions, or organic solvents, such as hexane.

c) proteins anchored by a hydrophobic region into the lipid bilayer (e.g. melittin),

d) peripheral proteins anchored to the lipid bilayer by a covalently attached glycolipid (e.g. alkaline phosphate, acetylcholinesterase).

There is also an important group of soluble proteins which, under the correct conditions, insert into the membrane. Examples of these are toxins such as the colicins which kill cells by forming a large pore in the membrane, thus destroying the electrical gradient of the cell.

1.7. PROTEIN COMPOSITION

Proteins are polymers of amino acids formed by the formation of an amide bond between the α-amino and α-carboxyl groups of the amino acids to form a peptide linkage. The linking of the amino acids forms a polypeptide backbone of carbon, nitrogen and oxygen, with amino acid sidechains spaced at regular intervals along

the chain. Proteins are generally made up of a combination of the twenty common amino acids. It is the sequence of these amino acids along the polypeptide chain that determines the conformation and function of the protein.

1.7.1. Polypetide Backbone

The polypeptide backbone takes the form shown in Fig. 1.5 where R_i is the ith amino acid residue from the amino terminus.

The average length of the C'— N bond found from X-ray crystallography is 1.33 Å, which is between that observed for a normal C — N bond (1.45 Å) and a normal C = N bond (1.25 Å), indicating that in this environment the C'— N group is partially double bonded. This restricts rotational freedom, causing the peptide unit to be rigid and planar, with the hydrogen of the amino group almost always trans to the oxygen of the carbonyl group. Both the N_i — C_i^{α} and C_i^{α} — C_i bond are pure single bonds and allow rotational freedom either side of the peptide unit.

1.7.2. Amino Acids

Nineteen of the twenty common amino acids have the same general chemical structure as shown in Fig. 1.6a.

It is the composition of the side chain that gives the amino acid its properties. The various residues can

Fig. 1.5. The chemical structure of the polypeptide backbone.

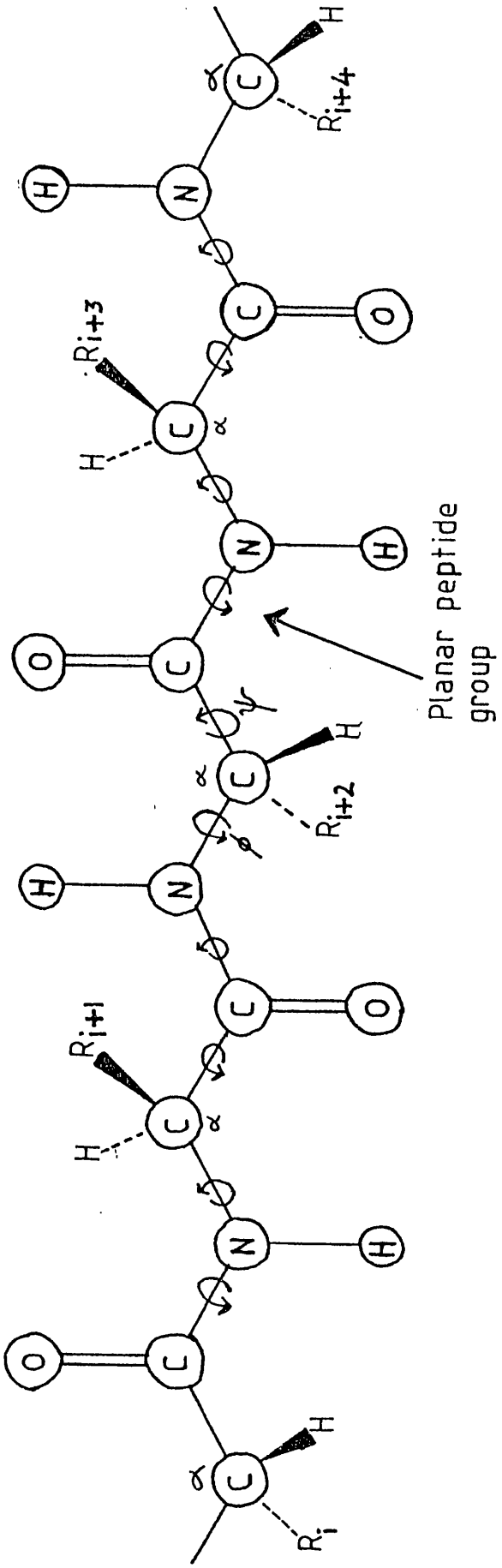
Planar peptide group

Fig. 1.6a) The basic chemical structure of amino acids.

b) The chemical structure of proline.

c) The chemical structure of α-aminoisobutyric acid.

a)

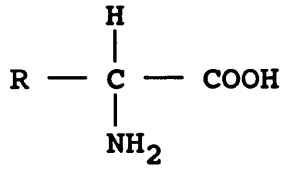

b)

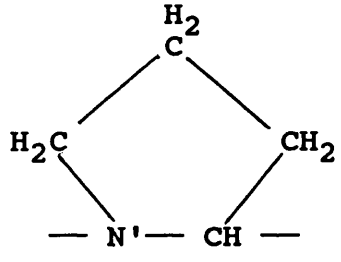

c)

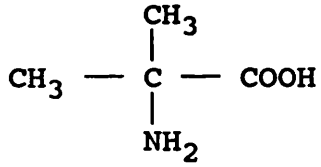

be categorised into nonpolar or hydrophobic, neutral (uncharged) polar, positively charged and negatively charged R groups in the pH range 6.0 - 7.0. These groupings are quite general and it must be borne in mind that each individual residue has differing characteristics.

The important exception to this general amino acid structure is proline, which is an imino, rather than an amino, acid and is illustrated in Fig. 1.6b. This residue is unable to hydrogen bond as the N is strongly bonded to a C atom and therefore does not possess an NH group.

Another important but rare amino acid is α-aminoisobutyric acid (see Fig. 1.6c). This amino acid occurs extensively in the alamethicin family of antibiotics and is thought to promote the formation of the 3_{10}-helical secondary structure (see Section 1.8.2.3).

The cysteine residue is the only amino acid normally capable of forming covalent bonds with other amino acids in the protein. Two cysteine residues can be oxidised to form a disulphide bridge, a bond that can only be cleaved in a reduction reaction, and not by adjusting the pH or by the use of high salt concentrations or denaturing agents. Therefore these bonds are important in protein stabilisation.

1.8. PROTEIN STRUCTURE

Protein structure can be subdivided into four separate categories; primary, secondary, tertiary and quaternary structure. The relationship and influence of each structure needs to be discussed in detail.

1.8.1. Primary Structure

The primary structure is defined as the sequence of the amino acids along the polypeptide chain. This is the most fundamental characterisation of a protein and many properties of the protein are derived from its primary structure.

Sanger first developed the techniques for sequencing with his studies on insulin (Sanger & Thompson, 1963; Sanger & Tuppy, 1961) by sequentially hydrolysing the peptide bonds in the backbone by heating with either an acid or base. Another technique has also been developed where the sequence is identified from information contained in the mRNA.

1.8.2. Secondary Structure

The secondary structure or conformation of a protein is the spatial arrangement of the amino acid residues within the molecule. A protein that is completely unfolded, i.e. there are no intramolecular hydrogen bonds, generally possesses no activity, with an exception being melittin which is unordered in solution yet still binds to membranes. It is the folding of the protein,

mainly driven by hydrophobic interactions and, to a lesser extent, by amino acid - amino acid interactions, that allows intramolecular hydrogen-bonding to occur and induces activity in the protein. Despite the huge number of conformations possible for any given protein, each protein folds into one (or, rarely, a few) conformation(s) under normal biological conditions.

1.8.2.1. α-Helix

The α-helix was the first secondary structure to be postulated (Pauling et al., 1951; Pauling & Corey, 1951a) that could be related to conformations in synthetic polypeptides (Pauling & Corey, 1951b), fibrous proteins (Perutz 1951) and globular proteins (Kendrew et al., 1960) and is the most commonly observed of the polypeptide conformations (Fig. 1.7a). It is also the predominant structure of protein domains within the lipid bilayer. Hydrogen bonds are formed between the backbone carbonyl oxygen of residue i and the backbone NH of the $i + 4$ residue along the chain. The hydrogen bonds all point in the same direction and are nearly parallel to the helix axis. Amino acid side chains project out from the helix and, except in the bulkiest cases, do not interfere with the structure. However, proline and glycine are rarely found in helical structures. The characteristics of different helical structures are given in Table 1.I.

Table 1-I. The hydrogen-bonding scheme of helical secondary structures, where N is the number of residues per rise and H is the rise per residue. (From Krimm & Bandekar, 1986).

HELIX	N	H	H-BONDING
α	3.60	1.495	5 → 1
α_{II}	3.60	1.5	5 → 1
3_{10}	2.99	2.01	4 → 1

Fig. 1.7. A schematic diagram of common secondary structures (H-bonds represented by the dotted lines):-

a) α-helix,
b) antiparallel β-sheet, and
c) type I β-turn.

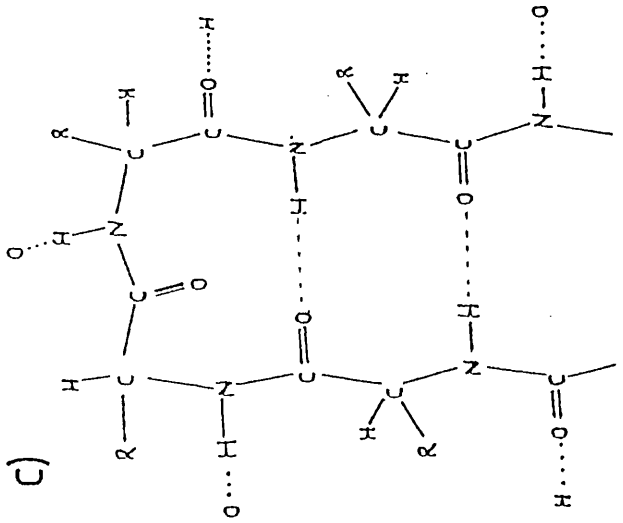

c)

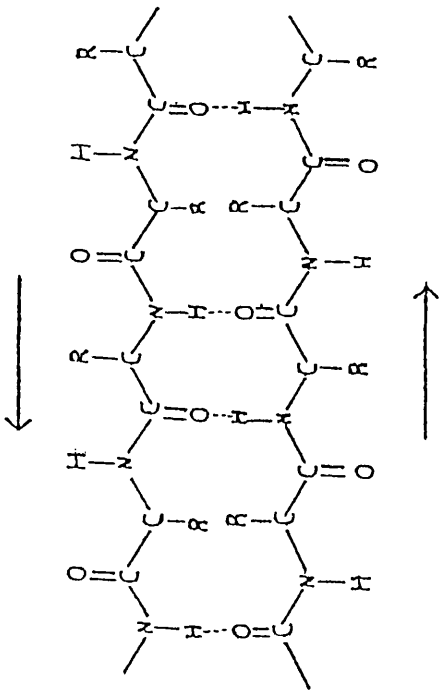

b)

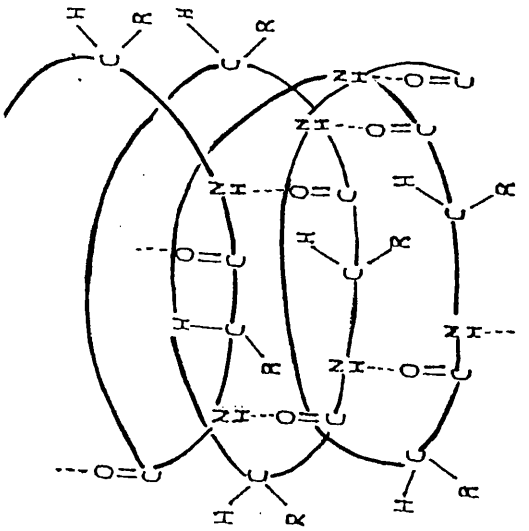

a)

1.8.2.2. α_{II}-helix

The α_{II}-helix is very similar to the α-helix, with hydrogen bonds formed between the carbonyl oxygen of i unit and hydrogen of the N — H of the $i + 4$ unit. However the plane of the peptide groups are not parallel to the helix axis as with the α-helix but tilted, with the N — H bonds pointing inwards towards the axis. This results in the slight lengthening, and weakening, of the C ═ O·····H — N hydrogen bonds, with the N····O distance being 3.00 Å for α_{II}-helix, compared to 2.86 Å for α-helix (Krimm & Dwivedi, 1982). This structure is not common in polypeptides and proteins, but has been observed in lysozyme (Némethy et al., 1967) and proposed to exist in bacteriorhodopsin (Krimm & Dwivedi 1982).

1.8.2.3. 3_{10}-Helix

This structure differs from the α-helix in that hydrogen-bonding occurs between the carbonyl oxygen of the i unit and hydrogen of the N — H group of the $i + 3$ unit (see Fig. 3.1 and 3.3). This structure is not common and, when observed, is usually at the end of regular α-helices. The amino acid α-aminoisobutyric acid (Aib) tends to promote the formation of the 3_{10}-helix, and this structure has been observed in homopolypeptides of this amino acid, in alamethicin, a protein containing 9 Aib residues out of 20, and has been proposed to occur in

other members of the alamethicin family.

1.8.2.4. β-Sheet

Intramolecular hydrogen bonds are formed between the carbonyl oxygen and NH groups of two or more extended polypeptide chains running parallel or anti-parallel, leading to the formation of parallel or anti-parallel β-sheet, respectively (Fig. 1.7b). Detailed coordinates for a steriochemically acceptable β-sheet structure were first provided in 1951 (Pauling & Corey, 1951a,b) and has since been observed in synthetic polypeptides and proteins. Amino acid residues protrude on alternate sides of the sheet structure, and β-sheets tend to be twisted rather than planar. The β-sheet structure is common in soluble proteins, but is rarely found in membrane proteins, with the important exception of porin. Intermolecular β-sheet has been observed to form between protein molecules, especially under denaturing conditions (Jackson 1990).

1.8.2.5. β-Turns

Reversal in the direction of the polypeptide chain is achieved by a β-turns, in which the carbonyl oxygen of $\underline{i}$ unit is H-bonded to the NH of the $\underline{i}$ + 3 residue (Fig. 1.7c). From steric hindrance considerations, three types of β-turns are possible. Type I and II are non-helical, whereas type III corresponds to one turn of a 3_{10}-helix. Soluble proteins tend to contain a significant proportion

of β-turns and these tend to be exposed to solvent on the surface of the protein. X-ray crystallography has indicated that carbohydrate groups tend to be observed attached to β-turns.

1.8.2.6. γ-turns

This structure is similar to the β-turn and is formed by three amino acid residues. Three energetically possible conformations have been proposed. The γ-turn and mirror-related γ-turn have H-bonds between the CO group of unit i and the NH group of the i + 2 unit (3 → 1 H-bond), and between the CO group of the i + 2 group and the NH of the i group (1 → 3 H-bond). The inverse γ-turn has a 3 → 1 H-bond and an H-bond between the CO of unit i - 1 and the NH of unit i + 3 (5 → 1 H-bond). γ-turns have been observed in peptides (Karle, 1981).

1.8.2.7. Random Structure

This term refers to areas within polypeptides and proteins that have no repetitive hydrogen-bonding pattern to promote a regular structure. Hydrogen bonding may still occur but no specific conformation is achieved. The proportion of random structures observed in proteins varies from casein, having nearly 100 % random structure, to membrane proteins, where it has yet to be observed within the bilayer.

1.8.3. Tertiary Structure

Tertiary structure is defined as the overall three dimensional architecture of the polypeptide chain, including the relationship of various secondary structures to one another. It is determined by the character of the amino acid side chains. For example, hydrophobic side chains will disrupt water far less when buried in the generally hydrophobic core of the protein. Hydrophilic sidechains will tend to remain exposed to water as large energies are required to drive them into a hydrophobic environment. Tertiary structure is also influenced by non-covalent interactions between different secondary structures, such as Van der Waals forces and polypeptide backbone interactions, and by the presence of disulphide bridges.

1.8.4. Quaternary Structure

This is defined as the relationship of subgroups in a protein required to give activity. For example haemoglobin is composed of four subunits, two α and two β chains, each of which is bound to a heme group. These chains have been shown to fit together in an approximate tetrahedral arrangement.

1.9 PROTEIN MOBILITY

Soluble proteins rotate rapidly in aqueous media and diffuse freely. However membrane proteins are restricted by the presence of the bilayer. Membrane proteins are able to rotate about an axis normal to the membrane. Lateral diffusion is limited by protein size and the phase of the bilayer. Diffusion of proteins is typically 2 - 3 orders of magnitude lower than for lipids, and is further reduced by a factor of 2 - 3 orders of magnitude below the phase transition of the bilayer.

T_m has a major effect on the proteins contained in the bilayer. Membrane proteins are approximately evenly distributed in membranes above T_m and generally function as monomeric proteins. At temperatures below T_m, proteins tend to be pushed into aggregates between areas of lipid in the crystalline phase, usually leading to a reduction in protein mobility and activity.

A number of soluble proteins that interact with the bilayer are unable to do so below T_m because the packing of the lipid headgroups is too close and the energy required to interrupt the close-packing of the acyl chains is too large. Interactions tend to occur at T_m when chain packing defects and vacancies formed in the bilayer are at a maximum, or above.

This introductory chapter sets out to discuss the composition and nature of biomembranes, and examines the

roles of the membrane components in relation to the various functions of biomembranes. Furthermore it describes the dynamic nature of biomembranes. The information gained from studies on biomembrane systems led to the "fluid mosaic" model proposed by Singer and Nicholson (1972). This widely-accepted model pictures membrane proteins floating in the lipid matrix "sea". However it has certain limitations. For example, it does not consider semi-crystalline arrays of lipids that exist in bacterial cell membranes nor does it consider possible influences on protein mobility in the membrane, such as protein-protein interactions, the formation of protein aggregates and the interaction of proteins with the intracellular protein skeleton.

The composition and structure of proteins has been described with respect to membrane and soluble proteins. The relationship between the structure and function of proteins has been considered, and the techniques commonly employed in determining protein structure will be discussed in the following chapter.

CHAPTER TWO

BIOPHYSICAL TECHNIQUES

2.1. INTRODUCTION

This chapter describes the techniques available in determining protein structure. Techniques based on similar theoretical principles are grouped together and in each case the advantages and disadvantages of each approach, and examples of the studies carried out, are discussed.

The techniques discussed are based on the interaction of electromagnetic (e.m.) radiation interacting with matter. The types of interaction are dependent on the energy, and hence wavelength, of the radiation and a brief summary of these is given in Table 2.I.

Table 2-I. The electromagnetic spectrum and interactions with matter.

Type of Radiation	Wavelength (m)	Photon energy (eV)	Interaction with matter
Gamma	10^{-10}	1.2×10^{3}	Nuclear
X-rays	10^{-8}	12.4	Inner shell electrons
Vacuum UV	2×10^{-7}	6.3	Ionisation
Near UV	4×10^{-7}	3.1	Valence electrons
Visible	7×10^{-7}	1.8	
Near IR	2.5×10^{-6}	0.5	Molecular vibrations
Mid IR	2.5×10^{-5}	5×10^{-2}	
Far IR	10^{-4}	1.2×10^{-3}	
Microwaves	4×10^{-4}	3×10^{-3}	Electron spin orientation
Radiowaves	3×10^{4}	4×10^{-11}	Nuclear spin orientation

2.2. X-Ray Crystallography and Electron Diffraction

The concept of these techniques is based on the principles that:-

a) crystals are composed of unit cells that are arranged in a regular, repeating lattice,

b) atoms can scatter a fraction of the incident radiation without altering the wavelength or relative phase of the incident radiation, and that

c) the amplitude of the scattered radiation depends on the composition of the atoms.

The regularity of the crystal lattice, which may be considered to be a three-dimensional diffraction grating for X-rays, and for electrons of sufficiently high energy, causes radiation scattered from atoms in the lattice to interfere to form a diffraction pattern. The diffraction pattern is dependent on the physical dimensions of the crystal lattice and the type and position of atoms contained within the subunits.

A simple theory derived by Bragg (1913) considers X-rays reflected from lattice planes within the crystal (Fig. 2.1) giving information about the crystal structure:-

$$2d\sin\theta = n\lambda \qquad \text{Equ. 2.1.}$$

where θ = angle of incident radiation,

d = spacing of lattice planes,

n = number of order reflection, and

λ = wavelength of incident radiation.

Fig. 2.1. The reflection and interference of electromagnetic radiation from a crystal lattice structure.

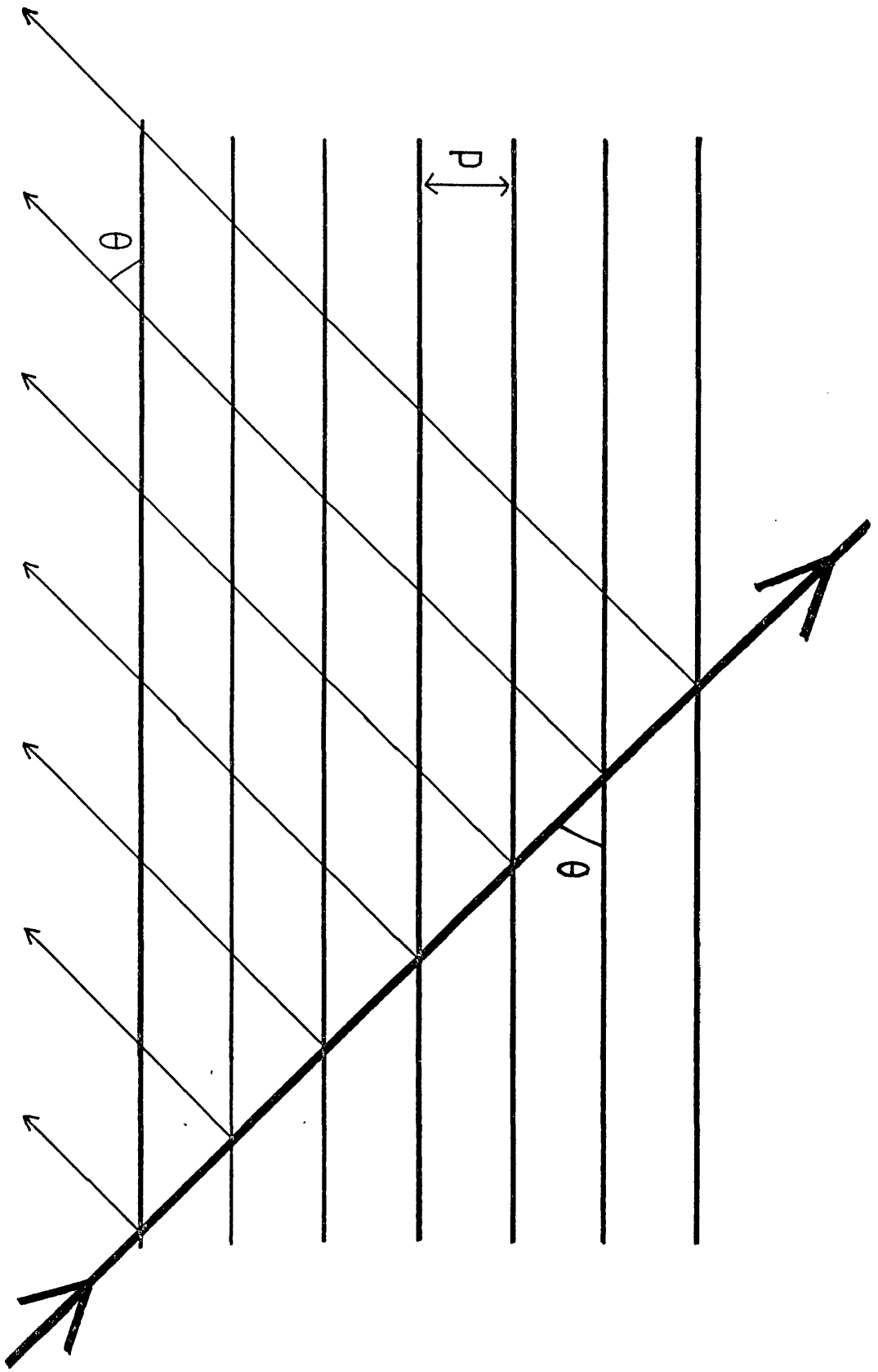
d
θ
θ

This result will give details of the characteristics of the unit cell.

In theory, the electron density in a crystal at point (x,y,z) can be determined using Equ. 2.2.

$$\rho(xyz) = \frac{1}{V}\Sigma\Sigma\Sigma|F(hkl)|\cos[2\pi(hx+ky+lz)-\alpha(hkl)] \qquad \text{Equ. 2.2}$$

where $\rho(xyz)$ = electron density at position (x,y,z),

V = unit cell volume,

(hkl) = crystal lattice indices,

$F(hkl)$ = amplitude of the structure factor, and

$\alpha(hkl)$ = phase of structural lattice factor.

Therefore, to make direct structural determination both the amplitude and phase of the diffracted radiation needs to be determined.

2.2.1. X-ray crystallography

F(hkl) can be determined from the X-diffraction results as it is related to the measured intensity. However, it is not possible to measure the phase, $\alpha(hkl)$, directly. The common way around this problem for proteins is to use the isomorphous replacement method. This technique depends on the preparation of protein crystals that contain a heavy atom, typically uranium, mercury, or platinum. The scattering of X-radiation from an atom possessing a high atomic number will dominate the amplitude and phase of the diffraction spectra. Once the position of the heavy atom has been determined using a

Patterson synthesis, its contribution to the phases of various spectra can be calculated. The technique of isomorphous replacement in determining protein secondary structure was first used by Kendrew et al. (1958) in determining the structure of myoglobin.

X-ray crystallography has been used to determine the secondary structure of a large number of soluble proteins to a resolution of less than 2Å in some cases (Creighton 1984). So far the photosynthetic reaction centre of Rhodopseudomonas viridis (Diesenhofer et al., 1985) and porin (Weiss et al., 1990) are the only membrane proteins that have been successfully studied by this technique. The structure and packing of lipid bilayers in two-dimensional lipid-water liquid crystals has been studied (for reviews see Luzzati 1968; Shipley 1972). X-ray diffraction has also been used to study lipids that have been crystallised (Hitchcock et al., 1974; Elder et al., 1977; Pearson & Pascher, 1979).

Problems associated with X-ray crystallography include the production of large (> 200 μm diameter) stable crystals and the assumption that the structure of the sample under crystallisation conditions is the same as that in the native environment. The most common technique for crystallising soluble proteins is precipitation from high concentration NH_3SO_4 solutions. Differences in structure between the crystallised protein and the protein in its native environment have been

reported (Haris et al., 1990; Fisher et al., 1989). Severe problems have been encountered in trying to crystallise integral membrane proteins because components of the proteins are in contact with both polar and non-polar phases of the membrane. To maintain the native conformation of the protein it is necessary to reproduce the bipolar environment in the crystal. For this reason membrane protein studies with this technique lag behind that of soluble proteins. Detergents used in attempts to crystallise membrane proteins may affect the protein structure.

2.2.2. Electron Diffraction

Electron diffraction is a technique that has been used to study two-dimensional arrays of membrane proteins. The arrays have to be highly ordered to produce high resolution, and successful studies have been carried out on membrane proteins in natural arrays (e.g. bacteriorhodopsin) and on proteins reconstituted from isolated membrane components (e.g. porin).

The experimental details of this technique differs from that of X-ray crystallography due to the difference in scattering power of chemical groups for X-rays and electrons. Electrons are charged particles and scatter from both atomic nuclei and atomic electrons. In practice, samples must be no more than a few hundred angstroms thick and have to be studied in a vacuum. Reducing radiation damage to the sample is achieved by

lowering the temperature to -180°C, and negative staining is often required to maintain the structure of the membrane during the experiment.

Electron microscopy is becoming a powerful technique for studying membrane proteins. The main success has been the application of the method to gain structural information on bacteriorhodopsin (Henderson et al., 1990) and porin (Jap et al., 1991). Other membranes appear perturbed by the severe experimental conditions. Disorder in the lattice can limit the resolution, and the intrinsic properties of the stains used limits the resolution to 15 - 20 Å at best. The resolution achieved by electron microscopy is generally poorer than that achieved by X-ray crystallography and is not yet at the atomic scale.

2.3. NUCLEAR MAGNETIC RESONANCE SPECTROSCOPY

NMR has been used for many years by organic chemists, but the recent developments in producing high field strength magnets, the advancement of computer-aided procedures and the advances in the isolation and preparation of biological macromolecules has enabled the technique to be applied to a wide range of biological systems.

The spinning of atomic nuclei possessing a spin quantum number, I, > 0 produces a magnetic moment. Placing the atoms in an external magnetic field causes

the magnetic moment of the atomic nuclei to align either with or against the external field. The magnetic moment interacting with the external magnetic field causes the atomic nuclei to precess around the line of force of the applied magnetic field in a similar manner to a spinning gyroscope acting in a gravitational field. The angle of precession with respect to the line of force of the applied external magnetic field is limited to a distinct number of allowed values dependent on I, each corresponding to a discrete energy level given by the equation

$$E = \frac{m\mu}{I}.\beta H_o \qquad \text{Equ. 2.3.}$$

where I = spin quantum number

m = magnetic quantum number

μ = magnetic moment of the nucleus

β = nuclear magneton = 5.049×10^{24} $ergG^{-1}$

H_o = external magnetic field strength

E = energy of transition.

The population of the energy levels at equilibrium is predicted by the Boltzmann distribution

$$n_u = n_l \exp(-\mu H_o/IkT) \qquad \text{Equ. 2.4.}$$

where n_u = number in upper level,

n_l = number in lower level,

k = Boltzmann's constant, and

T = absolute temperature.

The frequency of radiation needed to excite nuclei from one energy level to another is found by equating

Equ. 2.3 with the Planck quantum of energy

$$\triangle E = h\nu_o = m\mu\beta H_o/I \qquad \text{Equ. 2.5}$$

where h = Plank's constant

Therefore by applying radiation of the correct frequency, atomic nuclei will be excited from one energy level to another. After an excitation pulse, the nuclei will return to their equilibrium positions through spin-lattice and spin-spin relaxation.

Nearly all structural information on proteins is obtained from the nuclear Overhausen effect (NOE) and from spin-spin coupling (J). The NOE technique utilises the fact that protons have a shielding effect on other protons within a 5Å range, and, in the absence of intramolecular motion, the NOE is proportional to r^{-6}, where r is the internuclear separation. NOE therefore gives accurate details on the relative proton positions and hence the secondary structure. Spin-spin coupling of nuclei interacting with one another occurs due to the highly magnetic electrons in the intervening bonds. This leads to splitting of the resonant bands and information on the coupling constants.

NMR has provided a wealth of information on the nature of lipids and proteins. Many early important studies on bilayer order were carried out using ^2H NMR on selectively deuterated lipids. This gave valuable information on the configuration of the acyl chains in the different bilayer phases. Information has also been gained on the state of the headgroup region. Numerous

studies on soluble proteins have been carried out to gain information on polypeptide and protein conformation at atomic resolution.

Despite many improvements in this technique, its application to determining protein secondary structure is very time consuming, and is limited to proteins of molecular weight below approximately 15000 daltons due to the complexity of information obtained. However ^{13}C- or ^{15}N- labelled ligands have been used to gain information on the protein binding site without having to go through the time-consuming procedure of gaining information on the whole protein (Fesik et al., 1988).

Structural information on membrane-bound peptides and proteins is as yet limited due to the lipids restricting the rotational freedom of protein, hence causing line broadening. Some work on hydrophobic peptides has been done in solvents in the absence of lipids in an attempt to mimic the low polarity of the membrane environment, but recently FTIR studies have thrown some doubt on the validity of these systems (Kennedy et al., 1991; Jackson & Mantsch, 1991a).

2.4. CIRCULAR DICHROISM

This technique is based on the observation that left- and right-circularly polarised light is absorbed unevenly by asymmetric molecules. Even though most amino acids contain an asymmetric carbon atom, they tend not to exhibit strong anomalous absorption. Circular dichroism

spectra are obtained from polypeptides and proteins because of the asymmetric and periodic arrangement of the polypeptide units in these structures.

Plane polarised light can be considered to consist of two components, a beam of right- and a beam of left-circularly polarised light, with electric vectors E_r and E_l, respectively. Interaction with an optically active medium may slow down one of the components causing a change in angle of the plane polarised light. As the molar absorbtivities of each circularly polarised component is different, the circularly polarised light becomes elliptically polarised.

The differential absorption is measured by:-

$$\triangle\varepsilon \propto (\varepsilon_l - \varepsilon_r)$$

where $\triangle\varepsilon$ is the measure of circular dichroism, and ε_l and ε_r are the extinction coefficients for left and right circularly polarised light.

CD gives information on the conformation of the optically active polypeptide backbone. It is a widely used technique and has provided much valuable information on the structure of soluble proteins. It is a quick technique, uses proteins in low concentration in aqueous buffers, is not limited by protein size and provides qualitative and quantitative information on protein secondary structure (Drake, 1986; Chen et al., 1974).

However it is unable to provide high resolution

information on the samples under investigation, and the distinction between β-sheet and β-turn structure is not clear. Problems with light scattering has severely limited the application of CD to membrane suspensions.

2.5. VIBRATIONAL SPECTROSCOPY

Vibrational spectroscopy gives information on the vibrational energy of chemical groups within molecules. Photons whose energy is equal to the difference in energy, $\triangle E$, between two vibrational energy states of a chemical bond can be absorbed, thus exciting the bond from one vibrational energy level to another. From the relationship $\triangle E = h\nu$, only photons of specific energy, and therefore specific frequency, will be absorbed. This will produce discrete, rather than continuous, spectra.

2.5.1. Molecular Vibrations

The number of different vibrations possible for any molecule is 3n-6, where n is the number of atoms present. The type of vibrations that occur in a three atom molecule is illustrated in Fig. 2.2.

For an atom executing periodic harmonic motion, the relationship between the induced dipole moment, $\underline{M}$, and the amplitude of the electric field, $\underline{E}$, of the incident radiation can be given by the equation:-

$$\underline{M} = \alpha\underline{E} \qquad \text{Equ. 2.7}$$

where α is the polarisability of the sample.

Expressing $\underline{E}$ and α as functions of time

$$\underline{E} = \underline{E}_m \cos 2\pi\nu t, \qquad \text{Equ. 2.8}$$

where $\underline{E}_m$ = amplitude of the vibrating electric vector of the incident beam, and v is the frequency, and

$$\alpha = \alpha_o + \alpha_1 \cos 2\pi\nu_o t \qquad \text{Equ. 2.9}$$

Fig. 2.2. Vibrations of a three atom-molecule.

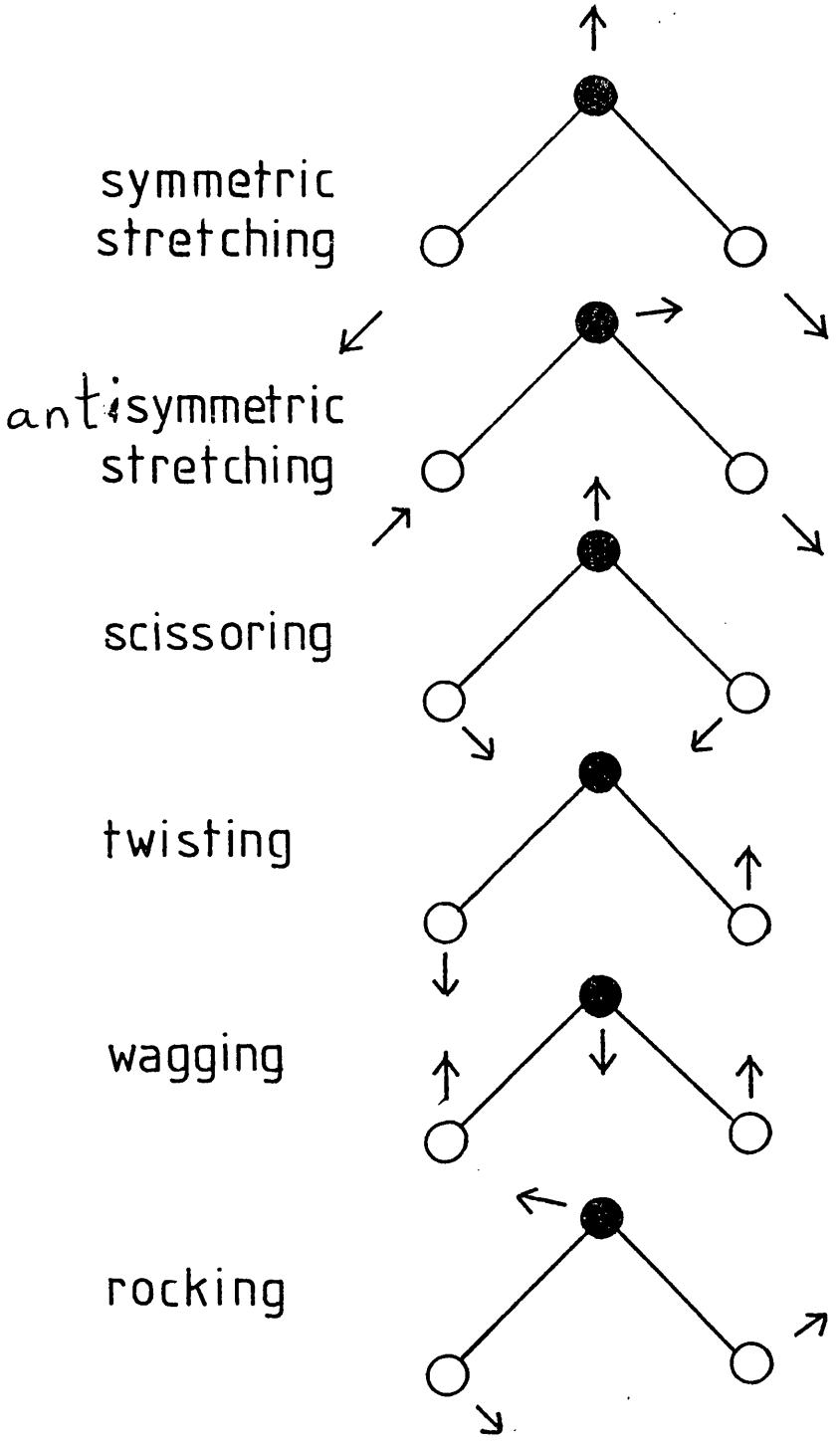
symmetric
stretching
antisymmetric
stretching
scissoring
twisting
wagging
rocking

where α_o is the polarisability of the equilibrium configuration of the atoms, and v_o is the frequency of the molecular vibrations of the atoms in the sample (assuming they all have the same phase).

The theory has been applied in both Raman and infrared spectroscopy.

2.5.2. Raman Spectroscopy

Changes in the polarisability of a molecule can give rise to three different types of scattering (Fig. 2.3.). The molecule may by excited from one energy level to another and then return to the ground state via the emission of a photon equal in energy to that of the incident radiation, hv. This is known as Rayleigh scattering (Fig. 2.3a). A molecule in an excited state may absorb a photon and be excited to a virtual excited state, and then decay to the ground state. The energy of the emitted radiation $\triangle E = h(v+v_o)$ and is known as the anti-Stokes line (Fig. 2.3b). Also the molecule may be excited from the ground state to a virtual excited state and then decay to an excited state with the energy of the photon emitted equal to the difference in energy between the virtual excited state and the excited state, $\triangle E = h(v-v_o)$. This emitted radiation is known as the Stokes line (Fig. 2.3c).

Samples are illuminated with an intense monochromatic radiation and the emitted radiation is detected at 90° to

Fig. 2.3. Schematic energy diagram of the excitation and relaxation of vibrational energy levels via photon absorption and emission.

a) Rayleigh scattering,
b) Production of the anti-Stokes line,
c) Production of the Stokes line.

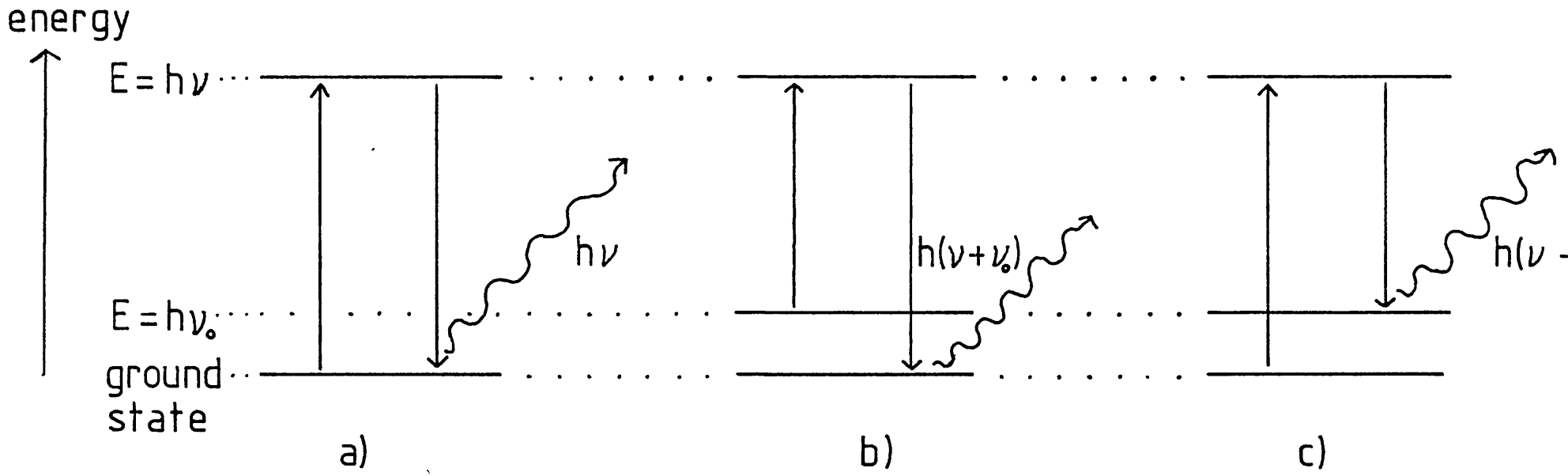
energy
E = hν
E = hν₀
ground state
hν
h(ν+ν₀)
h(ν -
a)
b)
c)

the direction of the incident radiation. The use of lasers has significantly enhanced the signal-to-noise ratio (s/n) achieved with this technique. A large amount of literature has been published on Raman spectroscopic studies of lipids, and soluble and membrane proteins (Williams 1983; Vogel & Gärtner, 1987). Samples can be examined in aqueous solution but the s/n is generally poor. Doubts have been raised over the use of quantitative analysis of protein secondary structure by this technique (Gibson & Cassim 1989).

Raman spectra of biological samples are usually affected by a strong luminescence signal, typically a broad featureless background over about a 3000cm^{-1} range. The origin of this signal is probably fluorescence or phosphorescence and has the effect of degrading the s/n ratio of the collected spectra. The development of Fourier transform near-Infrared Raman spectroscopy has reduced the luminescence background of many chemical samples, but has yet to produce spectra of significantly higher quality for biological samples when compared to spectra from conventional Raman instruments. Furthermore the intense excitation radiation required to produce an adequate signal can raise the sample temperature and may lead to protein denaturation.

2.5.3. Infrared Spectroscopy

Infrared spectroscopy differs from Raman spectroscopy in that chemical bonds are infrared "active" only if there is a periodic change in the dipole moment of the bond. If a linear molecule, e.g. CO_2, is considered, the molecule possesses a dipole due to the uneven distribution of electrons within the molecule caused by the relative electronegativity of the constituent atoms. The symmetric stretching vibration does not alter the overall distribution of electrons within the molecule. Therefore the centre of the dipole moment remains unchanged and hence is not infrared active. A periodic antisymmetric stretching vibration does move the centre of the dipole moment and hence is infrared active.

Infrared spectroscopy has been used in chemical analysis for many years but it is only recently that its application to biological studies of lipids, proteins, lipid-protein interactions and nucleic acids has been investigated. Samples can be examined in aqueous solution and information on proteins and lipids in the same sample can be gained at the same time.

The major disadvantage of IR spectroscopy used to be the very strong absorption of the H — O — H bending vibration of water in the region of the amide I and II bands (1700 cm^{-1} - 1500 cm^{-1}) of the protein which completely masked the protein signals (Fig. 2.4b). One way to overcome this problem was to view samples in D_2O solutions as the D — O — D bending vibration absorption

Fig. 2.4a) The IR transmission spectrum between 4000 cm^{-1} and 400 cm^{-1} of water vapour at room temperature.

b) The IR transmission spectrum between 4000 cm^{-1} and 400 cm^{-1} of H_2O at 20°C using a 6 μm pathlength.

c) The IR transmission spectrum between 4000 cm^{-1} and 400 cm^{-1} of D_2O at 20° C using a 50 μm pathlength.

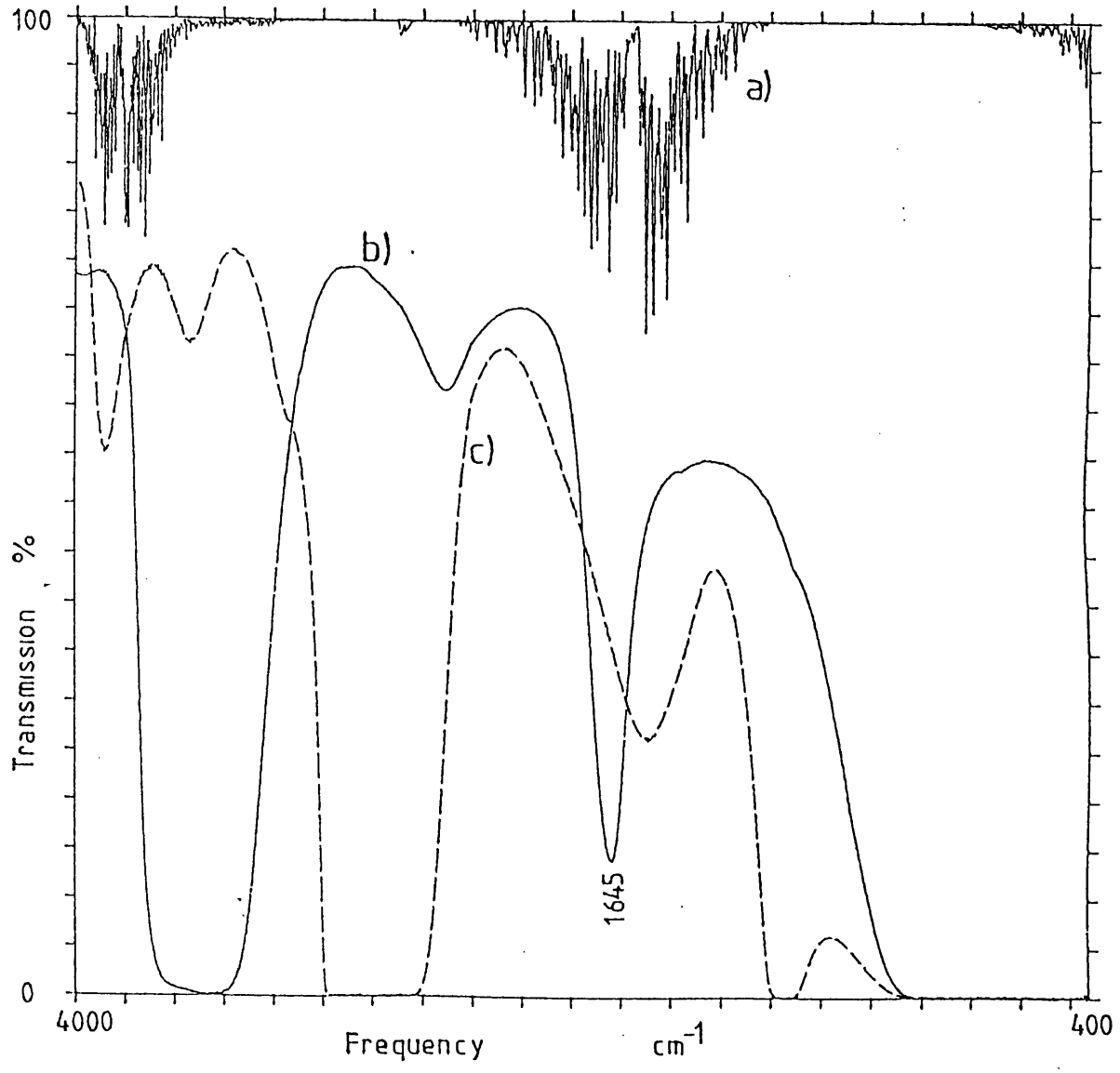
100
0
Transmission %
a)
b)
c)
1645
4000
Frequency
cm-1
400

band occurs approximately 100 cm^{-1} away from the protein amide I band. (Fig. 2.4c). However samples in H_2O buffer can now be studied due to the application of computers to IR spectroscopy and the development of the Fast Fourier transform algorithm. This allows accurate digital subtraction of H_2O bands from the sample spectra and the production of absorbance spectra with high signal-to-noise ratios.

2.5.3.1 Instrumentation

The development of FTIR spectroscopy from the conventional dispersive instruments is discussed in this section. Starting from a brief description of a dispersive IR instrument, the theory of FTIR spectroscopy will be covered.

2.5.3.2 Dispersive IR spectrometers

In basic terms, a dispersive or conventional IR spectrometer comprises of an IR source, a monochromator and a detector. The monochromator separates the radiation into its constituent frequencies and, by a series of slits, radiation of a narrow range of frequencies is selected to interact with the sample. This method is repeated until the spectral region of interest has been systematically covered. Increasing the resolution is achieved by narrowing the range of frequencies measured at any one time, but this has the effect of reducing the energy incident on the detector, hence reducing the s/n

ratio and increasing the scanning time. Digital subtraction of background spectra is possible, but the technique produced spectra with a poor s/n ratio.

2.5.3.3 Fourier Transform Infrared Spectroscopy

The application of the interferometer and the development of the fast Fourier transform to infrared spectroscopy has greatly reduced the time required to gather high quality IR spectra, and has increased the versatility of the technique in both research and routine applications.

2.5.3.4 Fourier Transforms

The study on the theory of heat conduction published by Fourier in 1822 is remarkable as it laid down the foundations of a tremendously powerful and flexible mathematical technique. The basic idea is that any periodic function can be expressed as a series of sine and cosine waves of the same period.

Any periodic function, F(t), with a repeat frequency v can be represented by

$$F(t) = 2\Sigma[f'(n)\cos 2\pi nvt + f''(n)\sin 2\pi nvt] \qquad \text{Equ. 2.11}$$

$$= \Sigma f(n) e^{2\pi invt} \qquad \text{Equ. 2.12}$$

This can be written as:-

$$F(t) = \int_{-\infty}^{\infty} f(v) e^{2\pi ivt} dv \qquad \text{Equ. 2.13}$$

$$= \int_{-\infty}^{\infty} f(v)\cos 2\pi vt.dv + i\int_{-\infty}^{\infty} f(v)\sin 2\pi vt.dv \qquad \text{Equ. 2.14}$$

where F(t) is the Fourier transform of f(v).

An important characteristic of this relationship is that

$$f(v) = \int_{-\infty}^{\infty} F(t) e^{-2\pi ivt} dt.$$

Therefore, in theory, we can determine F(t) from f(v), and vice versa.

In the simplest case, the Fourier transform (FT) of an infinitely narrow line of frequency v is a sinusoidal function from $-\infty$ to ∞. Similarly the FT of a number of discrete narrow lines with frequency v_n (where n is any number) is a waveform in which the individual sinusoidal functions interfere to produce a complex resultant waveform from $-\infty$ to ∞. Conversely a complex infinite sinusoidal waveform can undergo an inverse FT (FT^{-1}) to identify the frequencies of the input line sources.

2.5.3.5. Fourier Transforms Applied to Spectroscopy

In practice, experimental data collected in a given interval is digitised in the time domain, then undergoes Fourier transformation to give information of the frequencies of the radiation under examination. For example, in FT-NMR the nuclei held in the magnetic field experience a pulse, or series of pulses, of a wide range of radio frequency radiation. The radiation emitted during the free induction decay takes the form of a complex oscillation which is measured and digitised as a function of time. The FT of this oscillation gives information in the frequency domain of the nuclei under

investigation. However for IR spectroscopy, the frequencies being sampled ($\approx 10^{14}$ s^{-1}) are higher than that at which 'fast' electronic devices can operate ($\approx 10^{9}$ s^{-1}), so that information from the sample cannot be gained as a function of time. However the use of an interferometer overcomes this problem.

2.5.3.6. FTIR Instrumentation

The basic design of a FTIR spectrometer is shown in Fig. 2.5. IR radiation from the source is separated at the beamsplitter of the interferometer which, ideally, reflects 50% of the incident radiation to the stationary mirror and transmits 50% to the moving mirror. After reflection, the waves recombine and are directed to the detector.

Consider the simplest case of a beam of monochromatic radiation coming from the source. The intensity of the recombined beam at the detector depends on the path difference introduced between the two fractions of the beam. When the path difference is zero, the beams will be in phase and constructively interfere to produce a signal of intensity equal to that produced by the source. When the moving mirror has travelled $\frac{1}{4}\lambda$, thereby introducing a path difference of $\frac{1}{2}\lambda$, the beams will be 180° out of phase and destructively interfere to produce no signal at the detector. As the mirror moves at constant velocity, the intensity at the radiation incident on the detector

Fig. 2.5. The basic design of an FTIR spectrometer.

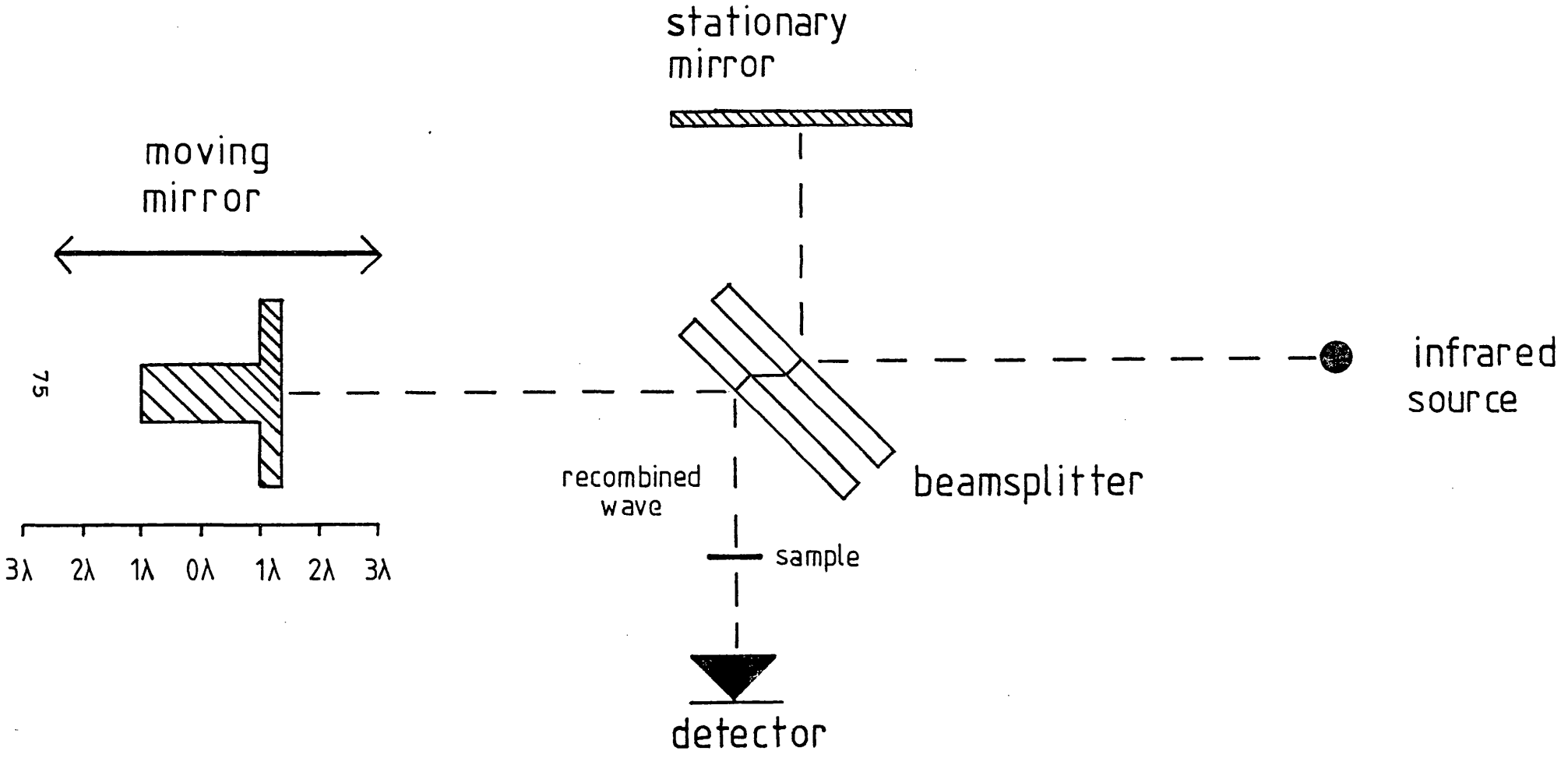
stationary
mirror
moving
mirror
75
3λ 2λ 1λ 0λ 1λ 2λ 3λ
infrared
source
recombined
wave
beamsplitter
sample
detector

will fluctuate sinusoidally.

When a source produces radiation of two or more wavelengths, the optical path difference for each will be different at any given position of the moving mirror as the optical path difference is a function of λ. This will cause the recombining beams to interfere, producing an interferogram of intensity against mirror displacement at the detector. The information is in the correct form to be analysed using Fourier transformation.

2.5.3.7. Generation of FTIR Spectra

The FT of an infinitely thin line is an infinite cosine train (Fig. 2.6a). In practice, the spectrometer can only measure a finite data set, and the inverse Fourier transform of a finite cosine train is a sinc function (Fig. 2.6b). The measured FT of a real IR absorption band of finite bandwidth, centred at frequency v, is an exponentially damped finite cosine train. The greater the bandwidth of the absorption band, the more severe the exponential damping (Fig. 2.7). The inverse FT of the exponentially damped finite cosine train is a broad band centred at frequency v.

2.5.3.8. Resolution Enhancement

If two or more broad bands are centred close to each other, the instrument may be unable to resolve them, thus

Fig. 2.6a) A schematic diagram illustrating the Fourier transformation of an infinitely thin line.
b) A schematic diagram illustrating the inverse Fourier transformation of a finite cosine train.

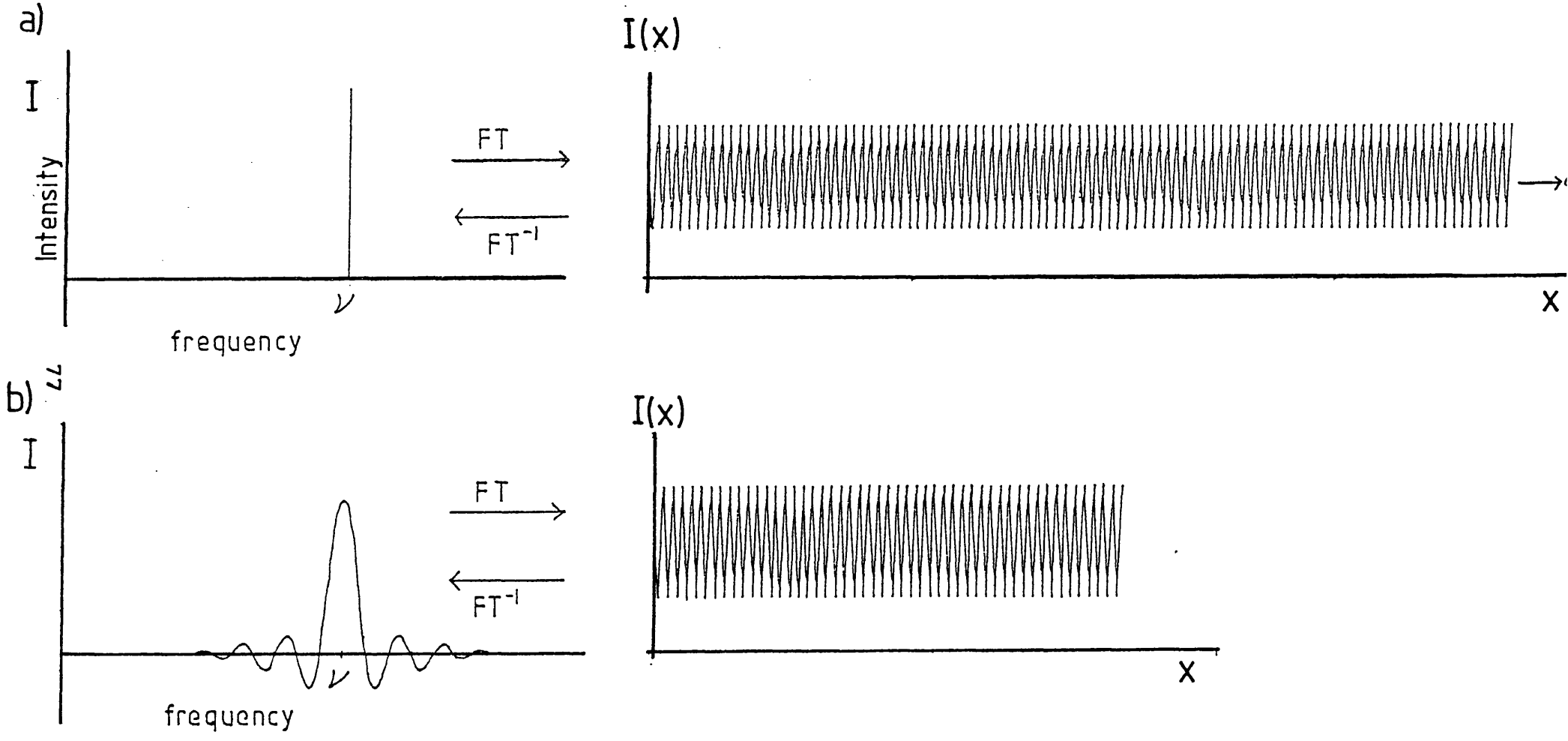
a)
I
Intensity
FT
FT⁻¹
ν
frequency
I(x)
X
b)
I
FT
FT⁻¹
ν
frequency
I(x)
X

Fig. 2.7) A schematic diagram of the Fourier transformations of bands of various halfwidths.

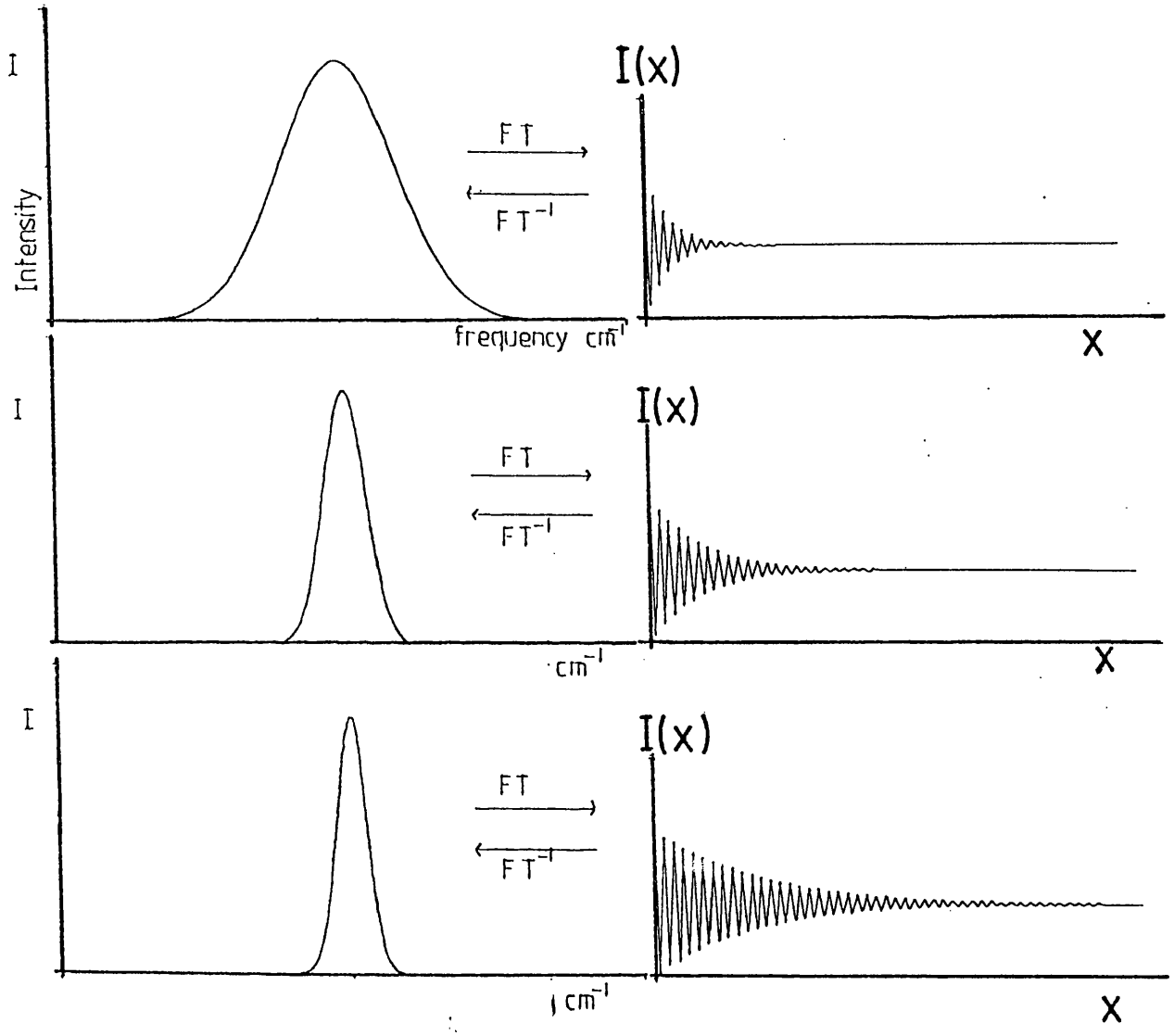
I
Intensity
frequency cm⁻¹
FT
FT⁻¹
I(x)
X
I
cm⁻¹
FT
FT⁻¹
I(x)
X
I
1 cm⁻¹
FT
FT⁻¹
I(x)
X

producing a resultant spectrum of a broad band envelope containing the real component bands. Two independent mathematical techniques, deconvolution and second derivation, have been developed to artificially narrow the widths of the component bands and hence allow accurate measurement of the component band frequencies. These techniques tend to be heavily relied upon in FTIR spectroscopic studies of biological molecules.

2.5.3.8.1. Deconvolution

Deconvolution manipulates the data in the Fourier domain. The width of the original band determines the rate of decay of the cosine train in the Fourier domain (Fig. 2.7), with wide bands causing faster decay than narrow bands. Therefore by multiplying the finite decaying exponential cosine train by a suitable finite rising exponential function (Fig. 2.8a), a finite constant amplitude cosine train can be obtained. The inverse transformation of the finite constant amplitude cosine train produces a sinc function, with a narrow peak at the position of the original band maximum and small side lobes on either side of the central peak (Fig. 2.8). In practice these side lobes interfere with component band identification of deconvolved complex band envelopes. The multiplication by the exponential function also results in the noise being increased exponentially. To reduce the problems of side lobes and increased noise in the deconvolved spectra, the constant

Fig. 2.8) The mechanism of deconvolution:-
a) multiplication of the decaying cosine train by an increasing exponential function,
b) multiplication of the finite cosine train by an apodization function.

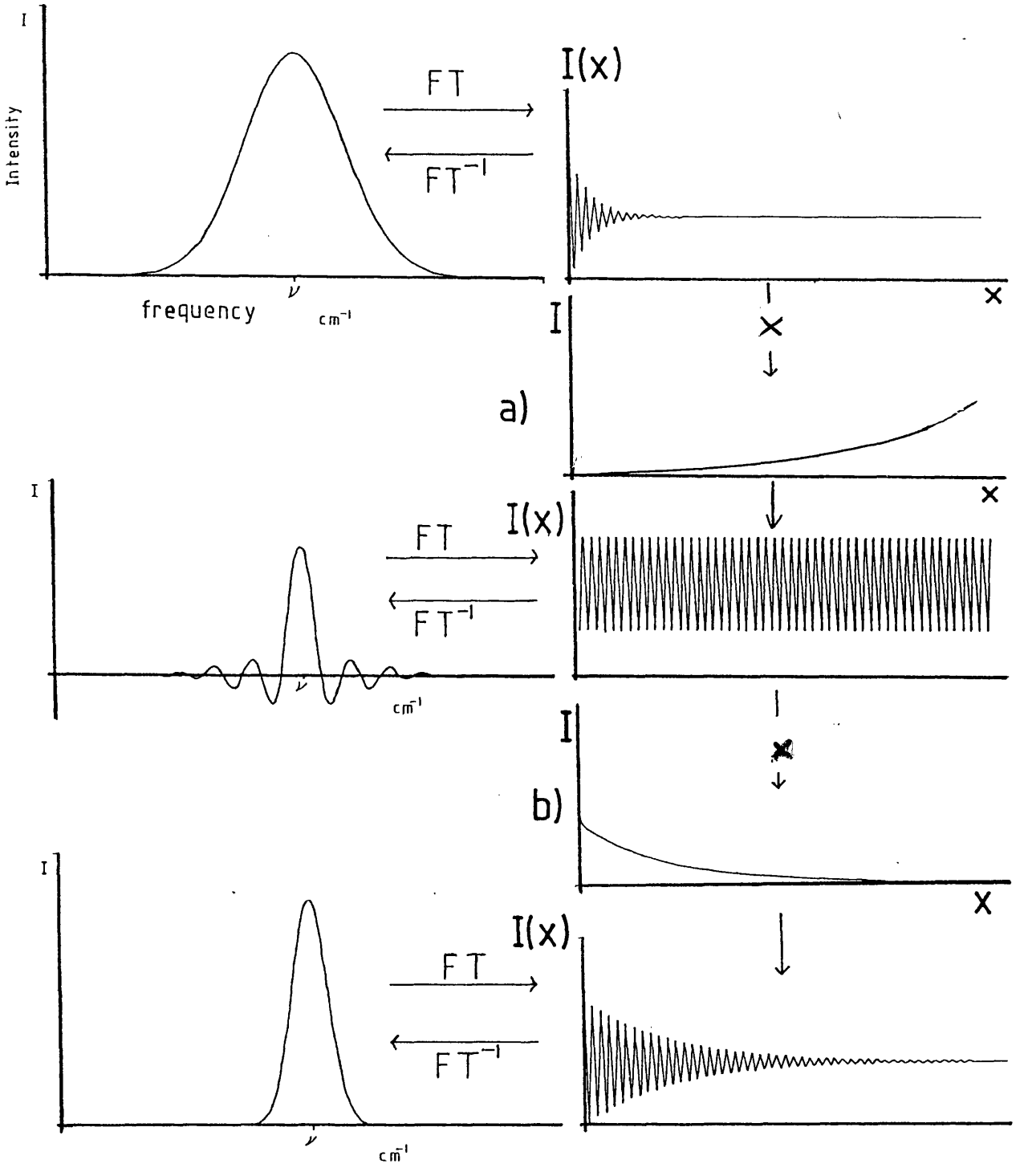
I
Intensity
frequency
ν
cm^{-1}
FT
FT^{-1}
I(x)
x
I
a)
b)

amplitude cosine form is multiplied by an apodization function, such as a $sinc^2$ or triangular function. This produces a decaying exponential train whose damping is less severe than that of the original cosine train (Fig. 2.8b). The transformation of this function produces a band narrower than the original whilst minimising the intensity of the side lobe artifacts. Furthermore, as apodization functions tend to zero, the noise is reduced in the cosine train and, hence, in the deconvolved spectrum.

2.5.3.8.2. Second Derivation

This technique utilises the fact that the position at which a component band occurs causes a point of inflection (i.e. where the rate of change of the gradient, $d^2I/dv^2 = 0$) on the band envelope.

The intrinsic shape of a single infrared absorption can be approximately represented by a Lorentzian function (Kauppinen et al., 1981b; Susi & Byler 1983)

$$I = (s/\pi)/(s^2+v^2)$$

where I = absorption intensity,

2s = width at half height, and

v = frequency of the band.

The second derivative of this function gives

$$\frac{d^2I}{dv^2} = -(1/\pi s)[\ 2a(1-3av^2)/(1+ av^2)^3]$$

where $a = 1/s^2$

The halfwidth of the second derivative, s'', is related to that of the original spectrum, s, by the equation

$$s'' = s/2.7$$

Therefore the component bandwidth is narrowed without altering the frequency.

Both second derivation and deconvolution techniques have been successfully applied to separate components within complex band envelopes. However absorption spectra must have a very high signal-to-noise ratio (s/n) for these techniques to be applied successfully as both enhance the level of noise in the resultant spectrum. Application of these techniques to poor s/n spectra leads to the production of spurious bands in the resolution-enhanced spectra.

2.5.3.9. Quantitative Analysis

A reliable method for quantification of IR spectra of biomolecules and other systems has long been sought. The main problem has been in trying to accurately determine the area of the component bands contained within the complex band envelope. Various methods have been developed to deal with this problem.

2.5.3.9.1. Curve fitting

This method relies on resolution enhancement to identify the positions of the component bands of a complex band envelope. A synthetic spectrum is then

generated by positioning component bands of known shape at the previously determined band positions. The characteristics (i.e. height, width and band type (Lorentzian, Gaussian or various combinations of the two)) of the component bands are altered until the synthetic band envelope matches that of the original spectrum. By calculating the areas of the component bands and assigning them to different vibrations, quantitative information can be gained (Fraser & Suzuki 1966, 1969; Villalain et al., 1989).

This method has been widely used but it relies on a number of assumptions:-

a) The computer programme assumes that the shape of the component bands are all the same and that all are symmetrical. Even though the IR absorption bands of simple molecules have a symmetrical Lorentzian form, there is no strong evidence to support either assumption when applied to complex molecules.

b) The assignment of the component bands to various secondary structures is based on the frequency of absorption. Recent evidence has shown that the IR spectra of a number of proteins cannot be explained using the results from some of the early IR protein and polypeptide studies.

c) The assumption that the molar absorptivity of all secondary structures are equal. Recent studies have shown that this is not the case for polypeptides of known conformation (Jackson et al., 1989a).

2.5.3.9.2. Factor Analysis

This method of quantification is based on fitting IR absorption spectra of known samples to an absorption spectrum of an unknown sample (Fredericks et al., 1985a,b). For quantifying protein structure, a library of FTIR absorption spectra of proteins whose structures are known from X-ray crystallography analysis is set up. These are then fitted to an absorption spectrum of the sample protein to generate a synthetic absorption band. The best statistical fit is found and the percentage content of the protein is determined from the reference spectra used to construct the synthetic band.

Recently published work has shown that this technique can quantitatively predict protein secondary structure to an accuracy of ± 3.9% for α-helix, ± 8.3% for β-sheet and ± 6.6% for β-turns (Lee et al., 1990). This method does not make any assumptions for band assignments, component band shapes or molar absorptivity. It does, however, assume that the secondary structure of proteins in their crystal state is the same as that in solution. There appears to be some difficulties applying this method to membrane proteins because the reference spectra are of soluble proteins. There are not enough membrane proteins of known structure to produce the required set of reference spectra.

2.5.3.10. Advantages of Fourier Transform Data Collection

a) The Multiplex Advantage (Fellgett's Advantage).

As the interferometer does not separate the source radiation into individual frequencies, the collected interferogram contains information on all the frequencies incident on the sample. Whereas the dispersive IR spectrometer systematically scans n individual frequencies to produce one spectrum, where n is any number, one FTIR scan produces a spectrum of all n frequencies, and is therefore much faster.

b) The Throughput Advantage (Jacquinot's Advantage)

The absence of frequency selection and the need for fewer optical elements than the dispersive instruments allows more energy to impinge on the sample and the detector, hence increasing the s/n ratio of FTIR spectrometers.

c) Frequency Precision (Conne's Advantage)

Frequency precision of dispersive spectrometers relied on calibration by external standards and on the uniform motion of the frequency selection mechanism. FTIR spectrometers typically use a helium-neon laser for internal frequency calibration, and for controlling the mirror movement of the interferometer, by monitoring interference fringes created from this monochromatic source.

2.5.3.11. Sampling Techniques

Acquisition of high s/n ratio absorption spectra of proteins and lipids requires the elimination of water vapour bands (Fig. 2.4a). This is important primarily for protein spectra because the narrow water vapour bands overlap with the protein amide I band (Table 2.II). Resolution-enhancement techniques enhance narrow bands more than broad absorption bands, thus resulting in spurious components from water vapour being identified within the amide I band.

Water vapour contributions may be reduced by purging the instrument with dry air or nitrogen, and by employing a sample shuttle which allows the background to be signal-averaging concurrently with the sample. Also a pre-recorded water vapour absorption spectrum can be subtracted from the protein absorption spectrum to reduce the vapour bands still further.

Samples may be prepared in KBr discs for investigation of materials in the dry state. 100 mg of KBr, an infrared transparent material, is mixed with approximately 1 mg of the sample and compressed into a thin disc. The acquisition of high s/n spectra is straightforward with this method.

The study of biological samples in aqueous media is more desirable. The strong H — O — H bending vibration of water (Fig. 2.4b) limits the sample thickness to 6 μm and necessitates the use of protein sample solutions of

20 - 50 mg/ml in order to obtain an adequate s/n ratio. 50 μm pathlengths can be used for samples in D_2O buffer (Fig. 2.4c), allowing a corresponding reduction in sample concentration.

The study of thin films, such as biological membranes, by transmission leads to poor s/n spectra due to the low amount of sample in the beam. This has been overcome by the development of Attenuated Internal Reflection (ATR) spectroscopy (Fig. 2.9). This technique utilises the phenomenon that e.m. radiation incident at the boundary of two media may be totally internally reflected at the boundary face when the angle of incidence, θ, $> \cos^{-1}(n_2/n_1)$, where n_1 and n_2 are the refractive indices of the internal and external media, respectively. For IR radiation, the evanescent beam passes a few microns into the external media before reflection occurs. By depositing the sample on a Ge crystal, the IR beam repeatedly samples the thin film on the surface of the crystal, thus enhancing the s/n ratio (Fig. 2.9). The number of reflections is determined by the dimensions of the crystal and, in practice, the thin film is sampled from six to thirty-six times, allowing high quality spectra to be produced from as little as 30 μg of sample.

This technique can be extended to study the orientation of components of thin films, such as lipids and proteins in biomembranes. The intensity, I, of IR absorption is related to the tranition moment of the molecule, M, by the equation

Fig. 2.9) A schematic diagram of an Attenuated Total Reflection.

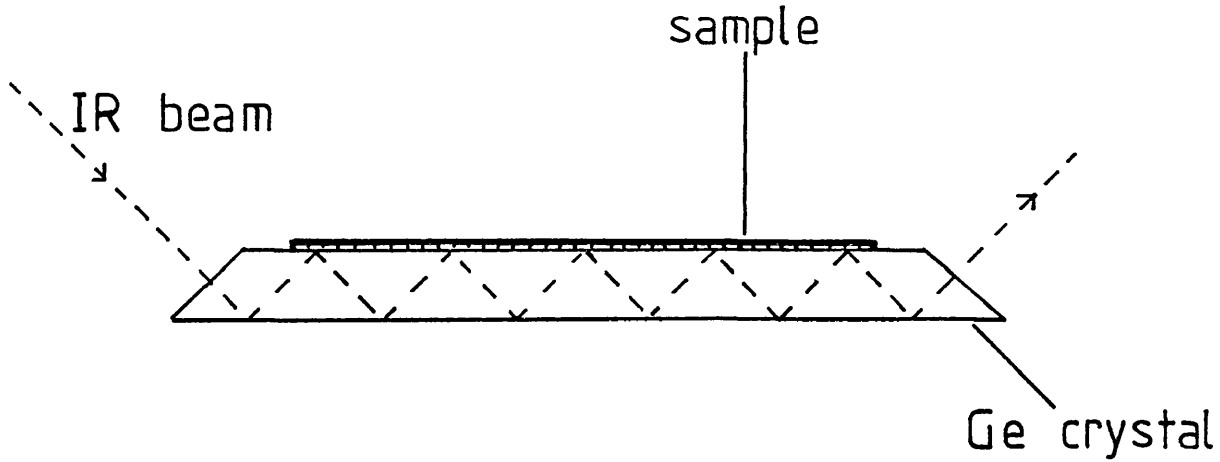
sample
IR beam
Ge crystal

$$I \propto M^2$$

From Equ. 2.7,

$$M = \alpha E \cos\theta$$

where θ = angle between the electric vector of the excitation radiation and the direction of the transition dipole moment.

Therefore, $I \propto \cos^2\theta$

If the incident radiation is linearly polarised, the IR absorption will be a maximum when the plane of polarisation coincides with the direction of the dipole moment, $\theta = 0°$, and a minimum when $\theta = 90°$. Therefore, information on the orientation of chemical groups within the sample layer can be gathered.

2.5.4. IR Active Bands In Biomolecules

2.6.4.1. Lipids

Lipids have been widely studied by IR spectroscopy (see Table 2.II). Information from the acyl chains is gathered from the CH_2 and CH_3 vibrations. The C = O band from the intermediate region of the lipid and the PO^{2-}, CH_2 and NH_3 vibrations from the headgroups can also be studied. The hydration of the lipids in bilayers and liposomes can be studied as the PO^{2-} stretching vibrations are sensitive water. Furthermore, lipid phase transition can be monitored due the shift of the CH_2 asymmetric stretching vibration, from 2919 cm^{-1} to 2924 cm^{-1} as the temperature is raised through T_m.

The C = O groups in the intermediate part of the lipid molecule are also sensitive to phase. The lipid carbonyl absorption has been shown by resolution enhancement techniques to comprise of two components. Initially these were thought to be from the sn-1 and sn-2 C = O groups absorbing at 1743 cm^{-1} and 1728 cm^{-1}, respectively. However FTIR studies on ^{18}O-substituted lipids suggest that the two bands arise from the C = O groups at different levels of hydration (Blume et al., 1988). As the temperature of the sample rises through T_m, the 1728 cm^{-1} component increases in intensity, indicating a higher level of hydration in the L_α phase. This results in a shift to a lower frequency of the lipid C = O absorption.

Table 2-II. The IR absorption frequencies of lipids.

IR BAND POSITION (CM^{-1})	ASSIGNMENT	
2956	CH_3 antisymmetric stretch	ACYL CHAIN GROUPS
2920	CH_2 antisymmetric stretch	
2870	CH_3 symmetric stretch	
2850	CH_2 symmetric stretch	
1470	CH_2 bending/scissoring	
1380	CH_2 symmetric deformation	
1380-1190	CH_2 wagging band progression	
1150-700	CH_2 rocking band progression	
3050	CH_3 antisymmetric stretch of $N(CH_3)_3$	HEADGROUPS
1740-1720	C = O ester stretch	
1490	CH_3 asymmetric bend of $N(CH_3)_3$	
1405	CH_3 symmetric bend of $N(CH_3)_3$	
1250	O – P = O asymmetric stretch	
1200-1000	C – O stretch	
1170	C – O from esters	
1085	O – P = O symmetric stretch	
1070	C – O from esters	
1040	C – N stretch	
900-800	P – O stretch	
800	C – N stretch	

The orientation of lipids within the bilayer has also been studied by polarised ATR spectroscopy in both the dry (Akutsu et al., 1975, 1981) and the hydrated state (Ter-Minassian-Saraga et al., 1988; Okamura et al., 1990). This has given valuable information on the orientation of the lipid acyl chains and the headgroups in the bilayer configuration.

A quantitative determination of the trans-gauche isomerisation at various positions along the lipid acyl chain as a function of phase, and of added cholesterol, has been developed (Mendelsohn et al., 1989, 1991). The experiments were based on observing the CD_2 rocking mode absorption of specifically deuterated acyl groups at different positions along the acyl chain. The absorption of the all trans CH_2 — CD_2 — CH_2 configuration occurs at 622 cm^{-1}, but shifts to about 650 cm^{-1} upon formation of gauche rotamers.

2.5.4.2. Proteins

Information on protein secondary structure is gained from the amide vibrations, shown in Table 2.III. As described in Chapter One each secondary structure has its own distinct hydrogen-bonding pattern between the oxygen of the C ═ O group and the hydrogen of the N — H group of the polypeptide backbone. This hydrogen-bonding is sufficiently strong to modify the electron density of the C ═ O group, and therefore the frequency of IR absorption, for each individual secondary structure. This

Table 2-III. The IR absorption frequencies of proteins.

AMIDE VIBRATION	FREQUENCY (CM^{-1})	ASSIGNMENT
A	3300	N — H (s)
B	3100	N — H (s)
I	1680-1600	80% C ═ O (s) 10% N — H (b) 10% C — N (s)
II	1580-1480	60% N — H (b) 40% C — N (s)
III	1300-1230	30% C — N (s) 30% N — H (b) 10% C ═ O (s) 10% O ═ C — N (b) 20% others
IV	770-626	40% O ═ C — N (b) 60% others
V	800-640	N — H (b)
VI	605-540	C ═ O (b)
VII	200	C — N (t)

s = stretch; b = bending; t = torsion

These results are gathered from Susi (1969), Thomas & Kyogoku (1977) and Wallach & Winzler (1974).

gives rise to the various secondary structures absorbing IR radiation of different frequencies. The amide I band is the most sensitive to protein secondary structure as this band is generated by an 80% C == O stretching vibration with a 10% coupling contribution from the N — H bending and C — N stretching vibrations, respectively (Miyazawa 1960). However the shift in position of the amide I absorption bands arising from different secondary structures is too small relative to their bandwidths to be resolved in the absorption spectra. Resolution enhancement techniques, such as second derivative and deconvolution, are employed to identify the frequency of the component bands present within the complex absorption band envelope and hence reveal the secondary structures present in the sample.

This has been applied successfully to reveal the secondary structure of many soluble and membrane proteins in aqueous solution, and binding various ligands (for reviews, see Jackson et al., 1989b; Krimm & Bandekar 1986; Susi & Byler 1986; Lee & Chapman 1986).

The orientation of secondary structures of membrane proteins has also been probed to gain more detailed information on the protein structure (Earnest et al., 1990; Nabedryk et al., 1981, 1988; Rothschild et al., 1980).

FTIR provides a powerful tool for investigating lipids and proteins in their native state. The initial difficulties in applying IR spectroscopy to biological systems have been overcome primarily by the application of Fourier transform methods. These became possible with the development of the Fast Fourier transform and the increasing availability of affordable microcomputers.

As with all techniques, FTIR spectroscopy does have certain disadvantages. The main limitation is that it is not able to give information at atomic resolution. It is a bulk technique as it gives information on the whole protein, and not on individual regions within it. Conformational changes induced by altering the environment, or by the interaction of ligands, such as metal ions, lipids or inhibitors, are therefore more likely to be observed in small proteins or polypeptides than in large biomolecules. One method used to gain more information about a specific fragment of a protein is to isolate the fragment, if possible, by proteolytic digestion. This has been tried with some success (Azpiazu et al., 1991) but it is important to realise that the environment of the fragment may be altered, hence altering its secondary structure. Another method is to isotopically label specific residues (Engelhard et al., 1985; Rothschild et al., 1986), or to use site-directed mutagenesis to change specific amino acid residues in the protein (Braiman et al., 1988; Rothschild et al., 1989).

Information is gained by identifying differences in the spectra of the native and modified protein. This is especially useful in determining the role of functional residues in a protein and their effect on structure.

CHAPTER THREE

FTIR STUDIES OF PEPTIDES FORMING 3_{10}- AND α-HELICES AND β-BEND RIBBON STRUCTURES IN ORGANIC SOLUTION AND IN MODEL BIOMEMBRANES

3.1. INTRODUCTION

The secondary structure of membrane proteins and signal peptides present within a lipid matrix is of considerable interest at the present time. Some workers suggest that the α-helix is the dominant motif in these systems (Henderson et al., 1990, Deisenhofer et al., 1985, Austen 1979; Briggs & Gierasch, 1984; Shinnar & Kaiser 1984; Batenburg et al., 1988; Rosenblatt et al., 1980) whereas other workers suggest that appreciable amounts of β-sheet (Kleffel et al., 1985, Reddy & Nagaraj, 1989) or some 3_{10}-helical structure may be present (Fox & Richards, 1982; Popot et al., 1990).

Understanding the mechanisms of insertion of proteins from an aqueous solution into a hydrophobic membrane environment has long been a problem faced by scientists. It is thought that a hydrophobic portion of the protein, normally situated in the hydrophobic core of the soluble protein, inserts into the bilayer. The "helical hairpin hypothesis" of Engelman and Steitz (1981) supposes that the insertion of proteins into membranes is initiated by the spontaneous penetration of an α- or 3_{10}-helical hairpin from a hydrophobic portion of the protein into the bilayer.

Even though a wealth of information is available on the secondary structures of soluble proteins at atomic resolution, the problems associated with X-ray

diffraction and NMR studies of membrane proteins has led to a lack of high resolution data of these membrane systems. Other methods and techniques are being applied in order to ease this information "bottleneck". X-ray diffraction studies of synthetic peptides crystallised from organic solvent in the absence of lipids is one approach used to gain information about the peptides. Another is to study peptides in low polarity solvents (e.g. $CDCl_3$) by ^1H NMR in an attempt to mimic the low polarity environment within the lipid bilayer. FTIR spectroscopy is a potentially useful technique as it gives information on the peptide secondary structure and on the lipid from the same sample in aqueous solution.

A recent survey of X-ray diffraction studies (Barlow & Thornton, 1988) has indicated that in addition to the α-helix, the 3_{10}-helical structure may also be present in various amounts in soluble proteins.

Various biophysical studies have shown that the $C^{\alpha,\alpha}$-dialkylated α-amino acid, α-aminoisobutyric acid (Aib), promotes $\alpha/3_{10}$-helical structures (Prasad & Balaram, 1984; Toniolo & Benedetti, 1988; Toniolo, 1989; Smith et al., 1981). This unusual α-amino acid occurs extensively in transmembrane channel-forming peptaibol antibiotics (Benedetti et al., 1982a; Bruckner & Graf, 1983). Biophysical studies of transmembrane channels, such as those formed by peptides of the alamethicin family, suggest that both α- and 3_{10}-helical structures

may occur (Mathew & Balaram, 1983; Menestrina et al., 1986). Two of these polypeptides, alamethicin and trichorzianine, were found to be predominantly α-helical by X-ray diffraction analysis, but short segments of 3_{10}-helix were also observed (Fox & Richards, 1982; Le Bars et al., 1988).

Conformation energy calculations, assuming a tetrahedral symmetric geometry for the four substituents on the C^{α} carbon of the Aib residue, predicted that an α-helical structure would be adopted by the Aib residue (Marshall 1971; Pletnev et al., 1973; Burgess & Leach, 1973). However, the assumption of symmetry has been shown to be invalid for crystallised peptides containing poly(Aib)$_n$. For a residue in a right-handed (incipient) 3_{10}-helical conformation, the bond angles involving the methyl group in the D-position tends to be larger than the tetrahedral value, whereas those involving the L-methyl group tend to be smaller. This slight distortion is due to steric hindrance as the formation of the 3_{10}-helix involves the methyl in the D-position being too close to the C == O of the preceding unit. Taking this asymmetry into account, Paterson et al., (1981) showed that the 3_{10}-helix is the most stable conformation for Aib homopeptides (Figs. 3.1 and 3.2).

A number of conformational studies on terminally-blocked Aib-containing peptides have been carried out using a range of techniques including X-ray diffraction, ^{1}H- and ^{13}C-NMR, vibrational CD and IR absorption

Fig. 3.1) A schematic diagram of pBrBz-$(Aib)_6$-OtBu indicating the H-bonding pattern.

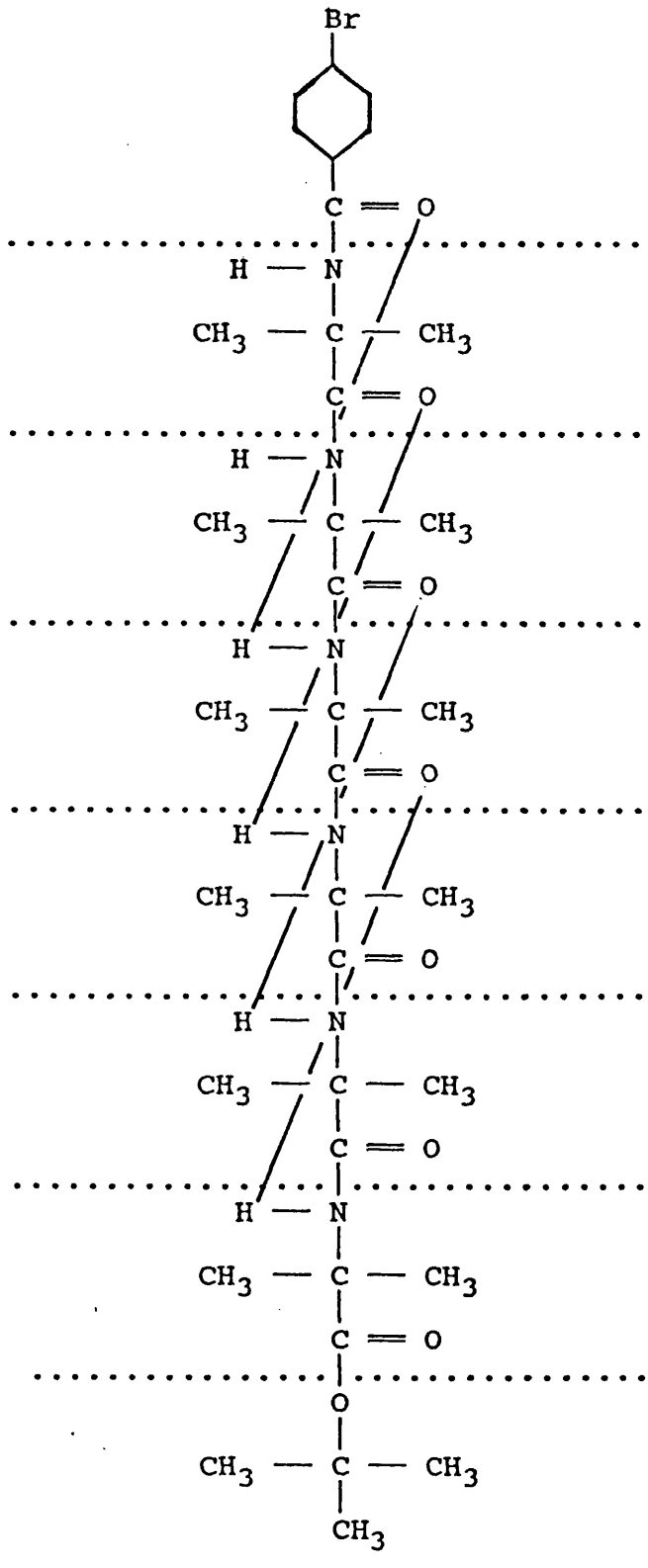

Fig. 3.2) The structure of the pBrBz-$(Aib)_6$-O*t*Bu solved by X-ray diffraction.

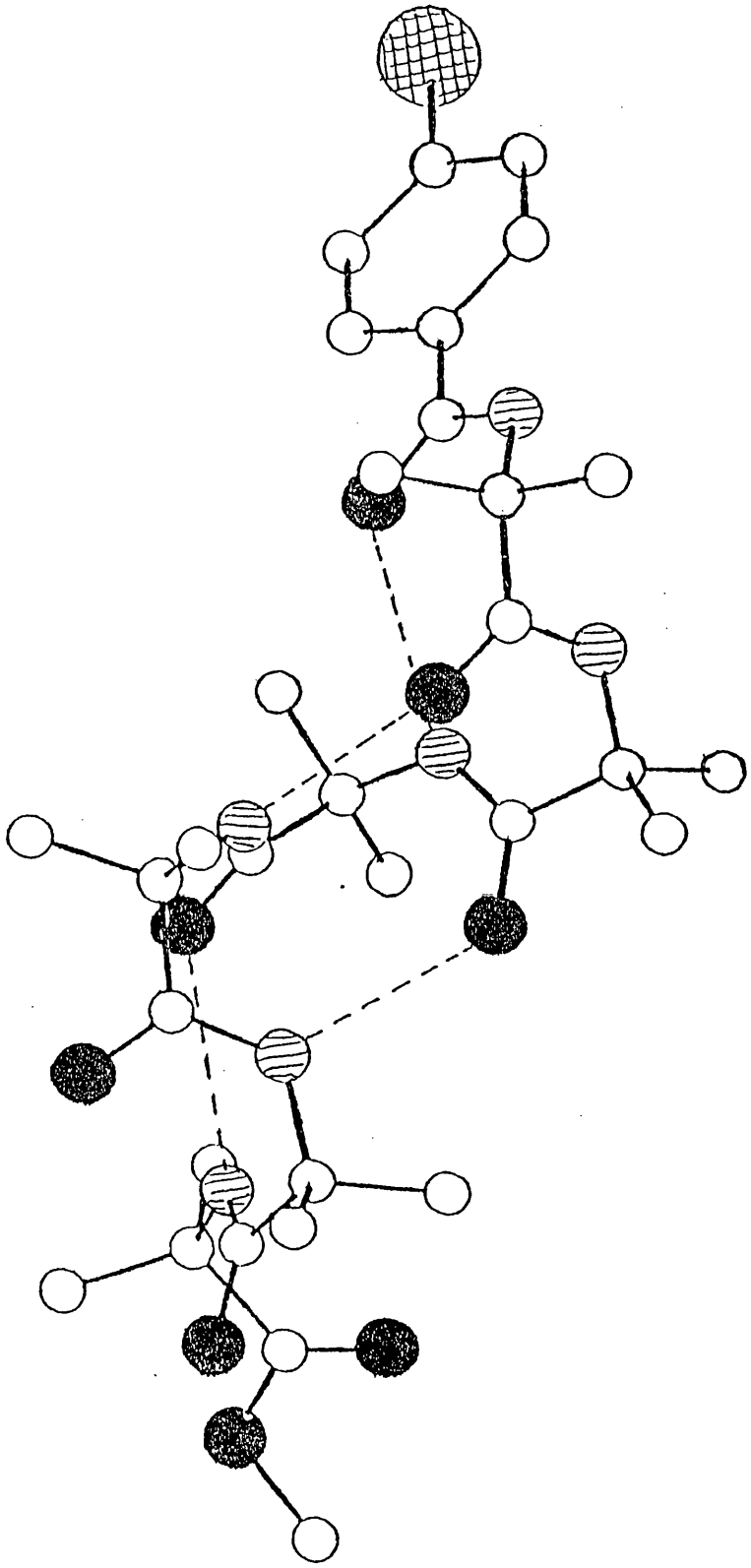

spectroscopy. A ^{13}C NMR study of Z-$(Aib)_n$-OMe (n = 3-8) by Saitô et al. (1988) showed that all these homopeptides contain incipient or fully developed 3_{10}-helices. ^{1}H NMR, IR absorption and X-ray diffraction studies of terminally-blocked, monodispersed $(Aib)_n$ (n = 2 - 5) homopeptides strongly support the formation of an intramolecular H-bonding pattern characteristic of the 3_{10}-helix occurring first at the trimer level (Benedetti et al., 1982b; Bavoso et al., 1986; Toniolo et al., 1985; Toniolo et al., 1986; Pavone et al., 1990a).

A diagram of the blocking groups used for these peptides is given in Fig. 3.3.

Toniolo et al., (1985, 1986) conclude from studies using X-ray diffraction and IR absorption spectroscopy that fully stable 3_{10}-helices are formed by Z-$(Aib)_n$-OtBu for n = 8 or more. However the current empirical view of Aib-rich (as opposed to poly(Aib)) peptides is that they tend to adopt a 3_{10}-helical structure when shorter than eight residues, and adopt either 3_{10}- or mixed $3_{10}/\alpha$-helical structure for eight residues or more (Bavoso et al., 1988). Marshall et al. (1990) concluded that the choice between the α- and 3_{10}- helical conformations assumed by peptides containing multiple $C^{\alpha,\alpha}$-dialkylated amino acids depends on peptide length, environment, and size and distribution of amino acid side chains.

Recent papers by Karle, Balaram and co-workers on Aib-rich peptides show that the peptide Boc-Trp-Ile-Ala-Aib-Ile-Val-Aib-Leu-Aib-Pro-OMe exhibit a predominantly

Fig. 3.3) A schematic diagram of the blocking groups used for the peptides:-

a) benzyloxycarbonyl, Z
b) para-bromobenzoyl, pBrBz
c) para-bromobenzyloxycarbonyl, pBrZ
d) tert-butoxycarbonyl, Boc
e) tert-butoxy, OtBu
f) methoxy, OMe

a)

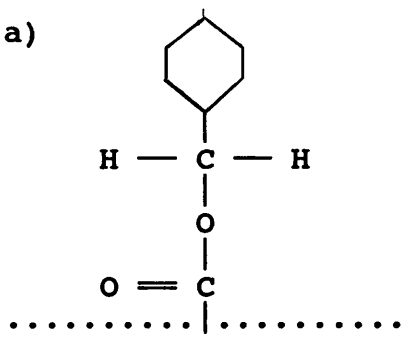

b)

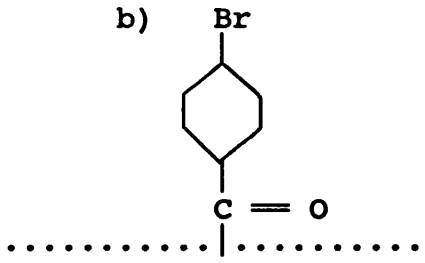

c)

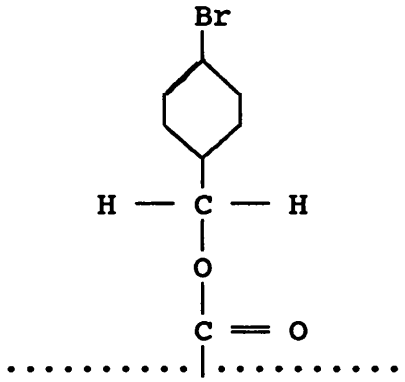

d)

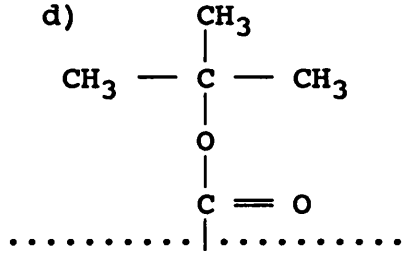

e)

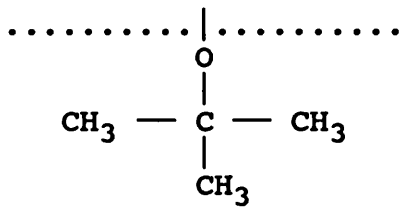

f)

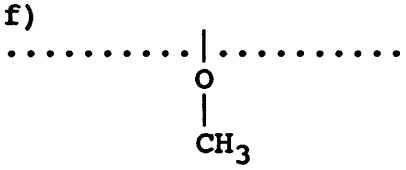

α-helical structure in triclinic crystals and a 3_{10}-helix in monoclinic crystals (Karle et al., 1989a). The same workers also reported that two molecules of the peptide Boc-Aib-Val-Aib-Aib-Val-Val-Val-Aib-Val-Aib-OMe cocrystallise in a triclinic cell with different helical conformations (Karle et al., 1989b), one molecule being totally α-helical and the other being a combination of α-helix and 3_{10}-helix. Solution studies using ^{1}H NMR on the same compound found it to be completely 3_{10}-helical in $CDCl_3$, and either α-helical or partially unfolded 3_{10}-helical in $(CD_3)_2SO$. Studies in $CDCl_3$ are widely carried out as this solvent has a low polarity, similar to the low polarity experienced in natural membranes. These studies illustrate the sensitivity of these peptide secondary structures to environment.

Dwivedi et al., (1984) calculate that the IR amide I band of poly(Aib)$_n$ in a 3_{10}-helical structure should absorb at 1665 cm^{-1}, whilst type III β-turns (a type III β-turn corresponds to the building unit of the 3_{10}-helix) should have amide I absorptions at 1686 cm^{-1} and 1646±3 cm^{-1}. A study of alamethicin (Haris & Chapman, 1988) assigned the main peak at 1663 cm^{-1} to a combination of absorptions from 3_{10}- and α-helices, and suggested that the weaker band at 1639 cm^{-1} may also be associated with the 3_{10}-helical structure.

X-ray diffraction studies of pBrBz-(Aib-L-Ala)$_{4,5}$-OMe crystallised from methanol have indicated that both peptides contain both α- and 3_{10}-helices under these

conditions (Benedetti et al., 1990; Pavone et al., 1990b).

Sequential oligomers containing the sequence Aib-L-Pro are also of interest as the presence of Pro in the sequence interrupts the H-bonding pattern. An NMR study by Venkatachalapathi & Balaram (1981) suggests that the peptides Z-(Aib-L-Pro)$_{3,4}$-OMe form a type of 3_{10}-helix that has the alternating presence/absence of the intramolecular H-bond due to the alkylation of the amide group in the Pro residue (Fig. 3.4). This structure is known as a β-bend ribbon and may be a conformational feature of some members of the alamethicin family, for example zervamicin (Karle et al., 1987). The longest β-bend ribbon, so far fully characterised by X-ray diffraction analysis, is that formed by pBrBz-Aib-(L-Pro-Aib)$_4$-OMe (Toniolo et al., 1991).

The IR absorption studies of terminally-blocked (Aib)$_n$ peptides (Benedetti et al., 1982b; Toniolo et al., 1985) related the position of the amide I maximum to the secondary structures present. This band, however, is not a pure band and consists of several components, each of which can be associated with various secondary structures. Resolution enhancement techniques such as second derivative and deconvolution can be used to identify the positions of the components of the amide I band, from which the secondary structures can be identified.

Fig. 3.4) The X-ray diffraction structure of pBrBz-(Aib-L-Pro)$_3$-OMe.

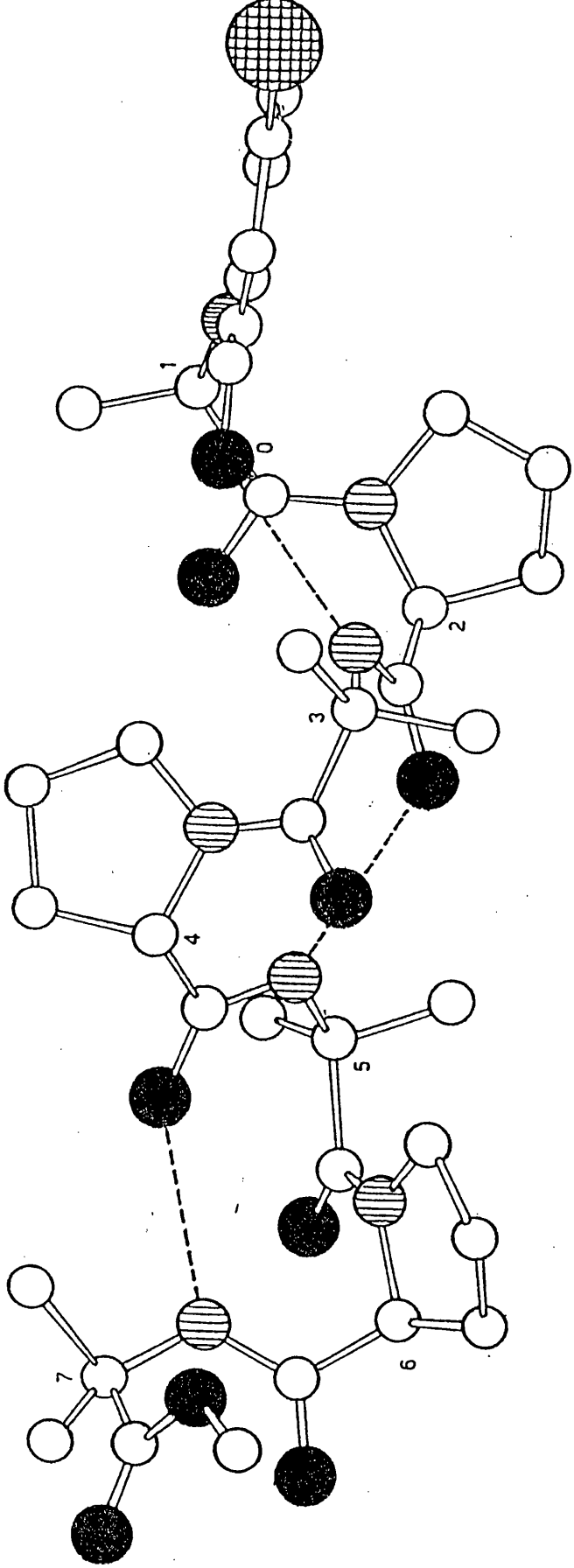
0
1
2
3
4
5
6
7

This chapter describes studies of peptides which are known to exist as 3_{10}-helical structures, a combination of 3_{10}- and α-helices, or β-bend ribbon in $CDCl_3$ solution using FTIR spectroscopy combined with resolution enhancement techniques. The characterisation of synthetic 3_{10}-helix and β-bend ribbon by FTIR spectroscopy is important in order to identify the IR absorption bands of these two structures. Once this has been established, the roles of these structures in protein secondary structure, in protein insertion and in the alamethicin family of proteins can be investigated by FTIR spectroscopy. Furthermore the assumption that these peptides have the same secondary structure in the low polarity solvent $CDCl_3$ as they do in natural membranes can also be investigated.

This work was carried out in collaboration with Prof. Claudio Toniolo and Dr. Mario Crisma of the University of Padua, Italy.

3.2. MATERIALS AND METHODS

The synthesis and characterisation of Z-$(Aib)_n$-O*t*Bu (*n* = 3-10) (Jones et al., 1965; Toniolo et al., 1985), Z-$(Aib\text{-}L\text{-}Ala)_n$-OMe (*n* = 2-5) and Z-L-Ala-$(Aib\text{-}L\text{-}Ala)_n$-OMe (*n* = 1-5) (Benedetti et al., 1990; Pavone et al., 1990b) and *p*BrZ-$(L\text{-}Pro\text{-}Aib)_n$-OMe (*n* = 1 - 5) (Toniolo et al., 1991) have already been described. The samples were generous gifts from Prof. C. Toniolo, University of Padua.

$CDCl_3$ and DMPC were both purchased from Sigma Chemicals Ltd., U.K. Solution studies were carried out in $CDCl_3$ at 20, 40 and 50°C.

The spectra in aqueous lipid dispersion were prepared by adding the peptide and DMPC to chloroform in a lipid/peptide ratio of 15:1. After drying the samples under N_2 and then under vacuum, small volumes of phosphate-buffered saline, pH 7.4, were added and the samples were incubated above the phase transition of the lipid for 2 - 3 hours. This is similar to the method of Rizzo et al. (1987) for incorporating alamethicin into the lipid dispersion. Samples in D_2O buffer, pD 7.4, were incubated at 33°C for 22 hours in order to allow hydrogen-deuterium exchange to occur in the peptide.

Spectra were obtained using a Perkin-Elmer 1750 FTIR spectrometer equipped with a TGS detector and a Perkin-Elmer 7300 computer for data acquisition and analysis. Samples were placed in a thermostated Beckman FH-01 CFT microcell fitted with CaF_2 windows, and a 50 μm teflon

spacer was used for measurements of the 16 mM samples in $CDCl_3$, and a 0.6 mm teflon spacer for 1.5 mM samples. For the aqueous solutions, a 6 μm tin spacer was used for samples in H_2O buffer, and a 50 μm teflon spacer for samples in D_2O buffer. Temperature control was achieved by means of a circulating water jacket. The spectrometer was continuously purged with dry air to eliminate water vapour absorptions from the spectral region of interest. A sample shuttle was used to permit the background to be signal averaged concurrently with the sample.

Solvent spectra were recorded under identical conditions as the sample spectra. Absorption spectra were obtained by digitally subtracting the solvent spectrum from the corresponding sample spectrum. If necessary, water vapour contributions were subtracted from the absorption spectrum using a previously recorded water vapour spectrum. Second derivative (Moffat et al., 1986) and deconvolution using the Perkin-Elmer ENHANCE routine (analogous to the method of Kauppinen et al., 1981a) were used to assign features of the composite amide I band to structural features present in the peptide.

3.3. RESULTS

3.3.1. Studies in organic solvent

The absorption spectra of the Z-$(Aib)_n$-O*t*Bu series (*n* = 3-10) at 1.5 mM concentration in $CDCl_3$ show the same pattern as those recorded by Toniolo et al., (1985). The position of the amide I band shows a similar decrease in the frequency as *n* increases. Similarly, the band from the free urethane and peptide N — H groups at 3450-3400 cm^{-1}, and the intramolecularly H-bonded N — H groups at 3380-3320 cm^{-1} behave as previously reported for the peptides in the absence of self-association.

Second derivative and deconvolution techniques give further information about the structure within the amide I band. The frequencies of the main band and of minor components of the amide I band for the 1.5 mM solutions of Z-$(Aib)_n$-O*t*Bu (*n* = 3-10) in $CDCl_3$ are given in Table 3.I. The absorption spectrum of Z-$(Aib)_8$-O*t*Bu in $CDCl_3$, known to adopt a stable 3_{10}-helical structure (Toniolo et al., 1985, 1986), is shown in Fig. 3.5a, with the deconvolved and second derivative spectra of the same peptide, shown in Figs. 3.5b and c, respectively).

For *n* = 8-10, the resolution enhanced spectra of the amide I band show three components: the main absorption band which occurs at 1666-1662 cm^{-1} and we assign to 3_{10}-helix, and two smaller components of approximately equal intensity, one at 1646-1644 cm^{-1}, which we assign to type III β-turns and one at 1681-1679 cm^{-1}, which may be

Table 3-I. The components of the resolution enhanced amide I and amide II bands of Z-$(Aib)_n$-O*t*Bu (*n* = 3-10) at 1.5 mM concentration in $CDCl_3$.

n	Amide I	Amide II
10	1681w,1662s,1646w	1533s
9	1681w,1663s,1644w	1532s,1558w
8	1679w,1666s,1646w	1532s
7	1680w,1670s,1648w	1531s,1557w
6	1677s,1664w,1649w	1531s,1537w
5	1680s,1668w	1526s,1537w
4	1682s,1662w	1517s,1530w
3	1687s,1664w	1523s,1538w

s = strong, w = weak

Fig. 3.5a) The FTIR absorption spectrum from 1800 cm^{-1} to 1500 cm^{-1} of Z-$(Aib)_8$-O<u>t</u>Bu in $CDCl_3$ at 20° C.

b) Deconvolved spectrum of Z-$(Aib)_8$-O<u>t</u>Bu in $CDCl_3$ at 20° C using resolution enhancement factor 2.125 and bandwidth 12.

c) Second derivative spectrum of Z-$(Aib)_8$-O<u>t</u>Bu in $CDCl_3$ at 20° C.

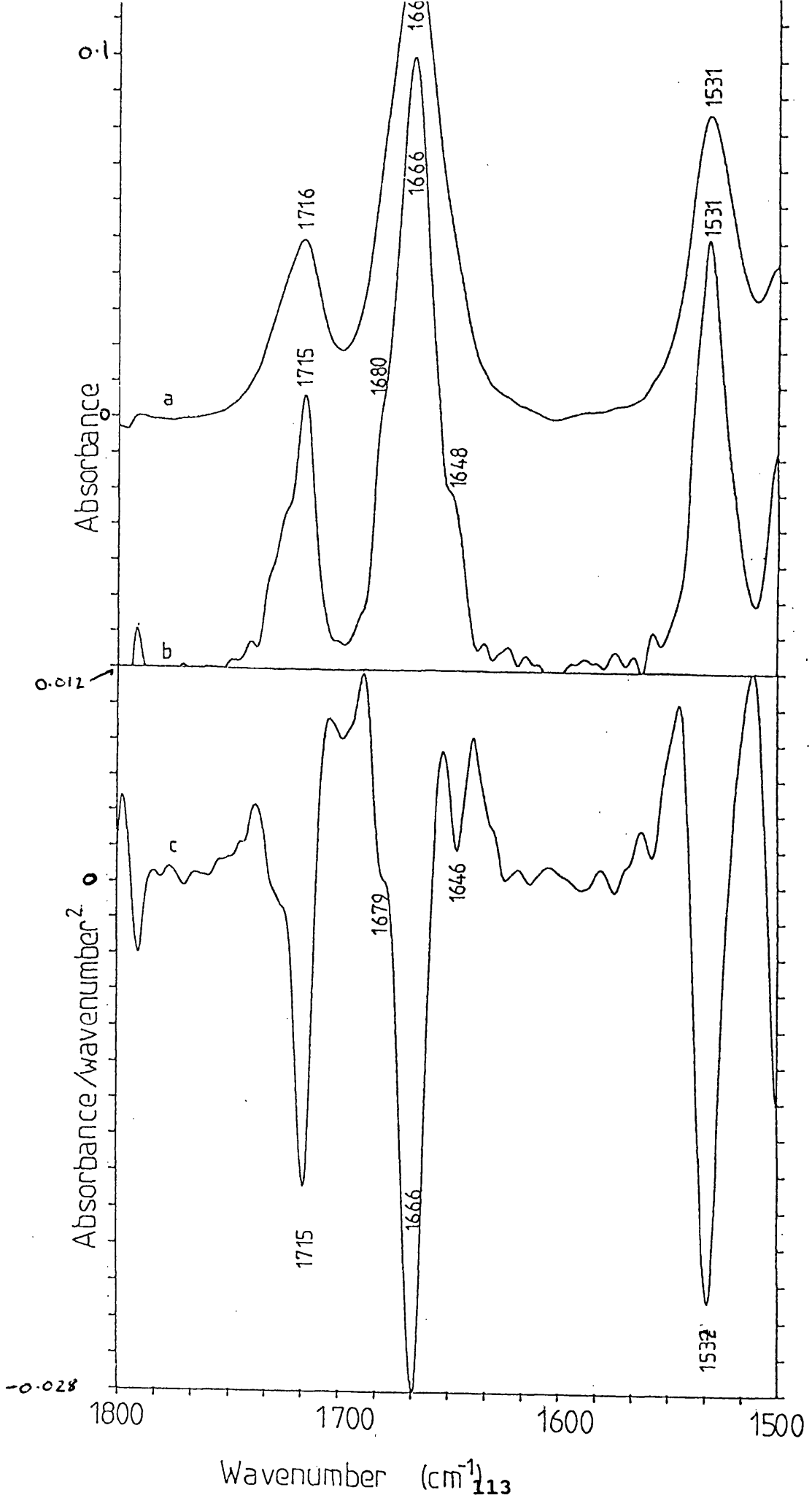
0.1
Absorbance
0
a
b
1716
1715
1680
1666
1648
1531
1531
0.012
-0.028
Absorbance/wavenumber^2
0
c
1715
1679
1666
1646
1532
1800
1700
1600
1500
Wavenumber (cm^{-1})

from type III β-turns and/or free carbonyl groups. The amide II band has one strong component, centred at 1533-1532 cm^{-1}. The band at 1716 - 1715 cm^{-1}, corresponding to the overlapping absorptions of H-bonded urethane C = O and free tert-butyl C = O ester of the N- and C-protecting moieties (Pulla Rao et al., 1980; Bonora et al., 1984) cannot be separated using resolution enhancement techniques.

The results of the studies of the Z-(Aib-L-Ala)$_n$-OMe (n= 2 - 5) peptides are listed in Table 3.II. The absorption spectrum of 1.5 mM Z-(Aib-L-Ala)$_5$-OMe is shown Fig. 3.6a, showing the amide I band at 1662 cm^{-1} and the amide II band at 1536 cm^{-1}. Deconvolution (Fig. 3.6c) is able to resolve the main amide I absorption into two components, one at 1662 cm^{-1}, assigned to 3_{10}-helix, and at 1659 cm^{-1}, assigned to α-helix. The band identified at 1681 cm^{-1} is assigned to type III β-turns and/or free carbonyl groups. The bands at 1649 cm^{-1} and 1641 cm^{-1} are either in, or very close to, the predicted frequency range for type III β-turns (Krimm & Bandekar, 1986). However the $3\pi/2$ vibration of the α-helix may also absorb in this region (Lee et al., 1985), making definite assignment of these bands difficult. The broad band centred around 1743 cm^{-1} is due to the free methyl ester carbonyl and the band centred at 1711-1713 cm^{-1} to the H-bonded urethane carbonyl of the blocking groups. The second derivative spectrum (Fig. 3.7a) is unable to resolve the two major bands and shows one asymmetric main

Table 3-II. The components of the resolution enhanced amide I and amide II bands of Z-(Aib-L-Ala)$_n$-OMe ($\underline{n}$ = 1-5) at 1.5 mM concentration in $CDCl_3$.

n	Amide I (cm^{-1})	Amide II (cm^{-1})
5	1681w,1662s,1659s,1649w,1641w	1537s
4	1673w,1664s,1644w	1535s
3	1673s,1657w	1528s
2	1681s,1664w	1534w,1514s
1	1677s	1513s

s = strong; w = weak

Fig. 3.6a) The FTIR absorption spectrum from 1800 cm^{-1} to 1500 cm^{-1} of 1.5 mM Z-(Aib-L-Ala)$_5$-OMe in $CDCl_3$ at 20° C.
b) The FTIR absorption spectrum from 1800 cm^{-1} to 1500 cm^{-1} of 1.5 mM Z-Ala-(Aib-L-Ala)$_5$-OMe in $CDCl_3$ at 20° C.
c) Deconvolved spectrum of Z-(Aib-L-Ala)$_5$-OMe in $CDCl_3$ at 20° C using bandwidth 12 and resolution enhancement factor 2.125.
d) Deconvolved spectrum of Z-L-Ala-(Aib-L-Ala)$_5$-OMe in $CDCl_3$ at 20° C using bandwidth 12 and resolution enhancement factor 2.125.

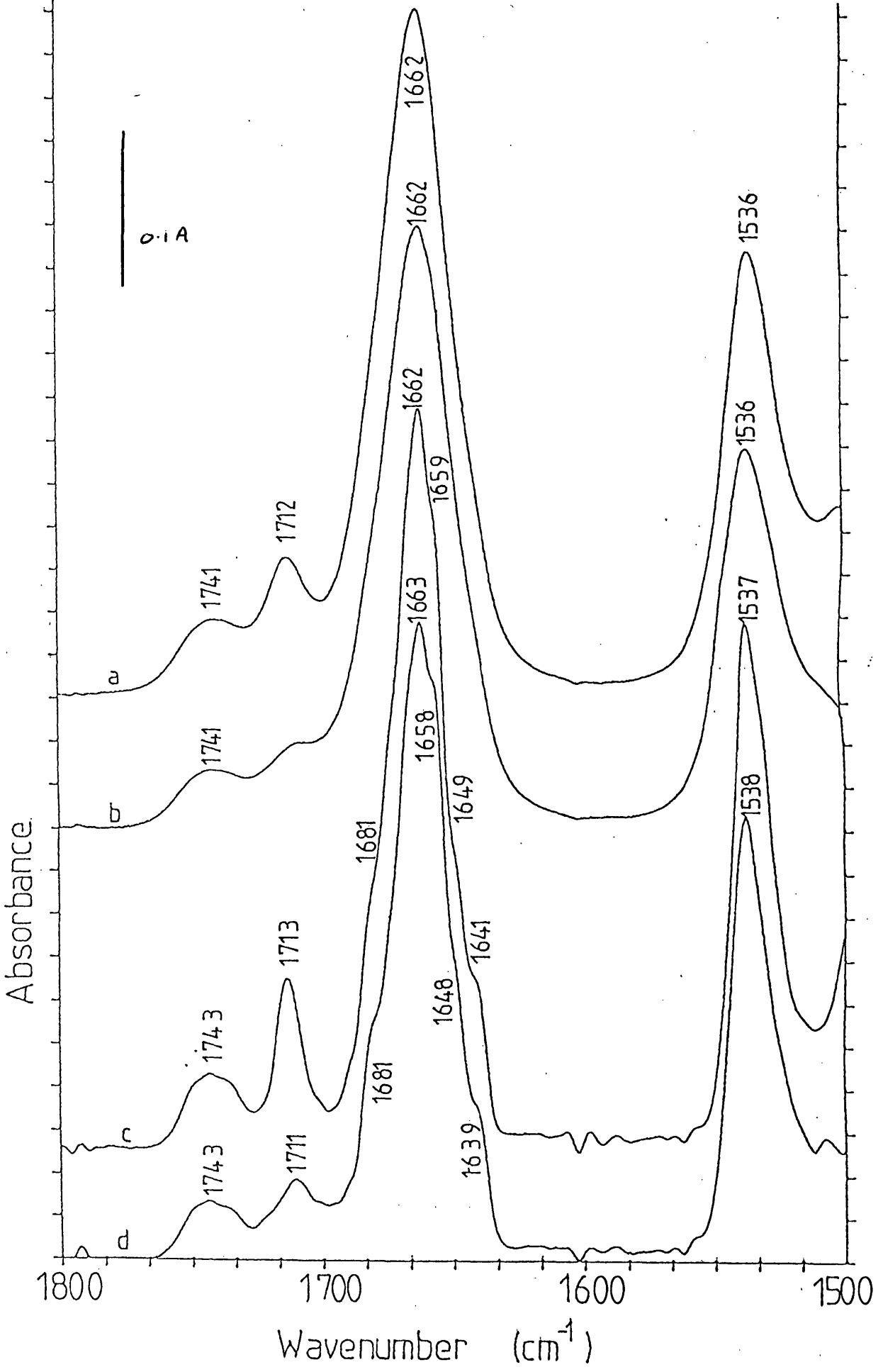
0·1 A
a
b
c
d
1662
1741
1712
1536
1662
1659
1741
1663
1658
1649
1537
1681
1538
1713
1641
1648
1743
1681
1639
1743
1711
Absorbance
1800
1700
1600
1500
Wavenumber (cm⁻¹)

Fig. 3.7a) Second derivative spectrum of Z-(Aib-L-Ala)$_5$-OMe in $CDCl_3$ at 20° C.
b) Second derivative spectrum of Z-L-Ala-(Aib-L-Ala)$_5$-OMe in $CDCl_3$ at 20°C.

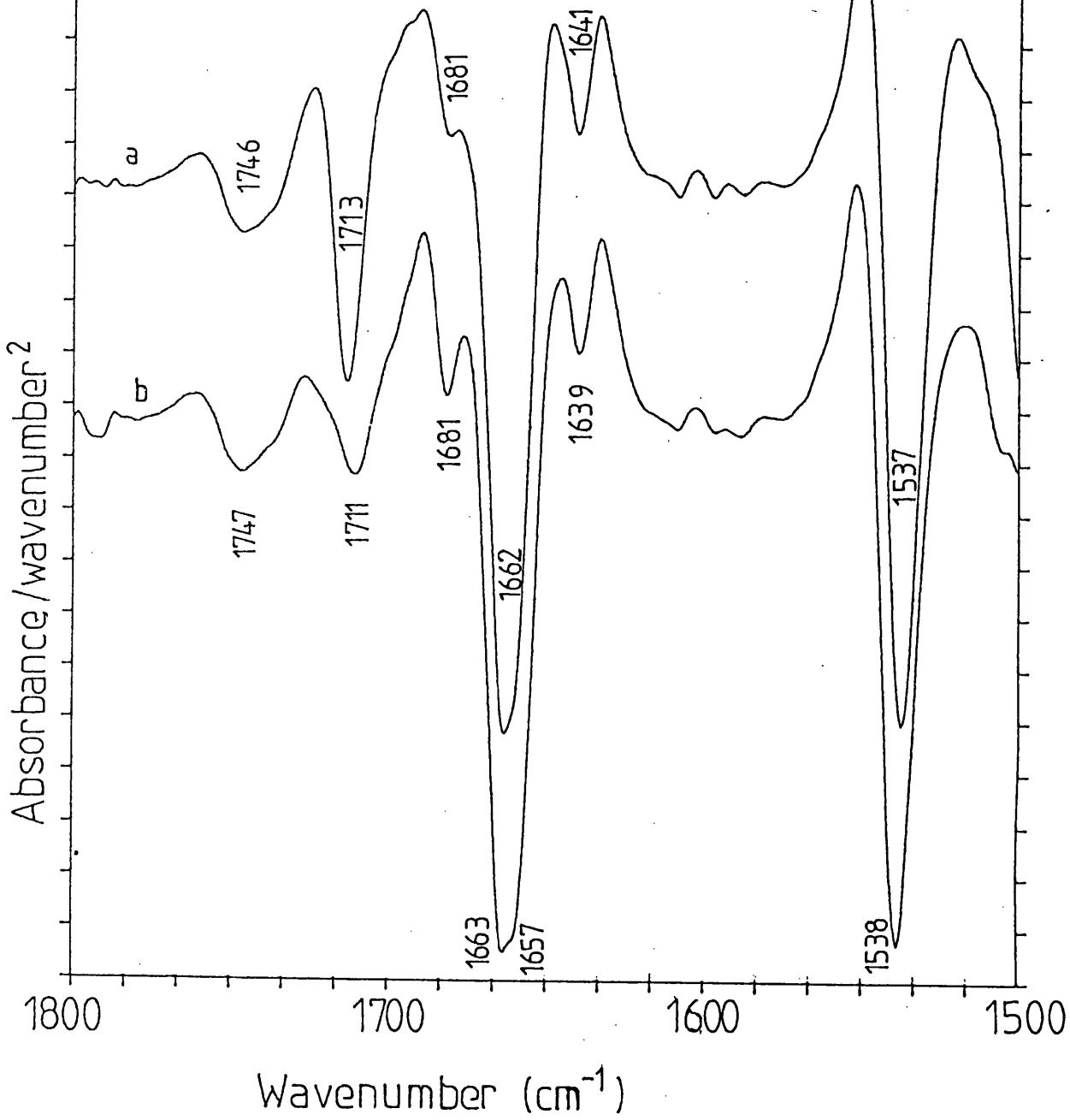
a
b
1746
1713
1681
1641
1747
1711
1681
1662
1639
1663
1657
1538
1537
Absorbance/wavenumber^2
1800
1700
1600
1500
Wavenumber (cm^{-1})

band at 1662 cm^{-1} which we assign to a combination of α- and 3_{10}-helices. Two smaller side bands are also seen at 1641 and 1681 cm^{-1} are identified, but the feature at 1649 cm^{-1} seen in the deconvolved spectrum is lost in the negative lobe of the main band.

The results of the study of the peptides Z-L-Ala-(Aib-L-Ala)$_n$-OMe (n = 1-5) are listed in Table 3.III. The IR absorption spectrum of 1.5 mM Z-L-Ala-(Aib-L-Ala)$_5$-OMe (Fig. 3.6b) shows the amide I band at 1662 cm^{-1} and the amide II band at 1536 cm^{-1}. The deconvolved and second derivative spectra (Fig. 3.6d and 3.7b, respectively) indicated that the main band is formed by two components, at 1663 cm^{-1} which we assign to 3_{10}-helix, and at 1657-1658 cm^{-1} which we assign to α-helix. Furthermore, the minor components at 1681 cm^{-1} we assign to type III β-turns and/or free carbonyl groups. The bands at 1639 cm^{-1} and 1648 cm^{-1} may be from type III β-turns, with a possible contribution from the $3\pi/2$ vibration of the α-helix. There is also a band 1743-1747 cm^{-1} which we assign to the free methyl ester carbonyl of the blocking group and one at 1711 cm^{-1}, assigned to the H-bonded urethane carbonyl group.

The absorption and resolution enhanced spectra of Z-L-Ala-(Aib-L-Ala)$_5$-OMe and Z-(Aib-L-Ala)$_5$-OMe in $CDCl_3$ at 16 mM concentration (shown in Figs 3.8 and 3.9) show similar spectra when compared to those at the lower concentration but better separation of the bands assigned

Table 3-III. The components of the resolution enhanced amide I and amide II bands of Z-L-Ala-(Aib-L-Ala)$_n$-OMe (n = 1- 5) at 1.5 mM concentration in $CDCl_3$.

n	Amide I	Amide II
5	1681w,1663s,1658s,1649w,1641w	1539s
4	1680w,1667s,1647w	1539
3	1679w,1667s,1647w	1536
2	1679w,1657w	1536s,1514w
1	1679w,1665w	1507w

s = strong, w = weak

Fig. 3.8a) Absorption spectrum of 16 mM Z-(Aib-L-Ala)$_5$-OMe in $CDCl_3$ at 20° C.

b) Absorption spectrum of 16 mM Z-Ala-(Aib-L-Ala)$_5$-OMe in $CDCl_3$ at 20° C.

c) Deconvolved spectrum of 16 mM Z-(Aib-L-Ala)$_5$-OMe in $CDCl_3$ at 20° C using bandwidth 12 and resolution enhancement factor 2.125.

d) Deconvolved spectrum of 16 mM Z-Ala-(Aib-L-Ala)$_5$-OMe in $CDCl_3$ at 20° C using bandwidth 12 and resolution enhancement factor 2.125.

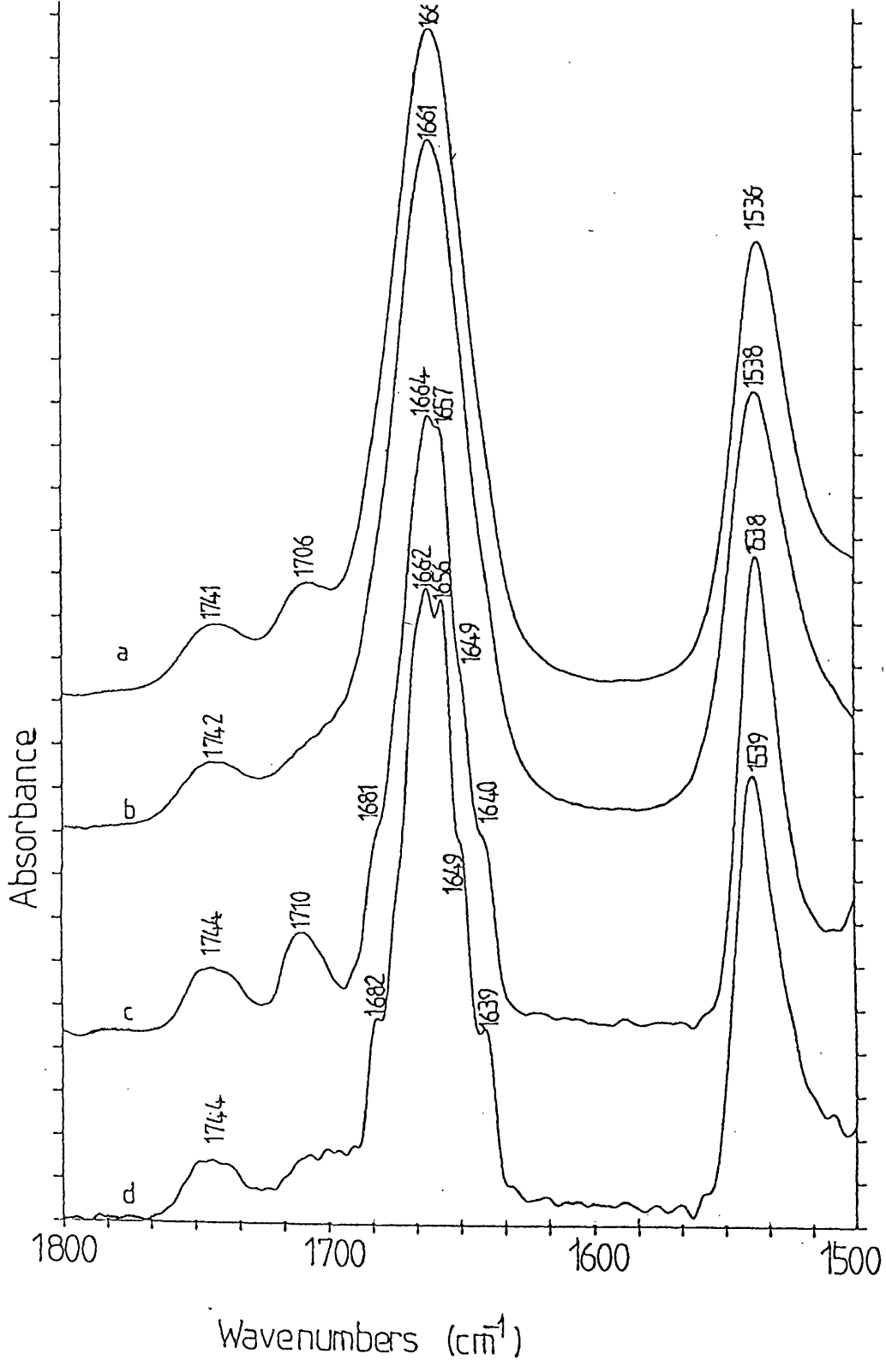
Absorbance
1800
1700
1600
1500
Wavenumbers (cm⁻¹)
a
b
c
d
1741
1706
1742
1744
1710
1744
1661
1664
1657
1662
1656
1649
1681
1640
1649
1682
1639
1536
1538
1538
1539

Fig. 3.9a) Second derivative spectrum of 16 mM Z-(Aib-L-Ala)$_5$-OMe in $CDCl_3$ at 20° C.
b) Second derivative spectrum of 16 mM Z-Ala-(Aib-L-Ala)$_5$-OMe in $CDCl_3$ at 20° C.

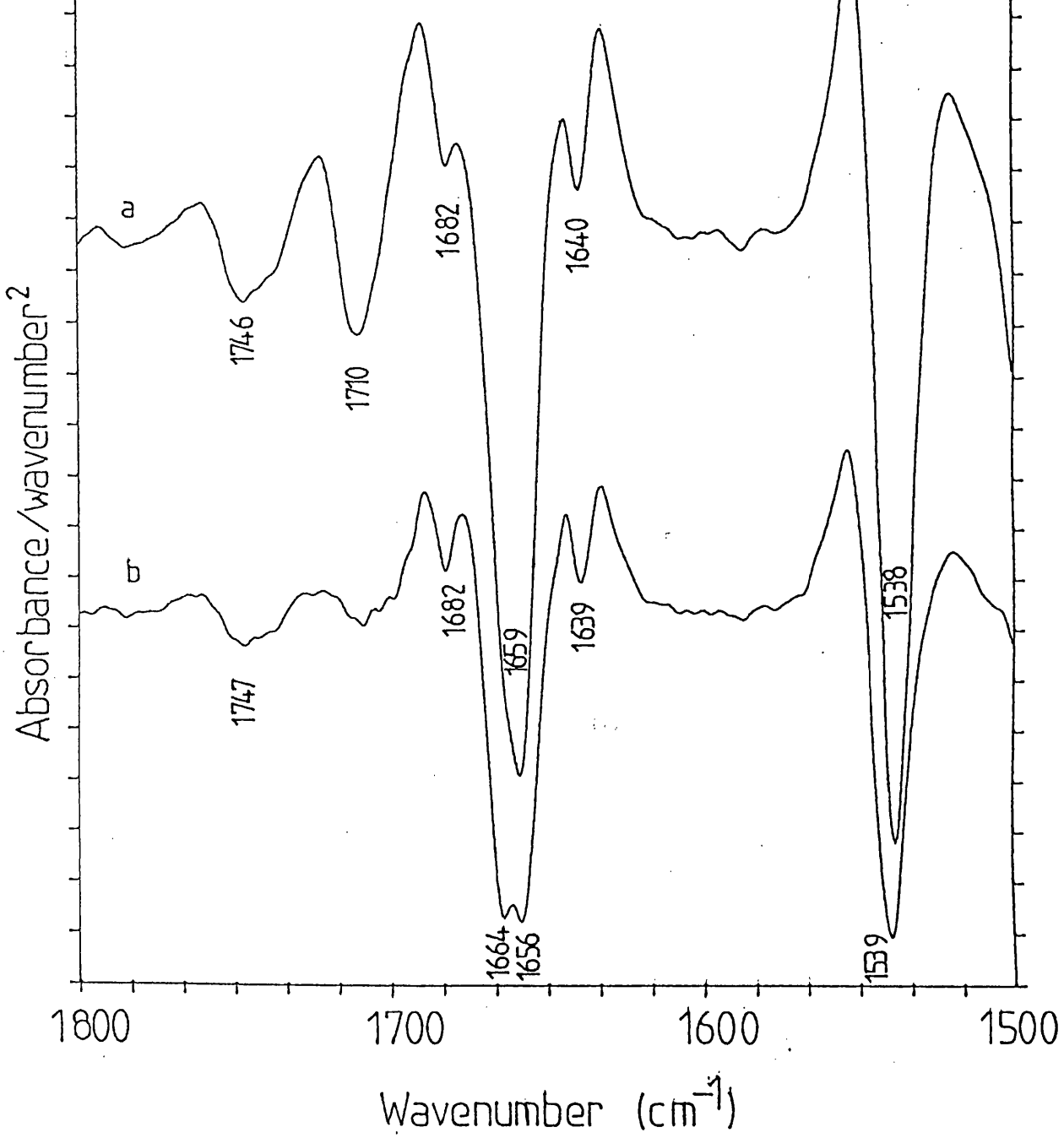
a
b
1746
1710
1682
1640
1747
1682
1659
1639
1538
1664
1656
1539
Absorbance/wavenumber^2
1800
1700
1600
1500
Wavenumber (cm^{-1})

to α- and 3_{10}-helices was achieved using the same resolution enhancement factors, probably due to an improved s/n ratio.

The results of the studies of the pBrZ-(L-Pro-Aib)$_n$-OMe (n= 2 - 5) peptides are given in Table 3.IV. The absorption spectrum of pBrZ-(L-Pro-Aib)$_5$-OMe, with the deconvolved and second derivative spectra, are shown in Fig. 3.10a, b and c, respectively. The absorption spectrum shows two amide I components, the main feature at 1645 cm^{-1}, which we assign to a combination of H-bonded secondary amide and free tertiary amide carbonyls present in a β-bend ribbon, and a smaller component at 1680 cm^{-1}, which we assign to free carbonyl groups. The amide II band is seen at 1538 cm^{-1}. Resolution enhancement techniques identify the position of the high frequency component at 1682 cm^{-1} and resolves a further band at 1661-1658 cm^{-1}. The band at 1736 cm^{-1} is assigned to the free methyl ester carbonyl group.

Table 3-IV. The components of the amide I and amide II bands of pBrZ-(L-Pro-Aib)$_n$-OMe (n = 2 - 5) at 1.5 mM concentration in $CDCl_3$.

n	Amide I	Amide II
5	1682w,1661w,1645s	1538s
4	1682w,1664w,1648s,1641w	1538s
3	1685s,1663s,1644w	1537s
2	1684s,1664w	1536s

s = strong, w = weak

Fig. 3.10a) The FTIR absorption spectrum from 1800 cm^{-1} to 1500 cm^{-1} of pBrZ-(L-Pro-Aib)$_5$-OMe in $CDCl_3$ at 20° C.

b) Deconvolved spectrum of pBrZ-(L-Pro-Aib)$_5$-OMe using bandwidth 12 and resolution enhancement factor 2.125.

c) Second derivative spectrum of pBrZ-(L-Pro-Aib)$_5$-OMe in $CDCl_3$ at 20°C.

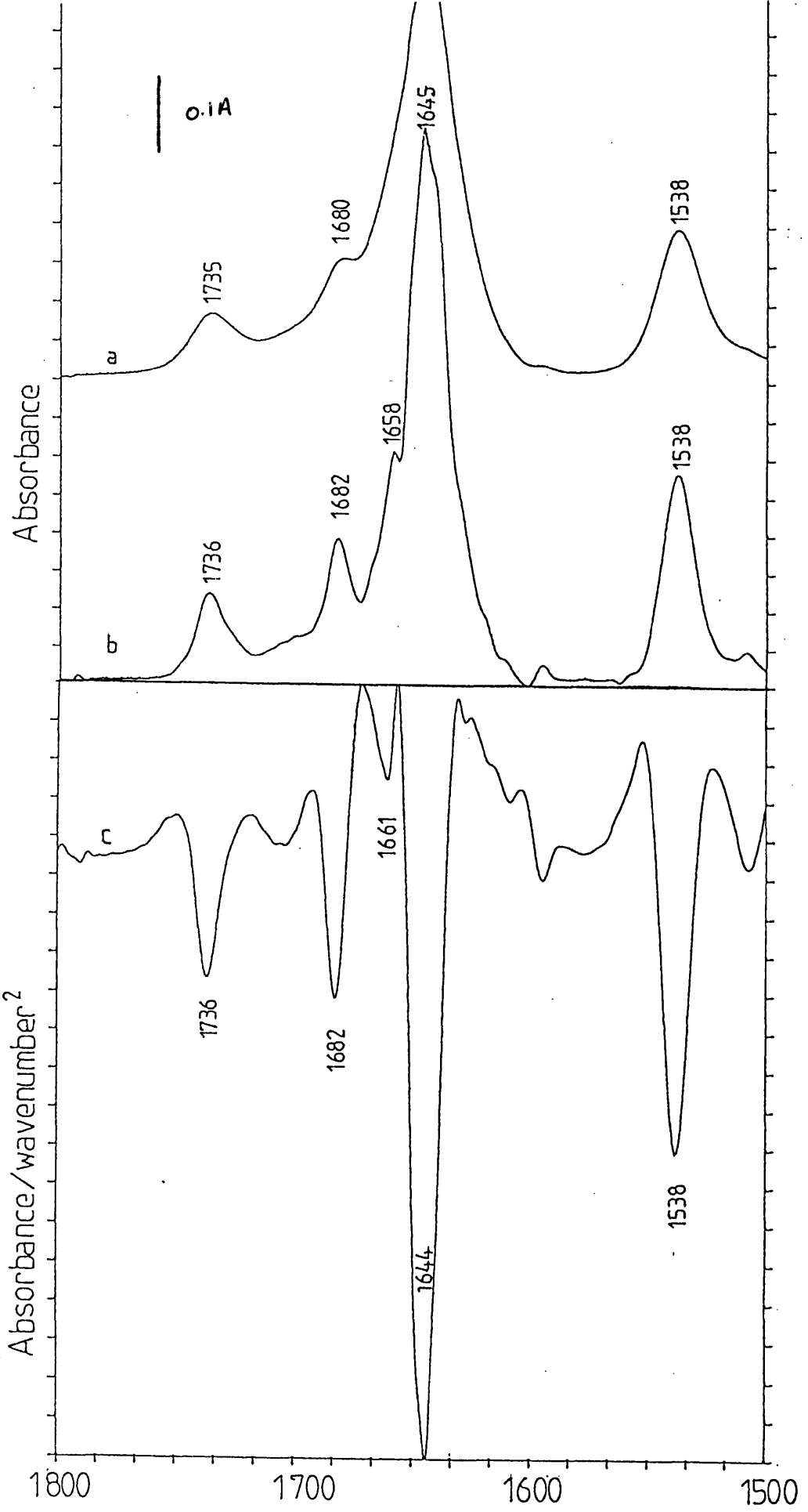
0.1A
1645
1680
1735
1538
a
Absorbance
1658
1682
1736
1538
b
1661
1736
1682
1644
1538
c
Absorbance/wavenumber^2
1800
1700
1600
1500
Wavenumber (cm^{-1})

3.3.2. Studies of peptides in aqueous lipid dispersion

The influence of lipids on the secondary structure of the peptides was investigated using DMPC vesicles. Fig. 3.11a shows the second derivative spectrum of Z-$(Aib)_8$-O*t*Bu in DMPC vesicles at 30° C (above T_m) in H_2O buffer. We assign the bands at 1743 and 1731 cm^{-1} to the lipid ester groups. The amide I band of the peptide exhibits two components, one at 1657 cm^{-1}, characteristic of α-helix, and the other at 1673 cm^{-1}, characteristic of β-turns and/or short, unstable 3_{10}-helix (from Section 3.3.1). We assign the band at 1702 cm^{-1} to the H-bonded urethane carbonyl group and the free tert-butyl ester carbonyl group. The frequencies of the amide I and II bands are unchanged at 20° C (below T_m). Similar results are obtained for Z-$(Aib)_n$-O*t*Bu (*n* = 9,10). The experiment was repeated in D_2O buffer, using Z-$(Aib)_8$-O*t*Bu in DMPC vesicles and the second derivative spectrum is shown in Fig. 3.12a. The spectrum is very similar to that of the sample in H_2O buffer and shows that despite the prolonged incubation in D_2O buffer little, if any, H → D exchange occurs. Similar results were obtained for Z-$(Aib)_n$-O*t*Bu (*n* = 9,10).

The second derivative spectrum of Z-$(Aib\text{-}L\text{-}Ala)_5$-OMe reconstituted in DMPC vesicles in H_2O buffer (Fig. 3.11b) shows two main components at 1652 cm^{-1}, assigned to α-helix, and at 1672 cm^{-1}, which we assign to short, unstable 3_{10}-helix and/or β-turns. The minor band at 1685

Fig. 3.11a) Second derivative spectrum of Z-$(Aib)_8$-O$\underline{t}$Bu in DMPC vesicles (approximate molar ratio 1:15) in pbs buffer, pH 7.4.
b) Second derivative spectrum of Z-$(Aib\text{-}L\text{-}Ala)_5$-OMe in DMPC vesicles (approximate molar ratio 1:15) in pbs buffer, pH 7.4.
c) Second derivative spectrum of Z-L-Ala-$(Aib\text{-}L\text{-}Ala)_5$-OMe in DMPC vesicles (approximate molar ratio 1:15) in pbs buffer, pH 7.4.

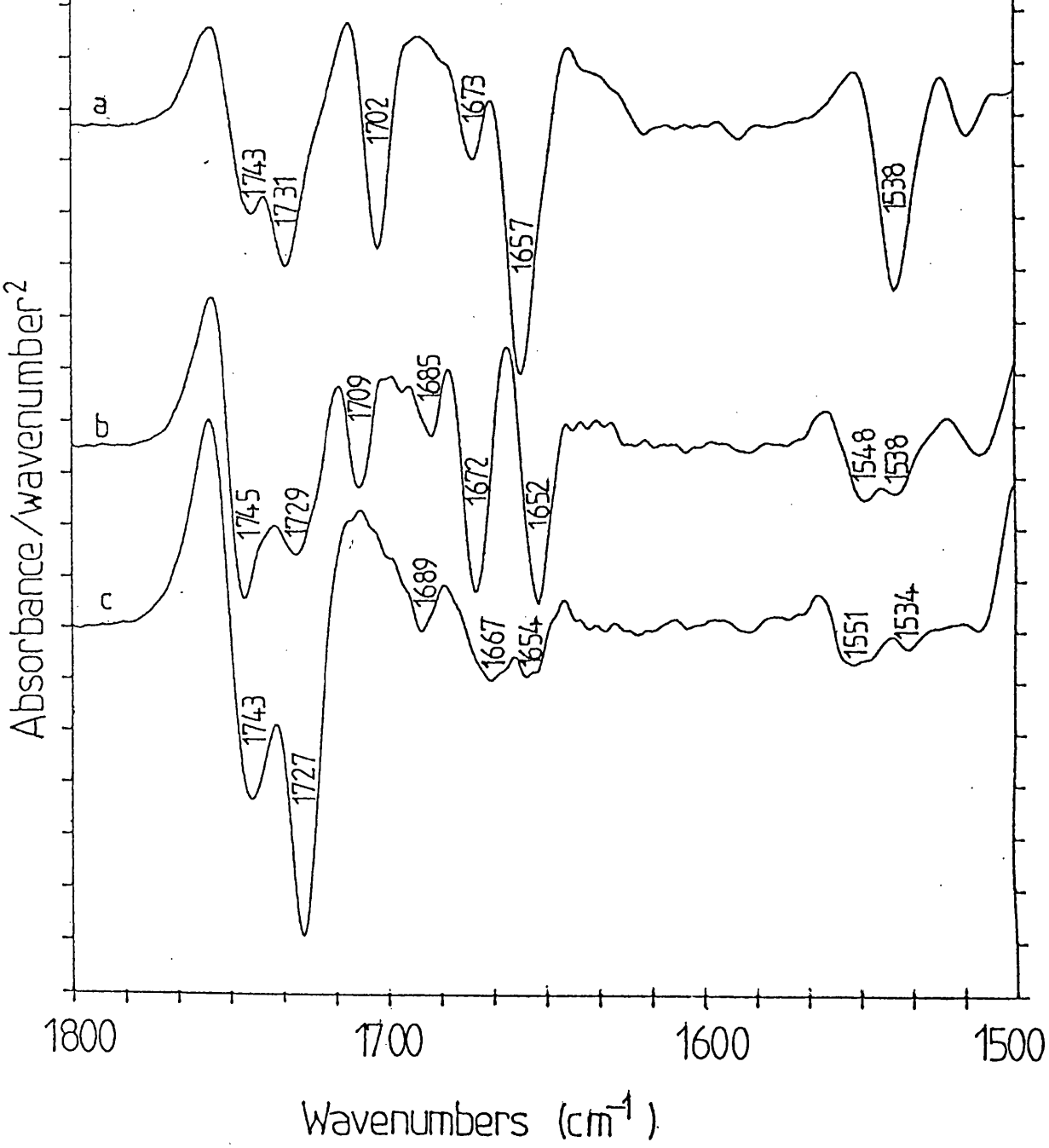
a
1743
1731
1702
1673
1657
1538
b
1709
1685
1745
1729
1672
1652
1548
1538
c
1743
1727
1689
1667
1654
1551
1534
Absorbance/wavenumber^2
1800
1700
1600
1500
Wavenumbers (cm^{-1})

Fig. 3.12a) Second derivative of Z-$(Aib)_8$-OMe in DMPC vesicles (approximate molar ratio 1:15) in pbs buffer, pD 7.4, after incubation at 33° C for 22-24 hours.

b) Second derivative spectrum of Z-$(Aib\text{-}L\text{-}Ala)_5$-OMe in DMPC vesicles (approximate molar ratio 1:15) in pbs buffer, pD 7.4 after incubation at 33° C for 22-24 hours.

c) Second derivative spectrum of Z-L-Ala-$(Aib\text{-}L\text{-}Ala)_5$-OMe in DMPC vesicles (approximate molar ratio 1:15) in pbs buffer, pD 7.4 after incubation at 33° C for 22-24 hours.

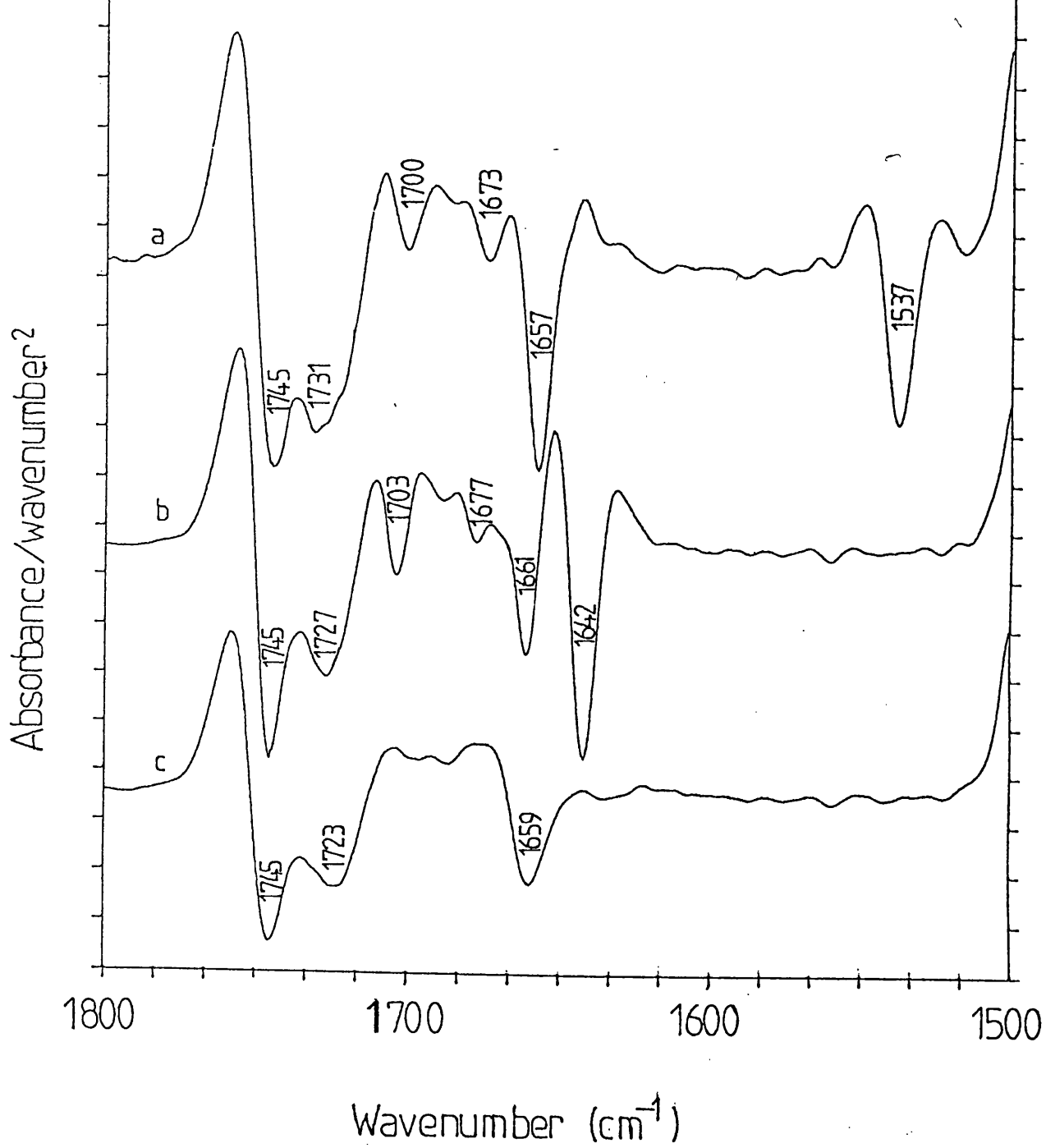
a
b
c
1700
1673
1745
1731
1657
1537
1703
1677
1661
1745
1727
1642
1745
1723
1659
Absorbance/wavenumber^2
1800
1700
1600
1500
Wavenumber (cm^{-1})

cm^{-1} is assigned to β-turns. The sharp band at 1709 cm^{-1} is assigned to the H-bonded urethane carbonyl of the N-protecting group and it is noted that the intensity of this band is greatly increased relative to the intensity in $CDCl_3$. Incubation of the sample in D_2O buffer induced a large shift in the amide II band, indicating a high level of H → D exchange. The second derivative spectrum (Fig. 3.12b) has components at 1677 cm^{-1}, which we assign to β-turns, 1661 cm^{-1}, assigned to exchanged 3_{10}-helix, and 1642 cm^{-1} which we assign to exchanged α-helix (see Section 3.4).

The second derivative spectrum of Z-L-Ala-(Aib-L-Ala)$_5$-OMe in DMPC vesicles in H_2O buffer (Fig. 3.11c) shows the main components of the amide I band at 1667 cm^{-1}, assigned to 3_{10}-helix, and 1654 cm^{-1}, assigned to α-helix. The intensity of the amide I absorption in this experiment is relatively weak and we were unable to improve on this result when repeating the experiment. The incubation of Z-L-Ala-(Aib-L-Ala)$_5$-OMe incorporated in DMPC vesicles in D_2O buffer caused the disappearance of the amide II band, indicating a high level of H → D exchange. The second derivative spectrum (Fig. 3.12c) shows the major amide I component at 1659 cm^{-1}. This is too high to be deuterated α-helix and therefore we assign the band to deuterated 3_{10}-helix, possibly with a contribution from α-helix. The small component at 1685 cm^{-1} is assigned to β-turn structures.

The second derivative spectrum of pBrZ-(L-Pro-Aib)$_5$-

Fig. 3.13a) Second derivative spectrum of pBrZ-(L-Pro-Aib)$_5$-OMe in DMPC vesicles (approximate molar ratio 1:15) in pbs buffer, pH 7.4.

b) Second derivative spectrum of pBrZ-(L-Pro-Aib)$_5$-OMe in DMPC vesicles in pbs buffer, pD 7.4 after incubation at 33° C for 22-24 h.

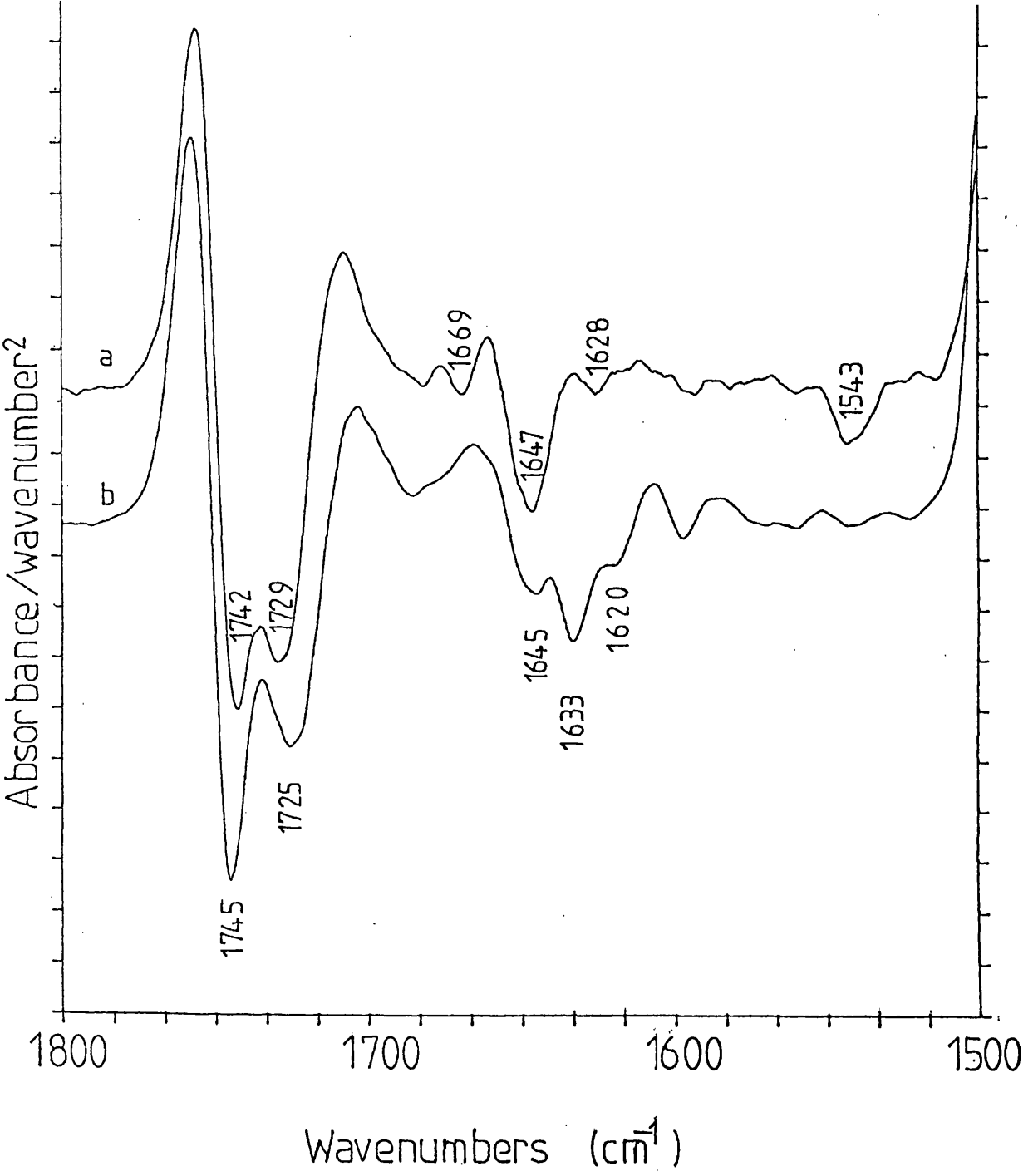
a
b
1745
1742
1729
1725
1669
1647
1645
1633
1628
1620
1543
1800
1700
1600
1500
Absorbance/wavenumber²
Wavenumbers (cm⁻¹)

OMe reconstituted in DMPC vesicles in H_2O buffer (Fig. 3.13a) gives the main amide I component at 1647 cm^{-1}, assigned to β-bend ribbon with smaller components at 1669 cm^{-1} assigned to β-turns, and the component at 1628 cm^{-1} tentatively assigned to aggregated peptides. The use of D_2O buffer causes H → D exchange in the peptide and the second derivative spectrum (Fig. 3.13b) shows three amide I components; 1633 cm^{-1} assigned to exchanged β-bend ribbon, 1645 cm^{-1} assigned to unexchanged β-bend ribbon and 1620 cm^{-1}, assigned to aggregated peptides.

3.4. DISCUSSION

The interpretation of the 1750-1700 cm^{-1} region of the IR absorption spectrum for these peptides is complicated by the presence of the N- and C-terminal protecting groups. These groups are required to protect the peptides during synthesis. The urethane C = O of the benzyloxycarbonyl protecting group is the acceptor of the first H-bond. A free urethane C = O occurs at a frequency > 1725 cm^{-1}, whereas the band from a H-bonded urethane C = O occurs at 1720-1715 cm^{-1} (Pulla Rao et al., 1980; Bonora et al., 1984). However the carbonyl of the tert-butyl ester group also occurs at 1720-1715 cm^{-1}, whilst the band from the carbonyl of the methyl ester occurs at 1740-1730 cm^{-1}.

In all the 3_{10}-helical peptides examined in the present study, the last two carbonyl groups are not H-bonded to NH groups (Fig. 3.1). As the number of Aib residues decreases, the absorption of the two free peptide carbonyls become relatively stronger with respect to that of the H-bonded peptide carbonyls. From Table 3.I as n decreases, the relative increase in intensity of the band centred around 1687-1677 cm^{-1} indicates that this band arises from free peptide carbonyls. The increase in intensity of the band in the range 1666-1662 cm^{-1} as n increases indicates that this is due to H-bonded peptide carbonyls. This frequency range, coupled with the position of the amide II at 1533-1531 cm^{-1}, agrees well

with the calculated frequencies of Krimm & Bandekar (1980) for the 3_{10}-helical structure.

The two minor components of the amide I band for the Z-$(Aib)_n$-O$\underline{t}$Bu ($\underline{n}$ = 8 - 10) homopeptides occur at 1681-1679 cm^{-1} and 1646-1644 cm^{-1}. These components remain after the sample has been diluted to a concentration approximately four times below the minimum level for self-aggregation, indicating that they derive from secondary structures present within the monomeric peptides. The observed frequencies agree well with the predicted values of 1686 and 1646±3 cm^{-1} for type III β-turn absorptions. Therefore, we assign the band at 1646-1644 cm^{-1} to type III β-turns, and the band at 1681 cm^{-1} to type III β-turns and/or free carbonyls.

We interpret the spectral shift observed with the Z-$(Aib)_n$-O$\underline{t}$Bu ($\underline{n}$= 8-10) peptides in DMPC vesicles to indicate that the peptides shift from a 3_{10}-helical conformation in $CDCl_3$ (1666-1662 cm^{-1}) to mainly α-helical (1657 cm^{-1}), with a contribution from β-turns and/or short unstable 3_{10}-helix (1673 cm^{-1}) in aqueous lipid dispersion. No further change in the peptide secondary structure is detected upon raising the temperature from below to above the phase transition temperature of the lipid. The asymmetrical geometry of the four substituents on the C^{α} carbon in the Aib residue required to stabilise the 3_{10}-helical conformation is lost when the peptide is inserted into a lipid bilayer,

making the α-helical structure more energetically favourable. Karle et al., (1988, 1989a) have shown that two different conformations are possible for the same Aib-rich peptide in its crystalline form, illustrating the sensitivity of the peptide secondary structure to its particular environment.

The inability of the peptide to undergo H → D exchange when incorporated in DMPC vesicles indicates the inaccessibility of the peptide to D_2O molecules in this environment.

We interpret the spectral changes observed when the peptide Z-(Aib-L-Ala)$_5$-OMe is incorporated into an aqueous lipid dispersion to indicate that 3_{10}- and α-helical structures are still present. The frequencies of the 1652 and 1642 cm^{-1} bands assigned to α-helix in the undeuterated and deuterated peptides respectively, are both low for regular α-helices. Karle et al. (1989b,c) reported the insertion of water molecules into the helical backbone of the apolar peptides Boc-Ala-Leu-Aib-Ala-Leu-Aib-OMe (Karle et al., 1989b) and Boc-Aib-(Val-Ala-Leu-Aib)$_3$-OMe (Karle et al., 1989c) when each was crystallised individually. In the first example, H-bonds are formed between the water and the C ═ O and NH groups of the Ala residues. This causes a bend in the backbone of the peptide and also increases the length of at least one of the intramolecular hydrogen bonds. This is similar to the highly solvated α-helical structure observed for troponin C, in which the intramolecular H-

bonding pattern of the B-helix is modified by approximately 20% of the C == O groups forming two H-bonds, one to NH groups and one to water molecules inserted into the helical backbone. This leads to a low frequency IR absorption for the solvated α-helix (Jackson et al., 1991). The rapid and almost complete deuteration of these peptides in the membrane also agrees with this hypothesis.

An increase in the intensity of the band assigned to the H-bonded urethane carbonyl grouped may indicate intermolecular H-bonding of this group in the peptide aggregate in the lipid environment, or possibly indicate H-bonding to the lipid headgroup.

The H → D exchange of Z-(Aib-L-Ala)$_5$-OMe and Z-L-Ala-(Aib-L-Ala)$_5$-OMe when incorporated in lipid vesicles indicates that in this environment the hydrogen atoms of the amide NH groups are readily accessible to D_2O molecules. This would tend to indicate that the peptides aggregate to form pores in the bilayer which allows the passage of water molecules. This would be similar to the model proposed by Fox and Richards (1976) for the action of alamethicin in which the protein aggregates in the membrane to form a pore.

The amide I band of Z-L-Ala-(Aib-L-Ala)$_5$-OMe incorporated in DMPC vesicles in H_2O buffer indicates the presence of two distinct components in the second derivative spectrum, at 1667 cm^{-1} and 1654 cm^{1}, assigned

to 3_{10}- and α-helix respectively. The same sample in D_2O buffer shows one strong feature at 1659 cm^{-1}. Assuming that the peptide adopts the same secondary structure in D_2O as in H_2O buffer, this band is assigned to deuterated 3_{10}-helix overlapping with non-deuterated α-helix. This is possible as the H-bonds in the 3_{10}-helix are weaker than in α-helix and exchange more readily.

NMR and IR absorption spectroscopy results for Z-(Aib-L-Pro)$_4$-OMe (Venkatachalapathi et al., 1981) indicate that the H-bonds formed may be slightly different from those of an ideal 3_{10}-helix due to the steric hindrance introduced by the presence of Pro residues. Unfavourable steric contacts required for an ideal 3_{10}-helix may be relaxed in this peptide by slight distortions introduced by nonplanar peptide units and deviations from the ideal 3_{10}-helical angles. These effects may alter the strength of the intramolecular H-bonds to produce the amide I absorption maximum at 1648-1645 cm^{-1} for pBrZ-(L-Pro-Aib)$_5$-OMe which is assigned to β-bend ribbon.

Incorporation of this peptide into DMPC vesicles produces very little effect on the amide I and II bands. The increased steric hindrance of the Pro-Aib peptides will reduce the number of possible conformations available and will require large perturbations to induce change. However, the peptide pBrZ-(L-Pro-Aib)$_5$-OMe does undergo H → D exchange when incorporated into DMPC vesicles in D_2O buffer, indicating that a pore may be

formed by aggregates of the peptide within the lipid bilayer. This is also supported by the observation of intermolecular β-sheet under these conditions.

Comparison of the results of peptides in aqueous lipid dispersion with those in $CDCl_3$ indicates that the secondary structure of the peptides differ in each environment. Organic solvents are frequently used in both NMR and CD spectroscopy because lipid aggregates hamper data collection due to line broadening effects from restricted protein mobility, and light scattering effects, respectively. Halogenated alcohols, especially trifluorethanol (TFE), are excellent solvents for proteins (Carver & Collins, 1990) and are frequently used when membrane mimetic solvents are required. However the dielectric constants of halogenated alcohols (> 20) are much greater than of biological membranes (typically 1). Furthermore, halogenated alcohols contain a potent hydrogen bond donor which may disrupt the native secondary structure of the protein (Jackson & Mantsch, 1991a). Dimethyl sulphoxide (DMSO; $(CH_3)_2SO$), another commonly used organic solvent, progressively disrupts the native secondary structure of the protein as the percentage of DMSO in H_2O increases due to the competition between the solvent S = O and peptide C = O groups to hydrogen bond to the peptide N — H groups (Jackson & Mantsch, 1991b). These studies indicate that solvents require more than just the property of low

polarity to mimic the membrane. Furthermore, the fact that solvents are more fluid than biomembranes may have consequences on the peptide structure.

$CDCl_3$ was used in this study because the structure of these peptides has been determined in this solvent by NMR spectroscopy. However these results raise questions over the suitability of $CDCl_3$ as a membrane-mimetic solvent.

3.5. SUMMARY

The primary aim of this work was to characterise the resolution enhanced FTIR spectra of peptides known, from X-ray diffraction and NMR studies, to contain 3_{10}-helical, mixed α- and 3_{10}-helical, and β-bend ribbon secondary structures. Studies of the peptides known to contain stable 3_{10}-helix in $CDCl_3$ show the main amide I absorption occurs at 1666-1662 cm^{-1} and the amide II band at 1533-1531 cm^{-1}. Resolution enhancement methods revealed small contributions at 1681-1678 cm^{-1}, assigned to free carbonyls and/or type III β-turns, and at 1646-1644 cm^{-1}, assigned to type III β-turns. Peptides known to contain both α- and 3_{10}-helices in their structure exhibit IR absorption bands characteristic of both types of conformation. Peptides known to fold into the β-bend ribbon structure show an amide I band maximum at 1648-1645 cm^{-1} with the amide II band at 1538-1536 cm^{-1}.

The secondary aim of this work was to investigate the effect of incorporation of these peptides into model membrane structures, e.g. DMPC vesicles, in aqueous buffer. Those peptides which possess a 3_{10}-helical structure in $CDCl_3$ solution change their secondary structure in DMPC vesicles to predominantly α-helical, with a contribution from β-turns and/or short, unstable 3_{10}-helix. These peptides are unable to undergo H → D exchange when the system is in D_2O buffer, indicating that they are unlikely to aggregate to form a pore

capable of allowing water molecules to pass through.

Those peptides which contain a combination of α- and 3_{10}-helical structures in $CDCl_3$ solution tend to retain some 3_{10}-helical structure within the lipid environment, although the overall H-bonding pattern is altered. This result, and those of the pure 3_{10}-helices, indicates that using a low polarity solvent to mimic the conditions of the lipid bilayer is not valid for these conformationally sensitive peptides. H → D exchange occurs rapidly for the $(Aib\text{-}L\text{-}Ala)_n$ peptides, indicating the probable aggregation of peptides to form pores in the lipid bilayer, which allow the passage of water molecules. The low frequency of the band assigned to α-helix in these spectra may indicate the interruption of the helix by water molecules H-bonded to the C == O groups of the peptide backbone.

Those peptides known to contain β-bend ribbon structure appear to be largely unaffected by the membrane environment, probably due to the severe steric hindrance of the amino acid chains.

This study represents the first complete characterisation of a pure 3_{10}-helix and a pure β-bend ribbon by FTIR spectroscopy using resolution enhancement techniques.

CHAPTER FOUR

PROBING THE MECHANISMS OF SPONTANEOUS PROTEIN INSERTION INTO MEMBRANES USING FTIR SPECTROSCOPY

4.1. INTRODUCTION

Protein insertion into a membrane necessitates the switch of the polypeptide chain from a water-soluble conformation to one that is more stable in the lipid bilayer. Two contrasting views of the process of insertion of membrane proteins into, and transport of secreted proteins across, the membrane bilayer have been proposed. The view that the motion of proteins across the membrane during protein synthesis is facilitated by specific protein assemblies within the bilayer has been put forward (Blobel & Dobberstein 1975; Nicchitta et al., 1991; Lingappa 1991). However Bretscher (1973) and Wickner (1979) considered that such specific protein assemblies were not required. However, the energy requirements and the three-dimensional structure, of the polypeptide backbone during insertion in either model are only beginning to be considered.

Experimental and theoretical prediction evidence of a number of membrane proteins, such as bacteriorhodopsin from Halobacterium halobium (Henderson et al., 1990), the photosynthetic reaction centre of Rhodopseudomonas viridis (Deisenhofer et al., 1985), rhodopsin (Findley & Pappin 1986; Haris et al., 1989) and the membrane-spanning sequences of the Ca^{2+} ATPase (MacLennan et al., 1985) indicate that the α-helix is the dominant secondary structure in the membrane. However one widely studied exception to these proteins is the porin matrix, a

membrane protein from Gram-negative bacteria which are neither α-helical nor hydrophobic. Porin forms assemblies of β-sheets stabilised by a dense network of H-bonds (Jap et al., 1991; Weiss et al., 1990; Nabedryk et al., 1988).

Furthermore, there has been a lot of work recently on the action of signal sequence polypeptides. These are part of the nascent protein containing a hydrophobic stretch from ten to fifteen residues long. As well as being essential for efficient and selective targeting of nascent protein chains either to the endoplasmic reticulum in eukaryotes, or to the cytoplasmic membrane in prokaryotes, they play a central role in the translocation of proteins across membranes. The signal sequence is cleaved after translocation. Surprisingly, signal sequences display a remarkable lack of primary sequence homology, even in closely-related proteins. Not all secretory and plasma proteins contain an amino-terminal signal sequence that is cleaved following translocation across the endoplasmic reticulum. Some proteins (e.g. ovalbumin) contain an internal signal sequence that serves the same function.

Structural studies have been carried out on a number of isolated signal sequences (for review, see Gierasch 1989). The structures observed for the sequences in aqueous solution tend to be random and/or β-structure. However, as the sequences are sparingly soluble in aqueous buffer, aggregation may occur. In the membrane environment, the α-helix motif tends to be adopted.

The secondary structure arrangement of proteins during spontaneous membrane insertion or transport across the membrane has been approached theoretically by Engelman & Steitz (1981). In a non-aqueous environment, where the possibility of groups forming H-bonds with water is absent, the free energy of each H-bonded pair compared to the unpaired state is 5.8 kcal/mol (Allen 1975). To avoid the large free energy cost of transferring an unsatisfied H-bond donor or acceptor from an aqueous to non-polar environment, or of the breaking of H-bonds in the non-polar environment, polypeptides containing a maximum number of H-bonds are more energetically favourable. As β-sheet structures contain a number of unpaired H-bonds, the most favourable secondary structure motifs in the non-polar membrane, in which most stable H-bonds in the polypeptide backbone will be formed, are the α- and 3_{10}-helices (Engelman & Steitz 1981). Therefore spontaneous insertion of a soluble protein into the membrane is thought to occur via a helical structure from the hydrophobic core of the soluble protein inserting into the bilayer. As the 3_{10}-helix has now been fully characterised by FTIR spectroscopy (see Chapter Three), it is possible to investigate the helical hairpin hypothesis using this technique. This chapter describes the experiments on the spontaneous insertion of a predominantly α-helical soluble protein, colicin A, and a predominantly β-sheet

soluble protein, aerolysin, into model membranes in order to gain experimental evidence concerning the method of insertion.

Studies on colicins have recently advanced our understanding of the insertion processes. Colicins are a family of plasmid-encoded protein antibiotics, such as colicin A, E_1, K and I_B with molecular weights of 60 - 80 kDa which kill bacteria closely related to the producing strain by depolarising the bacterial inner membrane (Parker et al., 1989). This is achieved by the insertion of part of the protein into the membrane, forming a voltage-gated ion channel (Schein et al., 1978; Konisky, 1982; Pattus et al., 1983). Colicins are also known to form voltage-gated ion channels in artificial planar bilayers (Frenette et al., 1989), and have been reconstituted with liposomes (Massotte et al., 1989).

The C-terminal, thermolytic fragment of colicin A (amino acid residues 389 - 592, with a molecular weight of 21 kDa) carries the pore-forming activity (Martinez et al., 1983). The X-ray diffraction structure of the soluble fragment reveals that it contains ten closely-packed α-helices (Parker et al., 1989), and, based on these results, a mechanism of membrane insertion has been proposed. It suggests that the fragment interacts with negatively-charged lipids in the membrane, and a helical hairpin from the hydrophobic core of the protein inserts into the membrane, perpendicular to the membrane surface. As this occurs, the fragment opens like an umbrella, with

the amphipathic helices lying parallel to the membrane surface. This may then be followed by oligomerisation of the protein to form voltage-gated ion channels.

An FTIR study of the thermolytic fragment of colicin E_1 has been published recently (Rath et al., 1991) which indicates that this peptide is predominantly α-helical when inserted into model membranes at pH 7.0, with low levels of β-structure. It also indicates that the average orientation of the helices is less than 55° relative to the membrane normal. However it is known that only 70-80 residues of this protein inserts under the experimental conditions (Morlon et al., 1988).

Aerolysin is a soluble, hydrophilic protein that forms pores in biomembranes and is largely responsible for the pathenogicity of Aeromonas Hydrophilia (Chakraborty et al., 1986). There are two precursor forms of the protein. Preproaerolysin contains a signal sequence polypeptide which is removed cotranslationally as the protein crosses the inner bacterial membrane. The protoxin, proaerolysin, is exported from the bacteria, and proteolytic removal outside the cell of 25 amino acids from the C-terminus yields the mature toxin (Buckley & Howard, 1985). Both the protoxin and the toxin can bind to membranes. However only the mature form of the toxin aggregates to form 3 nm diameter channels in the membrane, causing cell disruption (Howard & Buckley, 1982; Garland & Buckley, 1988). Aggregation of the mature

toxin is reversed in the presence of high concentrations of urea, indicating that covalent bonds are not formed in the aggregated state. Aerolysin binds with high affinity to a receptor in eukaryotic membranes which has been tentatively identified as glycophorin in rat erythrocytes, and also binds to artificial liposomes (Howard & Buckley, 1982). Furthermore, spontaneous aggregation of the mature toxin occurs at concentrations of 0.5 mg/ml or above, but can be prevented by the presence of Zn^{2+} ions (Buckley 1990). The protoxin remains soluble at high concentrations in the absence of Zn^{2+} ions.

The protein and its precursor are thought to be predominantly β-sheet in the soluble form based on preliminary X-ray crystallography results. From the amino acid sequence, the protein is quite hydrophilic, and has no obvious sequences which could form transbilayer helices (Green & Buckley, 1990).

The experiments presented in this chapter help elucidate the secondary structure of the pore-forming fragment of colicin A in solution, and inserted into a model biomembrane. It also provides the first direct experimental observations of the secondary structure of aerolysin, and proaerolysin, in solution and in the lipid environment.

4.2. MATERIALS AND METHODS

4.2.1. Colicin A

Colicin A and its pore-forming fragment were purified as described previously (Cavard & Lazdunski, 1987; Tucker et al., 1986) and were a generous gift from Dr. Franc Pattus, EMBL, Germany. Dimyristoyl phosphatidylglycerol (DMPG) and D_2O (99.9 atom % D) were purchased from Sigma, U.K.

Samples were prepared using a protein concentration of 20 mg/ml in buffer containing 20 mM MES, 100 mM NaCl at pH 5.0, or pH 7.0. The lyophilised protein was added to the buffer and, after vortexing for a few minutes, the solution was spun in a bench top centrifuge for 15 minutes to pellet any insoluble fraction in the preparation. The clear supernatant was used in the experiments, and the insoluble precipitate was discarded.

Samples in D_2O buffer were prepared by dissolving the lyophilised protein in H_2O buffer and centrifuging to as described above. The samples were then dialysed against D_2O buffer and concentrated using Amicon micro-concentrators, having a molecular weight cutoff of 10 kDa.

Samples used for D_2O experiments were incubated for at least 12 hours at 30° C, or at the temperature stated in the text.

Samples containing lipid were prepared by sonicating 3.5 mg of DMPG in 50 μl buffer above the phase transition

temperature for 15 minutes. The protein was added and vortexed to ensure mixing of the components.

4.2.2. Aerolysin

Proaerolysin was purified as described by Buckley (1989) and was a generous gift from Dr. Tom Buckley, University of Victoria, Canada.

Samples were prepared from a solution of approximately 1 mg/ml proaerolysin in buffer containing 20 mM Tris, 150 mM NaCl, pH 7.4. Some samples were dialysed against D_2O buffer containing 20 mM Tris, 150 mM NaCl, pD 7.4, washed and concentrated using an Amicon micro-concentrator to yield a protein concentration of approximately 2 - 5 mg/ml.

Conversion to the mature protein was accomplished by treatment with trypsin (protein: trypsin weight ratio 1000 : 1) for 15 minutes in H_2O buffer containing Zn^{2+} ions, pH 6.8 (J.T. Buckley, private communication). Tryptic digestion was stopped by the addition of excess PMSF. The sample was then dialysed against D_2O buffer to remove the cleaved polypeptide, trypsin and PMSF, and concentrated as described above.

For the membrane binding experiments, liposomes were prepared by dissolving dimyristoyl phosphatidylcholine (DMPC), cholesterol and dicetyl phosphate, in the molar ratio 7:2:1, in chloroform. After drying under N_2 gas and then under vacuum, buffer was added and the sample sonicated at 37° C. To prevent the mature toxin from

aggregating before interacting with the liposomes, the protoxin was incubated with the liposomes, and then trypsin was added. This allows the conversion of the protoxin to mature toxin and reduces the probability of the mature toxin aggregating outside the membrane.

The instrument conditions for collecting the FTIR spectra were the same as described in Section 3.2.

4.3.RESULTS

4.3.1. Colicin A

The absorption spectrum in the range 1800 - 1500 cm^{-1} of the pore-forming fragment of colicin A in H_2O buffer, pH 7.0 is given in Fig. 4.1a (upper trace). The two main absorption bands present are assigned to the amide I and II vibrations, centred at 1657 cm^{-1} and 1551 cm^{-1}. All band assignments are made are taken from Susi & Byler (1986), Chirgadze et al. (1975), Byler & Susi (1986), Krimm & Bandekar (1986) and Jackson et al. (1989).

The deconvolved and second derivative spectra of the pore-forming fragment are shown in Figs. 4.1a (lower trace) and 4.1b, respectively. The predominant band at 1656 cm^{-1} in the spectra can be assigned to α-helical and/or random structures. Further components present within the amide I band are at 1682 cm^{-1}, assigned to β-turns, at 1613 cm^{-1} assigned to tyrosine side chains, and at 1638 cm^{-1}. This weak feature may be associated with a small amount of β-sheet, either within the protein or from any remaining insoluble fragment, or from sidechain absorptions of arginine and lysine.

No differences between the pore-forming fragment at pH 7.0 and pH 5.0 were observed in the resolution-enhanced spectra (not shown).

Further information can be gained about the secondary structure can be gained by studying the samples in D_2O buffers. The absorption spectrum of the pore-forming

Fig. 4.1a) Absorption spectrum from 1800 cm^{-1} to 1500 cm^{-1} of the thermolytic fragment of colicin A in H_2O buffer (5% w/v), pH 7.0, (upper trace), with its deconvolved spectrum, using resolution enhancement factor 2.25 and bandwidth 11 cm^{-1} (lower trace).

b) Second derivative spectrum of colicin A in H_2O buffer, pH 7.0.

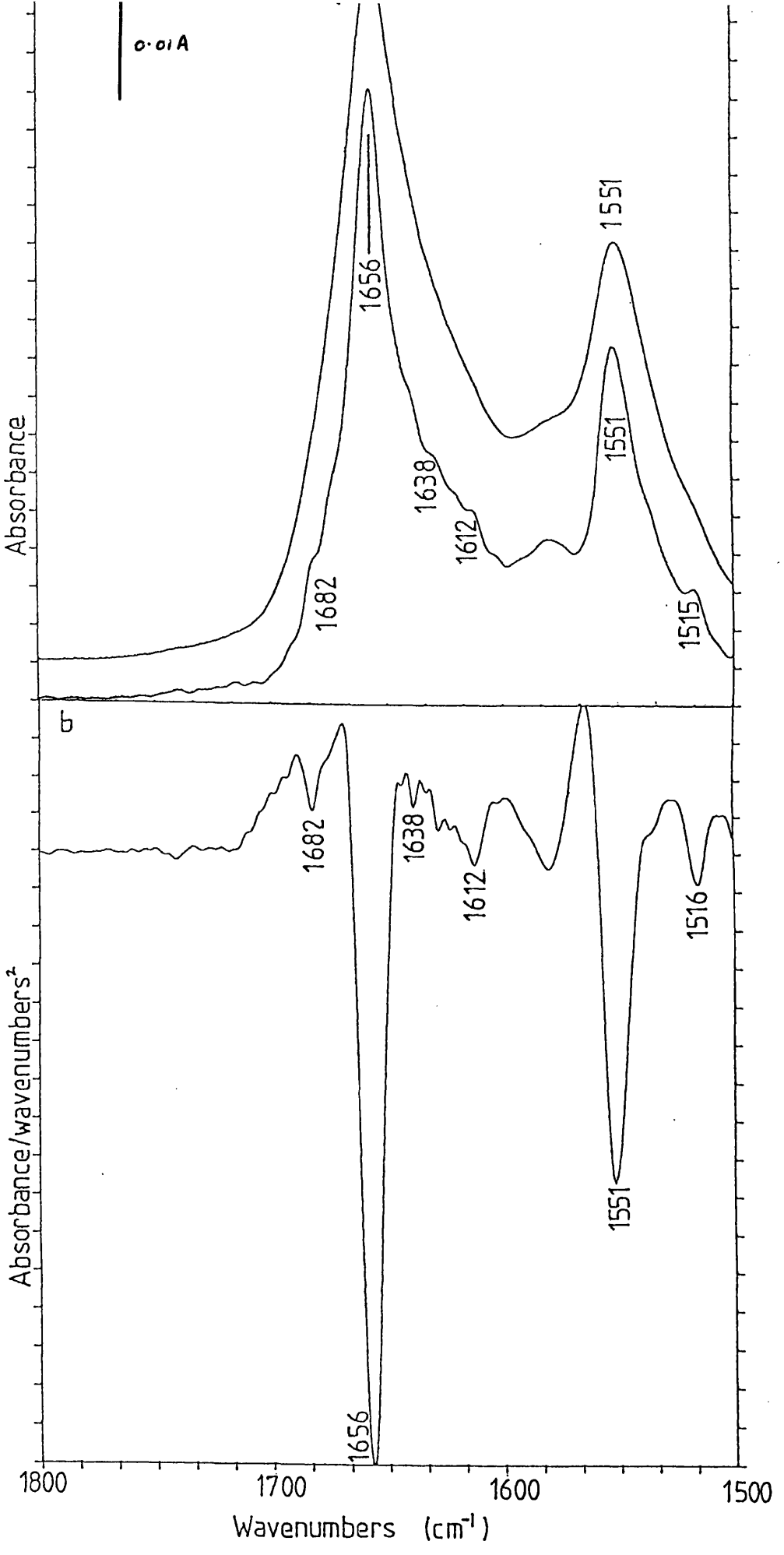
0·01A
Absorbance
1656
1551
1638
1612
1682
1551
1515
b
1682
1638
1612
1516
1551
1656
Absorbance/wavenumbers²
1800
1700
1600
1500
Wavenumbers (cm⁻¹)

fragment in D_2O buffer, pD.7.0, is shown in Fig. 4.2a (upper trace), showing the amide I' band at 1651 cm^{-1}, with the deconvolved spectrum (Fig. 4.2a lower trace). The second derivative spectra shown in Figs. 4.2b are of the sample at pD 7.0 (upper trace) and pD 5.0 (lower trace), respectively. The band positions, with assignments, are as follows: 1656-1657 cm^{-1} from unexchanged α-helix, 1672-1674 cm^{-1} from exchanged β-turns, 1643 cm^{-1} from exchanged random structures, 1584-1585 cm^{-1} from ionised carboxylate sidechains of aspartate residues, 1548-1549 cm^{-1} from amide II band, indicating that the protein has not undergone complete H → D exchange, and 1513-1514 cm^{-1} from tyrosine sidechains.

Using D_2O buffers, differences were observed in the second derivative spectra at pD 7.0 and pD 5.0 (Fig. 4.2b). A reduction in intensity of the band at 1643 cm^{-1}, assigned to exchanged random coil, occurs at pD 5.0.

The thermolytic fragment did not undergo any significant rearrangement of conformation between 20°C and 85°C at pD 5.0 or pD 7.0. However the main band in the resolution-enhanced spectra did shift from 1656 cm^{-1} to 1649 cm^{-1} at high temperatures, indicating an increased amount of H → D exchange in the α-helices with temperature.

The absorption spectrum of the thermolytic fragment of colicin A in the presence of DMPG liposomes above

Fig. 4.2a) Absorption spectrum of colicin A in D_2O buffer, pD 7.0, (upper trace), with its deconvolved spectrum, using resolution enhancement factor 2.125 and bandwidth 14 (lower trace).

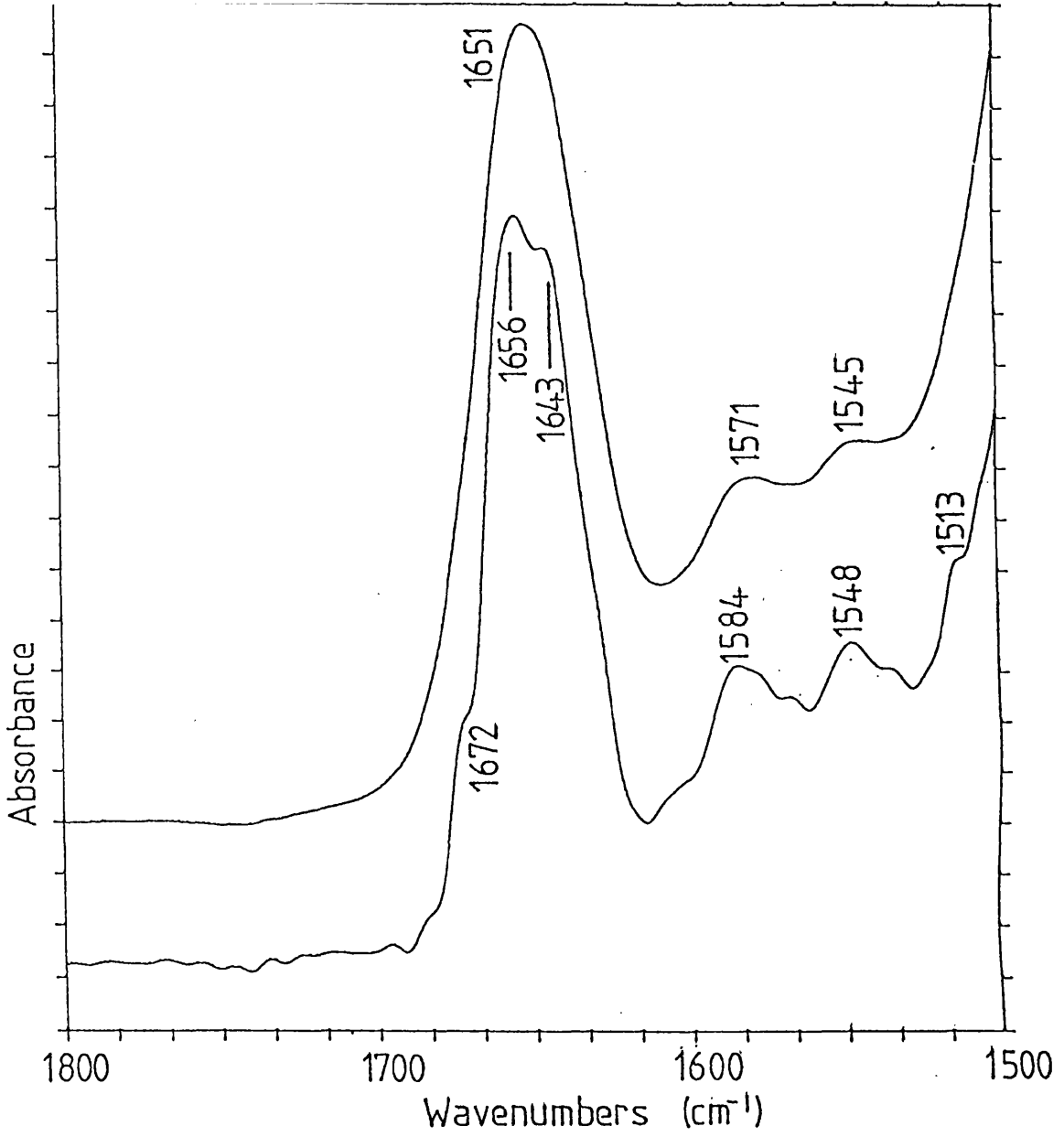
1651
1656
1643
1571
1545
1584
1548
1513
1672
Absorbance
1800
1700
1600
1500
Wavenumbers (cm⁻¹)

Fig. 4.2b) Second derivative spectra of colicin A in D_2O buffer, pD 7.0 (upper trace) and pD 5.0 (lower trace).

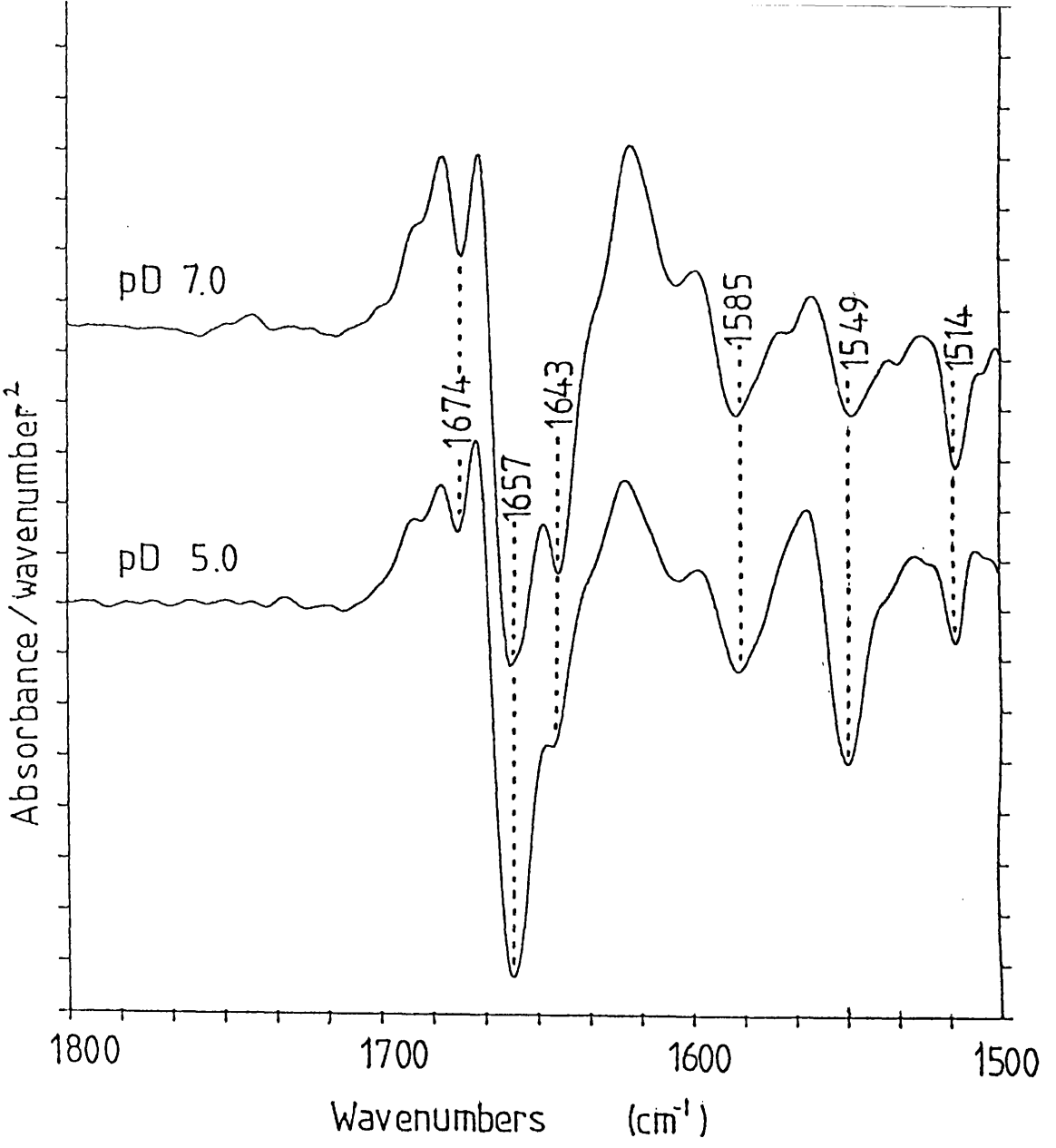
pD 7.0
pD 5.0
1674
1657
1643
1585
1549
1514
Absorbance / wavenumber^{-2}
1800
1700
1600
1500
Wavenumbers (cm^{-1})

phase transition temperature in H_2O buffer is shown in Fig. 4.3a, with the second derivative shown in Fig. 4.3b. From Fig. 4.3b, the bands at 1739 cm^{-1} and 1724 cm^{-1} are from the lipid ester carbonyl groups. The main component of the amide I band absorption appears at 1654 cm^{-1} and is assigned to α-helices. This is 2 cm^{-1} lower than the band assigned to α-helices in the spectrum of the soluble protein. The band at 1685 cm^{-1} is assigned to β-turns with a possible contribution from β-sheet, at 1633 cm^{-1} to β-sheet and arginine and lysine absorptions, at 1615 cm^{-1} to tyrosine sidechains.

Incubating the thermolytic fragment of colicin A with DMPG vesicles in D_2O buffer, pD 5.0, at 30° C (below phase transition temperature) produced no difference in the protein spectrum when compared to the sample in the absence of lipids. Raising the temperature of the sample above the phase transition temperature of the lipid produced an immediate change in the absorption spectrum and is illustrated clearly in the second derivative spectrum (Fig. 4.4). The bands at 1733 cm^{-1} and 1719 cm^{-1} are from the lipid ester carbonyl groups. The main amide I' component is shifted to 1649 cm^{-1} and is assigned to exchanged α-helix. A weak component at 1656 cm^{-1}, assigned to unexchanged α-helix, remained in the spectrum. This component disappears when the temperature is slightly raised. Bands are also observed at 1679 cm^{-1}, assigned to exchanged β-turns, and at 1692 cm^{-1} and 1630 cm^{-1}, which are assigned to β-sheet structures.

Fig. 4.3a) Absorption spectrum from 1800 cm^{-1} to 1500 cm^{-1} of colicin A incubated with DMPG vesicles above T_m, pH 5.0.

b) Second derivative spectrum of colicin A and DMPG vesicles above T_m, pH 5.0.

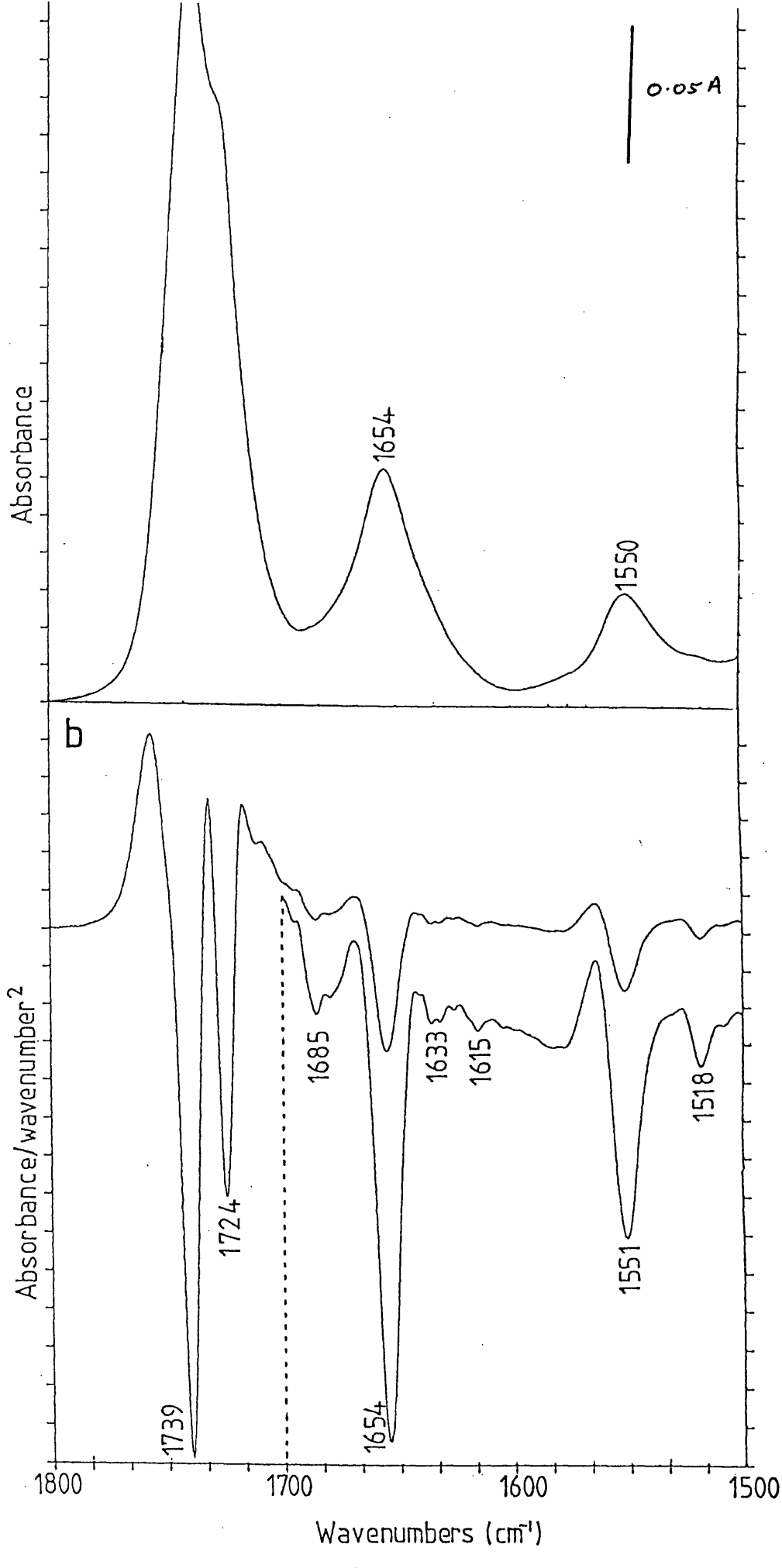
0·05 A
Absorbance
1654
1550
b
Absorbance/wavenumber^2
1739
1724
1685
1654
1633
1615
1551
1518
1800
1700
1600
1500
Wavenumbers (cm^{-1})

Fig. 4.4) Second derivative spectrum of colicin A with DMPG vesicles above T_m, pD 5.0.

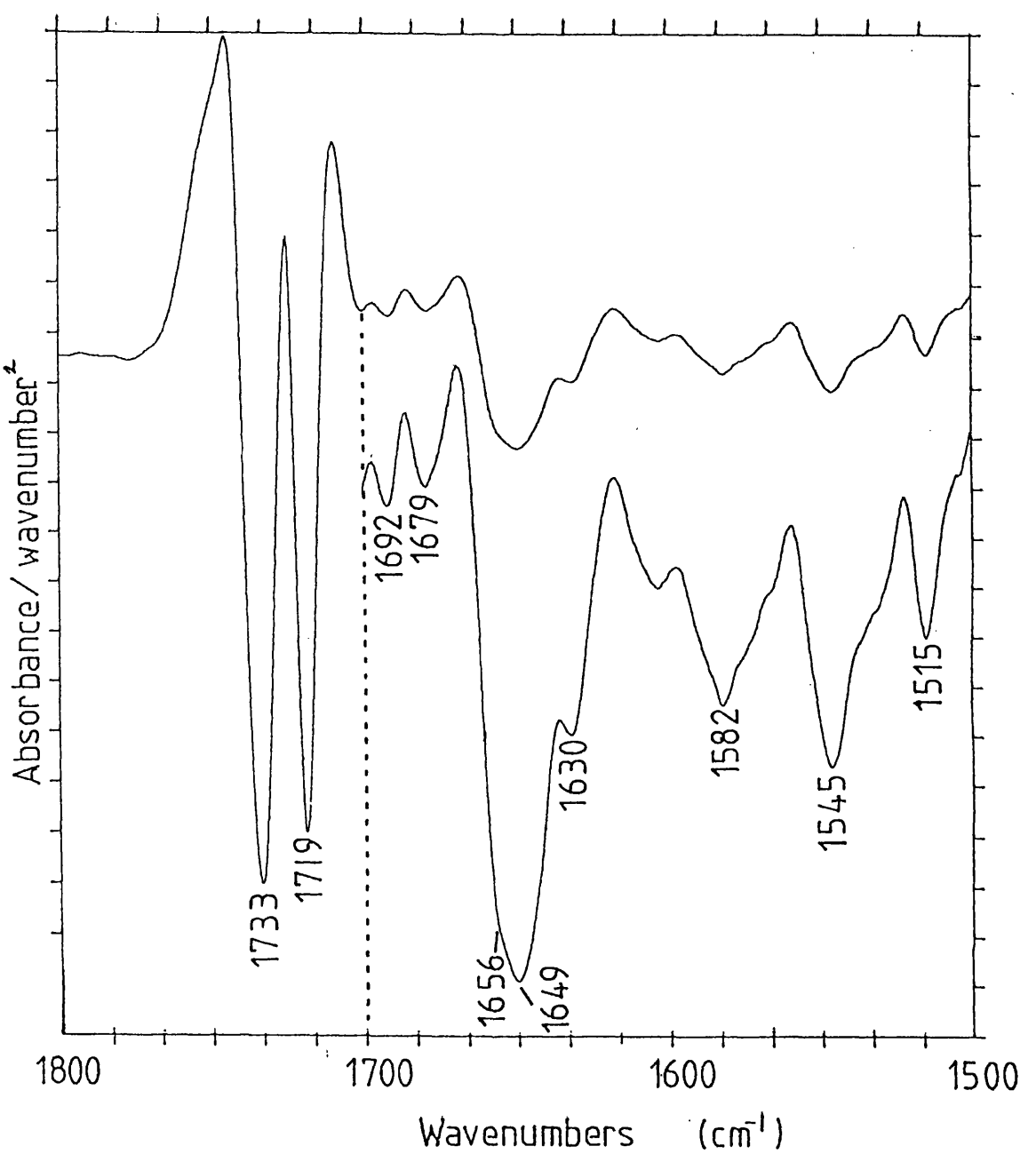
Absorbance / wavenumber²
1733
1719
1692
1679
1656
1649
1630
1582
1545
1515
1800
1700
1600
1500
Wavenumbers (cm⁻¹)

4.3.2. Aerolysin

The absorption spectra of proaerolysin in D_2O buffer is shown in Fig. 4.5a (upper trace) with the deconvolved spectrum shown in the lower trace, and the second derivative shown in Fig. 4.5b. The absorption spectrum of the protoxin shows the amide I' band maximum at 1641 cm^{-1}. The resolution enhanced spectra of the protoxin show components at 1683 cm^{-1}, assigned to β-sheet and β-turns, 1659 cm^{-1}, assigned to unexchanged α-helix, 1645 cm^{-1}, assigned to exchanged random structures with a possible contribution from exchanged α-helix, and 1633 cm^{-1} assigned to β-sheet. Bands are also seen at 1583 cm^{-1} and 1577 cm^{-1} which are assigned to the ionised carboxylate side chains of aspartate and glutamate, respectively. The weak feature at 1551 cm^{-1} is the amide II band, indicating that the protein has not undergo total deuteration, and the strong feature at 1515 cm^{-1} is from tyrosine sidechains.

Heating the protoxin has an effect on the spectrum at 50° - 55° C. In the second derivative spectrum, a band appears at 1618 cm^{-1} and, with time, increases in intensity with a corresponding loss in intensity of the 1633 cm^{-1} band (Fig. 4.6). The increasing intensity of the band at 1685 cm^{-1} coupled with the absorption at 1618 cm^{-1} is characteristic of the formation of intermolecular β-sheet. On lowering the temperature back to 20° C, the spectrum was similar to that at 55° C, indicting that the change was irreversible.

Fig. 4.5a) Absorption spectrum from 1800 cm^{-1} to 1500 cm^{-1} of proaerolysin in D_2O buffer, pD 7.4, at 20° C (upper trace) and its deconvolved spectrum using resolution enhancement factor 2 and bandwidth 12 cm^{-1}.

b) Second derivative spectrum of proaerolysin in D_2O buffer, pD 7.4.

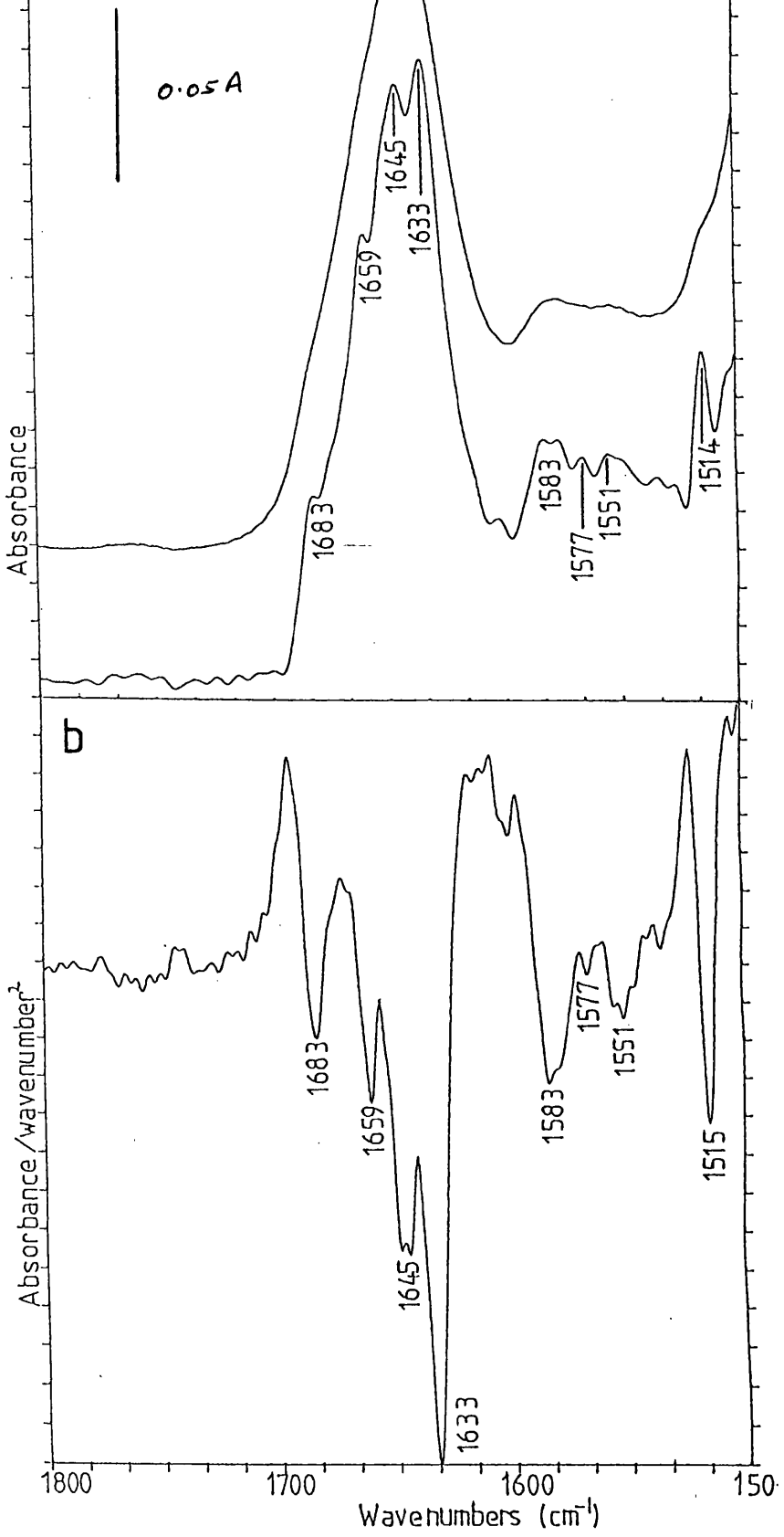
0·05 A
1645
1633
1659
1683
1583
1577
1551
1514
Absorbance
b
1683
1659
1645
1633
1583
1577
1551
1515
Absorbance /wavenumber⁻²
1800
1700
1600
150
Wavenumbers (cm⁻¹)

Fig. 4.6) Second derivative spectrum of heat denatured proaerolysin.

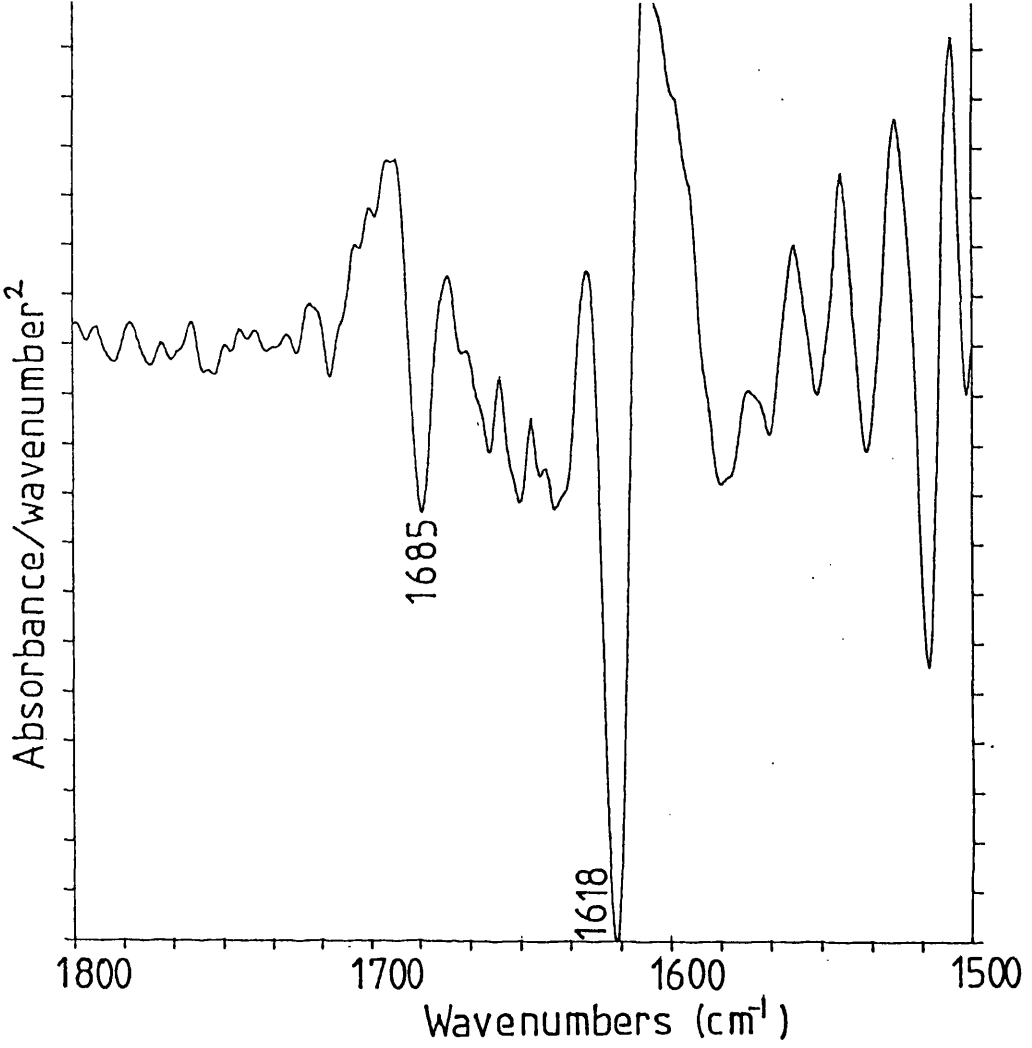
Absorbance/wavenumber^2
1685
1618
1800
1700
1600
1500
Wavenumbers (cm^{-1})

The spectrum of the mature toxin in D_2O buffer containing Zn^{2+} ions, pD 6.8, is shown in Fig. 4.7a (upper trace) with the deconvolved spectrum (lower trace), and the second derivative shown in Fig. 4.7b. The amide I' band occurs at 1638 cm^{-1}. Component bands, at 1684 and 1632 cm^{-1}, assigned to intramolecular β-sheet, and at 1644 cm^{-1}, assigned to exchanged random structure with a possible contribution from exchanged α-helix, are similar to that of the protoxin. The second derivative spectrum appears to have a weak component around 1659 cm^{-1}, which is assigned to unexchanged α-helix.

In the absence of Zn^{2+} ions, the aerolysin toxin has an amide I' absorption band at 1623 cm^{-1}. Second derivative analysis identifies component bands at 1616 and 1682 cm^{-1}, assigned to intermolecular β-sheet, similar to the spectrum shown in Fig. 4.6.

The spectrum of the mature toxin binding to liposomes is shown in Fig. 4.8a, with the second derivative spectra shown in Fig. 4.8b. The bands at 1745 cm^{-1} and 1722 cm^{-1} are from the lipid ester carbonyl groups. The poor s/n ratio of the spectrum restricts band assignment to the strongest bands:- at 1656 cm^{-1} to α-helix and at 1629 and 1620 cm^{-1} assigned to intra- and inter-molecular β-sheet, respectively.

Fig. 4.7a) Absorption (upper trace), and deconvolved spectra (lower trace) using resolution enhancement factor 2 and bandwidth 12 cm^{-1} of aerolysin in D_2O buffer in the presence of Zn^{2+} ions.

b) The second derivative spectrum of aerolysin in D_2O buffer in the presence of Zn^{2+} ions.

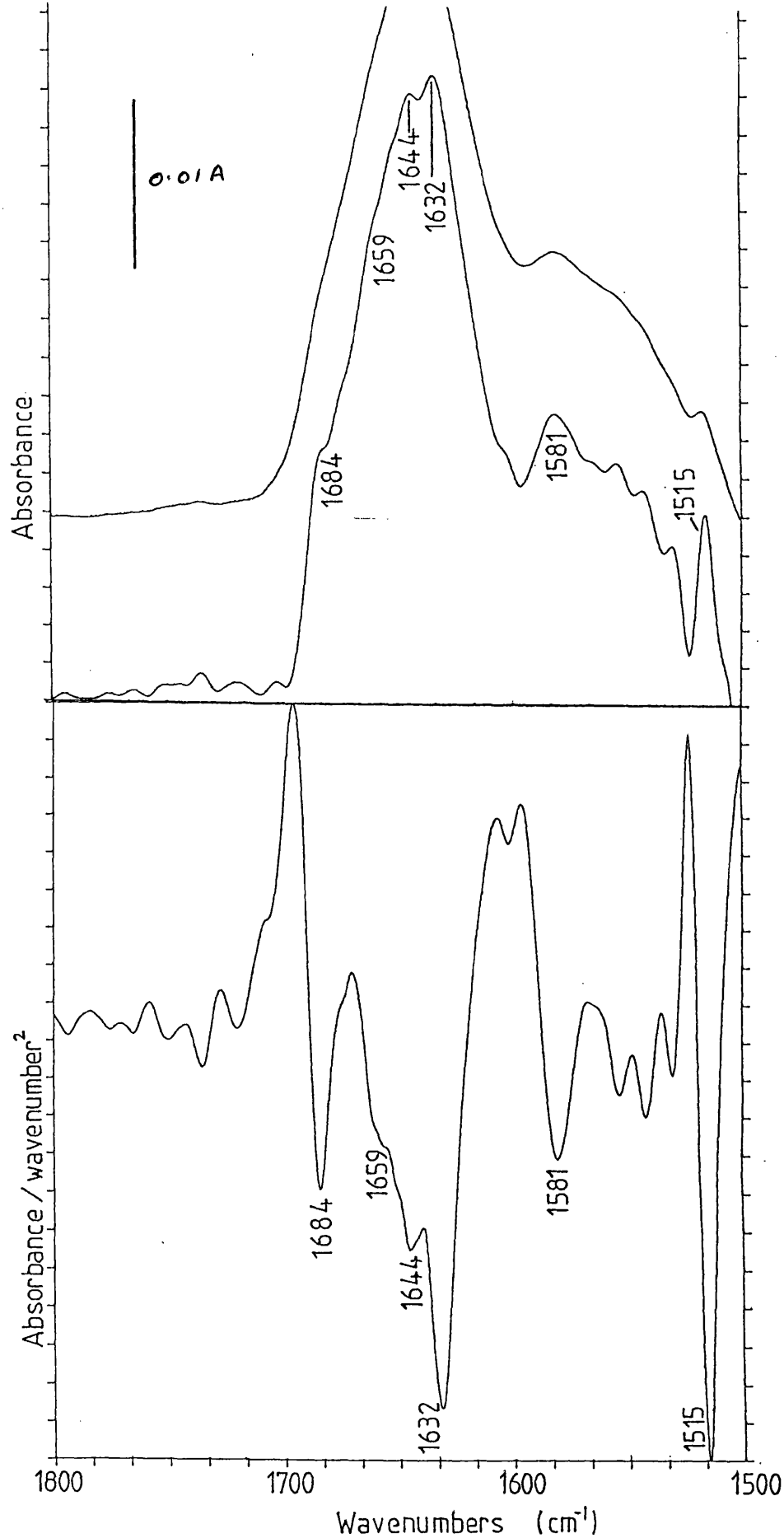
0·01A
Absorbance
1684
1659
1644
1632
1581
1515
Absorbance / wavenumber²
1684
1659
1644
1632
1581
1515
1800
1700
1600
1500
Wavenumbers (cm⁻¹)

Fig. 4.8a) The absorption spectrum of aerolysin in the presence of phosphatidylcholine - cholesterol - diacetyl phosphate vesicles (molar ratio 7:2:1) in D_2O buffer.
b) The second derivative spectrum of aerolysin bound to vesicles.

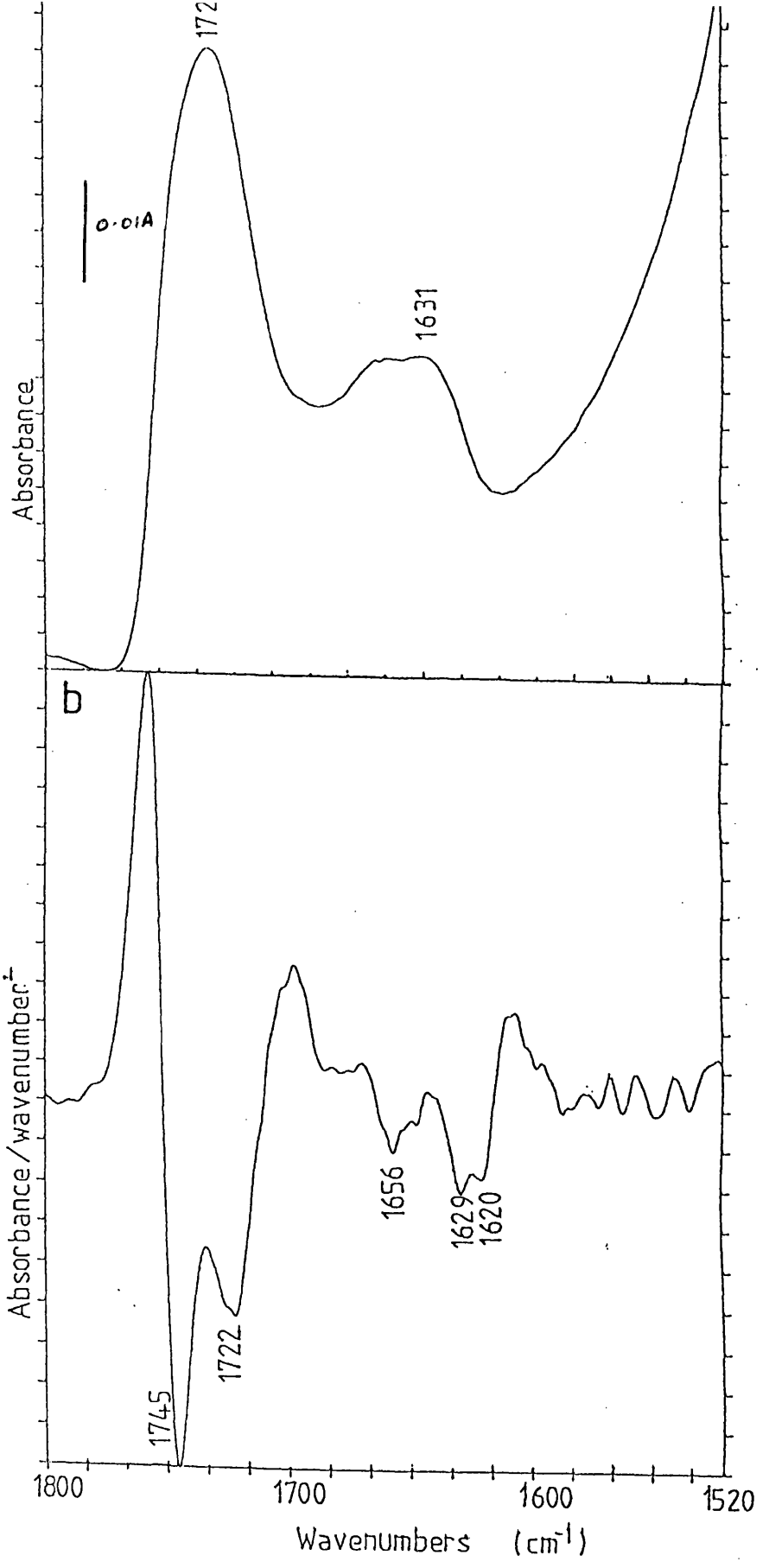
0·01A
1631
Absorbance
b
1656
1629
1620
1722
1745
Absorbance / wavenumber⁻¹
1800
1700
1600
1520
Wavenumbers (cm⁻¹)

4.4. DISCUSSION

The pore-inserting fragment of colicin A is a useful model in the investigation of protein insertion into the membrane. The structure of the pore-inserting fragment in the absence of the lipid matrix at atomic resolution has been determined by X-ray crystallography (Parker et al., 1989) and based on these results, a structural model of the inserted fragment has been proposed (Parker et al., 1990).

The assignment of the amide I component bands of the soluble pore-forming fragment in H_2O agree well qualitatively with the X-ray diffraction results of Parker et al. (1989). The structure is predominantly α-helical, with small amounts of β-turn and random structure present. The absorption around 1638-1639 cm^{-1} may indicate that some β-sheet is present, but this structure may occur in any residual insoluble fragment present in the sample. This band frequency may also be assigned to arginine and lysine sidechain absorptions.

Small differences were identified in the pore-forming fragment at pD 7 and pD 5 after identical incubation of the samples. This is supported by the resolution enhanced spectra, which indicate that the sample at pD 5 has a smaller proportion of exchanged random structures (with the possible contribution from exchanged α-helix) than at pD 7. This small change may be crucial in allowing protein insertion into the membrane.

The stability of the protein fragment was

investigated by thermal denaturation. At both pD 7.0 and 5.0, the protein was found to be stable up to at least 85° C (the maximum temperature obtainable). This indicates that, despite containing no disulphide bridges, the pore-forming fragment is extremely stable. This tends to agree with the X-ray diffraction model of the soluble fragment indicating that the ten α-helices in the fragment are in a very compact arrangement. This is not inconceivable as nearly 50% of the amino acids in the fragment are hydrophobic (Morlon et al., 1988).

The spectrum obtained of the fragment bound to DMPG lipids in H_2O buffer produced a 2 cm^{-1} shift in the band assigned to α-helix, which may be a result of the helices being in a more hydrated environment. The feature at 1633 cm^{-1} may indicate the presence of some β-sheet structure.

The results from the experiments repeated in D_2O buffer produced more information on the mechanism of protein insertion. Incubation of the fragment in the absence of liposomes, or in the presence of liposomes below the phase transition temperature show no difference in the amount of H → D exchange or in the amide I' band components, indicating that the soluble fragment has a similar secondary structure and solvent accessibility in the presence and absence of liposomes below the phase transition temperature.

Above the phase transition temperature, changes occur in the protein on insertion into the membrane. The

resolution enhanced spectrum indicates that most of the α-helices become accessible to the solvent and undergo H → D exchange, causing a disappearance of the band assigned to unexchanged α-helices at 1656 cm^{-1} in the soluble fragment, and the occurrence of a strong band at 1649 cm^{-1}, assigned to exchanged α-helices, in the membrane-inserted protein. The bands at 1630 cm^{-1} and 1692 cm^{-1} indicate that some β-sheet is also present in the membrane-inserted thermolytic fragment, which is similar to that observed for the thermolytic fragment of colicin E_1 bound to vesicles (Suga et al., 1991).

The high amount of H → D exchange in the inserted fragment of colicin A indicates that the structure of the protein in this environment is more solvent accessible and agrees with the model of Parker et al. (1989) in which the thermolytic fragment opens up into an "umbrella"-type structure on insertion. However a small amount of β-sheet structure is also observed. It is not known whether this is part of the membrane-inserted part of the fragment or is involved in stabilisation of the aggregated fragments in pore formation. The absence of a component band at 1666 - 1662 cm^{-1} in the resolution enhanced spectra indicates that no 3_{10}-helical structure is present. Therefore we conclude that the hairpin inserted into the membrane has α-helical structure.

Producing suitable samples of (pro)aerolysin from the initial proaerolysin samples supplied at 1 mg/ml in H_2O buffer caused problems. It was decided to use D_2O buffers

for all samples as the protein concentration was found to be too low in H_2O buffers to produce spectra with a high s/n ratio. Even though the use of microconcentrators proved successful in concentrating the sample, it resulted in the loss of approximately 70 - 80% of the starting material, presumably through adsorption to the concentrator membrane, and through protein aggregation.

The studies of aerolysin and its protoxin indicate that both contain predominantly β-sheet secondary structures, with small amounts of random structures also present. This generally agrees with the preliminary X-ray structure for the protoxin (Green & Buckley, 1990). The major difference between the protoxin and toxin is the decrease in intensity of the band assigned to unexchanged α-helix in the mature protein. The majority of the α-helix present in both proteins appears to be hydrophobic as judged by its high band frequency (1658 cm^{-1}).

Thermal denaturation of the protoxin occurred at 50°-55° C, with a formation of intermolecular β-sheet band at 1615 cm^{-1} with a corresponding decrease in the intramolecular β-sheet band at 1634 cm^{-1}. The 1658 cm^{-1} band assigned to unexchanged α-helix remained present in the spectrum at 85° C, indicating that this helix is hydrophobic as it does not undergo H → D exchange at high temperatures, or after protein denaturation. Denaturation at a temperature only 13°C- 18°C above its normal functional temperature indicates that the protein is not

highly stable, and is able to alter its H-bonding pattern in response to small changes in conditions.

Similar results were obtained for the mature toxin in the presence of Zn^{2+} ions. A buffer of pD 6.8 was used to avoid the precipitation of ZnOH which occurs at pD > 7. The band assigned to α-helix remained undeuterated, illustrating its hydrophobic nature. In the absence of Zn^{2+} ions, the protein aggregated immediately to form a milky solution at 20° C, with the main β-sheet absorption band shifting to 1616 cm^{-1}, indicating the formation of intermolecular β-sheet. The protein spectrum still retained a small 1658 cm^{-1} component from undeuterated α-helix.

Protein interactions with membranes were investigated using model membranes. Glycophorin has been tentatively identified as an aerolysin receptor in membranes. Investigating the binding of aerolysin to erythrocyte ghosts, membranes rich in glycophorin, similar to the study of Buckley et al.(1982), was considered. Even though it is possible to remove the structural proteins, such as actin and spectrin, using the technique of "alkali-stripping", the ghosts still contain significant amounts of membrane proteins in addition to glycophorin, such as the band III protein and the glucose transporter. The amide I' absorptions from these membrane proteins would dominate the FTIR absorption spectrum of aerolysin, and therefore be of little use.

An FTIR study of aerolysin interactions with model

membranes containing glycophorin would produce similar problems. Possible conformational changes in aerolysin on insertion into the membrane may be accompanied by changes in the environment and secondary structure of glycophorin. Assigning changes in the composite amide I' band to conformational changes in either protein would not be possible due to the overlap of their amide I' bands.

Aerolysin has been shown to form pores in model membranes (Howard & Buckley, 1982). Studying this type of system eliminates the problems of overlapping membrane protein IR absorption bands. However the disassociation constant for the aerolysin - model membrane system has not been determined, so the ratio of membrane-inserted to soluble aerolysin in the system is unknown. Separation of the vesicles containing the membrane-bound toxin from the soluble protein would be complex and cause further loss of the protein.

Therefore the approach used was to activate the protoxin bound to DMPC - cholesterol - dicetyl phosphate vesicles with trypsin. Changes would be identified in the resultant amide I' band that contained information on both membrane-inserted and soluble forms of the active protein. As the protoxin is known to bind to vesicles, this method also reduced the chance of protein aggregation occurring before interaction with the vesicles.

Interaction of the mature toxin with DMPC - cholesterol - dicetyl phosphate liposomes in D_2O buffer shows a second derivative spectrum with bands assigned to α-helix and intra- and intermolecular β-sheet. The presence of the band at 1656 cm^{-1} in the spectrum indicates that part of the membrane-inserted protein is α-helical. This may imply that the protein interaction with the membrane is initiated by the formation of an α-helical region within the protein.

The presence of strong β-sheet bands indicates that this structure is still present in the system. Whether the intermolecular β-sheet is formed to stabilise the aggregated membrane pore, or is present in aggregates of the soluble protein away from the membrane is not known.

4.5. SUMMARY

Fourier transform infrared spectroscopy has been used to investigate the mechanisms of membrane insertion of pore-forming fragment of colicin A and of aerolysin into the lipid matrix. Experiments carried out in H_2O and D_2O buffers show that the pore-forming fragment of colicin A is predominantly α-helical in solution. The protein undergoes a minor alteration of secondary structure in going from pD 7.0 to pD 5.0 (the condition required for membrane insertion). The pore-forming fragment retained its secondary structure at 85° C at both pD's indicating that, despite containing no disulphide bridges, the protein is very stable. This may be related to the hydrophobicity of the fragment core.

The secondary structure of the protein in the lipid matrix is again predominantly α-helical, but with a small proportion of β-sheet present. The high level of H → D exchange indicates that the protein has a relatively high solvent accessibility in this form. This may be due to the protein opening to an "umbrella"-type structure on insertion into the membrane and/or the protein aggregating in the membrane to form a large solvent-accessible pore.

Aerolysin and its precursor, proaerolysin, both possess predominantly β-sheet structure, with small regions of α-helical and random structure. Both proteins are solvent accessible as they undergo almost complete H → D exchange. Proaerolysin denatures at 50°-55° C where

the formation of intermolecular β-sheet is observed. The export of the protoxin may be initiated via the insertion of the hydrophobic α-helix into the membrane. The relative instability of the protoxin may be important in the transport across the membrane by allowing the breaking and reformation of intramolecular H-bonds. The main structural difference between the protoxin and toxin is the loss of the majority of α-helix on activation. However in the presence of vesicles, an increased amount of α-helix is identified in the active protein.

The absence of bands associated with the 3_{10}-helix in the thermolytic fragment of colicin A, proaerolysin and aerolysin indicates that membrane insertion may be initiated by insertion of an α-helical segment into the membrane.

CHAPTER FIVE

AN FTIR SPECTROSCOPIC STUDY OF TWO PANCREATIC AND ONE SNAKE VENOM PHOSPHOLIPASE A_2's AND THEIR INTERACTIONS WITH SUBSTRATE ANALOGUES AND A TRANSITION-STATE INHIBITOR

5.1. INTRODUCTION

Phospolipases are enzymes which are involved in the specific hydrolysis of phospholipid molecules. Each phospholipase acts on a different part of the phospholipid, as illustrated with PC in Fig. 5.1. Phospholipase A_1 and A_2 catalyse the specific hydrolysis of the 1-acyl and 2-acyl ester bonds of 3-sn phosphoglycerides, respectively, to release fatty acids. Phospholipases C and D catalyse the specific hydrolysis of the P — O bonds of the headgroup.

Phospholipases have been shown to occur in nearly all animal cells. They are crucial in the metabolic turnover of lipids in biomembranes and, as such, act as "triggers" in important processes such as membrane metabolism, haemostatis and blood clotting, prostaglandin synthesis, lung surfactant synthesis and pancreatitis. The role of prostaglandins are of particular interest. Prostaglandins are cyclic derivatives of certain fatty acids, containing twenty carbon atoms, such as arachidic and arachodonic acid, released mainly from the action of phospholipases A_1 and A_2 on phospholipids. Prostaglandins take part in the regulation of the diameter of blood vessels, kidney function, and are involved in platelet aggregation, the process of inflammation, and in human reproduction due to the high concentration of prostaglandins in seminal fluid (Euler 1976). Extracellular phospholipase A_2 (PLA_2) is involved in the digestion of dietary lipids, and in the

Fig. 5.1) The position of action of phospholipases on phosphatidylcholine lipids.

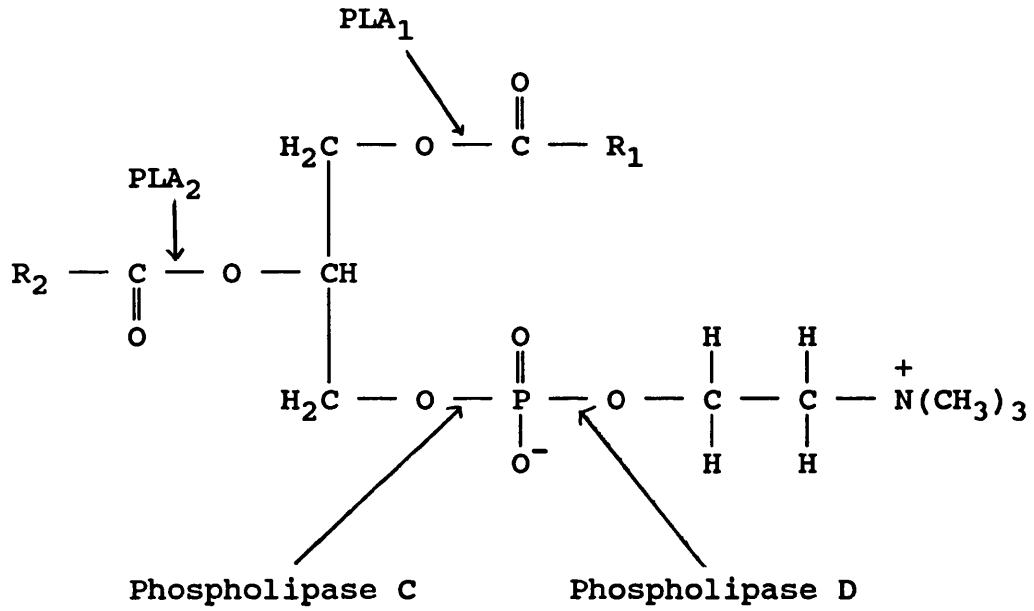
PLA1
PLA2
R2 — C — O — CH
H2C — O — C — R1
H2C — O — P — O — C — C — N(CH3)3
Phospholipase C
Phospholipase D

action of snake and bee venoms.

Despite existing in most cells, endocellular PLA_2 is generally found in low concentrations and has weak activity in experimental assays. This has severely limited studies on its structure and function. However in a few secretory organs, such as the pancreas and snake and bee venom glands, the extracellular enzyme is produced in high concentrations and can be isolated in large quantities. This has enabled the detailed study of the structure and functions of extracellular PLA_2. The detailed information on the structure-function relationship of the extracellular enzyme gives valuable information on the mechanisms of its action, and will aid the studies of the less-accessible endocellular and membrane-bound enzymes.

PLA_2 has an absolute requirement for Ca^{2+} ions. Although PLA_2's are able to hydrolyse substrate molecules present in monomeric dispersion (Roholt & Schamowitz 1961; De Haas et al., 1971; Wells 1972), the hydrolytic activity of the enzyme is greatly enhanced when the substrate is present as an organised lipid-water interface (Pieterson et al., 1974).

The amino acid sequences of a number of PLA_2's isolated from various sources have been determined. When comparing the sequences of pancreatic and elapid PLA_2's, of the 124 residues, 36 are conserved absolutely with a further 45 being substituted by residues with similar properties with respect to size, charge or hydrophobicity

(Slotboom et al., 1982). All contain 14 or 12 cysteine residues which form disulphide bridges, giving the enzyme rigidity and the properties of heat stability and resistance to denaturing agents (Van der Bergh et al., 1989).

Information on the secondary structure of pancreatic PLA_2 was first obtained using IR spectroscopy to study porcine PLA_2 in D_2O buffer (Abita et al., 1972). These workers suggested that, due to the high amide I frequency, both the enzyme and proenzyme have a high α-helical content. However no resolution enhancement techniques could be applied at this time and no quantitative estimates were made. A circular dichroism study of a number of pancreatic PLA_2's concluded that moderate amounts of α-helix were present in the enzyme (Jirgenson & De Haas, 1977). However these results may have been influenced by the X-ray diffraction studies of crystals of porcine PLA_2 (Drenth et al., 1976). The absence of regular α-helices and β-sheet deduced from these crystals suggested that the crystals contained denatured protein. Later detailed X-ray diffraction studies carried out on Ca^{2+}-containing crystals of the bovine enzyme at a resolution of 1.7 Å (Dijkstra et al., 1981) and of the porcine enzyme at a resolution of 2.4 Å (Dijkstra et al., 1983) showed that pancreatic enzymes have approximately 50% α-helical and 10% β-sheet content.

The main conformational differences elucidated

between the porcine and bovine enzymes in the crystal state occurs between residues 59 and 70 caused by the single substitution at position 63 of a Val residue in the bovine enzyme and a Phe residue in the porcine enzyme (Dijkstra et al., 1983). The side-chain of Val63 is at the surface of the bovine enzyme molecule, whereas the Phe63 side-chain of the porcine enzyme is buried within the molecule. The short α-helical section in the bovine enzyme between residues 59-66 is not present in the porcine molecule but there is a region of 3_{10}-helix, 1.5 turns long between residues 67 to 71. However a ^{1}H NMR study of bovine and porcine PLA_2 in solution suggested that the solution-state conformations of the two enzymes are very similar in this region (Fisher et al., 1989). Suitable crystals of PLA_2-lipid complexes have not been obtained, so that lipid-protein interactions of these enzymes have yet to be studied at atomic resolution by X-ray diffraction.

Studies of the neotropical rattlesnake Crotalus durissus terrificus venom PLA_2 are limited and, as yet, no X-ray structure of the soluble enzyme has been determined. An investigation using Raman and FTIR spectroscopy of PLA_2 from porcine pancreas and from the Crotalus durissus terrificus venom gives quantitative analyses from the Raman data of the two enzymes under various conditions (Aréas et al., 1989). This produced figures of 48% α-helix, 35% β-sheet and 18% random coil for the porcine pancreatic PLA_2 in solution, and 54% α-

helix, 35% β-sheet and 11% random coil for the snake venom PLA_2 in solution. This study also observed conformational changes in the enzymes caused by altering the physical state of the protein, and by altering the ionic species present in PLA_2 buffer solution.

Important work on PLA_2-lipid binding studies has been carried out using porcine and bovine pancreatic PLA_2 with n-alkylphosphocholines, non-degradable zwitterionic phospholipids (Soares de Araujo et al., 1979; Hille et al., 1981; Donné-Op den Kelder et al., 1981). Two possible binding mechanisms for the formation of PLA_2 - n-hexadecylphosphocholine complexes, involving two PLA_2 molecules interacting with each micelle have been proposed (Soares de Araujo et al., 1979). Further work using the anionic substrate analogue n-alkyl sulphate with porcine PLA_2 indicated that the enzyme would have to undergo a conformational change to gain full hydrolytic activity (Hille et al., 1983a,b). It has been suggested that the dramatic rate enhancement, observed for PLA_2 when the substrate concentration exceeds the CMC and a lipid-water interface is formed, is due to a conformational change in the protein, thereby resulting in an optimal alignment of the amino acids in the active site (Slotboom et al., 1982).

As well as studying the action of PLA_2 in hydrolysing lipids, it is believed that the inhibition of this enzyme could produce desirable pharmacological effects (Dennis

1987). Phospholipids having an amide linkage instead of an ester at the sn-2 position behave as potent transition-state inhibitors (Bonsen et al., 1972; De Haas et al., 1989). So far, no changes in secondary structure have been observed in pancreatic PLA_2 on binding to micelles of degradable or non-degradable zwitterionic lipids, or to inhibitor lipids.

Quantitative analysis of protein secondary structure can be obtained from FTIR absorption spectra using Factor Analysis. By correlating the amide I bands of a number of soluble proteins of known structure to the amide I band of the sample protein, quantitative estimates of the secondary structure of the sample protein can be made (Lee et al., 1990).

In this chapter we apply the technique of FTIR spectroscopy to examine qualitatively and quantitatively the secondary structure of porcine pancreatic phospholipase A_2. The interaction of n-alkylphosphocholine in monomer and micellar form, and of the inhibitor 1-heptanoyl-2-heptanoylamino-2-deoxy-sn-glycero-3-phosphoglycol (HHNP) with this phospholipase is also studied. These results are compared to those obtained for bovine pancreatic PLA_2 and Crotalus durissus terrificus PLA_2 in order to study the similarities in the secondary structures and modes of function of PLA_2's from pancreatic and snake venom sources.

5.2. MATERIALS AND METHODS

Deuterium oxide (99.8%) was obtained from Sigma, U.K. All other chemicals used were analytical grade from Sigma, U.K., when available, or from Aldrich, U.K.

Porcine (Niewenhuisen et al., 1974) and bovine (Fleer et al., 1978) pancreatic prophospholipase A_2 were purified from pancreatic tissue and converted into PLA_2 by limited proteolysis as described, and were generous gifts from Dr. Arend Slotboom and Prof. Gerard de Haas, University of Utrecht, Holland.

Snake venom phospholipase A_2 used was from Crotalus durissus terrificus and was obtained from Sigma, U.K.

The substrate analogues $C_{10}PN$ and $C_{18}PN$ were prepared and purified as described (Van Dam-Mieras et al., 1975), and 1-heptanoyl-2-heptanoylamino-2-deoxy-sn-glycero-phosphoglycol (HHNP) was prepared (Dijkman, R. & De Haas, G.H., unpublished results), and were generous gifts from Dr. Arend Slotboom and Prof. Gerard de Haas, University of Utrecht, Holland.

Samples used for experiments in D_2O were added to D_2O buffer and heated at 30°C for three hours, and then left at room temperature for a further 12 hours.

Calcium ions were removed from the (pro)enzymes by dialysing the sample for 36-48 hours against deionised water, adjusted to pH 3.5 with acetic acid. The samples were then lyophilised after the addition of a small amount of propan-2-ol.

Samples were prepared for studies in the absence of lipid with a protein concentration of 20-50 mg/ml in buffer containing 100mM $CaCl_2$, 100mM NaCl, 10mM MES, pH 6.0 or pD 6.0 as stated.

Values of pD were calculated according to the method of Glasoe and Long (1960).

Samples used to study the binding of monomeric lipids to porcine PLA_2 were prepared using 20 mg/ml of PLA_2 and 2 mg/ml $C_{10}PN$ in the same buffer as above.

Samples used to study the binding of PLA_2 to lipid micelles were prepared using 2 mg of PLA_2 and 11.2 mg $C_{18}PN$ in 100 μl of the same buffer as above. This will allow over 90% of the porcine PLA_2 to interact with the micelles (Donné-Op den Kelder, 1984). The preparation of PLA_2 for the study of protein-lipid binding in D_2O was carried out as described above. To one half of the sample was added $C_{18}PN$ whilst the other half was scanned in the absence of micelles. The PLA_2-micelle sample was scanned immediately afterwards to minimise the difference in $H \rightarrow D$ exchange between the samples.

The effect of the inhibitor above its CMC was studied by preparing a sample containing 20 mg/ml porcine PLA_2 and 10 mM inhibitor in H_2O or D_2O buffer containing 100 mM NaCl, 100 mM Na acetate and 20 mM $CaCl_2$, pH 5.95 or pD 5.95.

Spectra were gathered as described in Section 3.2.

Quantitative information on the different structures

present was achieved by using Factor Analysis, a technique based on CIRCOM (Lee et al., 1990; Fredericks et al., 1985a,b). This uses the FTIR absorption spectra of 5% (w/v) solutions in H_2O buffer of 18 reference proteins whose structures are known from X-ray diffraction studies. The amide I band of these reference proteins is then fitted to the amide I band of the sample spectrum to generate quantitative information about the sample protein.

The amide II/I ratio is the ratio of the area of the amide II band to the area of the amide I band.

5.3. RESULTS

5.3.1. Porcine PLA_2 and proPLA_2

The absorption spectrum in the range 1800-1500 cm^{-1} of porcine pancreatic PLA_2 in H_2O buffer, pH 6.0 is given in Fig. 5.2a (top trace). Two main absorption bands present are assigned to the amide I and II vibrations. Information on the secondary structure is mainly found from the overlapping components of the amide I band.

The deconvolved spectrum of porcine PLA_2 is shown in Fig. 5.2a (lower trace), with the second derivative shown in Fig. 5.2b. The predominant band at 1657-1658 cm^{-1} in the spectra can be assigned to a combination of α-helical and/or random structures. Further components present within the amide I band are the broad bands at 1678 cm^{-1}, assigned to β-turns and possibly β-sheet, and at 1635 cm^{-1}, assigned to β-sheet, whilst the band at 1617 cm^{-1} is assigned to tyrosine side chains. The main amide II band occurs at 1551-1552 cm^{-1}, whilst the sharp band at 1517 cm^{-1} is assigned to tyrosine side chains.

Further information on protein secondary structure can be gained by studying the samples in D_2O. The absorption spectrum of porcine PLA_2 dissolved in D_2O buffer is shown in Fig. 5.3a (solid line), with the component bands clearly visible in the deconvolved and second derivative spectra in Fig. 5.3b and 5.3c (upper traces) respectively. The band positions taken from the second derivative spectrum (Fig. 5.3c) are as follows:-

Fig. 5.2a) The absorption spectrum from 1800 cm^{-1} to 1500 cm^{-1} of 5% (w/v) porcine PLA_2 in H_2O buffer, pH 6.0 (top trace, solid line), its deconvolved spectrum using a resolution enhancement factor 2.25 and bandwidth of 11 cm^{-1} (lower trace, solid line) and the absorption spectrum of porcine PLA_2 in the presence of $C_{18}PN$ micelles in H_2O buffer, pH 6.0 (top trace, broken line).

b) Second derivative spectrum of 5% (w/v) porcine PLA_2 in H_2O buffer.

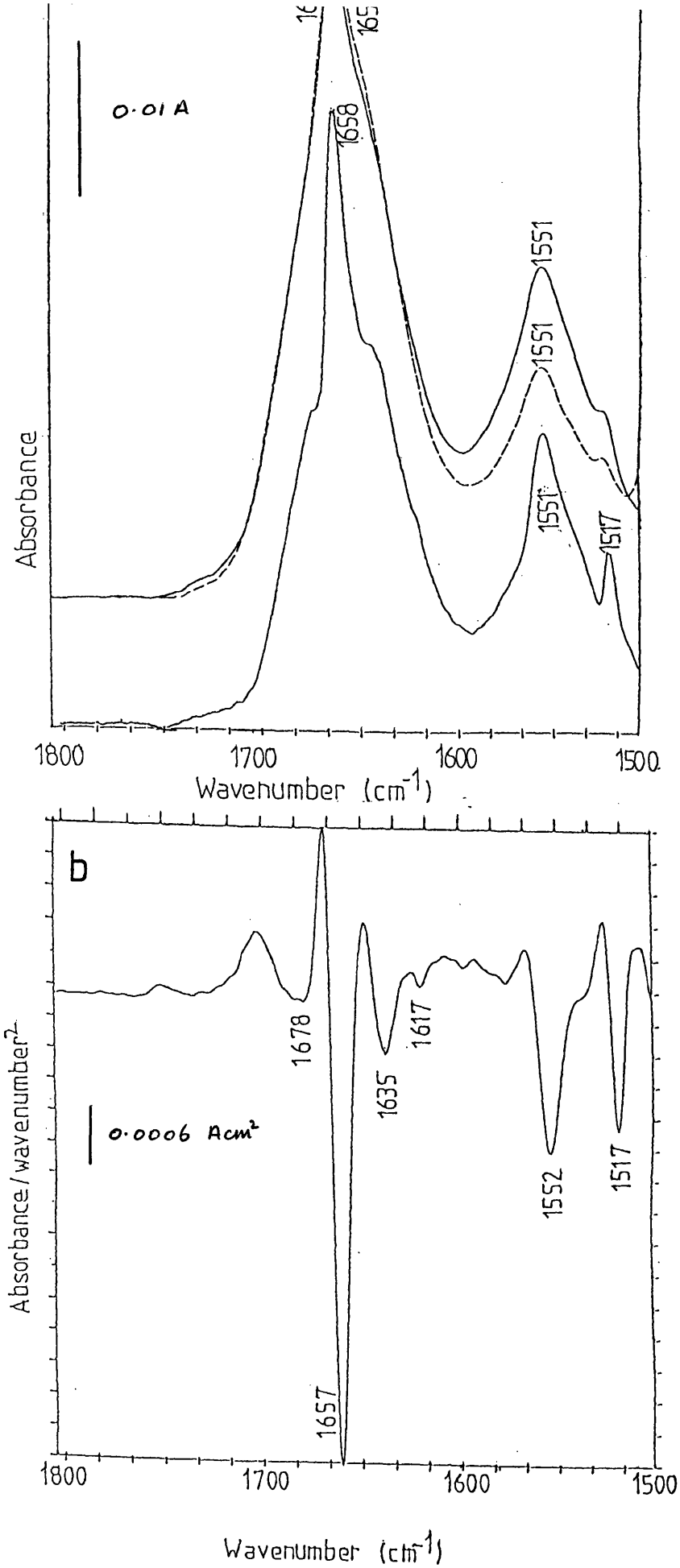
0·01 A
1658
1551
1551
1551
1517
Absorbance
1800
1700
1600
1500
Wavenumber (cm⁻¹)
b
0·0006 Acm²
1678
1657
1635
1617
1552
1517
Absorbance / wavenumber²
1800
1700
1600
1500
Wavenumber (cm⁻¹)

FIG. 5.3a) Absorption spectrum of partially deuterated porcine PLA_2 in D_2O buffer, pD 6.0, in the presence (dotted line) and absence (solid line) of $C_{18}PN$ micelles.

b) Deconvolved spectra of deuterated porcine PLA_2 in D_2O buffer, pD 6.0, using resolution enhancement factor 2.75 and bandwidth 15 cm^{-1} in the presence (lower trace) and absence (upper trace) of $C_{18}PN$ micelles.

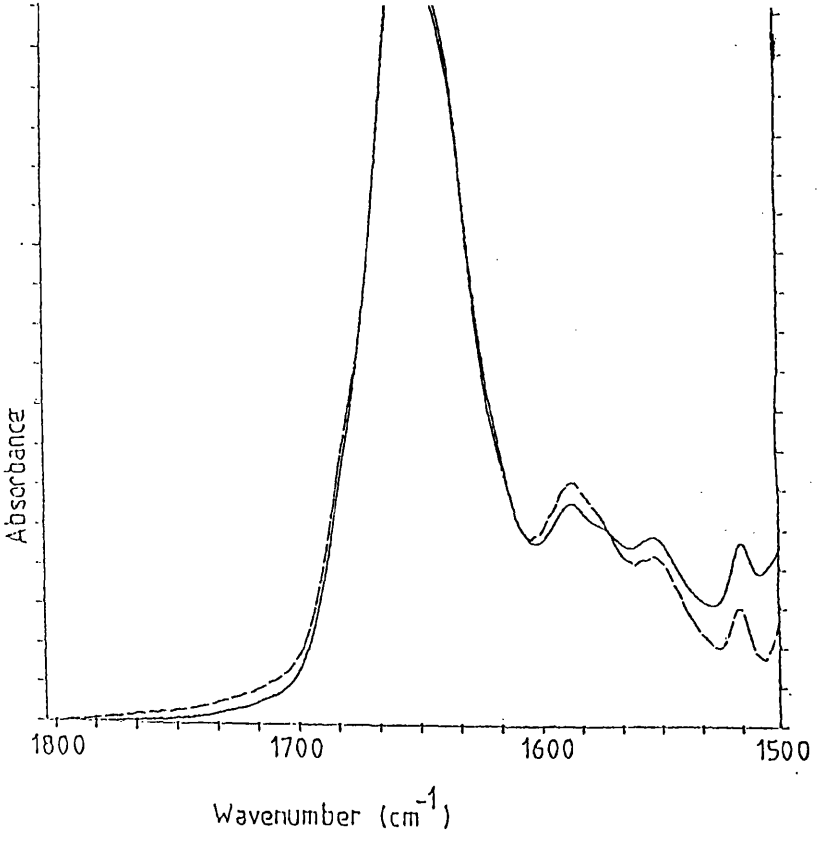
Absorbance
1800
1700
1600
1500
Wavenumber (cm-1)

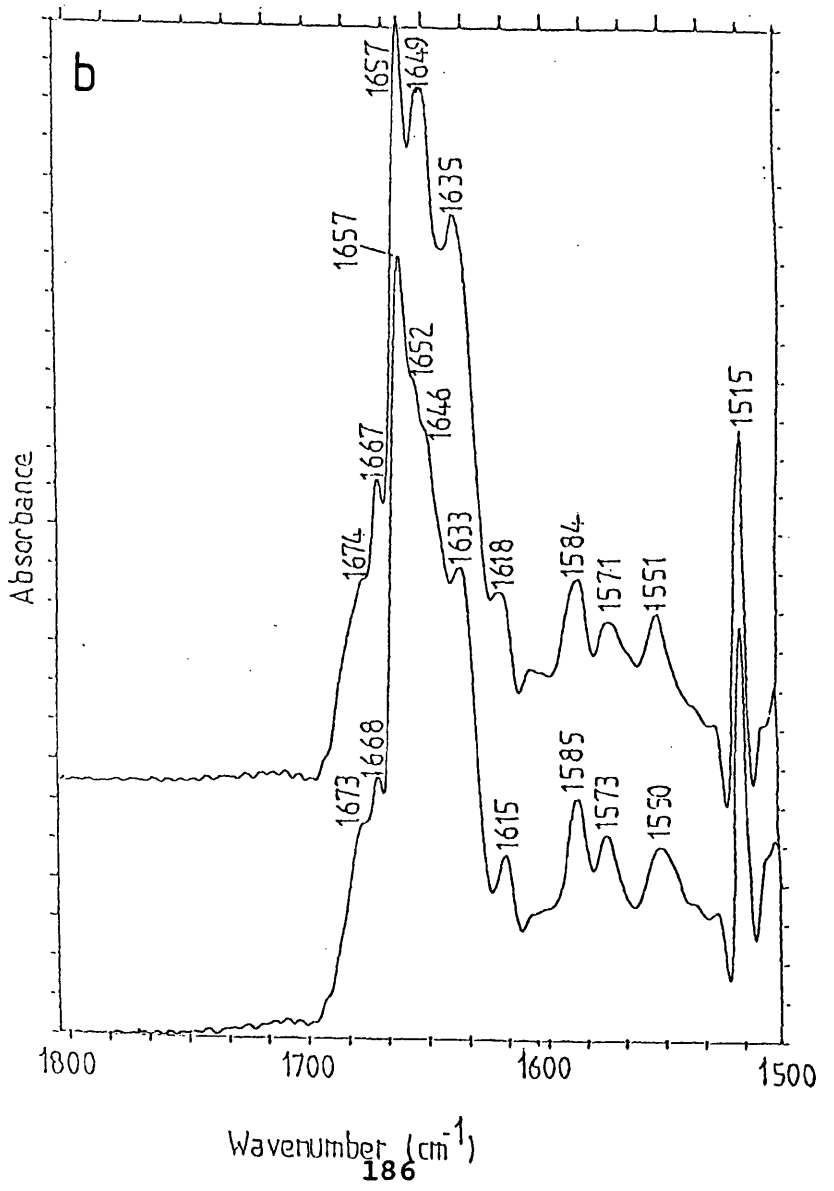
b
1657
1649
1635
1657
1652
1646
1667
1674
1633
1618
1584
1571
1551
1515
1668
1673
1615
1585
1573
1550
Absorbance
1800
1700
1600
1500
Wavenumber (cm-1)

Fig. 5.3c) Second derivative spectrum of partially deuterated porcine PLA_2 in D_2O buffer, pD 6.0, in the presence (lower trace) and absence (upper trace) of $C_{18}PN$ micelles.

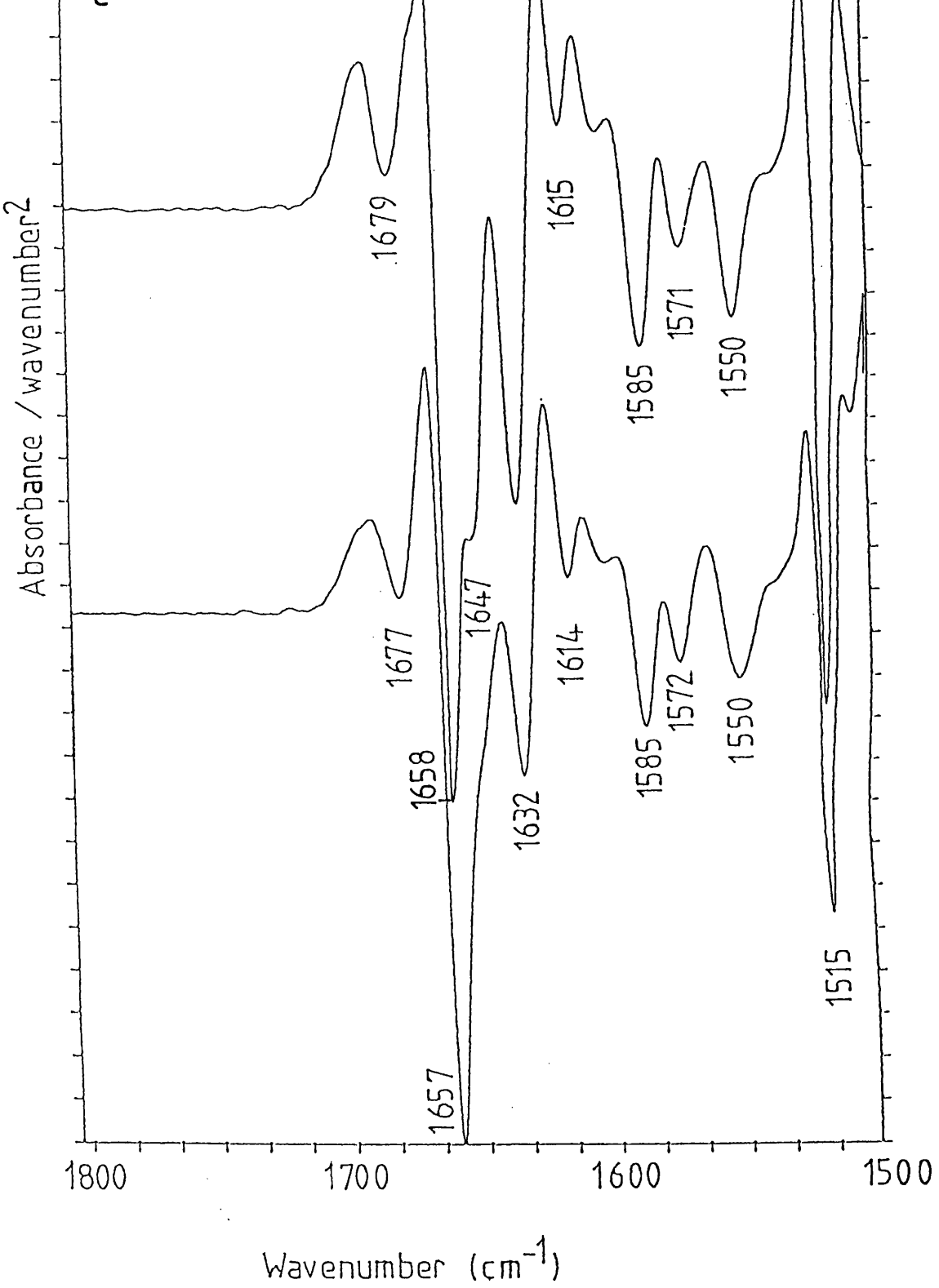
Absorbance / wavenumber2
1679
1615
1585
1571
1550
1677
1647
1658
1632
1614
1585
1572
1550
1657
1515
1800
1700
1600
1500
Wavenumber (cm-1)

1679 cm^{-1} from β-turns and/or β-sheet, 1658 cm^{-1} from unexchanged α-helix, 1647 cm^{-1} from exchanged α-helix and exchanged random structure, 1632 cm^{-1} β-sheet and 1615 cm^{-1} from tyrosine side chains. The bands at 1585 cm^{-1} and 1571 cm^{-1} are assigned to the ionised carboxylate side chains of the aspartate and glutamate residues respectively. The band at 1550 cm^{-1} is the amide II band that arises from the unexchanged N - H groups in the protein, indicating that complete H → D exchange has not occurred. The band at 1515 cm^{-1} is from tyrosine side chains. The only significant difference in the deconvolved spectrum (Fig. 5.3b) is a band at 1667 cm^{-1}, assigned to 3_{10}-helix (Krimm & Bandekar, 1986; Kennedy et al., 1991). This band is probably lost in the side lobe of the main band of the second derivative spectrum (upper trace, Fig. 5.3c).

The absorbance spectrum of deuterated porcine PLA_2 dried as a solid film on a Ge crystal is shown in Fig. 5.4a, with the second derivative spectrum shown in Fig. 5.4b. The main band in the second derivative spectrum occurs at 1652 cm^{-1}, with smaller bands occurring at 1682 cm^{-1}, 1636 cm^{-1} and 1615 cm^{-1}. Comparing this to the second derivative of the partially deuterated protein in solution (Fig. 5.3b), we see a decrease in the intensity of the 1636 cm^{-1} component in the dry protein, which is assigned to β-sheet.

The protein was dried from D_2O in an attempt to remove the possibility of absorption from H_2O molecules

Fig. 5.4a) Absorption spectrum of deuterated porcine PLA_2 in a thin lyophilised film on a Ge crystal.

b) Second derivative spectrum of porcine PLA_2 in a thin lyophilised film on Ge crystal.

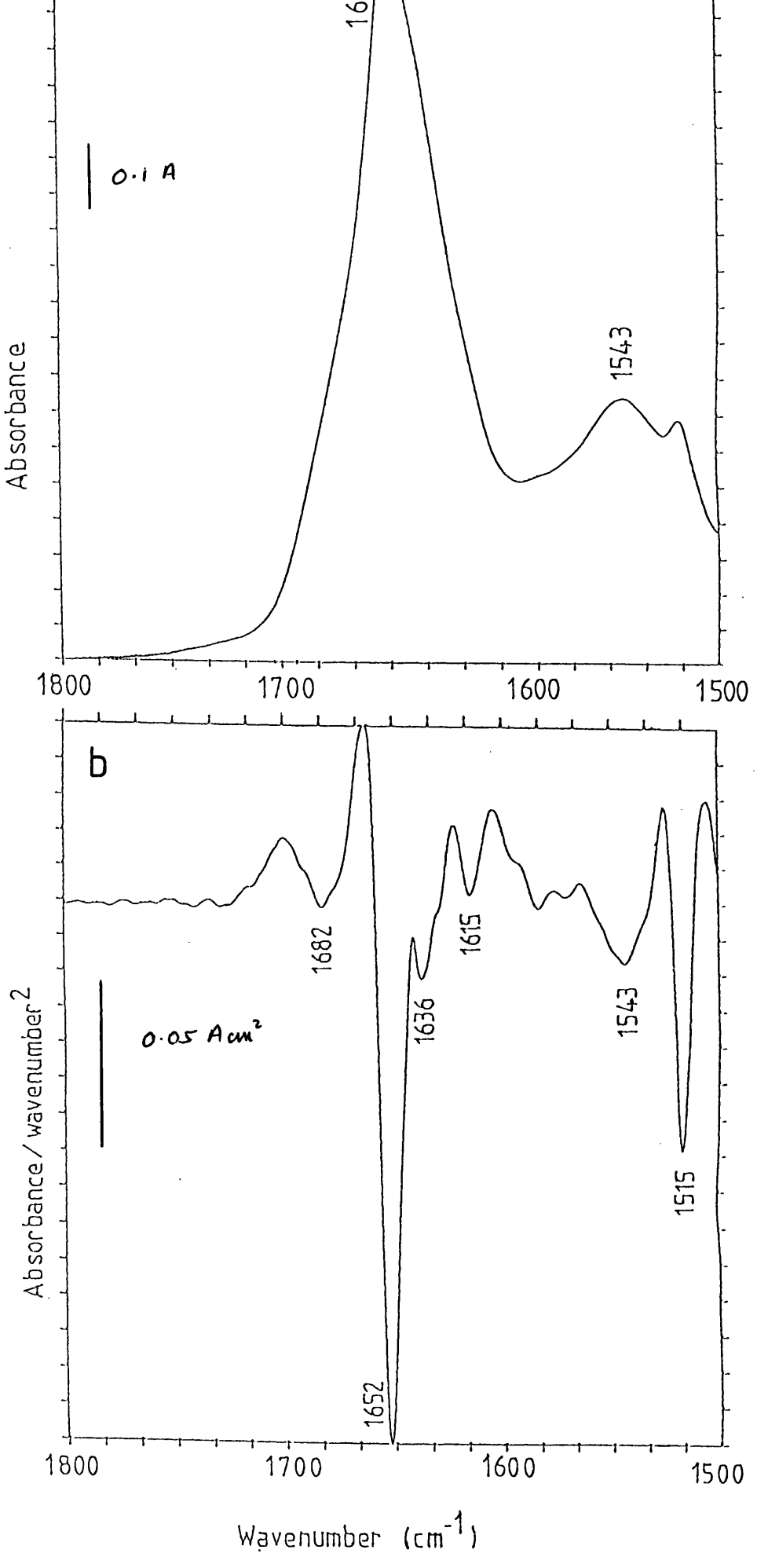
0.1 A
1543
Absorbance
1800
1700
1600
1500
b
1682
1652
1636
1615
1543
1515
0.05 Acm²
Absorbance / wavenumber²
Wavenumber (cm⁻¹)

remaining in the sample. Spectra of (pro)PLA_2 dried from H_2O have already been published (Aréas et al., 1989).

The absorption spectrum for porcine proPLA_2 in H_2O buffer is similar to that of the active enzyme in solution. No significant differences between the zymogen and the enzyme could be detected in the resolution enhanced spectra (not shown).

No significant difference in the spectra of porcine PLA_2 in the presence or absence of Ca^{2+} ions could be detected. No major changes occur in the enzyme in the temperature range 10^{o}-45^{o} C.

The rate of H → D exchange for porcine proPLA_2, Ca^{2+}-free and Ca^{2+}-bound PLA_2 was also studied over a 26 hour period. No significant difference in rates of exchange could be detected between the three samples by monitoring the amide II/amide I ratio.

Interactions of $C_{10}PN$ monomeric lipids with porcine (pro)PLA_2 were investigated in H_2O and D_2O buffers. No differences in the amide I region of these proteins could be detected in the presence and absence of $C_{10}PN$ lipid monomers (not shown).

Structural changes of the enzyme on $C_{18}PN$ micelles were also studied using porcine PLA_2. Fig. 5.2a (top trace, broken line) shows the amide I and II band of porcine PLA_2 in the presence of micelles at 35^{o}C in H_2O buffer. When compared to PLA_2 in buffer alone (Fig. 5.2a top trace, solid line), the amide II/amide I ratio is reduced by a factor of greater than 2.

To gain further insight into protein-micelle interactions, the experiments were repeated using PLA_2 in D_2O buffer. The absorption spectrum of partially deuterated porcine PLA_2 in the presence of $C_{18}PN$ micelles in D_2O buffer is shown in Fig. 5.3a (dotted line), with the amide I' maxima at 1653 cm^{-1}, compared to 1651 cm^{-1} in the absence of micelles (Fig. 5.3a, solid line). The deconvolved and second derivative spectra are shown in Figs. 5.3b (lower trace) and 5.3c (lower trace) respectively. Comparing the deconvolved spectra of porcine PLA_2 in D_2O in the presence and absence of micelles (Fig. 5.3b), there is an apparent decrease in the 1649 cm^{-1} band on incorporation into the micelle and an increase in the 1657 cm^{-1} band. The band at 1571 cm^{-1} shifts to 1572-1573 cm^{-1} on binding.

The difference spectrum of partially deuterated PLA_2 in the presence and absence of micelles is shown in Fig. 5.5. The difference spectrum was generated by subtracting the normalised absorption spectrum of deuterated porcine PLA_2 in the absence of $C_{18}PN$ micelles from the normalised absorption spectrum in the presence of $C_{18}PN$ micelles. A positive band at 1657 cm^{-1} is observed, with a major negative feature centred around 1632-1633 cm^{-1}. Two smaller negative features are also seen at 1669 cm^{-1} and 1686 cm^{-1} and a minor feature is noted around 1646 cm^{-1}. Subtraction of D_2O buffer containing varying amounts of H_2O contamination from the protein spectra produces

Fig. 5.5) Difference spectrum generated by subtracting the absorption spectrum of deuterated porcine PLA_2 in the absence of $C_{18}PN$ micelles from the absorption spectrum of deuterated porcine PLA_2 in the presence of $C_{18}PN$ micelles.

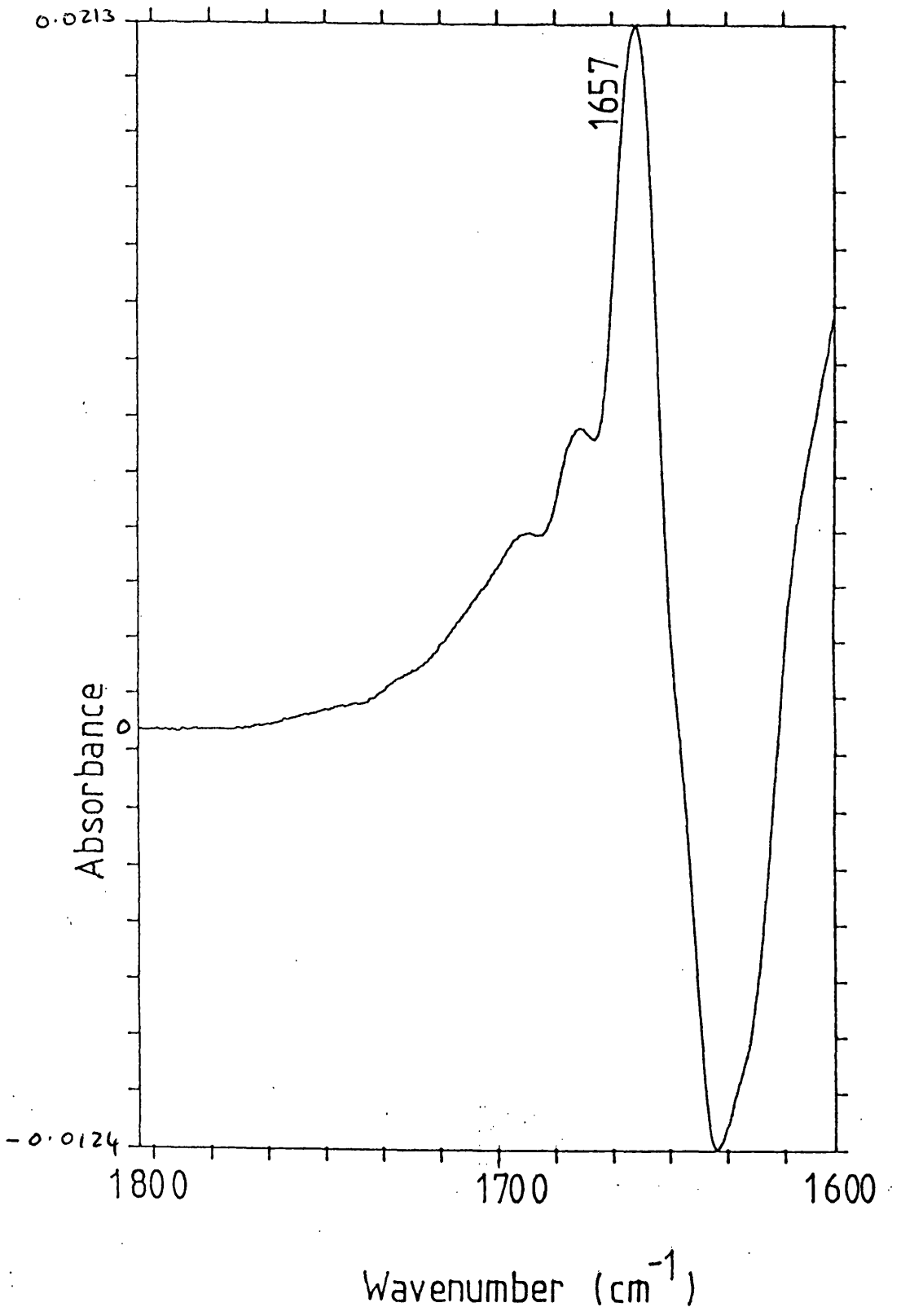
0.0213
1657
Absorbance
0
-0.0124
1800
1700
1600
Wavenumber (cm-1)

changes in the difference spectrum in the 1620-1635 cm^{-1} region. Therefore conclusions from this part of the difference spectrum must be treated with caution.

The absorption spectrum of porcine PLA_2 in the presence of inhibitor HHNP above its CMC in H_2O buffer is shown in Fig. 5.6. The amide I band occurs at 1657 cm^{-1} with the amide II band at 1551 cm^{-1}. The deconvolved spectrum does not differ significantly from that of the enzyme in solution. The absorption spectrum of partially deuterated PLA_2 in the presence of inhibitor micelles in D_2O buffer is shown in Fig. 5.7a (upper trace). The amide I' band is shifted from 1651 cm^{-1} in the absence of micelles to 1652 cm^{-1} on addition of HHNP micelles. The deconvolved spectrum is shown in Fig. 5.7a (lower trace) and second derivative spectrum in Fig. 5.7b. These spectra are similar to the resolution enhanced spectra of porcine PLA_2 in the presence of $C_{18}PN$ micelles, with bands assigned to α-helix at 1657 cm^{-1} and 1651 cm^{-1}, and the band at 1631-1632 cm^{-1}, assigned to β-sheet. Compared to the deconvolved spectrum in the absence of micelles (Fig 5.7a, lower trace), the β-sheet band appears to be reduced and the α-helix increased.

Quantitative analysis was carried out using Factor Analysis on the absorption spectra of porcine (pro)PLA_2 in H_2O under different conditions with the results shown in Table 5.I. Meaningful results could not be obtained for the protein interacting with micelles (see Discussion).

Table 5-I. A comparison of the quantification of three PLA_2's by FTIR Factor Analysis with other biophysical techniques.

		Percentage Content	
Protein	Structure	FTIR+	X-RAY*
Porcine proPLA$_2$	α-helix	56	55
	β-sheet	13	10
	β-turns	22	
Porcine PLA$_2$	α-helix	50	50
	β-sheet	14	10
	β-turns	24	
Bovine PLA$_2$	α-helix	55	50
	β-sheet	18	10
	β-turns	24	

*From Dijkstra et al. (1981, 1983)

		FTIR+	Raman*
Crotalus durissus	α-helix	46	54
	β-sheet	23	35
	β-turns	15	11

*From Aréas et al., 1989.

+The root mean square deviations of the FTIR values are 3.7% for α-helix, 8.3% β-sheet and 6% for β-turns (Lee et al., 1990).

Fig. 5.6) Absorption spectrum of porcine PLA_2 in the presence of HHNP above its cmc, pH 6.0.

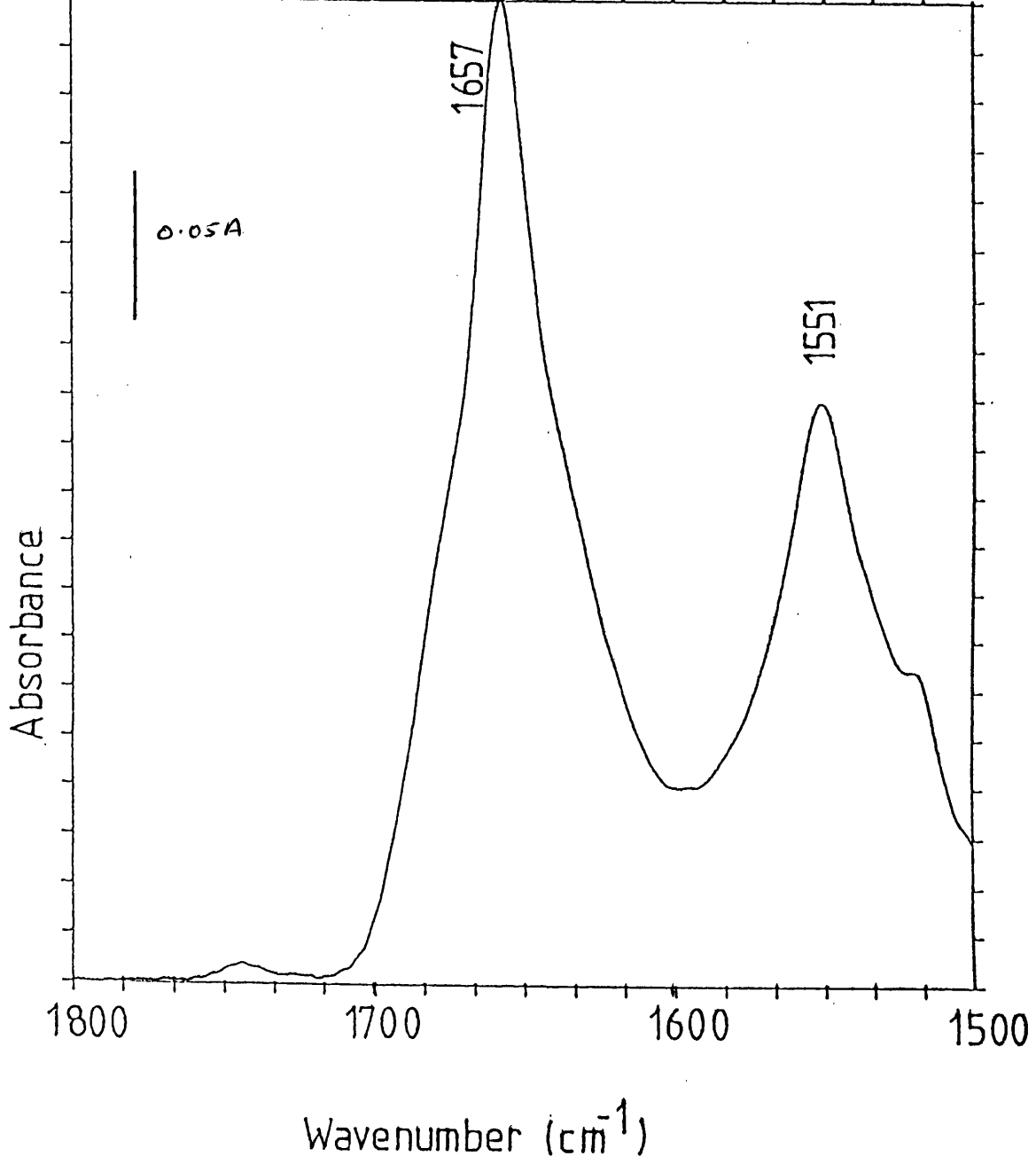
1657
1551
0.05A
Absorbance
1800
1700
1600
1500
Wavenumber (cm-1)

Fig. 5.7a) Absorption spectrum of partially deuterated porcine PLA_2 in the presence of HHNP micelles, pD 5.95 (upper trace) and its deconvolved spectrum using resolution enhancement factor 2.75 and bandwidth 15 cm^{-1} (lower trace).
b) Second derivative spectrum of partially deuterated porcine PLA_2 in the presence of HHNP micelles, pD 5.95.

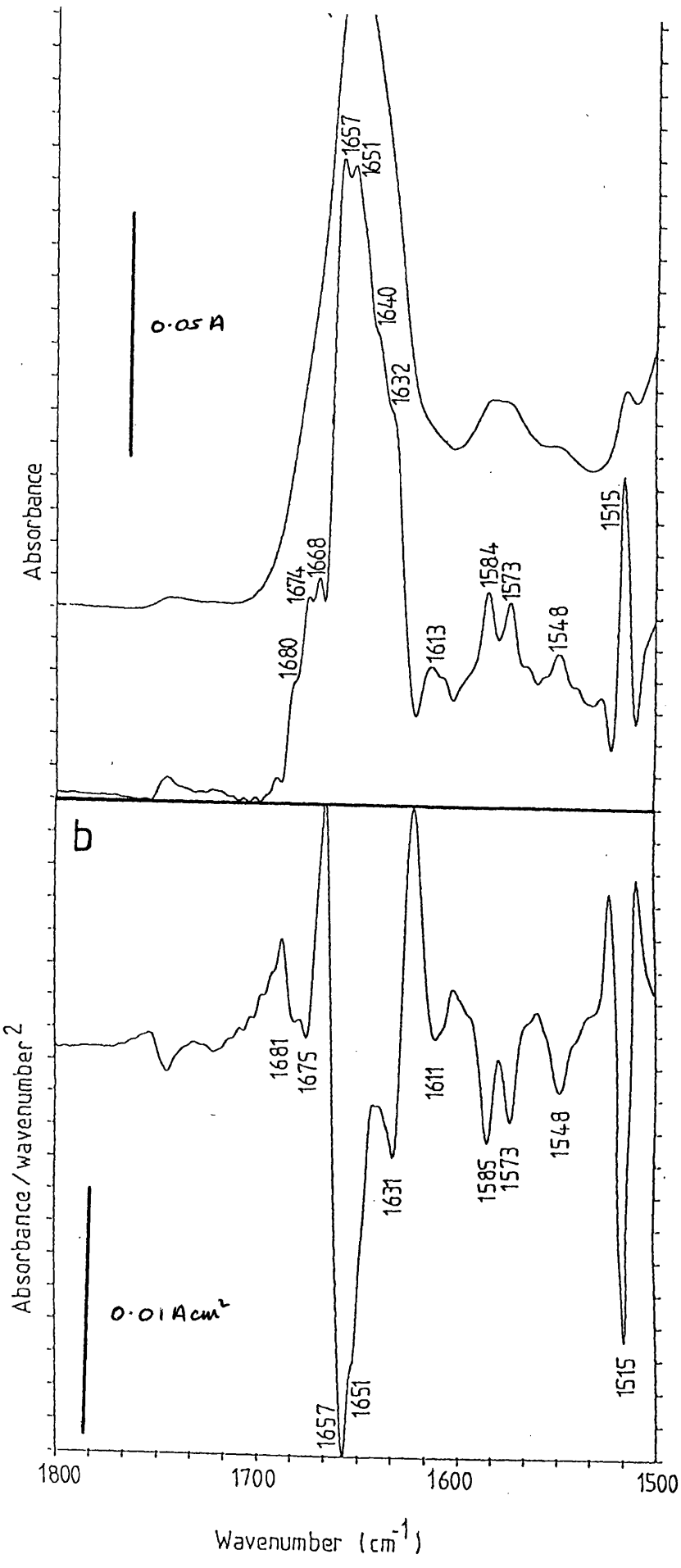
0·05 A
Absorbance
1657
1651
1640
1632
1680
1674
1668
1613
1584
1573
1548
1515
b
0·01 Acm⁻²
Absorbance / wavenumber⁻²
1681
1675
1657
1651
1631
1611
1585
1573
1548
1515
1800
1700
1600
1500
Wavenumber (cm⁻¹)

5.3.2. Bovine PLA_2

The use of bovine PLA_2 in a similar set of experiments produced similar results. The absorption spectrum of bovine PLA_2 in the absence (solid line) and presence (dotted line) of $C_{18}PN$ micelles in H_2O buffer (Fig. 5.8a), shows the amide I band at 1658 cm^{-1} and the amide II band at 1550 cm^{-1}. Results of the Factor Analysis of the protein in the absence of micelles are shown in Table 5.I. The amide II/I ratio is again reduced on binding to micelles. Further details are identified from the second derivative spectrum of the protein in the absence of micelles (Fig. 5.8b) showing components at 1683 cm^{-1}, assigned to β-turns and/or β-sheet, at 1657 cm^{-1}, assigned to α-helix and/or random structure, 1635 cm^{-1} assigned to β-sheet and 1616 cm^{-1} assigned to tyrosine sidechains. The amide II band is seen at 1550 cm^{-1} and the band assigned to tyrosine sidechains occurs at 1516 cm^{-1}.

The partially deuterated bovine PLA_2 showed an amide I' maximum at 1652 cm^{-1} in the absence of $C_{18}PN$ micelles after undergoing the same incubation in D_2O buffer as the porcine enzyme (Fig. 5.9a, upper trace), and at 1654 cm^{-1} in the presence of $C_{18}PN$ micelles (Fig. 5.9a, lower trace). The deconvolved spectra are shown in Fig. 5.9b, with the top spectrum being bovine PLA_2 in the absence of micelles and the lower trace being of the bovine enzyme bound to micelles. The band assignments from the deconvolved spectra are as follows:- β-sheet and/or

Fig. 5.8a) Absorption spectrum of bovine PLA_2 in H_2O buffer, pH 6.0 in the absence (solid line) and presence (broken line) of $C_{18}PN$ micelles.
b) Second derivative spectrum of bovine PLA_2 in H_2O buffer.

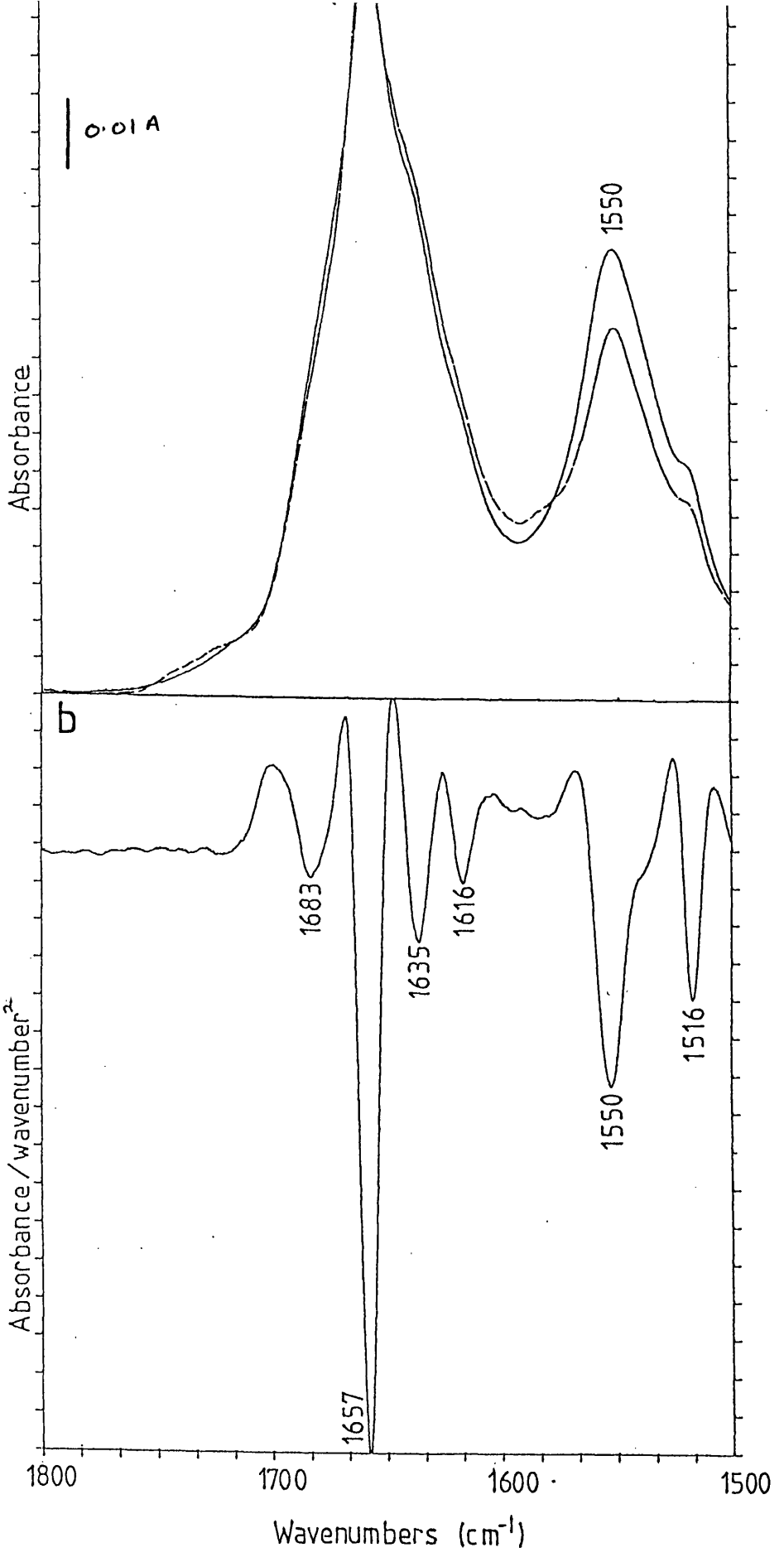
0.01 A
Absorbance
1550
b
1683
1657
1635
1616
1550
1516
Absorbance / wavenumber^2
1800
1700
1600
1500
Wavenumbers (cm^{-1})

Fig. 5.9a) Absorption spectra of partially deuterated bovine PLA_2 in the absence (upper trace) and presence (lower trace) of $C_{18}PN$ micelles, pD 6.0.

b) Their deconvolved spectra, using a resolution enhancement factor 2.5 and bandwidth 15 cm^{-1}.

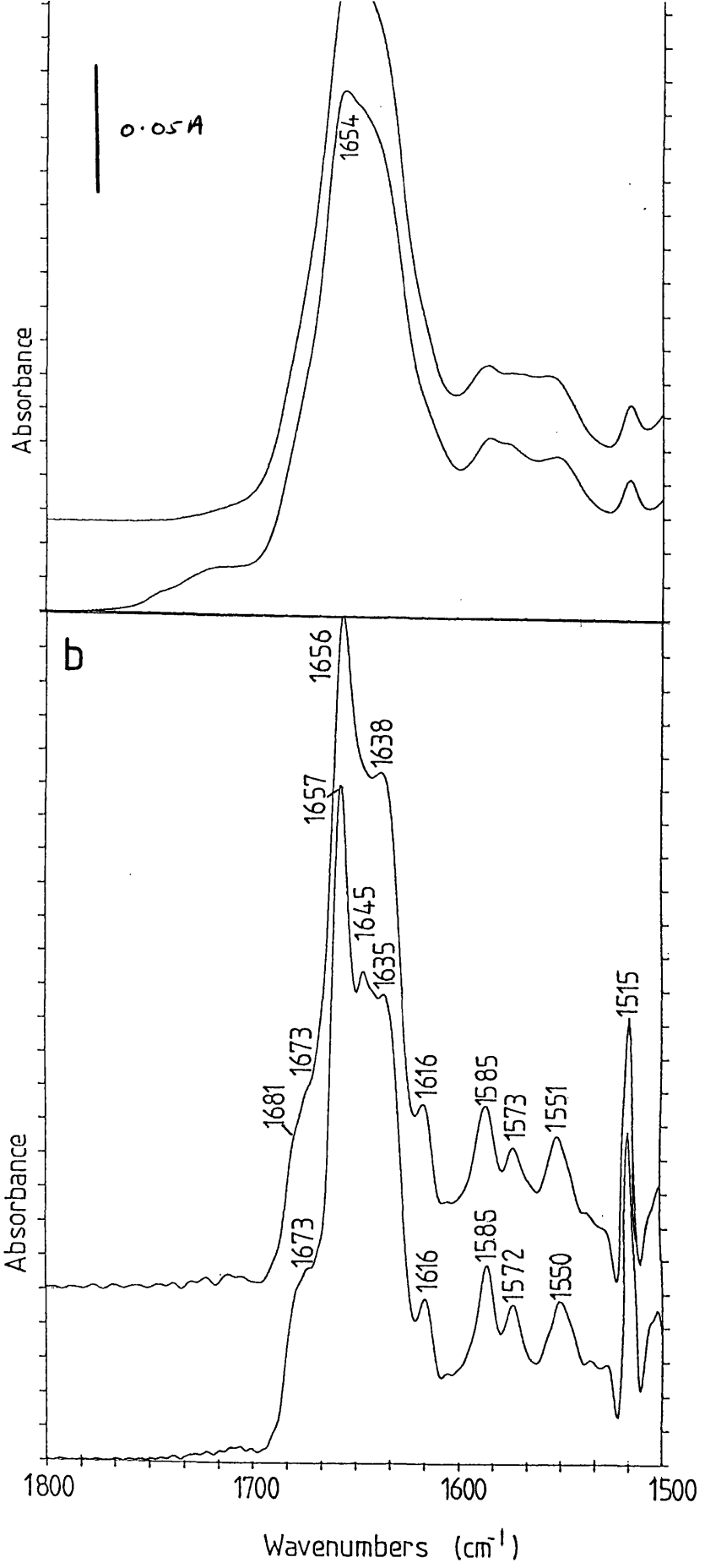
0·05A
1654
Absorbance
b
1656
1638
1657
1645
1635
1681
1673
1616
1585
1573
1551
1515
1673
1616
1585
1572
1550
Absorbance
1800
1700
1600
1500
Wavenumbers (cm⁻¹)

β-turns at 1681 cm^{-1}, β-turns at 1673 cm^{-1}, unexchanged α-helix at 1656-1657 cm^{-1}, exchanged random structure (with the possibility of deuterated α-helix) at 1645 cm^{-1}, β-sheet at 1635-1638 cm^{-1} and tyrosine sidechains at 1616 cm^{-1}. The relative intensity of the component 1635-1638 cm^{-1} is reduced on binding compared to the intensity of the main α-helical component, which shifts from 1656 cm^{-1} to 1657 cm^{-1}.

Similar changes are observed when the partially deuterated bovine enzyme binds to HHNP micelles, with Fig. 5.10 showing the deconvolved spectrum. The component bands in the deconvolved spectrum display a strong similarity to those of the deconvolved spectrum bound to $C_{18}PN$ (Fig. 5.9b, lower trace).

5.3.3. Snake venom PLA_2

The absorption spectra of the venom PLA_2 in H_2O buffer in the absence (solid line) and presence (dotted line) of $C_{18}PN$ micelles are shown in Fig. 5.11a. The amide I band is seen at 1657 cm^{-1} and amide II band at 1550 cm^{-1}. The amide II/I ratio is again reduced on interaction with the micelles. The second derivative spectrum of the protein in the absence of micelles is shown in Figs. 5.11b, with the peaks identified at 1682 cm^{-1}, assigned to β-turns and/or β-sheet, 1658 cm^{-1}, assigned to α-helix and/or random structures, 1633 cm^{-1}, assigned to β-sheet, and at 1615 cm^{-1}, assigned to tyrosine side chains. The amide II band is centred at

Fig. 5.10) Deconvolved spectrum of partially deuterated bovine PLA_2 in the presence HHNP micelles, pD 6.0, using a resolution enhancement factor 2.5 and bandwidth 15 cm^{-1}.

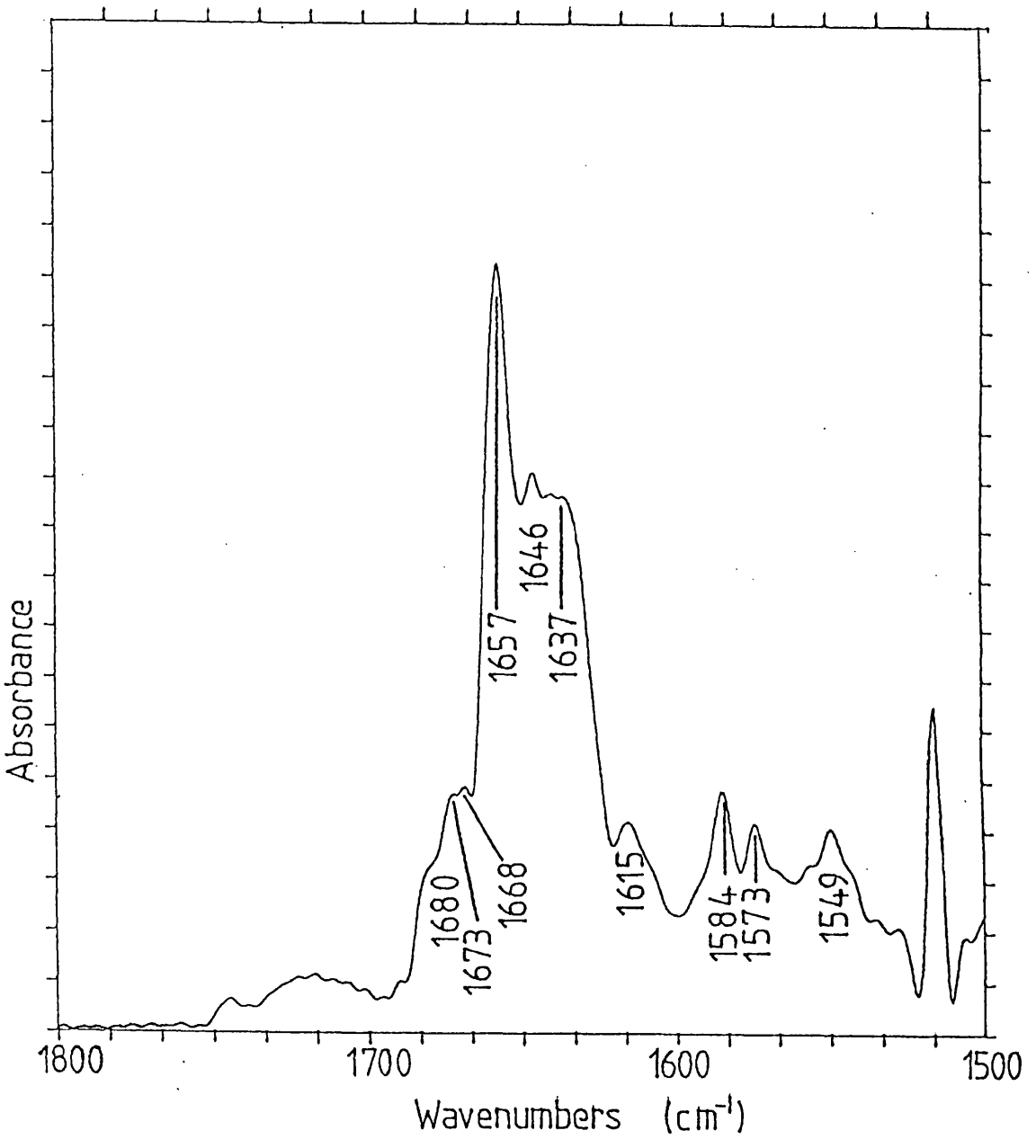
Absorbance
1800
1700
1600
1500
Wavenumbers (cm⁻¹)
1680
1673
1668
1657
1646
1637
1615
1584
1573
1549

Fig. 5.11a) Absorption spectra of snake venom PLA_2 in H_2O buffer in the absence (solid line) and presence (broken line) of $C_{18}PN$ micelles.
b) Second spectra of snake venom PLA_2 in H_2O buffer.

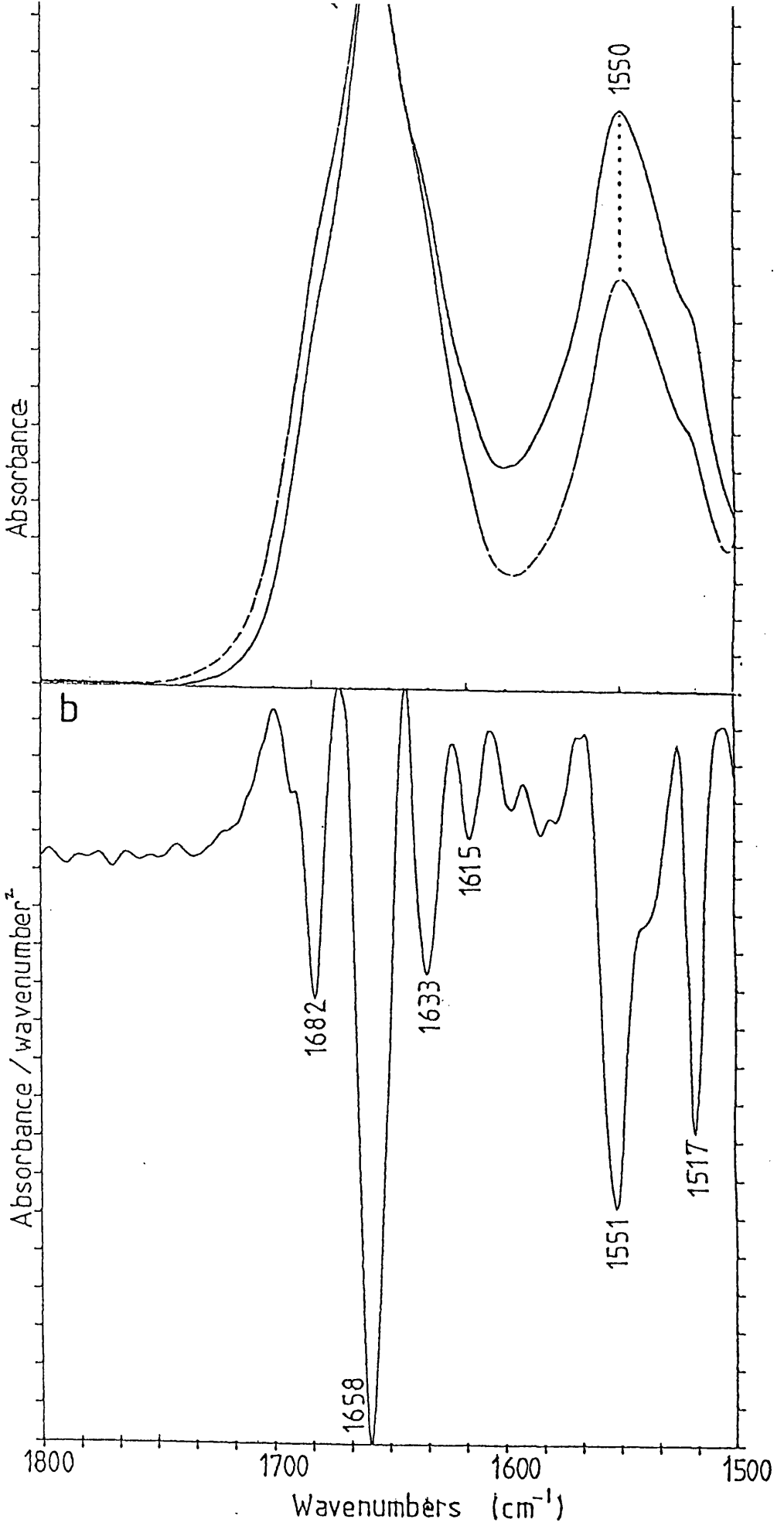
Absorbance
1550
b
Absorbance / wavenumber²
1682
1658
1633
1615
1551
1517
1800
1700
1600
1500
Wavenumbers (cm⁻¹)

1551 cm^{-1}, with the tyrosine band at 1517 cm^{-1}. Factor Analysis results of the snake venom PLA_2 in the absence of micelles in H_2O buffer are shown in Table 5.I.

The absorption spectrum of partially deuterated snake venom PLA_2 in the absence (upper trace) and presence (lower trace) of $C_{18}PN$ micelles are shown in Fig. 5.12a, indicating a shift from 1649 cm^{-1} to 1651 cm^{-1} on binding. Their respective deconvolved spectra are shown in Fig. 5.12b, with the respective second derivative spectra in Fig. 5.12c.

The band positions are similar for both spectra, with the following assignments:- β-turns and/or β-sheet at 1673-1677 cm^{-1}, unexchanged α-helix at 1655-1656 cm^{-1}, exchanged α-helix at 1650 cm^{-1}, exchanged random structure at 1644 cm^{-1}, β-sheet at 1633 cm^{-1} and tyrosine sidechains at 1611-1612 cm^{-1}. The main difference between the two spectra is the decrease in the intensity of the 1633 cm^{-1} band, assigned to β-sheet, occurring on interaction with the micelles, relative to the 1655-1656 cm^{-1} band, assigned to α-helix.

The absorption and second derivative spectra of the deuterated sample dried down onto Ge are shown in Fig. 5.13a and b, showing the amide I' band at 1653 cm^{-1}. The second derivative spectrum shows the main amide I' component band at 1656 cm^{-1} assigned to α-helix, with the band at 1634 cm^{-1} assigned to β-sheet, at 1682 cm^{-1} assigned to β-turns and β-sheet, and 1613 cm^{-1} assigned to tyrosine sidechains. Compared to the second derivative

Fig. 5.12a) Absorption spectra of partially deuterated snake venom PLA_2 in the absence (upper trace) and presence (lower trace) of $C_{18}PN$ micelles.

b) Their deconvolved spectra using resolution enhancement factor 2.125 and bandwidth 15 cm^{-1}.

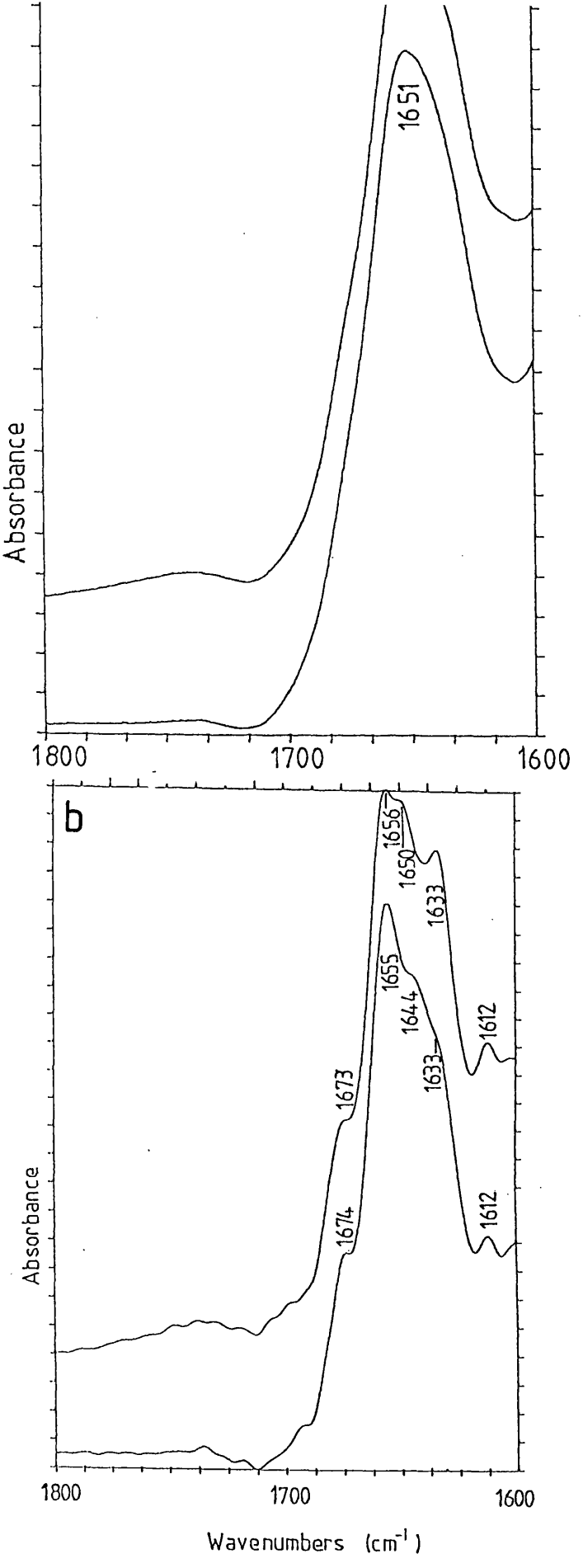
1651
Absorbance
1800
1700
1600
b
1656
1650
1633
1655
1644
1633
1612
1673
1674
1612
Absorbance
1800
1700
1600
Wavenumbers (cm⁻¹)

Fig. 5.12c) Second derivative spectra of partially deuterated snake venom PLA_2 in the absence (upper trace) and presence (lower trace) of $C_{18}PN$ micelles.

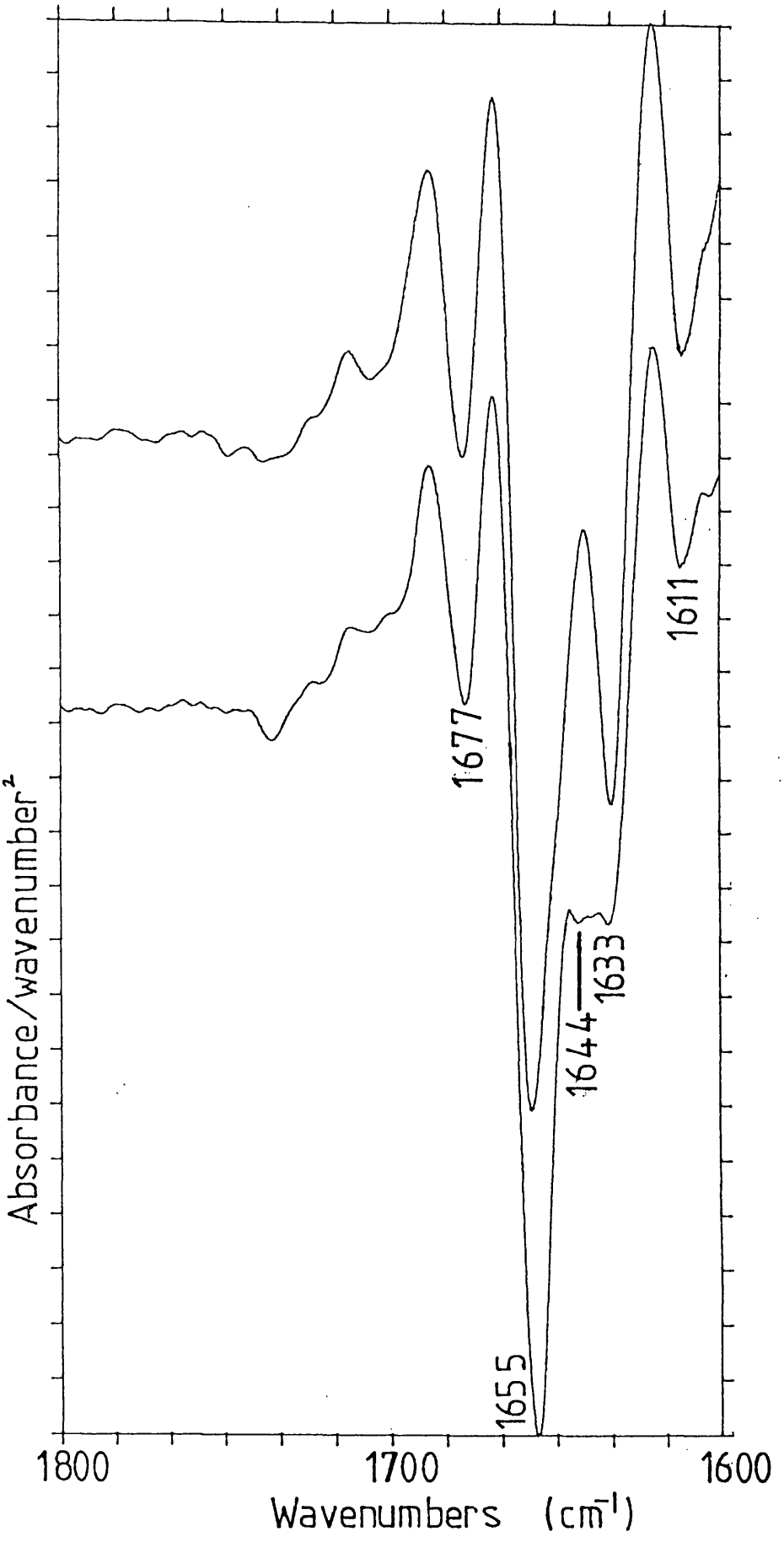
Absorbance/wavenumber²
1677
1655
1644
1633
1611
1800
1700
1600
Wavenumbers (cm⁻¹)

Fig. 5.13a) Absorption (upper trace) and second derivative (lower trace) spectra of partially deuterated snake venom PLA_2 in a thin lyophilised film on a Ge crystal.

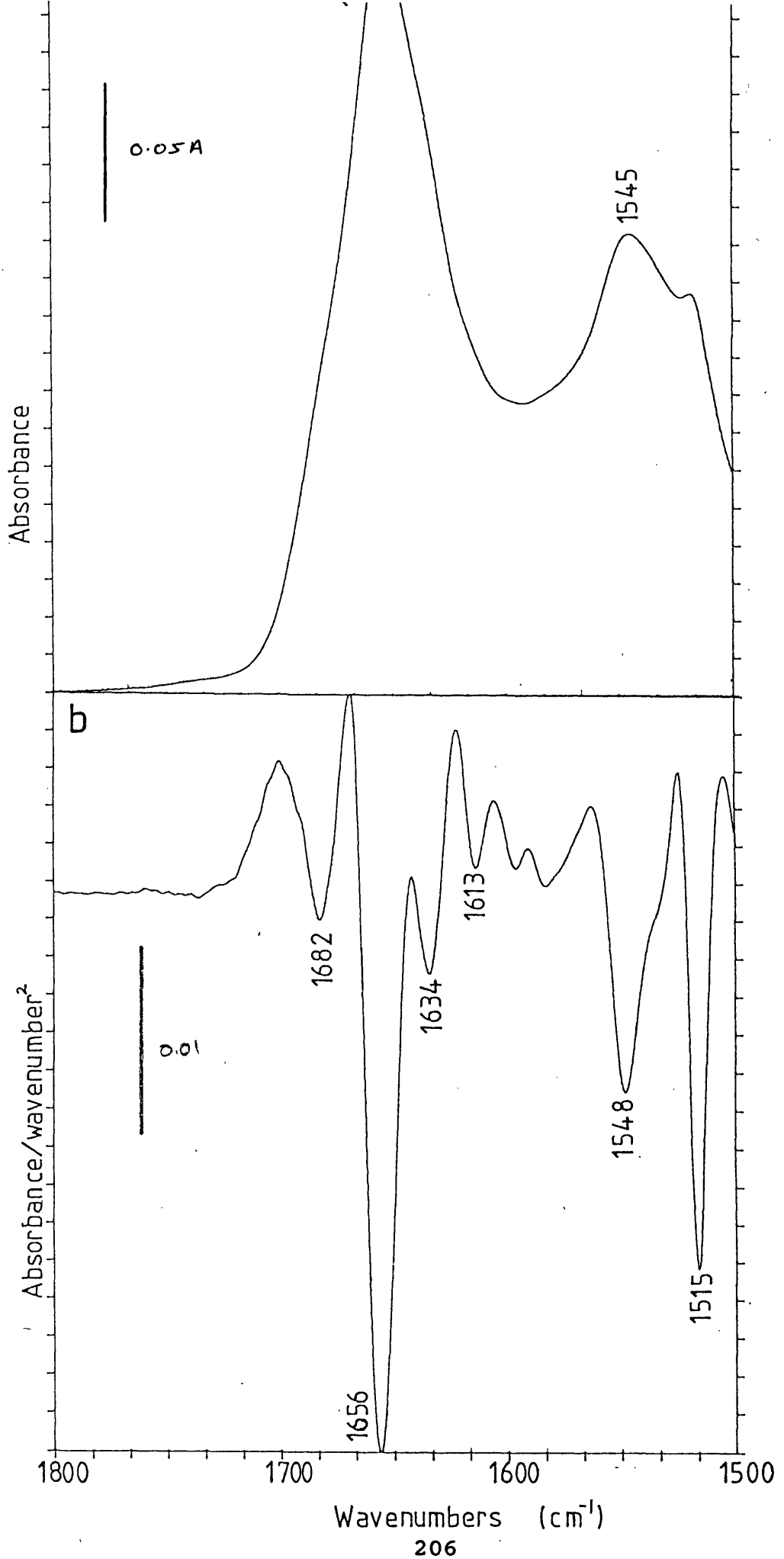
0.05A
1545
Absorbance
b
1682
1634
1613
1548
1515
1656
0.01
Absorbance/wavenumber²
1800
1700
1600
1500
Wavenumbers (cm⁻¹)

spectrum of snake venom PLA_2 in D_2O buffer (Fig. 5.12c), a decrease in intensity of the band assigned to β-sheet is observed.

5.4. DISCUSSION

The assignment of the components of the amide I band of porcine pancreatic (pro)PLA_2 and bovine pancreatic PLA_2 in H_2O and of the amide I' band in D_2O agree qualitatively with the results from X-ray diffraction work (Dijkstra et al., 1981, 1983).

Quantitative results of the pancreatic proteins in H_2O buffer using the Factor Analysis technique produced results which also agree well with those obtained from the X-ray structure (Table 5.I). This indicates that the structure of these proteins in aqueous solution is similar to that in the crystal form. The small difference in α-helical content between porcine proPLA_2 and PLA_2 may indicate that the seven amino acid sequence cleaved from the protein on activation has an α-helical structure. Our results disagree with those of Aréas et al. (1989) who observed an increase in α-helical content of more than 10% on the transition from porcine proenzyme to enzyme. The quantitative analysis of the Crotalus durissus terrificus venom PLA_2 gave values approximately 10% lower for both α-helix and β-sheet when compared to the results quoted by Aréas et al. (1989) calculated from Raman spectra. There is no X-ray structure published for the snake venom PLA_2, but our results indicate a slightly lower percentage of α-helix and a slightly higher percentage of β-sheet for the venom PLA_2 than for the pancreatic proteins.

Factor Analysis failed to produce meaningful results when applied to the spectra of porcine or snake venom PLA_2 bound to $C_{18}PN$ micelles. The second derivative spectra failed to identify any significant changes in the positions of the amide I components in H_2O buffer during protein-micelle interactions. However the Factor Analysis programme is based on the known structure of soluble proteins. This may indicate that, even though the positions of the amide I components remained unchanged, their band shapes may alter on going from the soluble to membrane-bound form.

The results of the enzymes dried down on the Ge crystal suggests that β-sheet structure is lost upon dehydration, and agrees with the results of Aréas et al., (1989). It should be noted that the crystals of PLA_2 will contain water of crystallisation to stabilise the protein whereas the lyophilised samples were virtually free of water judging by the absence of the 2125 cm^{-1} IR water absorption band.

The absence of any significant differences in spectra of porcine PLA_2 on the binding of Ca^{2+} ions or the binding of monomeric lipids indicates that both substrates fit into their respective position in the enzyme without causing a major change in secondary structure.

A change in all protein spectra were observed on the binding of $C_{18}PN$ micelles. Although there is no

significant change in the amide I band on protein-micelle interaction in H_2O, the amide II/I ratio is reduced by a factor of approximately 2. Changes in amide II/I ratios for polypeptides in different environments has been previously reported for melittin, where the amide II/I ratio of melittin and two of its fragments in the membrane is lower than that of the protein in solution (Lavialle et al., 1982). The marked differences in the spectra of partially deuterated porcine and bovine pancreatic PLA_2, and venom PLA_2, in solution and in membrane-bound form indicate that there is a conformational difference between the protein in the two different environments.

When comparing the deconvolved spectra of deuterated porcine PLA_2 in the presence and absence of micelles (Fig. 5.3b), the apparent reduction in intensity of the 1648 cm^{-1} band on binding to the $C_{18}PN$ micelles may be interpreted as a reduction of random structure with an increase in α-helix content, or as deuterated α-helix going from a hydrated to a hydrophobic environment on binding to micelles. However the difference spectrum of porcine PLA_2 in the presence and absence of micelles in D_2O (Fig. 5.5) does not support this concept. The striking features of the difference spectrum is the sharp positive feature at 1657 cm^{-1} and the broader negative feature at 1632-33 cm^{-1}. A loss in random structure, or a modification of the α-helices on going from a solution to membrane environment, would be expected to provide a

negative feature around 1646-1651 cm^{-1} in the difference spectrum. Therefore a reduction in β-sheet content, with a possible loss of β-turns, along with an increase in α-helical structure may be occurring.

Similar results were also observed for the partially deuterated bovine and snake venom PLA_2's on binding to $C_{18}PN$ micelles. This would indicate that a similar conformational change occurs within the snake venom enzyme during this binding interaction as occurs during the pancreatic PLA_2 binding, that is, an increase in α-helix and a loss in β-sheet, with a possible loss of some β-turn structure.

The binding of partially deuterated porcine enzyme to HHNP micelles increased the α-helical content of the protein at the expense of mainly β-sheet (Fig. 5.6b). In H_2O buffer the presence of micellar inhibitor does not induce the change in the amide II/I ratio of the enzyme as observed in the presence of $C_{18}PN$ micelles. The effect of environment on the amide II/I ratio has not been studied in depth, and it is unclear what induces changes of this type. The similarity of the bands in the resolution enhanced spectra of the enzyme bound to $C_{18}PN$ and HHNP micelles in D_2O buffer would indicate that the secondary structure of the protein in both systems is similar. Therefore the difference in the amide II/I ratio observed in H_2O buffer is unlikely to be connected to changes in secondary structure. It may possibly be

associated with the state of aggregation of the protein.

Despite there only being a 23% sequence homology (in optimised conditions of chain alignment) between porcine pancreatic and Crotalus durissus terrificus PLA_2's (Aréas et al., 1989), our results indicate that both enzymes undergo a similar conformational change on binding to lipid micelles, and when lyophilised as a thin film onto a Ge ATR crystal. Both results indicate that β-sheet, and possibly β-turn structure, is lost and α-helical structure is gained on binding to lipid micelles and when lyophilised. This, coupled with similar observations with the pancreatic enzymes, may indicate that when the protein interacts with the lipid bilayer, part of the protein becomes "dehydrated", possibly due to insertion into the hydrophobic core of the lipid bilayer.

5.5. SUMMARY

This chapter describes the study of the secondary structure of proPLA$_2$, the zymogen of porcine pancreatic proPLA$_2$, porcine and bovine pancreatic PLA$_2$ and Crotalus durissus terrificus PLA$_2$ in aqueous media. Quantitative analysis of the pancreatic proteins in solution made using Factor Analysis gave average values of 54% α-helix, 15% β-sheet and 23% β-turns, which agree well with those deduced from X-ray diffraction studies (Dijkstra et al., 1981,1983). Quantitative analysis of the snake venom PLA$_2$ gave values of 46% α-helix, 23% β-sheet and 15% β-turns.

Inducing catalytic activity in the enzymes through the binding of Ca^{2+} ions produced no significant differences in the secondary structure, or in the rate of H → D exchange, indicating that the ion binding can induce only a small structural change, if any at all. Furthermore no changes were observed in the temperature range 10° - 45° C. Similarly, no changes are observed on binding the non-degradable phospholipid analogue n-alkylphosphocholine in monomeric form. Considering these proteins contain seven disulphide bridges, it would be expected that they are rigid and difficult to perturb.

Conformational changes are observed between the lyophilised and hydrated samples. The observations are consistent with the loss of β-sheet upon dehydration, coupled with an increase in α-helical content.

The binding of porcine and bovine pancreatic PLA_2, and Crotalus durissus terrificus PLA_2 to n-alkylphosphocholine micelles produces changes which may indicate an increase in α-helical content, and a decrease in β-sheet, and possibly β-turn, content. Similar results were observed for the interaction of the pancreatic PLA_2 binding to substrate analogue inhibitor HHNP micelles.

The similarity of conformational changes occurring of the pancreatic and snake venom PLA_2's may indicate that the enzymes from different sources interact via a similar mechanism.

The conformational changes observed on binding to organised lipid surfaces indicate that the dramatic increase in catalytic activity is influenced by changes in the secondary structure. This would agree with Slotboom et al. (1982) who considered that the increase in activity must be caused by a conformational change leading to an optimal alignment of the amino acids in the active site.

CHAPTER SIX

FUTURE WORK

The work presented in this thesis illustrates the power of FTIR spectroscopy in elucidating protein secondary structure. It provides a valuable method of studying membrane-bound proteins to give researchers an accurate model of protein structure. The sensitivity of the technique is illustrated by the ability of identifying two similar, but structurally different, helices (the α- and 3_{10}-helices) occurring in polypeptide and protein samples.

Basic research is still required to study model peptides of known structure in order to accurately determine their IR absorption frequencies. The initial work in the application of IR and FTIR spectroscopy to elucidate protein secondary structure was based on theoretical calculations of proteins in the absence of water, and by empirical methods of the assignment of IR absorptions based on the known structure of the protein from X-ray diffraction models. The development of FTIR microscopy has provided a method of producing spectra of single protein crystals, thus enabling the direct comparison of the secondary structures deduced from X-ray diffraction with those deduced by FTIR spectroscopy. This will generate a more reliable method of IR band assignment and enable the direct comparison of the protein structure in a crystalline and soluble environment.

The accurate band assignment of IR absorptions of

types I, II and III β-turns is required to enhance the power of FTIR spectroscopy. This work could be done by the same methods as described in Chapter Three using the systematic study of model peptides whose structure is known from NMR spectroscopy or X-ray diffraction studies, in order to generate a more reliable method of protein band assignment. This method of approach is increasingly important in the study of small peptides, such as the alamethicin family, as their unusual amino acid sequences are likely to generate unusual secondary structures, such as the 3_{10}-helix and the β-bend ribbon. Furthermore the position of IR absorptions of small peptides is likely to deviate from the calculated and observed frequencies of structures found in large polypeptides and proteins.

The development of Factor Analysis has provided an important breakthrough in the application of FTIR spectroscopy to biomolecular systems in providing quantitative, as well as qualitative, information on protein secondary structures (Lee et al., 1990). However the predicted values have large error values. Even though the synthetic spectrum compares well with the absorption spectrum of the sample, resolution enhancement techniques identify differences between the spectra. Work is required to investigate the significance of these differences and to reduce the error values.

The development of site-directed mutagenesis has opened up a wide range of possibilities for many

biophysical techniques, including FTIR spectroscopy. The insertion into the amino acid sequence of residues sensitive to proteolytic digestion allows specific parts of the protein to be investigated. For example, cytoplasmic strands of membrane proteins could be cleaved, thus allowing an investigation of the membrane-bound portion of the protein by polarised ATR FTIR spectroscopy. Furthermore, important functional residues may be replaced, modifying the activity of the protein. Investigation of the effect of the amino acid substitution on the protein secondary structure and protein activity can easily be monitored by this technique.

The suitability of FTIR spectroscopy in studying protein-protein interactions needs to be thoroughly assessed. The absorption spectra of these systems are, at present, difficult to interpret because the amide I and II bands from the proteins in the sample overlap completely. However there is potential if the one protein or polypeptide is synthesised so that it has ^{13}C atoms in its polypeptide backbone. The shift induced in its amide I band position may be sufficient to reduce the overlap of the amide bands, thus allowing information on each of the proteins to be gained.

The improvement in scanning times has opened the way for the development of time-resolved FTIR spectroscopy. This technique allows information on protein dynamics to be gathered at a time resolution of $\approx$ 10 μs. For example,

the L, M and N intermediate states of the photocycle of bacteriorhodopsin have been characterised by time-resolved FTIR (Braiman et al., 1991) to give information on the changes occurring in the protein during the proton pumping and proton uptake cycle. The excellent time resolution gives this new technique tremendous potential of monitoring protein dynamics during ligand binding, and of protein folding.

Basic FTIR experiments need to be carried out to investigate DNA structure. The availability of milligram quantities of highly pure, synthetic oligonucleotides offers spectroscopists an exciting opportunity to probe the sequence-dependent effects on DNA-structural transitions and ligand-binding interactions. Work in this area has been carried out using NMR spectroscopy (Record et al., 1981; Williams et al., 1989; Braunlin & Bloomfield, 1991), but the application of FTIR spectroscopy has not yet been fully exploited in this area.

Another area of research that is suited to FTIR spectroscopy is the study of peptide - DNA interactions. Conformational changes occurring during these interactions need to be investigated in order to gain a better understanding of their structural basis. Examples of such proteins are restriction enzymes and transcription factors which are able to discriminate between a DNA-binding site and a random sequence, and

nucleases and chromosomal proteins which are able to bind to many different sequences (for review, see Churchill & Travers, 1991). FTIR spectroscopy is able to study both the peptide secondary structure and the DNA at the same time (Liquier et al., 1989; Dev & Walters 1990) and needs to be continued to develop this new field of research.

The development and success of FTIR spectroscopy in the field of biophysics has been mainly dependent on the advances made in the data acquisition techniques due to the application of computers and the development of the Fast Fourier transform. Future significant improvements with the instrumentation are thought to be limited, so the continuation of FTIR spectroscopy in the field of biophysics is now largely dependent on the vision, application and imagination of the spectroscopists.

REFERENCES

Abita, J-P., Lazdunski, M., Bonsen, P.P.M., Pieterson, W.A. & De Haas, G.H. (1972) Eur. J. Biochem. **30**, 37-47.

Akutsu, H., Kyogoku, Y., Nakahara, H. & Fukuda, K. (1975) Chem. Phys. Lipids **15**, 222-242.

Akutsu, H., Ikematsu, M. & Kyogoku, Y. (1981) Chem. Phys. Lipids **28**, 149-158.

Allen, L.C. (1975) Proc. Natl. Acad. Sci. (USA) **72**, 4701-4705.

Aréas, E.P.G., Laure, C.J., Gabilan, N., Araujo, P.S. & Kawana, Y. (1989) Biochim. Biophys. Acta **997**, 15-26.

Austen, B.M. (1979) FEBS Letters **103**, 308-313.

Azpiazu, I.A. & Chapman, D. (1991) Unpublished results.

Batenburg, A.M., Brasseur,R., Ruysschaert, J.M., van Scharrenburg, G.J.M., Slotboom, A.J., Demel, R.A. & de Kruijff, B. (1988) J. Biol. Chem. **263**, 4202-4207.

Barlow, D.J. & Thornton, J.M. (1988) J. Mol. Biol. **201**, 601-619.

Baty, D., Frenette, M., Lloubès, R., Howard, S.P., Géli, V., Pattus, F. & Lazdunski, C. (1988) Mol. Microbiol. **2**, 807 - 811.

Bavoso, A., Benedetti, E., Di Blasio, B., Pavone, V., Pedone, C., Toniolo, C., Bonora, G.M., Formaggio, F. & Crisma, M. (1988) J. Biomol. Struc. Dyn. **5**, 803-817.

Bavoso, A., Benedetti, E., Di Blasio, B., Pavone, V., Toniolo, C. & Bonora, G.M. (1986) Proc. Natl. Acad. Sci. USA **83**, 1988-1992.

Benedetti, E., Bavoso, A., Di Blasio, B., Pavone, C., Pedone, C., Toniolo, C. & Bonora, G.M. (1982a) Proc. Natl. Acad. Sci. USA **79**, 7951-7954.

Benedetti, E., Bavoso, A., Di Blasio, B., Pavone, V., Pedone, C., Crisma, M., Bonora, G.M. & Toniolo, C. (1982b) J. Am. Chem. Soc. **104**, 2437-2444.

Benedetti, E., Di Blasio, B., Pavone, V., Pedone, C., Santini, A., Bavoso, A., Toniolo, C., Crisma, M. & Sartore, L. (1990) J. Chem. Soc., Perkin Trans. **2**, 1829-1837.

Blobel, G. & Dobberstein, B. (1975) J. Cell Biol. **67**, 835-851.

Blume, A., Hubner, W. & Messner, G. (1988) Biochemistry **27**, 8239-8249

Bonora, G.M., Mappeli, C., Toniolo, C., Wilkening, R.R. & Stevens, E.S. (1984) Int. J. Biol. Macromol. **6**, 179-188.

Bonsen, P.P.M., De Haas, G.H., Pieterson, W.A. & van Deenen, L.L.M. (1972) Biochim. Biophys. Acta **270**, 364-382.

Bragg, W.L. (1913) Proc. Cambridge Phil. Soc. **17**, 43.

Braiman, M.S., Bousché, O. & Rothschild, K.J. (1991) Proc. Natl. Acad. Sci. (USA) **88**, 2388-2392.

Braiman, M.S., Mogi, T., Marti, T., Stern, L.J., Khorana, H.G. & Rothschild, K.J. (1988) Biochemistry **27**, 8516-8520.

Braunlin, W.H. & Bloomfield, V.A. (1991) Biochemistry **30**, 754-758.

Bretscher, M.S. (1973) Science **181**, 622-629.

Briggs, M.S. & Gierasch, L.M. (1984) Biochemistry **23**, 3111-3114.

Bruckner, H. & Graf, H. (1983) Experientia **39**, 528-530.

Buckley, J.T. (1990) Biochem. Cell Biol. **68**, 221-224.

Buckley, J.T. & Howard, S.P. (1985) J. Bacteriol. **161**, 1181.

Burgess, A.W. & Leach, S.J. (1973) Biopolymers **12**, 2599-2605.

Byler, D.M. and Susi, H. (1986) Biopolymers **25**, 469 - 487.

Carver, J.A. & Collins, J.G. (1990) Eur. J. Biochem. **187**, 645-650.

Cavard, D. & Lazdunski, C. (1979) Eur. J. Biol. **96**, 517-524.

Chakraborty, T., Huhle, B., Bergbauer, H. & Goebel, W. (1986) J. Bacteriol. **167**, 368-374.

Chen, Y-H., Yang, J.T. & Chau, K.H. (1974) Biochemistry **13**, 3350- 3359.

Chirgadze, Y. N., Fedorov, O.V. & Trushina, N.P. (1975) Biopolymers **14**, 679 - 694.

Churchill, M.E.A. & Travers, A.A. (1991) TIBS **16**, 92-97.

Creighton, T.E. (1984) in "Proteins: Structures and Molecular Principles", W.H. Freeman and Co., New York. pp. 200-203.

De Haas G.H., Bonsen, P.P.M., Pieterson, W.A. & Van Deenan L.L.M. (1971) Biochim. Biophys. Acta **239**, 252-266.

De Haas, G.H., Van Oort, M.G., Dilkman, R & Verger, R. (1989) Biochem. Soc. Trans. **17**, 274-276.

De Haas, G.H., Dijkman, R., Ransac, S. & Verger, R. (1991) Biochim. Biophys. Acta. in press.

Deisenhofer, J., Epp, O., Miki, K., Huber, R. & Michel, H. (1985) Nature **318**, 618-624.

Dennis, E.A. (1987) Drug Dev. Res. **10**, 205.

Derome, A.E. (1987) in "Modern NMR techniques for chemistry research". Pergamon, Oxford.

Dev, S.B. & Walters, L. (1990) Biopolymers **29**, 289-299.

Dijkman, R. & De Haas, G.H. (1991) Unpublished results.

Dijkstra, B.W., Kalk, K.H., Hol, W.G. & Drenth, J. (1981) J. Biol. Mol. **147**, 163-179.

Dijkstra, B.W., Renetseder, R., Kalk, K.W., Hol, W.G. & Drenth, J. (1983) J. Biol. Mol. **168**, 163-179.

Donné-Op den Kelder, G.M., Hille, J.D.R., Dijkman, R., De Haas, G.H. & Egmond, M.R. (1981) Biochemistry **20**, 4074-4078.

Donné-Op den Kelder, G.M. (1984) Ph.D Thesis from University of Utrect, The Netherlands.

Drake, A.F. (1986) Eur. Spectr. News **69**, 10-17.

Drenth, J., Enzing, C.M., Kalk, K.H. & Vessies, J.C.A. (1976) Nature **264**, 373-377.

Dwidedi, A.M., Krimm, S. & Malcolm, B.R. (1984) Biopolymers **23**, 2025-2065.

Earnst, T.N., Herzfeld, J. & Rothschild, K.J. (1990) Biophys. J. **58**, 1539-1546.

Elder, M., Hitchcock, P.B., Mason, R. & Shipley, G.G. (1977) Proc. R. Soc. A354, 157-170.

Engelhard, M., Gerwert, K, Hess, B., Kreutz, W. & Siebert, F. (1985) Biochemistry **24**, 400-407.

Engelman, D.E. & Steitz, T.A. (1981) Cell **23**, 411-422.

Euler, U.S. (1976) in "Prostoglandins" (ed. Curtis-Taylor, P.B.), Churchill-Livingstone, Amsterdam. pp. 3-7.

Fesik, S.W., Luly, J.R., Erikson, J.W. & Abad-Zapatero, C. (1988) Biochemistry **27**, 8297-8301.

Findlay, J.B. & Pappin, D.J. (1986) Biochem. J. **238**, 625-642.

Fisher, J., Primrose, W.U., Roberts, G.C.K., Dekker, N., Boelens, R., Kaptein, R. & Slotboom, A.J. (1989) Biochemistry **28**, 5929-5946.

Fleer, E.A.M., Verheij, H.M. & De Haas, G.H. (1978) Eur. J. Biochem. **82**, 261-269.

Fourier, J.B.J. (1822) Théorie analytique de la chaleur. Paris: Firmin Didot.

Fox, R. & Richards, F.M. (1982) Nature (London) **300**, 325-330.

Frazer, R.D.B. & Suzuki, E. (1966) Anal. Chem. **38**, 1770-1773.

Frazer, R.D.B. & Suzuki, E. (1969) Anal. Chem. **41**, 37-39.

Fredericks, P.M., Lee, J.B., Osbourn, P.R. & Swinkles, D.A.J. (1985a) Appl. Spectros. **39**, 303-310.

Fredericks, P.M., Lee, J.B., Osbourn, P.R. & Swinkles, D.A.J. (1985b) Appl. Spectros. **39**, 311-316.

Frenette, M., Knibiehler, M., Baty, D., Géli, V., Pattus, F., Verger, R. & Lazdunski, C. (1989) Biochemistry **28**, 2509 - 2519.

Garland, W.J. & Buckley, J.T. (1988) Infect. Immun. **56**, 1249-1253.

Gibson, N.J. & Cassim, J.Y. (1989) **28**, 2134-2139.

Gierasch, L.M. (1989) Biochemistry **28**, 923-930.

Glasoe, P.K. & Long, E.A. (1960) J. Phys. Chem. **64**, 188-191.

Green, M.J. & Buckley, J.T. (1990) Biochemistry **29**, 2177-2180.

Haris, P.I. & Chapman, D. (1988) Biochim. Biophys. Acta **943**, 375-380.

Haris, P.I., Chapman, D., Harrison, R.A., Smith, K.F. & Perkins, S.J. (1990) Biochemistry **29**,1377-1380.

Haris, P.I., Coke, M. & Chapman, D. (1989) Biochim. Biophys. Acta **995**, 160-167.

Henderson, R., Baldwin, J.M., Ceska, T.A., Zemlin, F., Beckmann, E. & Downing, K.H. (1990) J. Mol. Biol. **213**, 899-929.

Hille, J.D.R., Donné-Op den Kelder, G.M., Sauve, P., De Haas, G.H. & Egmond, M.R. (1981) Biochemistry **20**, 4063-4073.

Hille, J.D.R., Egmond, M.R., Dijkman, R., Van Oort, M.G., Sauve, P. & De Haas, G.H. (1983a) Biochemistry **22**, 5354-5358.

Hille, J.D.R., Egmond, M.R., Dijkman, R., Van Oort, M.G., Jirgensons, B. & De Haas, G.H. (1983b) Biochemistry **22**, 5347-5353.

Hitchcock, P.B., Mason, R., Thomas, K.M. & Sipley, G.G. (1974) Proc. Natl. Acad. Sci. (USA) **71**, 3036-3040.

Howard, S.P. & Buckley, J.T. (1982) Biochemistry **21**, 1662-1666.

Huang, C.H. (1977) Lipids **12**, 348 - 356.

Jackson, M. (1990) Ph.D Thesis, University of London.

Jackson, M., Haris, P.I. & Chapman, D. (1989a) Biochim. Biophys. Acta **998**, 75-79.

Jackson, M., Haris, P.I. & Chapman, D. (1989b) J. Molec. Structure **214**, 329-355.

Jackson, M., Bailey, P., Martin, S. & Chapman, D. (1991) Biochemistry (in press).

Jackson, M. & Mantsch, H.H. (1991a) Biochim. Biopys. Acta. **1078**, 231-235.

Jackson, M. & Mantsch, H.H. (1991b) Manuscript in preparation.

Jap, B.K., Walian, P.J. & Gehring, K. (1991) Nature **350**, 167-170.

Jirgenson, B. & De Haas, G.H. (1977) Biochim. Biophys. Acta **494**, 285-292.

Jones, D.S., Kenner, G.W., Preston, J. & Sheppard, R.C. (1965) J. Chem. Soc. 6227-6239.

Karle, I.L. (1981) in "Perspectives in Chemistry" (Eberle, R., Geiger, R. & Weiland, T. eds.) pp. 261-271, Karger, Basel.

Karle, I.L., Flippen-Anderson, J., Sukumar, M. & Balaram, P. (1987) Proc. Natl. Acad. Sci. (USA) **84**, 5087-5091.

Karle, I.L., Flippen-Anderson, J.L., Sukumar, M. & Balaram, P. (1988) Int. J. Pept. Protein Res. **31**, 567-576.

Karle, I.L., Flippen-Anderson, J.L., Uma, K., Balaram, H. & Balaram, P. (1989a) Proc. Natl. Acad. Sci. USA **86**, 765-769.

Karle, I.L., Flippen-Anderson, J.L., Uma, K. & Balaram, P. (1989b) Biopolymers **28**, 773-781.

Karle, I.L., Flippen-Anderson, J.L., Uma, K. & Balaram, P. (1989c) Biochemistry **28**, 6696-6701.

Kauppinen, J.K., Moffatt, D.J., Mantsch, H.H. & Cameron, D.G. (1981) Anal. Chem. **53**, 1454-1457.

Kendrew, J.C., Bodo, G., Dintzis, H.M., Parrish, R.G., Wyckoff, H. W. & Phillips, D.C. (1958) Nature **181**, 662-666.

Kendrew, J.C., Dickerson, R.E., Stranber, B.E., Hart, R.G., Davies, D.R., Phillips, D.C. & Shore, V.C. (1960) Nature **185**, 422-427.

Kennedy, D.F., Crisma, M., Toniolo, C. & Chapman, D. (1991) Biochemistry **30**, 6541-6548.

Kleffel, B., Gravito, R.M., Baumeister, W. & Rosenbusch, J.P. (1985) EMBO J. **4**, 1586-1592.

Konisky, J. (1982) Annu. Rev. Microbiol. **36**, 125 - 144.

Krimm, S. & Bandekar, J. (1986) Adv. Protein Chem. **38**, 181 - 364.

Krimm, S. & Dwivedi, A.M. (1982) Science **216**, 407-408.

Lavialle, F., Adams, R.G. & Levin, I.W. (1982) Biochemistry **21**, 2305-2312.

Le Bars, M., Bachet, B. & Mornon, J.P. (1988) Zeit. Kristallogr. **185**, 588.

Lee, D.C. & Chapman, D. (1986) Bioscience Reports **6**, 235-256.

Lee, D.C., Haris, P.I., Chapman, D. & Mitchell, R.C. (1990) Biochemistry **29**, 9185-9193.

Lingappa, V.R. (1991) Cell **65**, 527-530.

Liquier, J., Mchami, A. & Taillandier, E. (1989) J. Biomolec. Struct. **7**, 119-126.

Luzzati, V. (1968) in "Biological Membranes" (ed. Chapman, D.), Academic Press, New York, pp. 71-123.

MacLennan, D.H., Brandl, C.J., Korczac, B. & Green, N.M. (1985) Nature **316**, 597-607.

Marshall, G.R. In "Intra-Science Chemistry Reports"; Kharasch, N. Ed.; Gordon and Breach: New York, 1971; pp. 305-316.

Marshall, G.R., Hodgkin, E.E., Langs, D.A., Smith, G.D., Zabrocki, J. & Leplawy, M.T. (1990) Proc. Natl.Acad. Sci. U.S.A. **87**, 487-491.

Martinez, M.C., Lazdunski, C. & Pattus, F. (1983) EMBO J. **2**, 1501-1507.

Massotte, D., Dasseux, J.L., Sauve, P., Cyrklaff, M., Loenard, K. and Pattus, F. (1989) Biochemistry **28**, 7713-7719.

Mathew, M.K. & Balaram, P. (1983) Molec. Cellul. Biochem. **50**, 47-64.

Mendelsohn, R., Davies, M.A., Brauner, J.W., Schuster, H.F. & Dluhy, R.A. (1989) Biochemistry **28**, 8934-8939.

Mendelsohn, R., Davies, M.A., Schuster, H.F., Xu, Z. & Bittman, R. (1991) Biochemistry **30**, 8558-8563.

Menestrina, G., Voges, K.P., Jung, G. & Boheim, G. (1986) J. Membrane Biol. **93**, 111-132.

Merrill, A.R. & Cramer, W.A. (1990) Biochemistry **29**, 8529-8534.

Miyazawa, T. (1960) J. Chem. Phys. **32**, 1647- 1652.

Moffat, D.J., Kauppinen, J.K., Cameron, D.G., Mantsch, H.H. & Jones, R.N. (1986) Computer programs for infrared spectrophometry, N.R.C.C. Bulletin No. **18**, Ottawa, Canada.

Morlon, J., Chartier, M., Bidaut, M. & Lazdunski, C. (1988) Mol. Gen. Genet. **211**, 232-243.

Nabedryk, E., Garavito, R.M. & Breton, J. (1988) Biophys. J. **53**, 671-676.

Nabedryk, E., Tiede, D.M., Dutton, P.L. & Breton, J. (1981) Biochim. Biophys. Acta **682**, 273 - 280.

Némethy, G., Phillips, D.C., Leach, S.J. & Scheraga, H.A. (1967) Nature **214**, 363-365.

Nicchitta, C.V., Migliaccio, G. and Blobel, G. (1991) Cell **65**, 587-598.

Niewenhuizen, W., Kunze, H. & De Haas, G.H. (1974) Methods Enzymol. **32B**, 147-154.

Okamura, E., Umemura, J. and Takenaka, T. (1990) Biochim. Biophys. Acta **1025**, 94-98.

Oldfield, E. & Chapman, D. (1972) FEBS Lett. **23**, 285-297.

Parker, M.W., Pattus, F., Tucker, A.D. & Tsernoglou, D. (1989) Nature **337**, 93 - 96.

Parker, M.W., Tucker, A.D., Tsernoglou, D. & Pattus, F. (1990) Trends Biochem. Sci. **15**, 126-129.

Paterson, Y., Rumsey, S.M., Benedetti, E., Nemethy, G. & Scheraga, H.A. (1981) J. Am. Chem. Soc. **103**, 2947-2955.

Pattus, F., Cavard, D., Verger, R., Lazdunski, C., Rosenbusch, J. & Schindler, H. (1983) in "Physical Chemistry of Transmembrane Ion Motions" (Spach, G., Ed.) pp. 407 - 413, Elsevier, Amsterdam.

Pauling, L., Corey, R.B. & Branson, H.R. (1951) Proc. Natl. Acad. Sci. (USA) **37**, 205-211.

Pauling, L. & Corey, R,B, (1951a) Proc. Natl. Acad. Sci. (USA) **37**, 235-340.

Pauling, L. & Corey, R.B. (1951b) Proc. Natl. Acad. Sci. (USA) **37**, 241-50.

Pavone, V., Di Blasio, B., Santinti, A., Benedetti, E., Pedone, C., Toniolo, C. & Crisma, M. (1990a) J. Mol. Biol. **214**, 63 633-635.

Pavone, V., Benedetti, E., Di Blasio, B., Pedone, C., Santini, A., Bavoso, A., Toniolo, C., Crisma, M. & Sartore, L. (1990b) J. Biomol. Struct. Dyn. **7**, 1321-1331.

Pearson, R.H. & Pascher, I. (1979) Natue **281**, 499-501.

Perutz, M.F. (1951) Nature **167**, 1053-1054.

Pieterson, W.A., Volwerk, J.J. & De Haas, G.H. (1974) Biochemistry **13**, 1439-1445.

Pletnev, V.Z., Gromov, E.P. & Popov, E.M. (1973) Khim. Prir. Soedin. **9**, 224-229.

Popot, J-L. & Engelman, D.M. (1990) Biochemistry **29**, 4031-4037.

Popot, J-L., Engelman, D.M., Gurel, O. & Zaccai, G. (1990) J. Mol. Biol. **210**, 829-847.

Prasad, B.V.V. & Balaram, P. (1984) C.R.C. Crit. Rev. Biochem. **16**, 307-348.

Pulla Rao, C., Nagaraj, R., Rao, C.N.R. & Balaram, P. (1980) Biochemistry **19**, 425-431.
Rath, P., Bouché, O., Merrill, A.R., Cramer, W.A. & Rothschild, K.J. (1991) Biophys. J. **59**, 516-522.

Record, M.T.,Jr., Mazur, S.J., Melancon, P., Roe, J.M., Shaner, S.L. & Unger, L. (1981) Ann. Rev. Biochem. **50**, 997-1024.

Reddy, G.L. & Nagaraj, R. (1989) J. Biol. Chem. 264, 16591-16597.

Rizzo, V., Stankowski, S. & Schwarz, G. (1987) Biochemistry **26**, 2751-2759.

Roholt, O.A., & Schlamowitz, M. (1961) Arch. Biochem. Biophys. **94**, 364.

Rosenblatt, M., Beaudette, N.V. & Fasman, G.D. (1980) Proc. Natl. Acad. Sci. (USA) **77**, 3983-3987.

Rothschild, K.J., Gray, D., Mogi, T., Marti, T., Braiman, M.S., Stern, L.J. & Khorana, H.G. (1989) Biochemistry **28**, 7052-7059.

Rothschild, K.J., Roepe, P., Ahl, P.L., Earnest, T.N., Bogomolni, R.A., Das Gupta, S.K., Mulliken, C.M. & Herzfeld, J. (1986) Proc. Natl. Acad. Sci. (USA) **83**, 347-351.

Rothschild, K.J., Sanches, R., Hsaio, R.L. & Clark, N.A. (1980) Biophys. J. **31**, 53-64.

Saitô, H., Tabeta, R., Formaggio, F., Crisma, M. & Toniolo, C. (1988) Biopolymers **27**, 1607-1617.

Sanger, F. & Thompson, E.O.P. (1963) Biochem. J. **53**, 353 - 374.

Sanger, F. & Tuppy, H. (1961) Biochem. J. **49**, 463-490.

Schein, S.J., Kagan, B. and Finkelstein, A. (1978) Nature **276**, 159 - 169.

Shinnar, A.E. & Kaiser, E.T. (1984) J. Am. Chem. Soc. **106**, 5006-5007.

Shipley, G.G. (1972) in "Biological Membranes 2" (ed. Chapman, D. & Wallach, D.F.H.) Academic Press, London, pp. 1-89.

Singer, S.J. & Nicolson, G.L. (1972) Science **175**, 720-731.

Slotboom, A.J., Verheij, H.M. & De Haas, G.H. (1982) in "Phospholipids", (Hawthorne, J.N. & Ansell, G.B., eds.) Vol. **4**, pp. 359-434, Elsevier, Amsterdam.

Smith, G.D., Pletnev, V.Z., Duax, W.L., Balasabramanian, T.M., Bosshard, H.E., Czerwinski, E.W., Kendrick, N.E., Matthews, F.S. & Marshall, G.R. (1981) J. Am. Chem. Soc. **103**, 1493-1501.

Soares de Araujo, P., Rosseau, M.Y., Kremer, J.M.H., Van Zoelen, E.J.J. & De Haas (1979) Biochemistry **18**, 580-586.
Suga, H., Shirabe, K., Yamamoto, T., Tasumi, M., Umeda, M., Nishimura, C., Nakazawa, A., Nakanishi, M. & Arata, Y. (1991) J. Biol. Chem. **266**, 13527-13543.

Susi, H. in "Structure and Stability of Biological Macromolecules" (Timasheff, S.N. & Fasman, G.D., eds.) pp. 575-663, Decker, New York.

Susi, H. & Byler, D.M. (1986) Methods Enzymol. **130**, 290-311.

Ter-Minassian-Saraga, L., Okamura, E., Umemura, J. & Takenaka, T. (1988) Biochim. Biophys. Acta **946**, 417-423.

Thomas, G.J. & Kyogoku, Y. (1977) in "Infrared and Raman Spectroscopy", Part C, Practical Spectroscopy Vol. 1 (Braine, E.G. & Grasselli, J.G., eds.) Marcel Dekker Inc., New York.

Toniolo, C. (1989) Biopolymers **28**, 247-257.

Toniolo, C. & Benedetti, E. (1988) ISI Atlas of Science: Biochemistry **1**, 225-230.

Toniolo, C., Bonora, G.M., Barone, V., Bavoso, A., Benedetti, E., Di Blasio, B., Grimaldi, P., Lelj, F., Pavone, V. & Pedone, C. (1985) Macromolecules **18**, 895-902.

Toniolo, C., Bonora, G.M., Bavoso, A., Benedetti, E., Di Blasio, B., Pavone, V. & Pedone, C. (1986) Macromolecules **19**, 472-479.

Toniolo, C., Crisma, M., Anzolin, M., Benedetti, E., Di Blasio, B., Pavone, V., Pedone, C. & Santini, A. (1991) manuscript in preparation.

Tucker, A.D., Pattus, F. & Tsernoglou, D. (1986) J. Mol. Biol. **190**, 133-134.

Venkatachalapathi, Y.V. & Balaram, P. (1981) Biopolymers **20**, 1137-1145.

Van Dam-Mieras, M.C.E., Slotboom, A.J., Pieterson, W.A.& De Haas, G.H. (1975) Biochemistry **14**, 5387-5393.

Van der Bergh, C.J., Slotboom, A.J., Verheij, H.M. & De Haas, G.H. (1989) J. Cell Biochem. **39**, 379-390.

Villalain, J., Gomez-Fernandez, J.C., Jackson, M. & Chapman, D. (1989) Biochim. Biophys. Acta **978**, 305-312.

Vogel, H. & Gärtner, W. (1987) J. Biol. Chem. **262**, 11464-11469.

Waite, M. (1987) Handbook of Lipid Research Vol. **5**, Plenum Press, New York.

Wallach, D.F.H. & Winzler, R.J. (1974) "Evolving Strategies and Tactics in Membrane Research" pp. 140-189, Springer-Verlag, New York.

Weiss, M.S., Wacker, T., Weckesser, J., Welte, W. & Schultz, G.E. (1990) FEBS Lett. **267**, 268-272.

Wells, M.A. (1972) Biochemistry **11**, 1030-1041.

Wichner, W. (1979) Ann. Rev. Biochem. **48**, 23-45.

Williams, A.P., Longfellow, C.E., Freier, S.M., Kierzek, R. & Turner, D.M. (1989) Biochemistry **28**, 4283-4291.

Williams, R.W. (1983) J. Mol. Biol. **166**, 581-603.

Wüthrich, K. (1986) in "NMR of proteins and nucleic acids" John Wiley, New York; VCH.

PUBLICATIONS

1. "A Fourier Transform Infrared Spectroscopic Study of Porcine and Bovine Phospholipase A_2 and their Interaction with Substrate Analogues and a Transition-State Inhibitor."
Kennedy, D.F., Slotboom, A.J., De Haas, G.H. & Chapman, D. (1990) Biochim. Biophys. Acta **1040**, 317-326.

2. "Studies of Peptides Containing 3_{10}-helical, α-helical and β-bend Ribbon Conformations in Organic Solution and in Model Biomembranes by Fourier Transform Infrared Spectroscopy."
Kennedy, D.F., Crisma, M., Toniolo, C. & Chapman, D. (1991) Biochemistry (1991) **30**, 6541-6548.

3. "A Fourier Transform Infrared Spectroscopic Study of Colicin A in its Soluble and Membrane-bound Form."
Kennedy, D.F., Pattus, F. & Chapman, D. (1991) Submitted to Biochim. Bioiphys. Acta.

A Fourier transform infrared spectroscopic (FTIR) study of porcine and bovine pancreatic phospholipase A_2 and their interaction with substrate analogues and a transition-state inhibitor

D.F. Kennedy [1], A.J. Slotboom [2], G.H. de Haas [2] and D. Chapman [1]

[1] *Department of Protein and Molecular Biology, Division of Basic Medical Sciences, Royal Free Hospital School of Medicine, University of London, London (U.K) and* [2] *Centre for Biomembranes and Lipid Enzymology, University of Utrecht, Utrecht (The Netherlands)*

(Received 7 November 1989)
(Revised manuscript received 22 June 1990)

Key words: Phospholipase A_2; Fourier transform infrared spectroscopy; Protein conformation

Fourier transform infrared spectroscopy has been used to investigate the secondary structure of porcine and bovine pancreatic phospholipase A_2 (PLA_2) and the zymogen of porcine PLA_2, prophospholipase A_2 (proPLA_2), in both H_2O and D_2O media. Detailed qualitative analysis was made of these proteins using second derivative and deconvolution techniques. Quantitative studies of the proteins in solution made using Factor Analysis gave average values of 54% α-helix, 15% β-sheet and 23% β-turns. These values agree well with the secondary structures deduced from previous studies of single crystals using X-ray techniques. No significant differences in secondary structure were observed for porcine pancreatic (pro)phospholipase A_2 in the presence or absence of Ca^{2+} ions, or in the temperature range 10–45°C. The binding of the non-degradable phospholipid analogue, *n*-alkylphosphocholine, in monomeric form produced no significant difference in the secondary structure of either enzyme. Conformational differences were, however, observed between the enzyme lyophilised in a solid film and in aqueous solution. The change is probably due to the formation of β-sheet upon hydration, coupled with a loss of random structures. Conformational differences in both porcine and bovine pancreatic PLA_2 were observed on binding to *n*-alkylphosphocholine micelles. This change may be due to a small increase in the α-helical structure and a decrease in the β-sheet, and/or possibly β-turn content. Similar conformational changes were observed for the interaction of porcine and bovine PLA_2 with the substrate analogue inhibitor 1-heptanoyl-2-heptanoylamino-2-deoxy-*sn*-glycero-3-phosphoglycol in micellar form.

Introduction

Pancreatic phospholipase A_2 (EC 3.1.1.4, phosphatidylcholine α-acylhydrolase) (PLA_2) catalyses the specific hydrolysis of the 2-acyl ester bonds of 3-*sn*-phosphoglycerides to release fatty acids, especially arachadonic acid [1]. The enzyme has an absolute requirement for Ca^{2+} ions. Phospholipase A_2 belongs to a class of lipolytic enzymes, which are esterases hydrolysing in vivo substrates. Although such enzymes are able to hydrolyse substrate molecules present in monomeric dispersion [2–4], the hydrolytic activity of the enzyme is greatly enhanced when the substrate is present at an organised lipid–water interface [5].

The amino acid sequences of a number of PLA_2's isolated from various sources have been determined. When comparing the sequences of pancreatic and elapid PLA_2's, of the 124 residues, 36 are conserved absolutely with a further 45 being substituted by residues with similar properties with respect to size, charge or hydrophobicity [6]. All contain 14 or 12 cysteine residues which form disulphide bridges, giving the enzyme rigidity and the properties of heat stability and resistance to denaturing agents [7].

Abbreviations: (pro)PLA_2, (pro)phospholipase A_2; FTIR, Fourier transform infrared; CD, circular dichroism; NMR, nuclear magnetic resonance; $C_{18}PN$, *n*-octadecylphosphocholine; $C_{10}PN$, *n*-decylphosphocholine; cmc, critical micelle concentration; EGTA, ethylene glycol-bis(β-aminoethyl ether)-*N*,*N*,*N'*,*N'*-tetra-acetic acid; HHNP, 1-heptanoyl-2-heptanoylamino-2-deoxy-*sn*-glycero-3-phosphoglycol; Ge, germanium.

Correspondence: D. Chapman, Department of Protein and Molecular Biology, Division of Basic Medical Sciences, Royal Free Hospital School of Medicine, University of London, Rowland Hill Street, London NW3 2PF, U.K.

Information on the secondary structure of pancreatic PLA_2 was first obtained using IR spectroscopy to study porcine PLA_2 in D_2O buffer [8]. From infrared studies on the enzyme and its zymogen in D_2O buffer, these workers suggested that due to the high amide I frequency, both the enzyme and proenzyme have a high α-helical content. However no resolution enhancement techniques could be applied at this time and no quantitative estimates were made. A circular dichroism study on a number of pancreatic PLA_2's concluded that moderate amounts of α-helix were present in the enzyme [9]. However, these results may have been influenced by the X-ray diffraction studies of crystals of porcine PLA_2 [10]. The absence of regular α-helices and β-sheet deduced from these crystals suggested that the crystals contained denatured protein. Later detailed X-ray diffraction studies carried out on Ca^{2+}-containing crystals of the bovine enzyme at a resolution of 1.7 Å [11] and of the porcine enzyme at a resolution of 2.4 Å [12] showed that pancreatic enzymes have approx. 50% α-helical and 10% β-sheet content.

The main conformational differences elucidated between the porcine and bovine enzymes occurs between residues 59 and 70 caused by the single substitution at position 63 of a Val residue in the bovine enzyme and a Phe residue in the porcine enzyme [12]. The side-chain of Val-63 is at the surface of the bovine enzyme molecule, the Phe-63 side-chain of the porcine enzyme is buried within the molecule. The short α-helical section in the bovine enzyme between residues 59–66 is not present in the porcine molecule, but there is a region of 3_{10}-helix, 1.5 turns long between residues 67 to 71. However, a recent ^{1}H-NMR study of bovine and porcine PLA_2 in solution suggested that the solution-state conformations of the two enzymes are very similar in this region [13]. Suitable crystals of PLA_2-lipid complexes have yet to be obtained, so that lipid–protein interactions of these enzymes have yet to be studied by X-ray diffraction.

A recent investigation using Raman and FTIR spectroscopy of PLA_2 from porcine pancreas and from *Crotalus durissus terrificus* venom gives quantitative analyses from the Raman data of the two enzymes under various conditions [14]. This produced figures of 48% α-helix, 35% β-sheet and 18% random coil for the porcine pancreatic PLA_2 in solution, and 54% α-helix, 35% β-sheet and 11% random coil for the snake venom PLA_2 in solution. This study also observed conformational changes in the enzymes caused by altering the physical state of the protein, and by altering the ionic species present in PLA_2 buffer solution.

Important work on PLA_2-lipid binding studies has been carried out using porcine and bovine pancreatic PLA_2 with *n*-alkylphosphocholines, nondegradable zwitterionic phospholipids [15–17]. Two possible binding mechanisms for the formation of PLA_2-*n*-hexadecanylphosphocholine complexes, involving two PLA_2 molecules interacting with each micelle have been proposed [15]. Further work using the anionic substrate analogue *n*-alkyl sulphate with porcine PLA_2 indicated that the enzyme would have to undergo a conformational change to gain full hydrolytic activity [18,19]. It has been suggested that the dramatic rate enhancement observed for PLA_2 when the substrate concentration exceeds the CMC and a lipid–water interface is formed is due to a conformational change in the protein bound by the micelle, thereby resulting in an optimal alignment of the amino acids in the active site [6].

As well as studying the action of PLA_2 in hydrolysing lipids, it is believed that the inhibition of this enzyme could produce desirable pharmacological effects [20]. Phospholipids having an amide linkage instead of an ester at the *sn*-2 position behave as potent transition-state inhibitors [21,22]. So far, no changes in secondary structure have been observed in pancreatic PLA_2 on binding to micelles of degradable or nondegradable zwitterionic lipids or to inhibitor lipids.

FTIR spectroscopy is an established technique for studying protein secondary structure in aqueous solution. The frequency of the strong amide I and amide II bands can be related to the content of α-helical, β-sheet, turns and random coil conformations in the protein under study [23–26]. Fourier transform methods of data acquisition combined with digital subtraction of water absorption have enabled acquisition of high-quality spectra of proteins and polypeptides in aqueous solution [25–27]. Second derivative and deconvolution methods can then be applied to obtain the position of the overlapping components of the broad amide bands and assign them to different secondary structure components [23,25,26]. FTIR spectroscopy combined with resolution enhancement techniques and hydrogen-deuterium exchange can also be successfully applied to reveal small conformational differences in protein structure [23,25,28,29]. FTIR spectroscopy has been used to study successfully the effect of the binding of metal ions on protein conformation [30,31], and has also been widely used for the study of biomembranes and lipoproteins [25,32]. Information on both the lipid and protein components in the system can be deduced from these biological systems.

Quantitative analysis of protein secondary structure can also be obtained from FTIR absorption spectra by using the technique of Factor Analysis. By correlating the amide I bands of a number of soluble proteins of known structure to the amide I band of the sample protein, quantitative estimates of the secondary structure of the sample protein can be made [33].

In the present paper we apply the technique of FTIR spectroscopy to examine qualitatively and quantitatively the secondary structure of porcine and bovine pancreatic phospholipase A_2. The interaction of *n*-al-

of the inhibitor 1-heptanoyl-2-heptanoylamino-2-deoxy-*sn*-glycero-3-phosphoglycol, HHNP, with these phospholipases is also studied.

Materials and Methods

Deuterium oxide (99.8%) was obtained from Sigma, U.K. All other chemicals used were analytical grade from Sigma when available, or from Aldrich.

Porcine and bovine pancreatic prophospholipase A_2 were purified from pancreatic tissue and converted into PLA_2 by limited proteolysis as described (Refs. 34 and 35 respectively).

The substrate analogues $C_{10}PN$ and $C_{18}PN$ were prepared and purified as described [36].

1-Heptanoyl-2-heptanoylamino-2-deoxy-*sn*-glycero-phosphoglycol (HHNP) was prepared as described [48].

Samples used for experiments in D_2O were added to D_2O buffer and heated at 30°C for 3 h, and then left at room temperature for a further 12 h.

Calcium ions were removed from the (pro)enzymes by dialysing the sample for 36–48 h against deionised water, adjusted to pH 3.5 with acetic acid. The samples were then lyophilised after the addition of a small amount of propan-2-ol.

Samples were prepared for studies in the absence of lipid with a protein concentration of 20–50 mg/ml in buffer containing 100 mM $CaCl_2$, 100 mM NaCl, 10 mM Mes, pH 6.0 or p*D* 6.0 as stated. Spectra were recorded at the stated temperature by signal averaging 200 scans at a resolution of 4 cm^{-1}.

Values of p*D* were calculated according to the method of Glasoe and Long [37].

Samples used to study the binding of monomeric lipids to porcine PLA_2 were prepared using 20 mg/ml of PLA_2 and 2 mg/ml $C_{10}PN$ in the same buffer as above.

Samples used to study the binding of PLA_2 to lipid micelles were prepared using 2 mg of PLA_2 and 11.2 mg $C_{18}PN$ in 100 μl of the same buffer as above. This will allow over 90% of the porcine PLA_2 to interact with the micelles [38]. The preparation of PLA_2 for the study of protein–lipid binding in D_2O was carried out as described above. To one-half of the sample was added $C_{18}PN$ whilst the other half was scanned in the absence of micelles. The PLA_2-micelle sample was scanned immediately afterwards to minimise the difference in H–D exchange between the samples.

The effect of the inhibitor above its CMC was studied by preparing a sample containing 20 mg/ml porcine PLA_2 and 10 mM inhibitor in H_2O or D_2O buffer containing 100 mM NaCl, 100 mM Na acetate and 20 mM $CaCl_2$, pH 5.95 or p*D* 5.95.

Spectra were obtained using a Perkin-Elmer 1750 FTIR spectrometer equipped with a TGS detector and analysis. Double-sided interferograms were collected and apodized using a raised cosine function prior to Fourier transformation of the data. Samples were placed in a thermostated Beckman FH-01 CFT microcell fitted with CaF_2 windows and a 6 μm tin spacer for measurements in H_2O, or a 50 μm Teflon spacer for D_2O. Temperature control was achieved by means of a cell jacket of circulating water. The spectrometer was continuously purged with dry air to eliminate water vapour absorptions from the spectral region of interest. A sample shuttle was used to permit the background to be signal-averaged concurrently with the sample.

Solvent spectra were recorded with the same cell and under the same instrument conditions as sample spectra. Difference spectra were obtained by digitally subtracting solvent spectra from the corresponding sample spectra [39]. Great care was taken with the D_2O spectra to ensure that the contamination of D_2O buffers with H_2O was the same for the sample spectra as for the buffer spectra, otherwise contributions from small amounts of H_2O would effect the amide I absorption.

The large intrinsic widths of the individual components present in the amide I band means that they cannot be resolved by increasing instrument resolution. Resolution enhancement techniques such as second derivative [40] calculated over a 13 cm^{-1} data range, and deconvolution using the Perkin-Elmer ENHANCE routine (analogous to the method in Ref. 41) were used to assign features of the composite amide I band to structural features present in the molecule.

Quantitative information on the different structures present was achieved by using Factor Analysis, a technique based on CIRCOM [33,42,43]. This uses the FTIR spectra of 5% (w/v) solutions in H_2O of 18 reference proteins whose structures are known from X-ray diffraction studies. The amide I band of these reference proteins is then fitted to the amide I band of the sample spectrum to generate quantitative information about the sample protein.

The amide II/I ratio is the ratio of the area of the amide II band to the area of the amide I band.

Results

Porcine PLA_2 in solution

The absorption spectrum in the range 1800–1500 cm^{-1} of porcine pancreatic PLA_2 in H_2O buffer, pH 6.0 is given in Fig. 1a. Two main absorption bands present are assigned to the amide I and II vibrations. Information on the secondary structure is mainly found from the overlapping components of the amide I band. All band assignments made in this work are taken from Refs. 23 and 44–46.

The deconvolved spectrum of porcine PLA_2 is also shown in Fig. 1a, with the deconvolved and the second

derivative shown in Fig. 1b. The predominant band at 1657 cm^{-1} in the spectra can be assigned to a combination of α-helical and/or random structures. Further components present within the amide I band are the broad bands at 1672 cm^{-1}, assigned to β-turns and possibly β-sheet, and at 1635 cm^{-1} is assigned to a combination of β-turns and β-sheet, whilst the band at 1618 cm^{-1} is assigned to tyrosine side chains. The main amide II band occurs at 1552 cm^{-1}, whilst the sharp band at 1517 cm^{-1} is assigned to tyrosine side chains.

Further information on protein secondary structure can be gained by studying the samples in D_2O solution. The absorption spectrum of porcine PLA_2 dissolved in D_2O is shown in Fig. 2a (solid line), with the component bands clearly visible in the deconvolved and second derivative spectra in Fig. 2b and c, respectively. The band positions taken from the second derivative spectrum (Fig. 2c) are as follows: 1679 cm^{-1} β-turns and/or β-sheet, 1658 cm^{-1} α-helix, 1647 cm^{-1} exchanged α-helix and exchanged random coil, 1632 cm^{-1} β-sheet and β-turns and 1615 cm^{-1} tyrosine side chains. The bands at 1585 cm^{-1} and 1571 cm^{-1} are assigned to the ionised carboxylate side chains of the aspartate and glutamate residues respectively. The band at 1550 cm^{-1} is the amide II band that arises from the unexchanged N–H bonds in the protein, indicating that complete exchange has not occurred. The band at 1515 cm^{-1} is from tyrosine side chains. The only significant difference that the deconvolved spectrum (Fig. 2b) picks out is a band at 1667 cm^{-1}, assigned to 3_{10}-helix (46, unpublished data). This band is probably lost in the side lobe of the main band of the second derivative spectrum (Fig. 2c).

Porcine PLA_2 in solid film

The absorbance spectrum of deuterated porcine PLA_2 in a solid film on a Ge crystal is shown in Fig. 3a, with the second derivative spectrum shown in Fig. 3b. The main band in the second derivative spectrum occurs at 1652 cm^{-1}, with smaller bands occurring at 1682 cm^{-1} and 1636 cm^{-1}. Comparing this to the second derivative of the protein in solution (Fig. 1b), we see a decrease in the intensity of the 1635 cm^{-1} component, which we have assigned to β-sheet, in the dry protein.

The protein was dried down from D_2O in an attempt to remove the possibility of H_2O absorption from molecules remaining in the sample. Spectra of (pro)PLA_2 dried from H_2O have already been published [14].

Porcine $proPLA_2$

The absorption spectrum for porcine $proPLA_2$ in H_2O buffer is very similar to that of the active enzyme in solution. No significant differences between the zymogen and the enzyme could be detected in the deconvolved or second derivative spectrum (not shown).

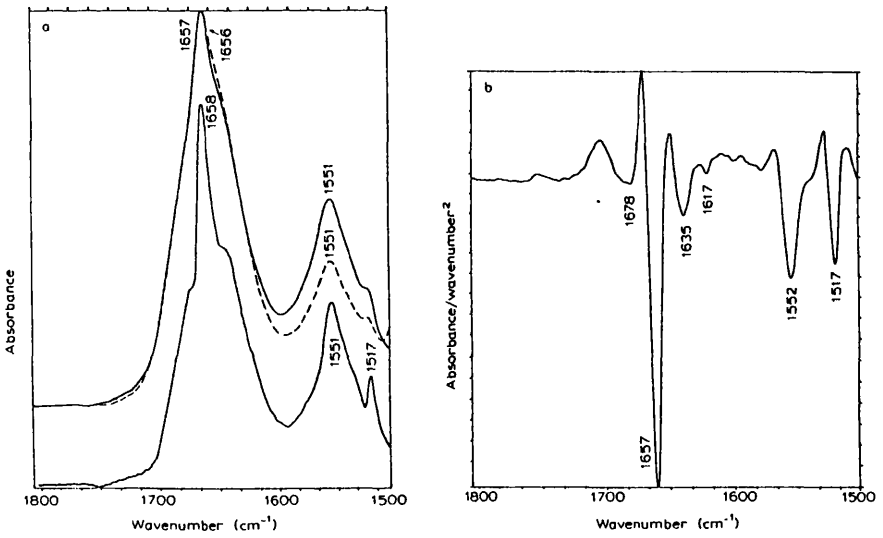

Fig. 1. (a) The absorption spectrum from 1800 cm^{-1} to 1500 cm^{-1} of 5% (w/v) porcine PLA_2 in H_2O buffer, pH 6.0 (top trace, solid line), its deconvolved spectrum using a resolution enhancement factor 2.25 and bandwidth of 11 cm^{-1} (lower trace, solid line) and the absorption spectrum of porcine PLA_2 in the presence of $C_{18}PN$ micelles in H_2O buffer, pH 6.0 (top trace, broken line). (b) Second derivative spectrum of 5% (w/v) porcine PLA_2 in H_2O buffer.

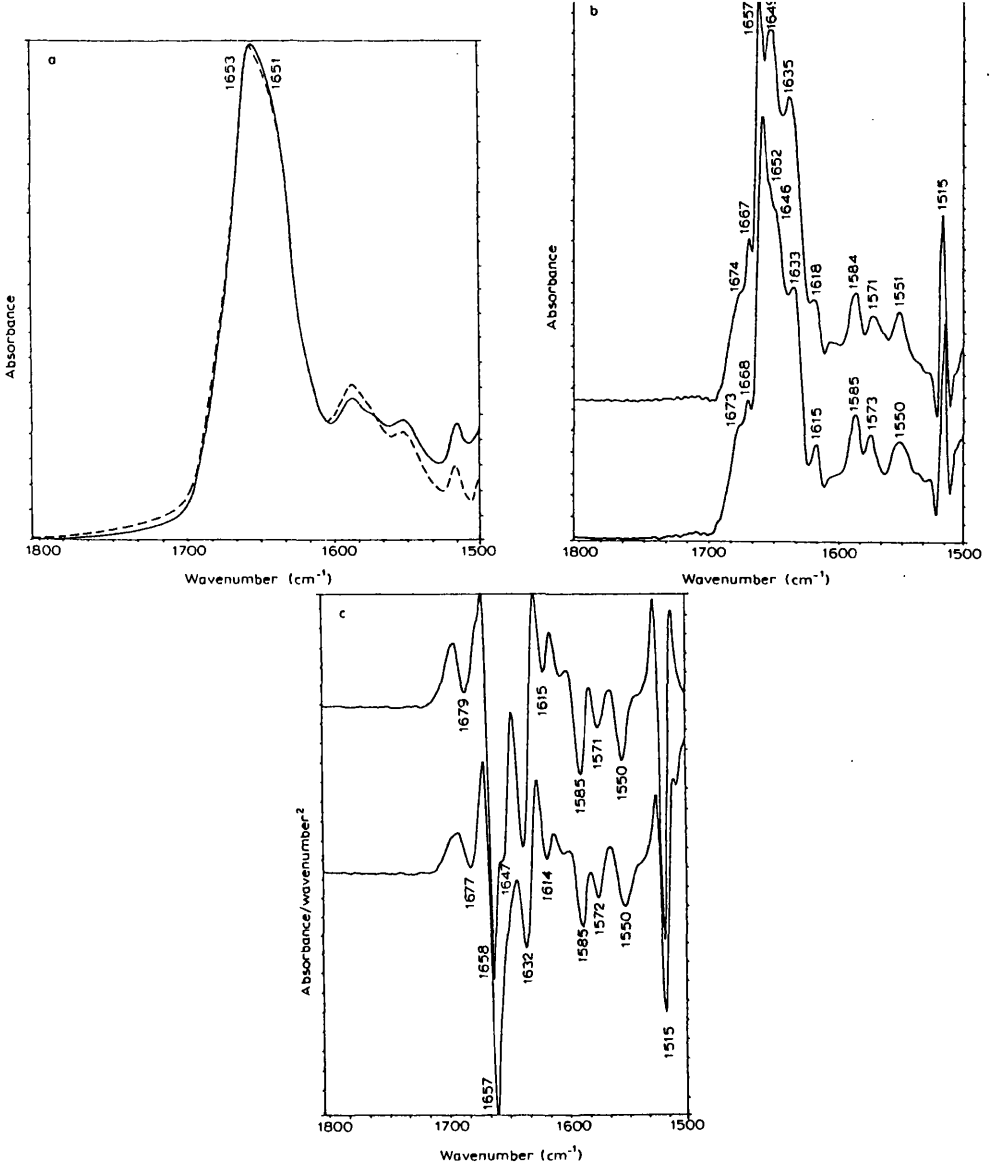

Fig. 2. (a) Absorption spectrum of partially deuterated porcine PLA_2 in D_2O buffer, p*D* 6.0, in the presence (dotted line) and absence (solid line) of $C_{18}PN$ micelles. (b) Deconvolved spectrum of deuterated porcine PLA_2 in D_2O buffer, p*D* 6.0, using resolution enhancement factor 2.75 and bandwidth 15 cm^{-1} in the presence (lower trace) and absence (upper trace) of $C_{18}PN$ micelles. (c) Second derivative spectrum of partially deuterated porcine PLA_2 in D_2O buffer, p*D* 6.0, in the presence (lower trace) and absence (upper trace) of $C_{18}PN$ micelles.

No significant difference in the spectra of porcine PLA_2 in the presence or absence of Ca^{2+} ions could be detected. No major changes occur in the enzyme in the temperature range 10–45 °C.

The rate of H–D exchange for porcine proPLA_2, Ca^{2+}-free and Ca^{2+}-bound PLA_2 was also studied over a 26 h period. No significant difference in rates of exchange could be detected for the three samples.

Porcine PLA_2 interactions with monomeric lipids

Interactions of $C_{10}PN$ monomeric lipids with porcine (pro)PLA_2 were investigated in H_2O and D_2O buffers.

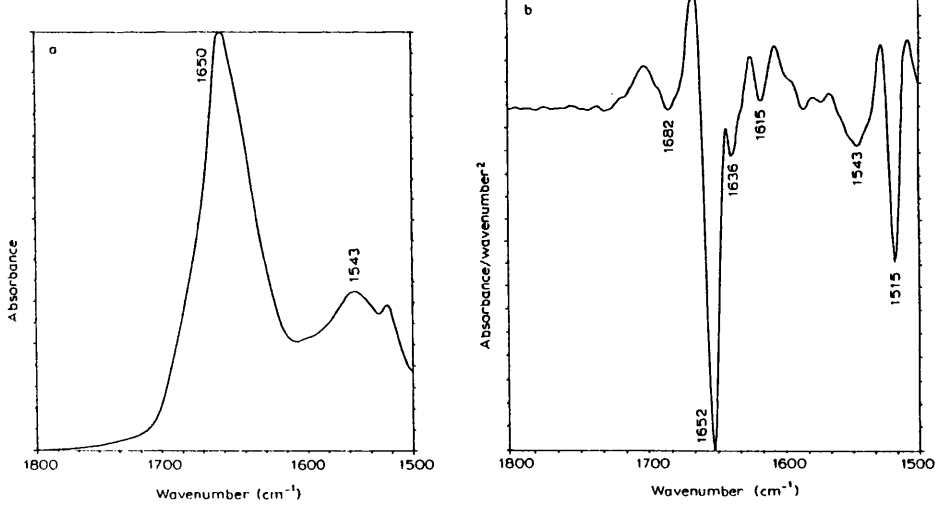

Fig. 3. (a) Absorption spectrum of deuterated porcine PLA_2 in a thin lyophilised film on a Ge crystal. (b) Second derivative spectrum of porcine PLA_2 in a thin lyophilised film on Ge crystal.

No change in the amide I region of these proteins could be detected in the presence and absence of $C_{10}PN$ lipid monomers (not shown).

Porcine PLA_2 interacting with $C_{18}PN$ micelles

Structural changes of the enzyme on binding lipid micelles were also studied using porcine PLA_2. Fig. 1a (top trace, broken line) shows the amide I and II band of porcine PLA_2 in the presence of micelles at 35°C in H_2O buffer. When compared to PLA_2 in buffer alone (Fig. 1a top trace, solid line), the position of the amide I is slightly shifted to 1657 cm^{-1} and the amide II/amide I ratio is reduced by a factor of greater than 2. The second derivative spectrum of the bound PLA_2 has its main peak at 1656 cm^{-1} (not shown).

To gain further insight into the protein-micelle interaction, the experiments were repeated using PLA_2 in D_2O buffer. The absorption spectrum of partially deuterated porcine PLA_2 in the presence of $C_{18}PN$ micelles in D_2O buffer is shown in Fig. 2a (dotted line), with the amide I′ maxima at 1653 cm^{-1}, compared to 1651 cm^{-1} in the absence of micelles (see Fig. 2a). The deconvolved and second derivative spectra are shown in Fig. 2b (lower trace) and c (lower trace), respectively. Comparing the deconvolved spectra of porcine PLA_2 in D_2O in the presence and absence of micelles (Fig. 2b), there is an apparent decrease in the 1649 cm^{-1} band on incorporation into the micelle and an increase in the 1657 cm^{-1} band. The band at 1571 cm^{-1} shifts to 1573 cm^{-1} on binding.

The difference spectrum of partially deuterated PLA_2 in the presence and absence of micelles is shown in Fig. 4. A positive band at 1657 cm^{-1} is observed, with a major negative feature centered around 1632–1633 cm^{-1}, Two smaller negative features are also seen at 1669 cm^{-1} and 1686 cm^{-1} and a minor feature is noted around 1646 cm^{-1}. Subtraction of D_2O buffer containing varying amounts of H_2O contamination from the

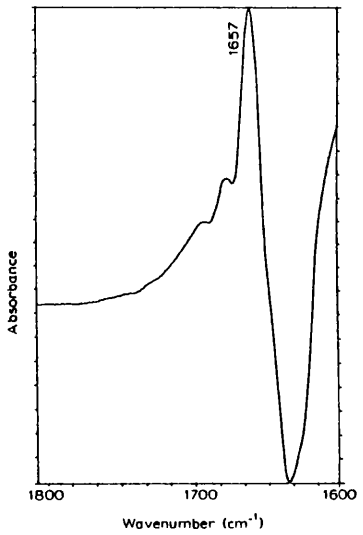

Fig. 4. Difference spectrum generated by subtracting the absorption spectrum of deuterated porcine PLA_2 in the absence of $C_{18}PN$ micelles from the absorption spectrum of deuterated porcine PLA_2 in the presence of $C_{18}PN$ micelles.

protein spectra produces changes in the difference spectrum in the 1620–1635 cm^{-1} region. Therefore conclusions from this part of the difference spectrum must be treated with caution.

Porcine PLA_2 binding to HHNP inhibitor

The absorption spectrum of porcine PLA_2 in the presence of inhibitor HHNP above its CMC in H_2O is shown in Fig. 5a. The amide I band occurs at 1657 cm^{-1} with the amide II band at 1550 cm^{-1}. The deconvolved spectrum does not differ significantly from that of the enzyme in solution. The absorption spectrum of partially deuterated PLA_2 in the presence of inhibitor micelles in D_2O buffer is shown in Fig. 5b (upper trace). The amide I′ band is shifted 2 cm^{-1} on interacting with the micelles. The deconvolved spectrum is shown in Fig.

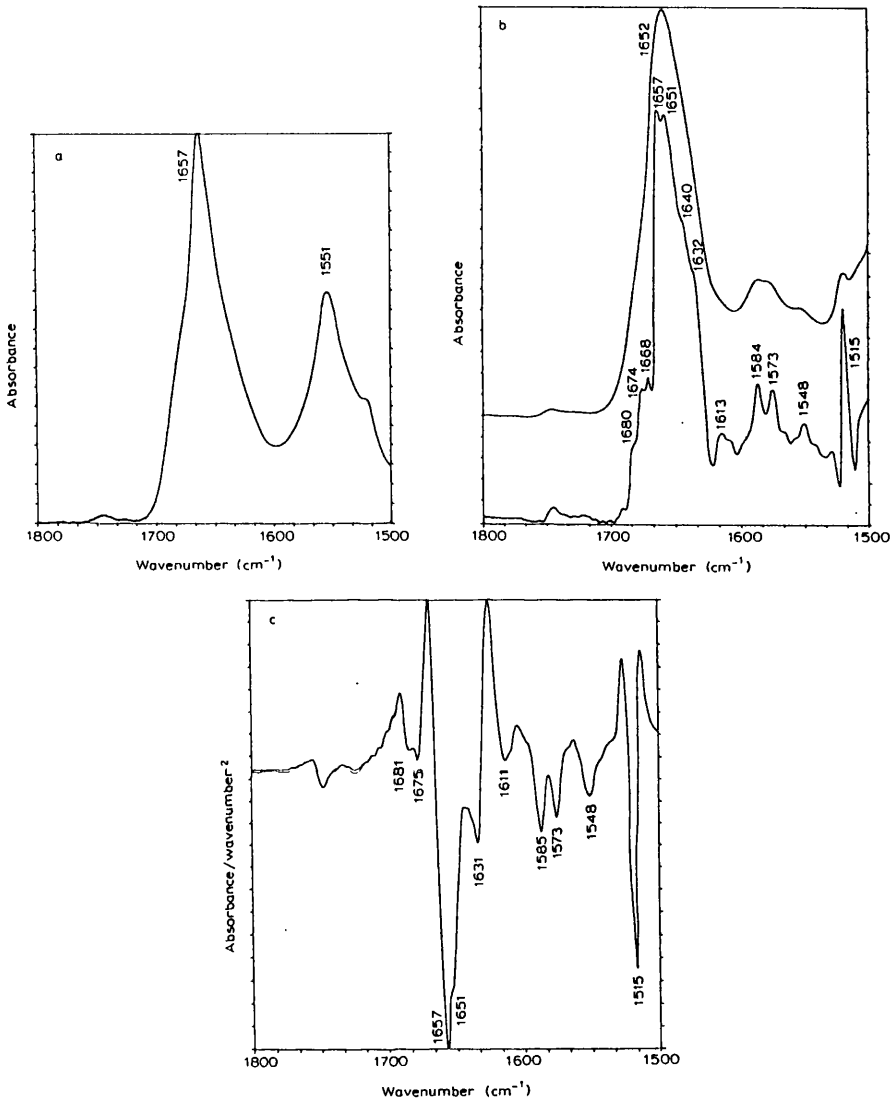

Fig. 5. (a) Absorption spectrum of partially deuterated porcine PLA_2 in the presence of HHNP above its cmc, pH 6.0. (b) Absorption spectrum of partially deuterated porcine PLA_2 in the presence of HHNP micelles, p*D* 5.95 (upper trace) and its deconvolved spectrum using resolution enhancement factor 2.75 and bandwidth 15 cm^{-1} (lower trace). (c) Second derivative spectrum of partially deuterated porcine PLA_2 in the presence of HHNP micelles, p*D* 5.95.

TABLE I

Comparitive results of the quantitative analysis of secondary structures present in PLA_2's by X-ray diffraction and FTIR spectroscopy

Protein	Structure	Percentage content	
		FTIR [a]	X-ray [b]
Porcine proPLA$_2$	α-helix	56	55
	β-sheet	13	10
	β-turns	22	
Porcine PLA$_2$	α-helix	50	50
	β-sheet	14	10
	β-turns	24	
Bovine PLA$_2$	α-helix	55	50
	β-sheet	18	10
	β-turns	24	

[a] The root mean square deviations of the FTIR values are 3.7% for α-helix, 8.3% β-sheet and 6% for β-turns [33].
[b] From Refs. 11 and 12.

5b (lower trace) and second derivative spectrum in Fig. 5c. These spectra are similar to the resolution enhanced spectra of porcine PLA$_2$ in the presence of C_{18}PN micelles, with the band at 1657 cm^{-1} enhanced and the one at 1632 cm^{-1} reduced in the deconvolved spectrum. The intensity of the band at 1646 cm^{-1} also appears to be reduced in the presence of the inhibitor. The difference spectrum of partially deuterated porcine PLA$_2$ in the presence and absence of inhibitor again shows a sharp peak at 1657 cm^{-1}, with a negative feature around 1620–1630 cm^{-1} (not shown).

Quantitative analysis of porcine PLA_2

Quantitative analysis was carried out using Factor Analysis on the absorption spectra of porcine (pro)PLA$_2$ in H_2O under different conditions with the results shown in Table I. Results could not be obtained for the protein interacting with micelles.

Bovine PLA_2

The use of bovine PLA$_2$ in a similar set of experiments produced similar results. The partially deuterated bovine PLA$_2$ showed an amide I′ maximum at 1652 cm^{-1} after undergoing the same treatment as the porcine enzyme, and shifted as low as 1647 cm^{-1} after full exchange (spectra not shown).

The spectrum of deuterated bovine PLA$_2$ dried down as a solid film was similar to that of the equivalent porcine spectrum, with the deconvolved spectrum showing a reduction in the intensity of the 1634 cm^{-1} band and a narrowing of the dominant 1656 cm^{-1} band.

Again conformational changes were identified when the deuterated enzyme interacted with the lipid micelles, causing a 2 cm^{-1} shift of the amide I′ band from 1652 cm^{-1} in the absence of micelles to 1654 cm^{-1} in the presence of C_{18}PN micelles. The deconvolved spectra show that the relative intensity of the components at 1646 cm^{-1} and 1636 cm^{-1} are reduced on binding compared to the intensity of the main component, which shifts from 1656 cm^{-1} to 1657 cm^{-1} on binding. The difference spectrum (equivalent to Fig. 4 for porcine PLA$_2$) showed a narrow positive band at 1658 cm^{-1} and a negative feature around 1633 cm^{-1}, Similar results were also obtained for the bovine enzyme on interacting with HHNP micelles.

Discussion

The assignment of the components of the amide I band of porcine pancreatic (pro)PLA$_2$ and bovine pancreatic PLA$_2$ in H_2O and of the amide I′ band in D_2O agree qualitatively with the results from X-ray diffraction work [11,12].

Quantitative results of the three proteins in H_2O buffer using the Factor Analysis technique produced results which also agree well with those obtained from the X-ray structure (Table I). This indicates that the structure of these proteins in aqueous solution is similar to that in the crystal form. The small difference in α-helical content between porcine proPLA$_2$ and PLA$_2$ may indicate that the 7 amino acid residue cleaved from the protein on activation has an α-helical structure. However, our results disagree with those of Ref. 14 who observed an increase in α-helical content of more than 10% on the transition from porcine proenzyme to enzyme.

The Factor Analysis technique of fitting the spectra of 18 soluble proteins of known structure to the spectrum of porcine PLA$_2$ bound to C_{18}PN micelles failed to produce meaningful results. The second derivative spectra failed to identify any significant changes in the positions of the amide I components during protein–micelle interactions.

The results from the enzyme dried down on the Ge crystal suggests that β-sheet structure is formed upon hydration and agree with the results of Ref. 14. It should be noted that the crystals of PLA$_2$ will contain water of crystallisation to stabilise the protein whereas the lyophilised sample was virtually free of water judging by the absence of the 2125 cm^{-1} water band.

The absence of any significant differences in spectra of PLA$_2$ on the binding of Ca^{2+} ions or the binding of monomeric lipid substrates indicates that both substrates fit into their respective position into the enzyme molecule without causing a major change in secondary structure.

A change in the protein spectra were observed on the binding of C_{18}PN micelles. Although there is no significant change in the amide I band on protein–micelle interaction in H_2O, the amide II/I ratio is dramatically reduced. Changes in amide II/I ratios for polypeptides in different environments has been previously reported

existing as a tetramer is higher than that for the monomeric form [47]. The marked differences in the spectra of both partially deuterated porcine and bovine PLA_2 in solution and in membrane-bound form indicate that there is a conformational difference between the protein in the two different environments.

When comparing the deconvolved spectra of deuterated porcine PLA_2 in the presence and absence of micelles (Fig. 2b), the reduction in intensity of the 1648 cm^{-1} band on binding to the $C_{18}PN$ micelles may be interpreted as a reduction of some random structure with an increase in α-helix content. However, the difference spectrum of porcine PLA_2 in the presence and absence of micelles in D_2O (Fig. 4) does not support this concept. The striking features of the difference spectrum is the sharp positive feature at 1657 cm^{-1} and the broader negative feature at 1632–33 cm^{-1}. A loss in random structure, or a structural modification of the α-helices on going from a solution to membrane environment, would be expected to provide a negative feature around 1646–1649 cm^{-1} in the difference spectrum. Therefore, a reduction in β-sheet content and/or possibly β-turns, along with an increase in α-helical structure may be occurring.

The changes seen on the binding of deuterated bovine PLA_2 to micelles are smaller than those observed for deuterated porcine PLA_2. This is probably due to the fact that the dissociation constant of bovine PLA_2 with $C_{18}PN$ micelles is greater than that of porcine enzyme with the same lipid, thus a smaller percentage of the bovine enzyme molecules will be bound by micelles. The positive band in the difference spectrum at 1658 cm^{-1} is again high for deuterated α-helices, indicating that they are in a hydrophobic part of the complex.

The potent transition-state inhibitor HHNP produced a similar effect on the secondary structure of partially deuterated porcine pancreatic PLA_2 as that observed with the interaction of $C_{18}PN$ micelles. The deconvolved spectra of the partially deuterated enzyme in the presence of inhibitor micelles (Fig. 5b) and $C_{18}PN$ micelles (Fig. 2c) are similar, showing the increase in the band at 1656 cm^{-1} and the loss in intensity in the 1620–1630 cm^{-1} region. The similarity of the deconvolved, second derivative and difference spectra of partially deuterated porcine PLA_2 in the presence of $C_{18}PN$ micelles with the respective spectra in the presence of HHNP micelles indicates that the enzyme undergoes a similar conformational change in the presence of inhibitor in micellar form as occurs when interacting with $C_{18}PN$ micelles. However, in H_2O buffer the presence of micellar inhibitor does not induce the change in the amide II/I ratio of the enzyme as observed in the presence of $C_{18}PN$ micelles.

Our work shows that pancreatic PLA_2 from two different sources undergo conformation changes on dislipids. Both conformational changes may be associated with the β-sheet, and/or β-turn, portion of the molecule.

Acknowledgements

We would like to thank Dr. David Lee of Smith, Kline and Beecham Ltd. for carrying out the Factor Analysis of the spectra and for many useful discussions. We (D.F.K. and D.C.) would also like to thank S.E.R.C. (C.A.S.E. award sponsored by Perkin Elmer Ltd.) for financial support and also the Wellcome Trust.

References

1 Waite, M. (1987) Handbook of Lipid Research Vol. 5, Plenum Press, New York.
2 Roholt, O.A. and Schlamowitz, M. (1961) Arch. Biochem. Biophys. 94, 364.
3 De Haas, G.H., Bonsen, P.P.M., Pieterson, W.A. and Van Deenen (1971) Biochim. Biophys. Acta 239, 252–266.
4 Wells, M.A. (1972) Biochemistry 11, 1030–1041.
5 Pieterson, W.A., Volwerk, J.J. and De Haas, G.H. (1974) Biochemistry 13, 1439–1445.
6 Slotboom, A.J., Verheij, H.M. and De Haas, G.H. (1982) in Phospholipids, (Hawthorne, J.N. and Ansell, G.B., eds.) Vol. 4, pp. 359–434, Elsevier, Amsterdam.
7 Van der Bergh, C.J., Slotboom, A.J., Verheij, H.M. and De Haas, G.H. (1989) J. Cell Biochem. 39, 379–390.
8 Abita, J-P., Lazdunski, M., Bonson, P.P.M., Pieterson, W.A. and De Haas, G.H. (1972) Eur. J. Biochem. 30, 37–47.
9 Jirgenson, B. and De Haas, G.H. (1977) Biochim. Biophys. Acta 494, 285–292.
10 Drenth, J., Enzing, C.M., Kalk, K.H. and Vessies, J.C.A. (1976) Nature 264, 373–377.
11 Dijkstra, B.W., Kalk, K.H., Hol, W.G. and Drenth, J. (1981) J. Biol. Mol. 147, 97–123.
12 Dijkstra, B.W., Renetseder, R., Kalk, K.W., Hol, W.G. and Drenth, J. (1983) J. Biol. Mol. 168, 163–179.
13 Fisher, J., Primrose, W.U., Roberts, G.C.K., Dekker, N., Boelens, R., Kaptein, R. and Slotboom, A.J. (1989) Biochemistry 28, 5929–5946.
14 Arêas, E.P.G., Laure, C.J., Gabilan, N., Araujo, P.S. and Kawana, Y. (1989) Biochim. Biophys. Acta 997, 15–26.
15 Soares de Araujo, P., Rosseau, M.Y., Kremer, J.M.H., Van Zoelen, E.J.J. and De Haas, G.H. (1979) Biochemistry 18, 580–586.
16 Hille, J.D.R., Donne-Op den Kelder, G.M., Sauve, P., De Haas, G.H. and Egmond, M.R. (1981) Biochemistry 20, 4063–4073.
17 Donné-Op den Kelder, G.M., Hille, J.D.R., Dijkman, R., De Haas, G.H. and Egmond, M.R. (1981) Biochemistry 20, 4074–4078.
18 Hille, J.D.R., Egmond, M.R., Dijkman, R., Van Oort, M.G., Jirgensons, B. and De Haas, G.H. (1983) Biochemistry 22, 5347–5353.
19 Hille, J.D.R., Egmond, M.R., Dijkman, R., Van Oort, M.G., Sauve, P. and De Haas, G.H. (1983) Biochemistry 22, 5353–5358.
20 Dennis, E.A. (1987) Drug. Dev. Res. 10, 205.
21 Bonsen, P.P.M., De Haas, G.H., Pieterson, W.A. and van Deenen, L.L.M. (1972) Biochim. Biophys. Acta 270, 364–382.
22 De Haas, G.H., Van Oort, M.G., Dijkman, R. and Verger, R. (1989) Biochem. Soc. Trans. 17, 274–276.
23 Susi, H. and Byler, D.M. (1986) Methods Enzymol. 130, 290–311.
24 Krimm, S. and Bandekar, J. (1986) Adv. Protein Chem. 38, 181–364.

952, 115–130.
26 Jackson, M., Haris, P.I. and Chapman, D. (1989) J. Molec. Structure 204, 329–355.
27 Koenig, J.L. and Tabb, D.L. (1980) in Analytical applications of FT-IR to Molecular and Biological Systems (Dufir, J.R., ed.), pp. 241–255, Reidel, Boston.
28 Downer, N.W., Bruchman, T.J. and Hazzard, J.H. (1986) J. Biol. Chem. 261, 3640–3647.
29 Haris, P.I., Lee, D.C. and Chapman, D. (1986) Biochim. Biophys. Acta 874, 255–265.
30 Alvarez, J., Haris, P.I., Lee, D.C. and Chapman, D. (1987) Biochim. Biophys. Acta 916, 5–12.
31 Villalain, J., Gomez-Fernandez, J.C.,, Jackson, M. and Chapman, D. (1989) Biochim. Biophys. Acta 978, 305–312.
32 Herzyk, E., Lee, D.C., Dunn, R.C., Bruckdorfer, K.R. and Chapman, D. (1987) Biochim. Biophys. Acta 922, 145–154.
33 Lee, D.C., Haris, P.I., Chapman, D. and Mitchell, R.C. (1989) in Spectroscopy of Biological Molecules - State of the Art. Proceedings of the 3rd. European Conference on the Spectroscopy of Biological Molecules, Bologna, Italy (Bretoluzza, A., Fangano, C. and Monti, P., eds.), pp.57–58, Societa Editrice Bologna.
34 Nieuwenhuizen, W., Kunze, H. and De Haas, G.H. (1974) Methods Enzymol. 32B, 147–154.
35 Fleer, E.A.M., Verheij, H.M. and De Haas, G.H. (1978) Eur. J. Biochem. 82, 261–269.
De Haas, G.H. (1975) Biochemistry 14, 5387–5393.
37 Glasoe, P.K. and Long, E.A. (1960) J. Phys. Chem. 64, 188–191.
38 Donné-Op den Kelder, G.M. (1984) Ph.D Thesis from University of Utrecht.
39 Lee, D.C. and Chapman, D. (1986) Bioscience Reports 6, 235–256.
40 Moffatt, D.J., Kauppinen, J.C., Cameron, D.G., Mantsch, H.H. and Jones, R.N. (1986) Computer programs for infrared spectrophometry, N.R.C.C. Bulletin No. 18, Ottawa.
41 Kauppinen, J.K., Moffatt, D.J., Mantsch, H.H. and Cameron, D.G. (1981) Anal. Chem. 53, 1454.
42 Fredricks, P.M., Lee, J.B., Osbourn, P.R. and Swinkles, D.A.J. (1985) Appl. Spectros. 39, 303–310.
43 Fredricks, P.M., Lee, J.B., Osbourn, P.R. and Swinkles, D.A.J. (1985) Appl. Spectros. 39, 311–316.
44 Chirgadze, Yu. N., Fedorov, O.V. and Trushina, N.P. (1975) Biopolymers 14, 679–694.
45 Byler, D.M. and Susi, H. (1986) Biopolymers 25, 469–487.
46 Krimm, S. and Bandekar, J. (1986) Adv. Protein Chem. 38, 181–364.
47 Lavialle, F., Adams, R.G. and Levin, I.W. (1982) Biochemistry 21, 2305–2312.
48 De Haas, G.H., Dijkman, R., Ransac, S. and Verger, R. (1990) Biochim. Biophys. Acta, in press.

Studies of Peptides Forming 3_{10}- and α-Helices and β-Bend Ribbon Structures in Organic Solution and in Model Biomembranes by Fourier Transform Infrared Spectroscopy†

D. F. Kennedy,‡ M. Crisma,§ C. Toniolo,§ and D. Chapman*,‡

Department of Protein and Molecular Biology, Division of Basic Medical Science, Royal Free Hospital School of Medicine, University of London, London NW3 2PF, United Kingdom, and Biopolymer Research Centre, CNR, Department of Organic Chemistry, University of Padua, 35131 Padua, Italy

Received November 20, 1990; Revised Manuscript Received March 20, 1991

ABSTRACT: In order to examine the potential correlation between infrared absorption spectra and 3_{10}- and α-helices and β-bend ribbon structures, the secondary structures of synthetic peptides known to contain pure 3_{10}-helices, mixed $3_{10}/\alpha$-helices, and pure β-bend ribbon structures, based upon X-ray diffraction and NMR studies, have been investigated by using FTIR spectroscopy incorporating resolution-enhancement techniques. Studies of the peptides known to contain a stable 3_{10}-helix in $CDCl_3$ show the main amide I band of fully stable 3_{10}-helices occurs at 1666–1662 cm^{-1}. Resolution-enhancement methods revealed small contributions at 1681–1678 and 1646–1644 cm^{-1}, while the amide II band occurs at 1533–1531 cm^{-1}. Peptides known to contain both α- and 3_{10}-helices in their structure exhibit bands characteristic of both types of conformation. Peptides known to fold into the β-bend ribbon structure show an amide I band maximum at 1648–1645 cm^{-1} with the amide II band at 1538–1536 cm^{-1}. Incorporation of these peptides into model membrane structures, e.g., DMPC vesicles, in aqueous buffer sometimes produces changes in the peptide secondary structure. Those peptides which possess a 3_{10}-helical structure in $CDCl_3$ solution change the secondary structure in DMPC vesicles to predominantly α-helical, plus a contribution from short, unstable 3_{10}-helix and/or β-turns. Those peptides which contain a combination of α- and 3_{10}-helical structures in $CDCl_3$ solution tend to retain some 3_{10}-helical structure within the lipid environment, although the overall H-bonding pattern is altered. Those peptides which form a β-bend ribbon structure appear to be largely unaffected in the membrane environment. This study represents the first complete characterization of a pure 3_{10}-helix and a pure β-bend ribbon by FTIR spectroscopy using resolution-enhancement techniques.

The secondary structure of membrane proteins and signal peptides present within a lipid matrix is of considerable interest at the present time. Some workers suggest that the α-helix is the dominant motif in these systems (Henderson et al., 1975; Deisenhofer et al., 1985; Austen, 1979; Briggs & Gierasch, 1984; Shinnar & Kaiser, 1984; Batenburg et al., 1988; Rosenblatt et al., 1980), whereas other workers suggest that appreciable amounts of β-sheet (Kleffel et al., 1985; Reddy & Nagaraj, 1989) or some 3_{10}-helical structure (Fox & Richards, 1982; Popot et al., 1990) may be present. Furthermore, the "helical hairpin hypothesis" of Engelman and Steitz (1981) supposes that the insertion of proteins into membranes is initiated by the spontaneous penetration of an α- or 3_{10}-helical hairpin from a hydrophobic portion of the protein into the bilayer.

Biophysical studies on transmembrane channels, such as those formed by peptides of the alamethicin family, suggest that both α- and 3_{10}-helical structures may occur (Mathew & Balaram, 1983; Menestrina et al., 1986). A recent survey of X-ray diffraction studies (Barlow & Thornton, 1988) has indicated that in addition to the α-helix, the 3_{10}-helical structure may also be present in various amounts in soluble proteins.

Various studies have shown that the α-aminoisobutyric acid (Aib)[1] residue promotes $\alpha/3_{10}$-helical structures (Prasad & Balaram, 1984; Toniolo & Benedetti, 1988; Toniolo, 1989; Smith et al., 1981). This unusual α-amino acid occurs extensively in the transmembrane channel forming peptaibol antibiotics (Benedetti et al., 1982a; Bruckner & Graf, 1983). Two of these polypeptides, alamethicin and trichorzianine, were found to be predominantly α-helical by X-ray diffraction analysis, but short segments of 3_{10}-helical were also observed (Fox & Richards, 1982; Le Bars et al., 1988).

Experimental evidence from electron diffraction photographs (Malcolm, 1983) and Raman and polarized IR absorption studies (Dwivedi et al., 1984) indicates that the 3_{10}-helix is the preferred conformation of polydisperse poly(Aib)$_n$. Dwivedi et al. (1984) calculate that the amide I band of poly(Aib)$_n$ in a 3_{10}-helical structure should absorb at 1665 cm^{-1}, while type III β-turns (a type III β-turn corresponds to the building unit of the 3_{10}-helix) should have amide I absorptions at 1686 and 1646 ± 3 cm^{-1}. A recent study of alamethicin by Haris and Chapman (1989) assigned the main peak at 1663 cm^{-1} to a combination of absorptions from 3_{10}- and α-helices, and suggested that the weaker band at 1639 cm^{-1} may also be associated with the 3_{10}-helical structure. ^1H NMR, IR absorption, and X-ray diffraction studies of terminally blocked, monodisperse (Aib)$_n$ (n = 2–10) homopeptides strongly support the formation of an intramolecular

† This work was supported by the SERC and the Wellcome Foundation.

‡ University of London.

§ University of Padua.

[1] Abbreviations; Z, benzyloxycarbonyl; *p*BrZ, *p*-bromobenzyloxycarbonyl; *p*BrBz, *p*-bromobenzoyl; Boc, *tert*-butoxycarbonyl; OMe, methoxy; O*t*Bu, *tert*-butoxy; Aib, α-aminoisobutyric acid; DMPC, dimyristoylphosphatidylcholine; pbs, phosphate-buffered saline; FTIR, Fourier transform infrared; NMR, nuclear magnetic resonance.

0006-2960/91/0430-6541$02.50/0

at the trimer level (Benedetti et al., 1982b; Bavoso et al., 1986; Toniolo et al., 1985, 1986; Pavone et al., 1990).

X-ray diffraction studies of *p*BrBz-(Aib-L-Ala)$_{4.5}$-OMe crystallized from methanol have indicated that both peptides contain both α- and 3_{10}-helices under these conditions (Benedetti et al., 1990; Pavone et al., 1990).

Sequential oligomers containing the sequence Aib-L-Pro are also of interest as the presence of Pro in the sequence interrupts the H-bonding pattern. An NMR study by Venkatachalapathi and Balaram (1981) suggests that the peptide Z-(Aib-L-Pro)$_4$-OMe forms a type of 3_{10}-helix that has the alternating presence/absence of the intramolecular H-bond due to the alkylation of the amide group in the Pro residue. This structure is known as a β-bend ribbon and may be a conformational feature of some members of the alamethicin family, for example, zervamicin (Karle et al., 1987). The longest β-bend ribbon, so far fully characterized by X-ray diffraction analysis, is that formed by *p*BrBz-Aib-(L-Pro-Aib)$_4$-OMe (Toniolo et al., unpublished results).

FTIR spectroscopy is now an established technique for determining the secondary structure of proteins. The primary information on the polypeptide conformation is found in the amide I band. The IR absorption studies of terminally blocked (Aib)$_n$ peptides (Benedetti et al., 1982b; Toniolo et al., 1985) related the position of the amide I maximum to the secondary structures present. This band, however, is not a pure band and consists of several components, each of which can be associated with various secondary structures. Resolution-enhancement techniques such as second derivative and deconvolution can be used to identify the positions of the components of the amide I band, from which the secondary structures can be identified.

This paper describes studies of peptides which are known to exist as 3_{10}-helical structures, a combination of 3_{10}- and α-helices, or β-bend ribbon in $CDCl_3$ solution using FTIR spectroscopy combined with resolution-enhancement techniques. We ask the questions: (a) are there IR absorption bands which are characteristic, and can be used to indicate the presence of the 3_{10}-helical and the β-bend ribbon secondary structures, and (b) are the secondary structures which exist in solution modified when the peptides are incorporated into a model lipid biomembrane?

Materials and Methods

The synthesis and characterization of Z-(Aib)$_n$-O*t*Bu (n = 3–10) (Jones et al., 1965; Toniolo et al., 1985), Z-(Aib-L-Ala)$_n$-OMe (n = 2–5) and Z-L-Ala-(Aib-L-Ala)$_n$-OMe (n = 1–5) (Benedetti et al., 1990; Pavone et al., 1990), and *p*BrZ-(L-Pro-Aib)$_n$-OMe (n = 1–5) (Toniolo et al., unpublished results) have already been described.

$CDCl_3$ and DMPC were both purchased from Sigma Chemicals Ltd., England. Solution studies were carried out in $CDCl_3$ at 20, 40, and 50 °C.

The spectra in aqueous lipid dispersion were prepared by adding DMPC and the peptide to chloroform in a lipid:peptide ratio of 15:1. After the samples were dried under N_2 and then under vacuum, small volumes of phosphate-buffered saline, pH 7.4, were added, and the samples were incubated above the phase transition of the lipid for 2–3 h. This is similar to the method of Rizzo et al. (1987) for incorporating alamethicin into the lipid dispersion. Samples in D_2O buffer, pD 7.4, were incubated at 33 °C for 22–24 h in order to allow hydrogen–deuterium exchange to occur in the peptide.

Spectra were obtained with a Perkin-Elmer 1750 FTIR spectrometer equipped with a TGS detector and a Perkin-Elmer 7300 computer for data acquisition and analysis. Samples were placed in a thermostated Beckman FH-01 CFT microcell fitted with CaF_2 windows, and a 50-μm Teflon spacer was used for measurements of the 16 mM samples in $CDCl_3$ and a 0.6-mm Teflon spacer for 1.5 mM samples. For the aqueous solutions, a 6-μm tin spacer was used for samples in H_2O buffer, and a 50-μm Teflon spacer for samples in D_2O buffer. Temperature control was achieved by means of a cell jacket of circulating water. The spectrometer was continuously purged with dry air to eliminate water vapor absorptions from the spectral region of interest. A sample shuttle was used to permit the background to be signal-averaged concurrently with the sample.

Solvent spectra were recorded in a similar cell and under identical instrument conditions as the sample spectra. Difference spectra were obtained by digitally subtracting the solvent spectrum from the corresponding sample spectrum. Second-derivative (Moffat et al., 1986) and deconvolution using the Perkin-Elmer ENHANCE routine [analogous to the method of Kauppinen et al. (1981)] were used to assign features of the composite amide I band to structural features present in the peptide.

Amide II Bands of Z-(Aib)$_n$-O*t*Bu (n = 3–10) at 1.5 mM Concentration in $CDCl_3$[a]

n	amide I (cm^{-1})	amide II (cm^{-1})
10	1681 w, 1662 s, 1646 w	1533 s
9	1681 w, 1663 s, 1644 w	1532 s, 1558 w
8	1679 w, 1666 s, 1646 w	1532 s
7	1680 w, 1670 s, 1648 w	1531 s, 1557 w
6	1677 s, 1664 w, 1649 w	1531 s, 1537 w
5	1680 s, 1668 w	1526 s, 1537 w
4	1682 s, 1662 w	1517 s, 1530 w
3	1687 s, 1664 w	1523 s, 1538 w

[a] s = strong, w = weak.

Results

Studies in Organic Solvent. The absorption spectra of the Z-(Aib)$_n$-O*t*Bu series (n = 3–10) at 1.5 mM concentration in $CDCl_3$ show the same pattern as that recorded by Toniolo et al. (1985). The position of the amide I band shows a decrease in the frequency as n increases. Similarly, the bands from the free urethane and peptide N–H groups at 3450–3400 cm^{-1} and the intramolecularly H-bonded N–H groups at 3380–3320 cm^{-1} behave as previously reported for the peptides in the absence of self-association.

Second-derivative and deconvolution techniques give further information about the structure within the amide I absorption. The frequencies of the main band and of minor components of the amide I band for the 1.5 mM solutions of Z-(Aib)$_n$-O*t*Bu (n = 3–10) in $CDCl_3$ are given in Table I. The absorption spectrum of Z-(Aib)$_8$-O*t*Bu in $CDCl_3$, with the deconvolved and second-derivative spectra of the same peptide, is shown in Figure 1 (a, b, and c, respectively).

For n = 8–10, the resolution-enhanced spectra of the amide I band show three components: the main absorption band, which occurs at 1666–1662 cm^{-1} and we assign to 3_{10}-helix, and two smaller components of approximately equal intensity, one at 1646–1644 cm^{-1}, which we assign to type III β-turns, and one at 1681–1679 cm^{-1}, which may be from type III β-turns and/or free carbonyl groups. The amide II band has one strong component, whose peak is centered at 1533–1532 cm^{-1}. The band at 1716–1715 cm^{-1}, corresponding to the overlapping absorptions of H-bonded urethane C=O and free *tert*-butyl ester C=O groups of the N- and C-protecting moieties (Pulla Rao et al., 1980; Bonora et al., 1984), cannot

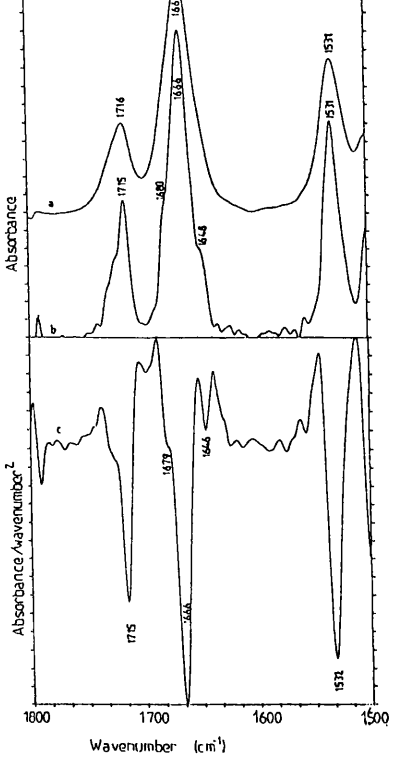

FIGURE 1: (a) FTIR absorption spectrum from 1800 to 1500 cm^{-1} of Z-(Aib)$_8$-O*t*Bu in $CDCl_3$ at 20 °C. (b) Deconvolved spectrum of Z-(Aib)$_8$-O*t*Bu in $CDCl_3$ at 20 °C using bandwidth 12 and resolution-enhancement factor 2.125. (c) Second-derivative spectrum of Z-(Aib)$_8$-O*t*Bu in $CDCl_3$ at 20 °C.

Table II: Components of the Resolution-Enhanced Amide I and Amide II Bands of Z-(Aib-L-Ala)$_n$-OMe (n = 1–5) at 1.5 mM Concentration in $CDCl_3$[a]

n	amide I (cm^{-1})	amide II (cm^{-1})
5	1681 w, 1662 s, 1659 s, 1649 w, 1641 w	1537 s
4	1673 w, 1664 s, 1644 w	1535 s
3	1673 s, 1657 w	1528 s
2	1681 s, 1664 w	1534 w, 1514 s
1	1677 s	1513 s

[a] s = strong, w = weak.

be separated by using resolution-enhancement techniques.

The results of the study of the Z-(Aib-L-Ala)$_n$-OMe (n = 1–5) peptides in $CDCl_3$ at 1.5 mM concentration are listed in Table II. The absorption spectrum of Z-(Aib-L-Ala)$_5$-OMe (Figure 2a) shows the amide I band at 1662 cm^{-1} and the amide II band at 1536 cm^{-1}. The deconvolved spectrum (Figure 2c) is able to resolve the main amide I absorption into two main components, one at 1662 cm^{-1}, assigned to 3_{10}-helix, and one at 1659 cm^{-1}, assigned to α-helix. The band identified at 1681 cm^{-1} is assigned to type III β-turns and/or free carbonyl groups. The bands at 1649 and 1641 cm^{-1} are either in or very close to the predicted frequency range for type III β-turns (Krimm & Bandekar, 1986). However, the $3\pi/2$ vibration of the α-helix may also absorb in this region (Lee et al., 1985), making definite assignment of the these bands difficult. The broad band centered around 1743 cm^{-1} should be related to the free methyl ester carbonyl group and the band centered at 1713 cm^{-1} to the H-bonded urethane carbonyl group. The second-derivative spectrum (Figure 3a) is unable to resolve the two major bands and shows one asymmetric main band at 1662 cm^{-1} which we assign to a combination of α- and

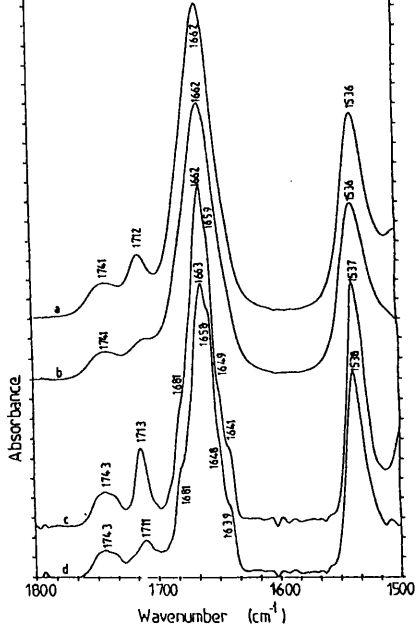

FIGURE 2: (a) FTIR absorption spectrum from 1800 to 1500 cm^{-1} of 1.5 mM Z-(Aib-L-Ala)$_5$-OMe in $CDCl_3$ at 20 °C. (b) FTIR absorption spectrum from 1800 to 1500 cm^{-1} of 1.5 mM Z-L-Ala-(Aib-L-Ala)$_5$-OMe in $CDCl_3$ at 20 °C. (c) Deconvolved spectrum of 1.5 mM Z-(Aib-L-Ala)$_5$-OMe in $CDCl_3$ at 20 °C using bandwidth 12 and resolution-enhancement factor 2.125. (d) Deconvolved spectrum of 1.5 mM Z-L-Ala-(Aib-L-Ala)$_5$-OMe in $CDCl_3$ at 20 °C using bandwidth 12 and resolution-enhancement factor 2.125.

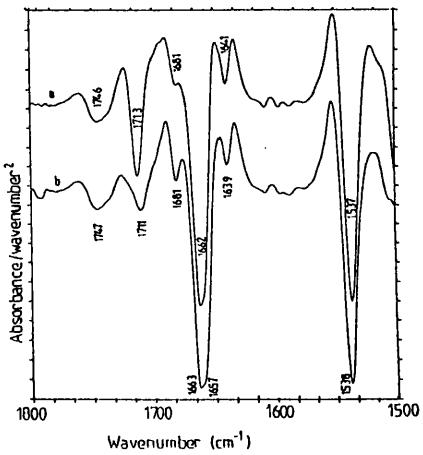

FIGURE 3: (a) Second-derivative spectrum of 1.5 mM Z-(Aib-L-Ala)$_5$-OMe in $CDCl_3$ at 20 °C. (b) Second-derivative spectrum of 1.5 mM Z-L-Ala-(Aib-L-Ala)$_5$-OMe in $CDCl_3$ at 20 °C.

Table III: Components of the Resolution-Enhanced Amide I and Amide II Bands of Z-L-Ala-(Aib-L-Ala)$_n$-OMe (n = 1–5) at 1.5 mM Concentration in $CDCl_3$[a]

n	amide I (cm^{-1})	amide II (cm^{-1})
5	1681 w, 1663 s, 1658 s, 1649 w, 1641 w	1538 s
4	1680 w, 1667 s, 1647 w	1533 s
3	1679 w, 1667 s, 1647 w	1533 s
2	1679 s, 1657 w	1533 w, 1514 s
1	1679 w, 1665 s	1507 w

[a] s = strong, w = weak.

3_{10}-helices. Two smaller side bands are also identified at 1641 and 1681 cm^{-1}, but the feature at 1649 cm^{-1} seen in the deconvolved spectrum is lost in the negative lobe of the main band.

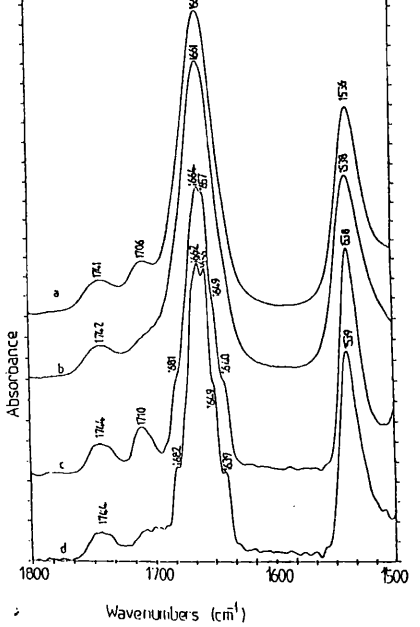

FIGURE 4: (a) Absorption spectrum of 16 mM Z-(Aib-L-Ala)$_5$-OMe in $CDCl_3$ at 20 °C. (b) Absorption spectrum of 16 mM Z-L-Ala-(Aib-L-Ala)$_5$-OMe in $CDCl_3$ at 20 °C. (c) Deconvolved spectrum of 16 mM Z-(Aib-L-Ala)$_5$-OMe in $CDCl_3$ at 20 °C using bandwidth 12 and resolution-enhancement factor 2.125. (d) Deconvolved spectrum of 16 mM Z-L-Ala-(Aib-L-Ala)$_5$-OMe in $CDCl_3$ at 20 °C using bandwidth 12 and resolution-enhancement factor 2.125.

Table IV: Components of the Resolution-Enhanced Amide I and Amide II Bands of *p*Brz-(L-Pro-Aib)$_n$-OMe (n = 2–5) at 1.5 mM concentration in $CDCl_3$[a]

n	amide I (cm^{-1})	amide II (cm^{-1})
5	1682 w, 1661 w, 1645 s	1538 s
4	1682 w, 1664 w, 1648 s, 1641 w	1538 s
3	1685 s, 1663 s, 1644 w	1537 s
2	1684 s, 1664 w	1536 s

[a] s = strong, w = weak.

The results of the study of the peptides Z-L-Ala-(Aib-L-Ala)$_n$-OMe (n = 1–5) in $CDCl_3$ at 1.5 mM concentration are listed in Table III. The absorption spectrum of Z-L-Ala-(Aib-L-Ala)$_5$-OMe (Figure 2b) shows the amide I band at 1662 cm^{-1} and the amide II band at 1536 cm^{-1}. The deconvolved and second-derivative spectra (Figures 2d and 3b, respectively) indicated that the main band is formed by two components, one at 1663 cm^{-1}, which we assign to 3_{10}-helix, and one at 1657–1658 cm^{-1}, which we assign to α-helix. Furthermore, the minor component at 1681 cm^{-1} we assign to type III β-turns and/or free carbonyl groups. The bands at 1639 and 1648 cm^{-1} may be from type III β-turns, with a possible contribution from the $3\pi/2$ vibration of the α-helix. There is also a band 1743–1747 cm^{-1} which we assign to the free methyl ester carbonyl group and one at 1711 cm^{-1}, assigned to the H-bonded urethane carbonyl group.

The absorption and resolution-enhanced spectra of Z-L-Ala-(Aib-L-Ala)$_5$-OMe and Z-(Aib-L-Ala)$_5$-OMe in $CDCl_3$ at 16 mM concentration show similar spectra when compared to those at the lower concentration, but better separation of the bands assigned to α- and 3_{10}-helices was achieved by using the same resolution-enhancement factors (Figures 4 and 5).

The results of the studies of the *p*BrZ-(L-Pro-Aib)$_n$-OMe (n = 2–5) peptides are given in Table IV. The absorption spectrum of *p*BrZ-(L-Pro-Aib)$_5$-OMe and the deconvolved and

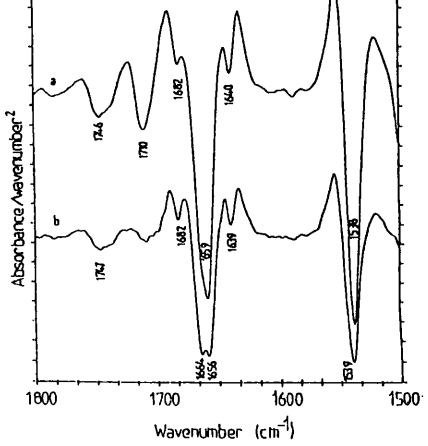

FIGURE 5: (a) Second-derivative spectrum of 16 mM Z-(Aib-L-Ala)$_5$-OMe in $CDCl_3$ at 20 °C. (b) Second-derivative spectrum of 16 mM Z-L-Ala-(Aib-L-Ala)$_5$-OMe in $CDCl_3$ at 20 °C.

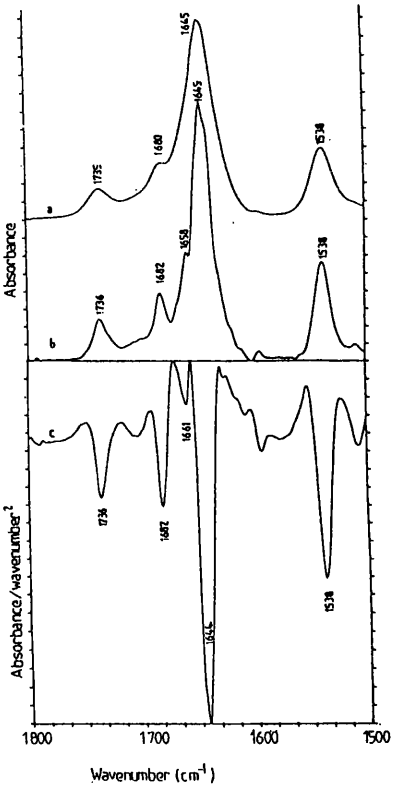

FIGURE 6: (a) FTIR absorption spectrum from 1800 to 1500 cm^{-1} of *p*BrZ-(L-Pro-Aib)$_5$-OMe in $CDCl_3$ at 20 °C. (b) Deconvolved spectrum of *p*BrZ-(L-Pro-Aib)$_5$-OMe using bandwidth 12 and resolution-enhancement factor 2.125. (c) Second-derivative spectrum of *p*BrZ-(L-Pro-Aib)$_5$-OMe in $CDCl_3$ at 20 °C.

second-derivative spectra are shown in Figure 6a–c, respectively. The absorption spectrum shows two amide I components: the main feature at 1645 cm^{-1}, which we assign to a combination of H-bonded secondary amide and free tertiary amide carbonyls present in a β-bend ribbon, and a smaller component at 1680 cm^{-1}, which we assign to free carbonyl groups. The amide II band is seen at 1538 cm^{-1}. Resolution-enhancement techniques identify the position of the high-frequency component at 1682 cm^{-1} and resolved a further band at 1661–1658 cm^{-1}. The band at 1736 cm^{-1} is assigned to the free methyl ester carbonyl group.

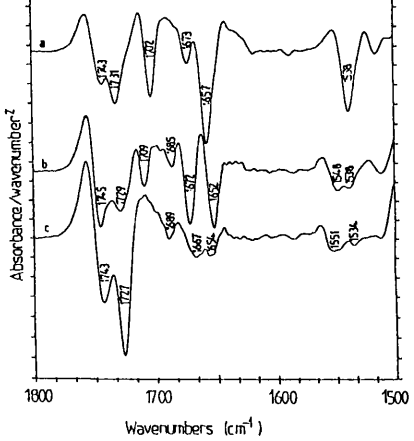

FIGURE 7: (a) Second-derivative spectrum of Z-(Aib)$_8$-O*t*Bu in DMPC vesicles (approximate molar ratio 1:15) in pbs buffer, pH 7.4. (b) Second-derivative spectrum of Z-(Aib-L-Ala)$_5$-OMe in DMPC vesicles (approximate molar ratio 1:15) in pbs buffer, pH 7.4. (c) Second-derivative spectrum of Z-L-Ala-(Aib-L-Ala)$_5$-OMe in DMPC vesicles (approximate molar ratio 1:15) in pbs buffer, pH 7.4.

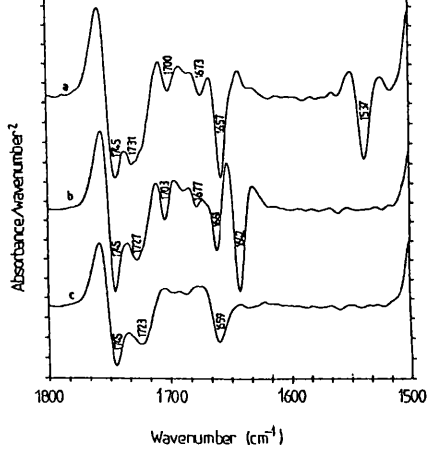

FIGURE 8: (a) Second-derivative of Z-(Aib)$_8$-O*t*Bu in DMPC vesicles (approximate molar ratio 1:15) in pbs buffer, pD 7.4, after incubation at 33 °C for 22–24 h. (b) Second-derivative spectrum of Z-(Aib-L-Ala)$_5$-OMe in DMPC vesicles (approximate molar ratio 1:15) in pbs buffer, pD 7.4, after incubation at 33 °C for 22–24 h. (c) Second-derivative spectrum of Z-L-Ala-(Aib-L-Ala)$_5$-OMe in DMPC vesicles (approximate molar ratio 1:15) in pbs buffer, pD 7.4, after incubation at 33 °C for 22–24 h.

Studies of Peptides in Aqueous Lipid Dispersion. The influence of lipids on the secondary structure of the peptides was investigated by using DMPC vesicles. Figure 7a shows the second-derivative spectrum of Z-(Aib)$_8$-O*t*Bu in DMPC vesicles at 30 °C (above T_c). We assign the bands at 1743 and 1731 cm^{-1} to the lipid ester groups. The amide I band of the peptide exhibits two components: one at 1657 cm^{-1}, characteristic of α-helix, and the other at 1673 cm^{-1}, characteristic of short, unstable 3_{10}-helix and/or β-turns. We assign the band at 1702 cm^{-1} to the H-bonded urethane carbonyl group and the *tert*-butyl ester carbonyl group. The frequencies of the amide I and II bands are unchanged at 20 °C (below the lipid transition temperature). Similar results are obtained for Z-(Aib)$_n$-O*t*Bu (n = 9, 10). The experiment was repeated in D_2O buffer, using Z-(Aib)$_8$-O*t*Bu in DMPC vesicles. The second-derivative spectrum is shown in Figure 8a. The spectrum is very similar to that of the sample in H_2O buffer and shows that, despite the long incubation in the D_2O buffer, little, if any, H ↔ D exchange occurs. Similar results were obtained for Z-(Aib)$_n$-O*t*Bu (n = 9, 10).

The second-derivative spectrum of Z-(Aib-L-Ala)$_5$-OMe reconstituted in DMPC vesicles (Figure 7b) shows two main components at 1652 cm^{-1}, assigned to α-helix, and at 1672 cm^{-1}, which we assign to a short, unstable 3_{10}-helix and/or β-turns. The small band at 1685 cm^{-1} is assigned to β-turns. The sharp band at 1709 cm^{-1} is assigned to the H-bonded urethane carbonyl of the N-protecting group, and it is noted that the intensity of this band is greatly increased relative to the intensity in $CDCl_3$. Incubation of the sample in D_2O buffer induced a large shift in the amide II band, indicating a high level of H ↔ D exchange. The second-derivative spectrum (Figure 8b) has components at 1677 cm^{-1}, which we assign to β-turns, 1661 cm^{-1}, assigned to exchanged 3_{10}-helix, and 1642 cm^{-1}, which we assign to α-helix (see Discussion).

The second-derivative spectrum of Z-L-Ala-(Aib-L-Ala)$_5$-OMe in DMPC vesicles (Figure 7c) shows the main components of the amide I band at 1667 cm^{-1}, assigned to 3_{10}-helix, and 1654 cm^{-1}, assigned to α-helix. The intensity of the amide I absorption in this spectrum is relatively weak, and we were unable to improve on this result when repeating the experiment. Incubation of Z-L-Ala-(Aib-L-Ala)$_5$-OMe incorporated in DMPC vesicles in D_2O buffer caused the disappearance of the amide II band, indicating a high level of H ↔ D exchange. The second-derivative spectrum (Figure 8c) shows the major amide I component at 1659 cm^{-1}. This is too high to be deuterated α-helix, and therefore we assign the band to deuterated 3_{10}-helix, possibly with a contribution from α-helix.

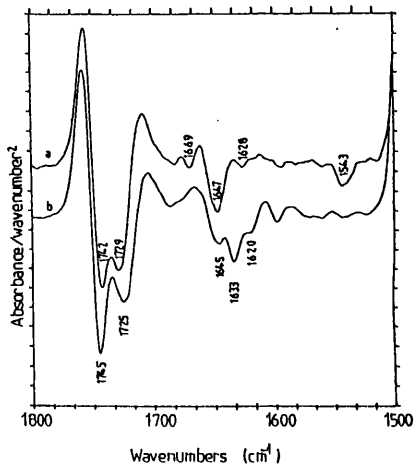

FIGURE 9: (a) Second-derivative spectrum of *p*BrZ-(L-Pro-Aib)$_5$OMe in DMPC vesicles (approximate molar ratio 1:15) in pbs buffer, pH 7.4. (b) Second-derivative spectrum of *p*BrZ-(L-Pro-Aib)$_5$-OMe in DMPC vesicles in pbs buffer, pD 7.4, after incubation at 33 °C for 22–24 h.

The second-derivative spectrum of *p*BrZ-(L-Pro-Aib)$_5$-OMe reconstituted in DMPC vesicles (Figure 9a) gives the main amide I component at 1647 cm^{-1}, assigned to β-bend ribbon, with smaller components at 1669 and 1628 cm^{-1}, both assigned to β-turns. The use of D_2O buffer causes H ↔ D exchange in the peptide, and the second-derivative spectrum (Figure 9b) shows three amide I components: 1633 cm^{-1}, assigned to exchanged β-bend ribbon; 1645 cm^{-1}, assigned to unexchanged β-bend ribbon; and 1620 cm^{-1}, assigned to β-turns.

Discussion

The $C^{\alpha,\alpha}$-dialkylated α-amino acid Aib has been shown to promote formation of helical conformations (Smith et al., 1981;

1988). Conformation energy calculations, assuming a tetrahedral symmetric geometry for the four substituents on the C^{α} carbon, predicted that an α-helical structure would be adopted by the Aib residue (Marshall, 1971; Pletnev et al., 1973; Burgess & Leach, 1973). However, the assumption of symmetry has been shown to be invalid for crystallized peptides containing poly(Aib)$_n$. For a residue in a right-handed (incipient) 3_{10}-helical conformation, the bond angles involving the methyl group in the D-position tend to be larger than the tetrahedral value, whereas those involving the L-methyl group tend to be smaller. This slight distortion is due to steric hindrance as the formation of the 3_{10}-helix involves the methyl in the D-position being too close to the C=O of the preceding unit. Taking this asymmetry into account, Paterson et al. (1981) showed that the 3_{10}-helix is the most stable conformation for Aib homopeptides.

A number of conformational studies on terminally blocked Aib-containing peptides have been carried out by using a range of techniques, including X-ray diffraction as well as ^1H and ^{13}C NMR and IR absorption spectroscopy. A ^{13}C NMR study of Z-(Aib)$_n$-OMe (n = 3–8) by Saitô et al. (1988) showed that all these homopeptides contain incipient or fully developed 3_{10}-helices. Toniolo et al. (1985, 1986) conclude from studies using X-ray diffraction and IR absorption spectroscopy that fully stable 3_{10}-helices are formed by Z-(Aib)$_n$-O*t*Bu for n = 8 or more.

Recent papers by Karle, Balaram, and co-workers on Aib-rich peptides show that the peptide Boc-Trp-Ile-Ala-Aib-Ile-Val-Aib-Leu-Aib-Pro-OMe exhibits a predominantly α-helical structure in triclinic crystals and a 3_{10}-helix in monoclinic crystals (Karle et al., 1989a). The same workers also reported that two molecules of the peptide Boc-Aib-Val-Aib-Aib-Val-Val-Val-Aib-Val-Aib-OMe cocrystallize in a triclinic cell with different helical conformations (Karle et al., 1989a), one molecule being totally α-helical and the other being a combination of α-helix and 3_{10}-helix. Solution studies using ^1H NMR on the same compound found it to be completely 3_{10}-helical in $CDCl_3$ and either α-helical or partially unfolded 3_{10}-helical in $(CD_3)_2SO$. Studies in $CDCl_3$ are widely carried out as this solvent has a low polarity, similar to the low polarity experienced in natural membranes.

Bavoso et al. (1988) summarized the current empirical view based on X-ray data that, while Aib-rich peptides shorter than eight residues tend to adopt a 3_{10}-helical structure, Aib-rich peptides of eight residues or longer may adopt either 3_{10}- or mixed $3_{10}/\alpha$-helical structure.

Marshall et al. (1990) concluded that the choice between the α- and 3_{10}-helical conformations assumed by peptides containing multiple $C^{\alpha,\alpha}$-dialkylated amino acids depends on peptide length, environment, and size and distribution of amino acid side chains.

The interpretation of the 1750–1600 cm^{-1} region of the IR absorption spectrum for these peptides is complicated by the presence of free peptide carbonyl groups and by the N- and C-terminal protecting groups. The urethane C=O of the benzyloxycarbonyl protecting group is the acceptor of the first H-bond. A free urethane C=O occurs at a frequency >1725 cm^{-1}, whereas the band from a H-bonded urethane C=O occurs at 1720–1715 cm^{-1} (Pulla Rao et al., 1980; Bonora et al., 1984). However, the carbonyl of the *tert*-butyl ester group also occurs at 1720–1715 cm^{-1}, while the band from the carbonyl of the methyl ester group occurs at 1740–1730 cm^{-1}.

In all the 3_{10}-helical peptides examined in the present study, the last two carbonyl groups are not H-bonded. As the number carbonyls become relatively stronger with respect to that of the H-bonded peptide carbonyls. From Table I, as n decreases, the relative increase in intensity of the band centered around 1687–1677 cm^{-1} indicates that this band arises from free peptide carbonyls. The increase in intensity of the band in the range 1666–1662 cm^{-1} as n increases indicates that this is due to H-bonded peptide carbonyls. This frequency range, coupled with the position of the amide II at 1533–1531 cm^{-1}, agrees well with the calculated frequencies of Krimm and Bandekar (1980) for the 3_{10}-helical structure.

The two minor components of the amide I band for the Z-(Aib)$_n$-O*t*Bu (n = 8–10) homopeptides occur at 1681–1679 and 1646–1644 cm^{-1}. These components remain after the sample has been diluted to a concentration approximately 4 times below the minimum level for self-aggregation, indicating that they derive from secondary structures present in the monomeric peptides. The observed frequencies agree well with the predicted values of 1686 and 1646 ± 3 cm^{-1} for type III β-turn absorptions. Therefore, we assign the band at 1646–1644 cm^{-1} to type III β-turns and the band at 1681 cm^{-1} to type III β-turns and/or free carbonyls.

The resolution-enhanced spectra of the Z-(Aib-L-Ala)$_n$-OMe and Z-L-Ala-(Aib-L-Ala)$_n$-OMe peptides in $CDCl_3$ indicate that in both peptide series the highest oligomers contain a combination of α- and 3_{10}-helix.

We interpret the spectral shift observed with the Z-(Aib)$_n$-O*t*Bu (n = 8–10) peptides using DMPC vesicles to indicate that the peptides shift from a 3_{10}-helical conformation in $CDCl_3$ to mainly α-helical, with a contribution from β-turns and/or short, unstable 3_{10}-helix, in aqueous lipid dispersion. No further change in the peptide secondary structure is detected upon raising the temperature from below to above the phase transition temperature of the lipid. Karle et al. (1988, 1989a) have shown that two different conformations are possible for the same peptide in its crystalline form, illustrating the sensitivity of the peptide secondary structure to its particular environment.

The inability of the peptide to undergo H ↔ D exchange when incorporated in DMPC vesicles indicates the inaccessibility of the peptide to D_2O molecules in this environment.

We interpret the spectral changes observed when the peptide Z-(Aib-L-Ala)$_5$-OMe is incorporated into an aqueous lipid dispersion to indicate that 3_{10}- and α-helical structures are still present. The frequencies of the 1652 and 1642 cm^{-1} bands assigned to α-helix in the undeuterated and deuterated peptide, respectively, are both low for regular α-helices. Karle et al. (1989b,c) reported the insertion of water molecules into the helical backbone of the apolar peptides Boc-Ala-Leu-Aib-Ala-Leu-Aib-OMe (Karle et al., 1989b) and Boc-Aib-(Val-Ala-Leu-Aib)$_3$-OMe (Karle et al., 1989c) when each was crystallized individually. In the first example, H-bonds are formed between the water and the C=O and NH groups of the Ala residues. This causes a bend in the backbone of the peptide and also increases the length of at least one of the intramolecular H-bonds, and may give rise to the low-frequency amide I components of the α-helical structure. This is similar to the low-frequency amide I′ band component assigned to the highly solvated α-helical structure observed for troponin C (Jackson et al., unpublished results), in which the intramolecular H-bonding pattern of the B-helix is interrupted by approximately 20% of the C=O groups H-bonding to water molecules inserted into the helical backbone.

An increase in the intensity of the band assigned to the H-bonded urethane carbonyl group may indicate intermole-

lipid environment, or possibly indicate H-bonding to the lipid head-group.

The H ↔ D exhange of Z-(Aib-L-Ala)$_5$-OMe and Z-L-Ala-(Aib-L-Ala)$_5$-OMe when incorporated in lipid vesicles indicates that in this environment the hydrogen atoms of the amide NH groups are easily accessible to D_2O molecules. This indicates that the peptides aggregate to form pores in the bilayer which allows the passage of water molecules.

The components of the amide I band of Z-L-Ala-(Aib-L-Ala)$_5$-OMe incorporated in DMPC vesicles in H_2O show bands at 1667 and 1654 cm^{-1}, assigned to 3_{10}-helix and to α-helix, respectively. In D_2O, the same peptide shows a dominant feature at 1659 cm^{-1}, which we assign to deuterated 3_{10}-helix with perhaps a contribution from α-helix.

The NMR and IR absorption spectroscopy results for Z-(Aib-L-Pro)$_4$-OMe (Venkatachalapathi et al., 1981) indicate that the H-bonds formed may be slightly different from those of an ideal 3_{10}-helix due to the steric hindrance introduced by the presence of Pro residues. Unfavorable steric contacts required for an ideal 3_{10}-helix may be relaxed in this peptide by slight distortions introduced by nonplanar peptide units and deviations from the ideal 3_{10}-helical angles. These effects may alter the strength of the intramolecular H-bonds to produce the amide I absorption maximum at 1648–1645 cm^{-1} for *p*BrZ-(L-Pro-Aib)$_5$-OMe, which we assign to β-bend ribbon.

Incorporation of this peptide into DMPC vesicles produces very little effect on the amide I and II bands. The increased steric hindrance of the Pro-Aib peptides will reduce the number of possible conformations available and will require large pertrubations to induce change. However, the peptide *p*BrZ-(L-Pro-Aib)$_5$-OMe does undergo H ↔ D exchange when incorporated into DMPC vesicles in D_2O buffer, indicating that a pore may be formed by aggregates of the peptide within the lipid bilayer.

This study represents the first characterization of the 3_{10}-helical and β-bend ribbon secondary structures of FTIR spectroscopy incorporating resolution-enhancement techniques. We have shown that the main absorption from the stable 3_{10}-helix occurs at 1666–1662 cm^{-1} and from the β-bend ribbon at 1648–1645 cm^{-1}. We also demonstrate that with resolution-enhancement techniques it can be possible to identify α- and 3_{10}-helices in the same peptide.

These reults indicate that Aib homopeptides have a 3_{10}-helical secondary structure in $CDCl_3$ and are predominantly α-helical when incorporated into lipid vesicles. Peptides with Aib-L-Ala as the repeat unit tend to retain some of the 3_{10}-helical structure that they exhibit in $CDCl_3$ when incorporated into an aqueous model membrane. Further, we have shown that the 3_{10}-helical structure is very sensitive to changes in environment.

Registry No. DMPC, 18194-24-6; Z-(Aib)8-OBu-t, 95842-05-0; Z-(Aib-L-Ala)5-OMe, 133850-20-1; Z-L-Ala-(Aib-L-Ala)5-OMe, 131738-94-8; *p*-Brz-(L-Pro-Aib)5-OMe, 133833-18-8.

References

Austen, B. M. (1979) *FEBS Lett. 103*, 308–313.

Barlow, D. J., & Thornton, J. M. (1988) *J. Mol. Biol. 201*, 601–619.

Batenburg, A. M., Brasseur, R., Ruysschaert, J. M., van Scharrenburg, G. J. M., Slotboom, A. J., Demel, R. A., & de Kruijff, B. (1988) *J. Biol. Chem. 263*, 4202–4207.

Bavoso, A., Benedetti, E., Di Blasio, B., Pavone, C., Toniolo, C., & Bonora, G. M. (1986) *Proc. Natl. Acad. Sci. U.S.A. 83*, 1988–1992.

C., Toniolo, C., Bonora, G. M., Formaggio, F., & Crisma, M. (1988) *J. Biomol. Struct. Dyn. 5*, 803–817.

Benedetti, E., Bavoso, A., Di Blasio, B., Pavone, V., Pedone, C., Toniolo, C., & Bonora, G. M. (1982a) *Proc. Natl. Acad. Sci. U.S.A. 79*, 7951–7954.

Benedetti, E., Bavoso, A., Di Blasio, B., Pavone, V., Pedone, C., Crimsa, M., Bonora, G. M. & Toniolo, C. (1982b) *J. Am. Chem. Soc. 104*, 2437–2444.

Benedetti, E., Di Blasio, B., Pavone, V., Pedone, C., Santini, A., Bavoso, A., Toniolo, C., Crisma, M., & Sartore, L. (1990) *J. Chem. Soc., Perkin Trans. 2*, 1829–1837.

Bonora, G. M., Mappeli, C., Toniolo, C., Wilkening, R. R., & Stevens, E. S. (1984) *Int. J. Biol. Macromol. 6*, 179–188.

Briggs, M. S., & Gierasch, L. M. (1984) *Biochemistry 23*, 3111–3114.

Bruckner, H., & Graf, H. (1983) *Experientia 39*, 528–530.

Burgess, A. W., & Leach, S. J. (1973) *Biopolymers 12*, 2599–2605.

Deisenhofer, J., Epp, O., Miki, K., Huber, R., & Michel, H. (1985) *Nature (London) 318*, 618–624.

Dwivedi, A. M., Krimm, S., & Malcolm, B. R. (1984) *Biopolymers 23*, 2025–2065.

Engelman, D. E., & Steitz, T. A. (1981) *Cell 23*, 411–422.

Fox, R., & Richards, F. M. (1982) *Nature (London) 300*, 325–330.

Haris, P. I., & Chapman, D. (1988) *Biochim. Biophys. Acta 943*, 375–380.

Henderson, R. (1975) *J. Mol. Biol. 93*, 123–138.

Jones, D. S., Kenner, G. W., Preston, J., & Sheppard, R. C. (1965) *J. Chem. Soc.*, 6227–6239.

Karle, I. L., Flippen-Anderson, J. L., Sukumar, M., & Balaram, P. (1987) *Proc. Natl. Acad. Sci. U.S.A. 84*, 5087–5091.

Karle, I. L., Flippen-Anderson, J. L., Sukumar, M., & Balaram, P. (1988) *Int. J. Pept. Protein Res. 31*, 567–576.

Karle, I. L., Flippen-Anderson, J. L., Uma, K., Balaram, H., & Balaram, P. (1989a) *Proc. Natl. Acad. Sci. U.S.A. 86*, 765–769.

Karle, I. L., Flippen-Anderson, J. L., Uma, K., & Balaram, P. (1989b) *Biopolymers 28*, 773–781.

Karle, I. L., Flippen-Anderson, J. L., Uma, K., & Balaram, P. (1989c) *Biochemistry 28*, 6696–6701.

Kauppinen, J. K., Moffat, D. J., Mantsch, H. H., & Cameron, D. G. (1981) *Appl. Spectrosc. 35*, 271–275.

Kleffel, B., Garavito, R. M., Baumeister, W., & Rosenbusch, J. P. (1985) *EMBO J. 4*, 1589–1592.

Krimm, S., & Bandekar, J. (1980) *Biopolymers 19*, 1–29.

Le Bars, M., Bachet, B., & Mornon, J. P. (1988) *Z. Kristallogr. 185*, 588.

Lee, D. C., Hayward, J. A., Restall, C. J., & Chapman, D. (1985) *Biochemistry 24*, 4364–4373.

Malcolm, B. R. (1983) *Biopolymers 22*, 319–322.

Marshall, G. R. (1971) in *Intra-Science Chemistry Reports* (Kharasch, N., Ed.) pp 305–316, Gordon and Breach, New York.

Marshall, G. R., Hodgkin, E. E., Langs, D. A., Smith, G. D., Zabrocki, J., & Leplawy, M. T. (1990) *Proc. Natl. Acad. Sci. U.S.A. 87*, 487–491.

Mathew, M. K., & Balaram, P. (1983) *Mol. Cell. Biochem. 50*, 47–64.

Menestrina, G., Voges, K. P., Jung, G., & Boheim, G. (1986) *J. Membr. Biol. 93*, 111–132.

Moffat, D. J., Kauppinen, J. K., Cameron, D. G., Mantsch, H. H., & Jones, R. N. (1986) *Computer programs for*

tawa, Canada.
Paterson, Y., Rumsey, S. M., Benedetti, E., Nemethy, G., & Sheraga, H. A. (1981) *J. Am. Chem. Soc. 103*, 2947–2955.
Pavone, V., Di Blasio, B., Santini, A., Benedetti, E., Pedone, C., Toniolo, C., & Crisma, M. (1990) *J. Mol. Biol. 214*, 633–635.
Pavone, V., Benedetti, E., Di Blasio, B., Pedone, C., Santini, A., Bavoso, A., Toniolo, C., Crisma, M., & Sartore, L. (1990) *J. Biomol. Struct. Dyn. 7*, 1321–1331.
Pletnev, V. Z., Gromov, E. P., & Popov, E. M. (1973) *Khim. Prir. Soedin. 9*, 224–229.
Popot, J. L., Engelman, D. M., Gurel, O., & Zaccai, G. (1990) *J. Mol. Biol. 210*, 829–847.
Prasad, B. V. V., & Balaram, P. (1984) *CRC Crit. Rev. Biochem. 16*, 307–348.
Pulla Rao, C., Nagaraj, R., Rao, C. N. R., & Balaram, P. (1980) *Biochemistry 19*, 425–431.
Reddy, G. L., & Nagaraj, R. (1989) *J. Biol. Chem. 264*, 16591–16597.
Rizzo, V., Stankowski, S., & Schwarz, G. (1987) *Biochemistry 26*, 2751–2759.
Proc. Natl. Acad. Sci. U.S.A. 77, 3983–3987.
Saitô, H., Tabeta, R., Formaggio, F., Crisma, M., & Toniolo, C. (1988) *Biopolymers 27*, 1607–1617.
Shinnar, A. E., & Kaiser, E. T. (1984) *J. Am. Chem. Soc. 106*, 5006–5007.
Smith, G. D., Pletnev, V. Z., Duax, W. L., Balasabramanian, T. M., Bosshard, H. E., Czerwinski, E. W., Kendrick, N. E., Matthews, F. S., & Marshall, G. R. (1981) *J. Am. Chem. Soc. 103*, 1493–1501.
Toniolo, C. (1989) *Biopolymers 28*, 247–257.
Toniolo, C., & Benedetti, E. (1988) *ISI Atlas Sci.: Biochem. 1*, 225–230.
Toniolo, C., Bonora, G. M., Barone, V., Bavoso, A., Benedetti, E., Di Blasio, B., Grimaldi, P., Lelj, F., Pavone, V., & Pedone, C. (1985) *Macromolecules 18*, 895–902.
Toniolo, C., Bonora, G. M., Bavoso, A., Benedetti, E., Di Blasio, B., Pavone, V., & Pedone, C. (1986) *Macromolecules 19*, 472–479.
Venkatachalapathi, Y. V., & Balaram, P. (1981) *Biopolymers 20*, 1137–1145.

Fourier Transform Infrared Study of the N Intermediate of Bacteriorhodopsin†

Jean-Marc Pfefferlé,‡ Akio Maeda,* Jun Sasaki, and Tôru Yoshizawa§
Department of Biophysics, Faculty of Science, Kyoto University, Kyoto 606, Japan
Received January 3, 1991; Revised Manuscript Received April 2, 1991

ABSTRACT: Visible absorption spectroscopic experiments show that the N intermediate is the main photoproduct of a highly hydrated film of the light-adapted bacteriorhodopsin (70% water by weight) at pH 10 and 274 K. The difference Fourier transform infrared spectrum between the N intermediate and unphotolyzed light-adapted bacteriorhodopsin was recorded under these conditions. A small amount of the M intermediate present did not affect this spectrum significantly. The difference spectrum exhibited a positive band at 1755 cm^{-1} (probably due to Asp-85) and a negative band at 1742 cm^{-1} (due to Asp-96), neither of which was observed for the M intermediate. The spectrum of the N intermediate at pH 7 was nearly identical with that at pH 10. Spectra at pH 10 also were measured with isotope-substituted samples. A vibrational band at 1692 cm^{-1} due to the peptide bond disappeared, and a band at 1558 cm^{-1} emerged upon formation of the N intermediate. The spectrum also displayed bands containing the N–H and C_{15}–H in-plane bending vibrational modes at 1394 and 1303 cm^{-1}. These frequencies are similar to those of the L intermediate while the intensities of these bands are larger than those in the L intermediate, suggesting that the Schiff bases of both the L and N intermediates have a strong hydrogen-bonding interaction with the protein and that the C_{12}–H to C_{15}–H region of the chromophore is less twisted in the N intermediate than in the L intermediate.

Bacteriorhodopsin in the purple membrane (bR)[1] is one of the retinoid proteins produced by *Halobacterium halobium* (Stoeckenius et al., 1979; Stoeckenius & Bogomolni, 1982). Its chromophore is retinal, linked to the protein moiety through the lysine-216 residue as a protonated Schiff base. Upon absorption of light by the chromophore, bR acts as a light-driven proton pump, by ejecting protons from the cell and taking up protons from the opposite side of the membrane. Asp-85 and -96, buried in the membrane, have been shown to be essential for these processes (Mogi et al., 1988), Asp-85 for the proton release step (Otto et al., 1990) and Asp-96 for the proton uptake step (Holz et al., 1989).

Resonance Raman experiments by Maeda et al. (1986) have revealed a photoproduct, L′, which is more stable at alkaline pH. By means of visible absorption spectroscopy, Drachev et al. (1987), Dancshazy et al. (1988), and Kouyama et al. (1988)

†This work was supported in part by Grants-in-Aid for Specially Promoted Research from the Japanese Ministry of Education, Science and Culture (63065002), by a research grant from the Human Frontier Science Program, and by the Joint Studies Program of the Graduate University for Advance Studies. J.-M.P. was supported by an exchange program between the Japan Society for the Promotion of Science and the Swiss National Science Foundation.
*Address correspondence to this author at the Department of Biophysics, Faculty of Science, Kyoto University, Kitashirakawa-Oiwakecho, Sakyo-ku, Kyoto 606, Japan.
‡Present address: KU 4.39, Ciba-Geigy, 1870 Monthey, Switzerland.
§Present address: Department of Applied Physics and Chemistry, The University of Electro-Communication, 1-5-1 Chofugaoka, Chofu, Tokyo 182, Japan.

[1] Abbreviations: bR, bacteriorhodopsin; FT-IR, Fourier transform infrared; BR^L, light-adapted bacteriorhodopsin; λ_{max}, wavelength of maximum absorption.

0006-2960/91/0430-6548$02.50/0